# Direct entry by RNase E

Justin Edward Clarke

Submitted in accordance with the requirements for the degree of Doctor of Philosophy

The University of Leeds

School of Molecular and Cellular biology

September 2015

## Statement of academic integrity

The candidate confirms that the work submitted is his/her own, except where work which has formed part of jointly-authored publications has been included. The contribution of the candidate and the other authors to this work has been explicitly indicated below. The candidate confirms that appropriate credit has been given within the thesis where reference has been made to the work of others.

The work in Chapter 3 has appeared in the publications as follows:

> Kime, L., Clarke, J. E., Romero A., D., Grasby, J. A. & McDowall., K. J. (2014) Adjacent single-stranded regions mediate processing of tRNA precursors by RNase E direct entry. *Nucleic Acids Research,* 42, 4577-4589.
>
> Clarke, J. E., Kime, L., Romero A., D. & McDowall, K. J. (2014) Direct entry by RNase E is a major pathway for the degradation and processing of RNA in *Escherichia coli. Nucleic Acids Research,* 42, 11733-11751.

*The candidate was responsible for all work shown in Chapter 3. Louise Kime was responsible for the preparation of the NTH-RNase T170V mutant.*

The work in Chapter 4 has appeared in the publication as follows:

> Clarke, J. E., Kime, L., Romero A., D. & McDowall, K. J. (2014) Direct entry by RNase E is a major pathway for the degradation and processing of RNA in *Escherichia coli. Nucleic Acids Research,* 42, 11733-11751.

*The candidate was responsible for all work shown in Chapter 4, except for the preparation of total RNA for the T170V in vitro RNA-seq analysis, which was prepared by Louise Kime.*

## Acknowledgements

First and foremost I would like to thank my supervisor Dr. Kenneth McDowall for his continuous support throughout my studies, providing valuable insight, and for never losing faith or interest in me or the project. I doubt I will ever have as good an advisor or mentor for the rest of my career.

I am also grateful to the members of Kenny's lab (Ayad, David, Louise, Tom, Fayez, Mia, Olatz, Kiran, Ayat) who I have had the pleasure to work with and form solid friendships. I would also like to thank all my fellow colleagues from Garstang level 8, the Stockley lab and various members of FBS for interesting discussions, help with the use of various equipment, and for many enjoyable "one-or-two pints". Specifically I would like to thank all members of the O'Neill lab (Liam, Victoria, Necoli, Nikki, Zeyad, Anna, Chris, to name a few and especially my reliable drinking buddy Arya who was always there to grab a drink with).

In addition, I would also like to thank all the students that I have supervised in lab throughout my Ph.D. Although tested at times, the experience has always reminded me that "when I am weak, then I am strong".

Finally, I would like to thank my family and my friends for their essential support during my Ph.D and life in general. Particular mention must be made to my soul mate Dave: *sine qua non.*

## Abstract

The rapid degradation of mRNA is central to the control of gene expression. In *Escherichia coli* (*E. coli*), the initiation of mRNA degradation is performed by RNase E, an essential endonuclease that is also involved in the processing of stable RNAs. Previous studies have found that the recognition of a 5'-monophosphate group by RNase E can stimulate RNA cleavage. However, more recent work has shown that this 5' monophosphate-dependent pathway may not be the major mechanism by which RNase E initiates mRNA decay, and that another pathway exists that has been termed 'direct' entry. However, the biochemical nature of this pathway has remained hypothetical and the exact importance of direct entry in RNA decay has yet to be established. The first results chapter presented here provides biochemical confirmation that direct entry cleavage by RNase E involves the simultaneous interaction of two or more unpaired regions of RNA. In addition, evidence is provided that shows that a 5'-monophosphate group does not enhance the catalytic activity of RNase E, a previous suggestion that contradicts the direct entry model. The second results chapter addresses the importance of direct entry in the cleavage of the *E. coli* transcriptome. It was found that a large proportion of cleavages dependent on RNase E were also sites of direct entry cleavage. The third results chapter provides evidence that post-transcriptional gene regulation by RNase E may extend beyond its ability to make endonucleolytic cleavages, by preventing the association of competing ribosomes to the mRNA and/or sequestering it to the inner membrane whereby the RNA decay machinery is associated. In summary, this thesis has shown that direct entry by RNase E is a simple yet prevalent mechanism involved in initiating mRNA decay in *E. coli* that is not exclusive with the 5' monophosphate-dependent pathway.

## Contents

## List of Figures

## List of Tables

## List of Abbreviations

| | |
|---|---|
| °C | Degrees Celsius |
| µ(unit) | Micro- |
| A | Adenosine |
| Å | Angstrom units |
| APS | Ammonium persulphate |
| *B. subtilis* | *Bacillus subtilis* |
| bp | Base pair |
| BPB | Bromophenol blue |
| BSA | Bovine serum albumin |
| C | Cytosine |
| c(unit) | Centi- |
| $CaCl_2$ | Calcium chloride |
| CTH | C-terminal half |
| Da | Daltons |
| DEPC | Diethyl pyrocarbonate |
| DMSO | Dimethyl sulphoxide |
| DNA | Deoxyribonucleic acid |
| DNase | Deoxyribonuclease |
| DTT | Dithiothreitol |
| *E. coli* | *Escherichia coli* |
| EDTA | Ethylenediaminetetraacetic acid |
| EMSA | Electrophoretic mobility shift assay |
| g | Grams |
| *g* | Gravity |
| G | Guanosine |
| h | Hours |
| HCl | Hydrochloric acid |
| IPTG | Isopropyl β-D-1-thiogalactopyranoside |
| k(unit) | Kilo |
| KCl | Potassium chloride |
| l | Litre |
| M | Molar |
| m(unit) | Milli- |

| | |
|---|---|
| $MgCl_2$ | Magnesium chloride |
| min | Minute |
| mol | Moles |
| mRNA | Messenger RNA |
| n(unit) | Nano- |
| NaCl | Sodium chloride |
| NAD | Nicotine adenine dinucleotide |
| NDP | Nucleotide diphosphate (see A, G, C, T, and U) |
| NMP | Nucleotide monophosphate (see A, G, C, T, and U) |
| nt | Nucleotide |
| NTH | N-terminal half |
| NTP | Nucleotide triphosphate (see A, G, C, T, and U) |
| $OD_{600}$ | Optical density at 600 nm |
| PCR | Polymerase chain reaction |
| PEP | Phoshphoenolpyruvate |
| psi | Pounds per square inch |
| RNA | Ribonucleic acid |
| RNase | Ribonuclease |
| rRNA | Ribosomal RNA |
| s | Second |
| S | Svedberg unit |
| SDS | Sodium dodecyl sulphate |
| sRNA | Small RNA |
| T | Thymine |
| TAE | Tris-acetate-EDTA |
| TAP | Tobacco Acid Pyrophosphatase |
| TBE | Tris-borate-EDTA |
| TEMED | Tetramethylethylenediamine |
| TEX | Terminator™ 5'-Phosphate-Dependent Exonuclease |
| $T_m$ | Melting temperature |
| tmRNA | Transfer-messenger RNA |
| Tris | Tris(hydroxymethyl)aminomethane |
| tRNA | Transfer RNA |
| U | Uracil |

| | |
|---|---|
| UCSC | University of California, Santa Cruz |
| UV | Ultraviolet |
| V | Volts |
| v/v | Volume to volume |
| w/v | Weight to volume |
| XyCy | Xylene cyanol FF |

# Chapter 1

# Introduction

## 1.1 General introduction to RNA decay

### 1.1.1 *Escherichia coli* as the model organism for elucidating principles of gene expression

*Escherichia coli* is a major model organism for understanding fundamental biological process, due to fact that the mechanisms involved in *E. coli* gene expression have been characterised in large detail. As a result, *E. coli* is the host of choice for producing macromolecules, such as recombinant hormones and vaccines, and for comparison of the function of genes conserved in less tractable organisms.

### 1.1.2 Importance of RNA decay and relation to transcription

The synthesis and degradation of RNA are the two factors that ultimately control cellular mRNA levels. Together they ensure a steady state level of RNA is achieved, which can be adjusted by an increase or decrease in either of these pathways. Since the level of protein production is dependent on the level of the encoding transcript, elements that affect mRNA production or turnover ultimately affect the final level of gene expression. When transcription is repressed, the rate of degradation decreases as the abundance of the RNA is reduced. The degradation of RNA is therefore often referred to as logarithmic, and its stability is described as by the half-life, *i.e.* the time it takes for the abundance to decrease by 50%. The half-life is used to compare the degradation of different transcripts, or the same transcripts under different conditions.

The half-life of bacterial mRNA tends to be short, for example in *E. coli* it ranges from tens of seconds to a few minutes (Bernstein et al., 2002, Selinger et al., 2003). Mammalian mRNA tends to be more stable with half-lives ranging from tens of minutes to a day (Tourriere et al., 2002). Due to the instability of bacterial mRNA, the translational machinery must follow closely changes in programmed levels of transcription, which are affected by alterations in the external or internal environment. Therefore, protein production ceases within seconds of transcriptional repression of the corresponding gene (Rauhut and Klug, 1999). As a result, bacteria can adapt rapidly to dynamic environmental conditions *e.g.* temperature changes (Goldstein et al., 1990) and nutrient deficiency (Hua et al., 2004).

More stable RNA components in prokaryotes can be found in the translational machinery, including transfer RNAs (tRNAs) and ribosomal RNAs (rRNAs), which tend to have half lives over 10 minutes (Deutscher, 2003). Maturation of these stable RNAs is still dependent on the RNA decay machinery, and segments produced upon processing of tRNA and rRNA precursors are degraded in a very similar fashion (Deutscher, 2006).

Nucleotides generated from the complete degradation of the RNA can be recycled to replenish the nucleotide pool, which will then be used as precursors for transcription. This harmony between synthesis and degradation illustrates a continuous fluidity in cellular nucleotide metabolism.

### 1.1.3 Interplay of RNA decay with translation and RNA quality control

Because degradation ultimately reduces the levels of substrates for translation, the interplay between translation and RNA decay can be complex and highly regulated. There exist several mechanisms in *E. coli* that dictate the fate of mRNA. One of the most studied mechanisms is translation regulation by small RNAs. Many sRNAs are believed to act as regulators for mRNA targets, by base pairing at particular regions on the transcript and hence affecting translation and/or stability. These antisense RNAs are usually 50-250 nt in length and fall into two groups. The first group are known as *cis*-acting sRNAs, as they are encoded within the DNA on the opposite strand of the gene encoding their mRNA target. Therefore, because they have the potential for complete pairing, *cis*-acting sRNAs may regulate mRNA targets by providing sites for RNase III cleavage, an endonuclease that cleaves double-stranded RNA only (Brantl, 2007). Most bacterial antisense RNAs are in the second group known as *trans*-acting sRNAs, as they are actually encoded far away from their targets. These sRNAs only have a short stretch of nucleotides that are complementary with the target and therefore require assistance of the RNA chaperone Hfq (Aiba, 2007). However, this low sequence complementarity means that many of these *trans*-acting sRNAs can regulate several different mRNA targets.

One of the most well studied *trans*-acting sRNAs is RyhB, which targets mRNAs that encode $Fe^{2+}$-binding proteins under conditions of iron deficiency, such as *sodB* (Masse and Gottesman, 2002). RyhB base pairs to *sodB*, inhibiting translation (Vecerek et al., 2003) and decreasing stability (Masse et al., 2003). Regulation of mRNAs by RyhB has been shown to be dependent on functional Hfq, which strengthens the sRNA-mRNA interaction (Geissmann and Touati, 2004), as well as protects unpaired RyhB from cleavage by RNase E (Masse et al., 2003, Moll et al., 2003). Further analyses into the RyhB-mediated degradation of *sodB* found that the RyhB-Hfq complex copurifies with RNase E, mediated by an interaction between RNase E and Hfq (Morita et al., 2005), leading to the theory that Hfq recruits RNase E to mRNA targets using sRNA as a guide.

However, this theory cannot account for the presence of sRNAs whose binding actually increases translation and stability of some mRNA targets, such as DsrA. Interestingly, DsrA requires Hfq to base pair and positively regulate some mRNAs such as *rpoS*, and negatively regulate others such as *hns* (Lease et al., 1998, Majdalani et al., 1998, Lease and Woodson, 2004), which would be improbable if

Hfq was involved in directly recruiting RNase E. More recently it has been suggested that sRNAs negatively regulate mRNAs by blocking the ribosome binding site, reducing ribosomal traffic and hence exposing the RNA to subsequent cleavage by RNase E (Udekwu et al., 2005, Morita et al., 2006).

It is important to note that the mechanism suggested above implies that mRNAs whose translation is repressed also become unstable. This reciprocal relationship between translation and mRNA decay has been shown in previous studies. Non-sense mutations that result in the production of premature termination codons (PTCs) upstream of sites of RNase E cleavage have been shown to increase susceptibility of the transcript to RNase E, whereas mutations that result in PTCs downstream of RNase E cleavage do not (Arnold et al., 1998, Braun et al., 1998). In addition, mRNA that is transcribed by T7 polymerase has been shown to be destabilised *in vivo* compared to the same mRNA transcribed by *E. coli* RNA polymerase. This is due to the increased speed of RNA synthesis by T7 polymerase, which paces far ahead of the translating ribosomes, effectively uncoupling transcription and translation and therefore leaving large segments of RNA exposed to endonucleolytic cleavage (Iost and Dreyfus, 1995). More recently it has been shown that increasing the binding of 30S subunits to the RBS of transcripts reduced cleavage by RNase E in the 5' UTR, whereas arresting ribosome translocation reduces cleavage by RNase E downstream of the RBS (Richards et al., 2012). These findings suggest a strong link between translational inhibition and RNA degradation, which ensures that mRNAs that are repressed are then subsequently degraded, irreversibly removing these transcripts and recycling the nucleotides for further rounds of transcription. The ability of the RNA decay machinery to rapidly degrade mRNAs whose translation is impaired also suggests a form of quality control to minimize the production of aberrant proteins. Such proteins could be produced as a result of mutations that result in PTCs or inefficient translation from RNA fragments produced by pervasive transcription (Deana and Belasco, 2005).

Ribosomes do not always play a "protective" role from RNA decay as suggested above. Recently, it has been found that translational pausing can sometime induce endonucleolytic cleavage near the stalled ribosomes. These "killer" ribosomes have been found on transcripts at sites that delay elongation or termination (Hayes and Sauer, 2003, Sunohara et al., 2004). Interestingly, the endonucleolytic cleavage occurs at the codon located specifically at the A site of the 50S subunit. As a result, the ribosome remains trapped on the mRNA due to removal of the stop codon. Release of the ribosome(s) is achieved via the *trans*-translation system, whereby transfer messenger RNA (tmRNA) recognises the stalled ribosome and binds to the empty A site. The tmRNA molecule resembles the clover-leaf structure of tRNA charged with an alanine amino acid, except that the

small anticodon loop is replaced with a larger open reading frame (ORF) loop. The alanine residue on the tmRNA is transferred to the C terminus of the polypeptide chain. The mRNA fragment is then replaced by the ORF of tmRNA, which is subsequently translated on to the C terminus of the polypeptide as a protein tag. The tagged protein is then released from the ribosome and is targeted for degradation by cellular proteases. Therefore, the action of tmRNA allows recovery of the stalled ribosome(s), further degradation of the mRNA, and degradation of the aberrant protein (Moore and Sauer, 2007, Keiler, 2008). It is important to note that the *trans*-translation system could be an important quality control mechanism for recovering stalled ribosomes and removing truncated proteins produced from RNA fragments that are generated by RNase E cleavage.

In addition to mRNAs, stable RNAs such as ribosomal and transfer RNAs are also subject to RNA quality control. Initially, one of the distinctions between the two groups of RNAs was the presence of oligo(A) tails formed by the action of poly(A) polymerase I (PAP I). Oligo(A) tails were associated solely with mRNAs, providing access for PNPase-mediated degradation (O'Hara et al., 1995, Mohanty and Kushner, 1999). However, it was later found that stable RNAs are also substrates for PAP I *in vivo* (Li et al., 1998b). Further analyses showed that mutated tRNAs that were readily denaturable in the cell did not accumulate in *E. coli*, except when PAP I or PNPase were inactivated, suggesting that the concordant activity of PAP I and PNPase is required for removal of defective tRNAs (Li et al., 2002). PNPase activity is not limited to removal of defective tRNAs. Analysis of rRNAs has found that mutations in both PNPase and RNase R results in the accumulation of defective rRNA fragments (Cheng and Deutscher, 2003). In fact, the role of RNase R and PNPase in the removal of defective or misfolded rRNAs may be one of the reasons why this double mutant expresses a lethal phenotype (Cheng et al., 1998).

Finally, the interplay of translation and RNA decay can under certain circumstances be concordant. Some minor components of the RNA decay machinery have a role in modifying the ribosomes and some mRNAs to direct the expression of specific genes. In *E. coli*, the stable toxin MazF is expressed along with its labile antitoxin MazE under normal conditions of growth (Marianovsky et al., 2001). Under various stressful conditions, such as the presence of ppGpp upon amino acid starvation, the *mazEF* module is no longer expressed. As a result, the labile MazE antitoxin is degraded by ClpAP, an ATP-dependent serine protease (Aizenman et al., 1996), releasing the stable MazF toxin to promote cell death (Kolodkin-Gal and Engelberg-Kulka, 2006). MazF-mediated cell death is also activated during phage infection to prevent the spread of infectious phages (Hazan and Engelberg-Kulka, 2004) and as a response to quorum-sensing factors as a form of population control (Kolodkin-Gal et al., 2007).

MazF makes endonucleolytic cleavages within single-stranded regions of mRNA at ACA sequences (Zhang et al., 2005). MazF activity has been shown to cause widespread cell death (Kolodkin-Gal and Engelberg-Kulka, 2006) and inhibition of protein synthesis (Christensen et al., 2003, Zhang et al., 2003). However, following MazF activation, around 10% of proteins were actually expressed in *E. coli*. Some of these proteins were also involved in mediating cell death, such as ClpP, a component of the ClpAP protease that could be involved in further degradation of the MazE antitoxin (Amitai et al., 2009). Interestingly, some of the proteins expressed during MazF activation were required for survival of a small subpopulation of cells, such as DeoC, a deoxy-ribose phosphate aldolase that allows *E. coli* to use deoxynucleotides as a carbon and energy source (Han et al., 2004, Amitai et al., 2009). MazF cleaves at ACA sites just upstream of the AUG start codon in these specific mRNAs, generating leaderless mRNAs (lmRNAs) that cannot make the canonical interaction with the 30S subunit. MazF also makes an endonucleolytic cleavage 43 nt from the 3' end of 16S rRNA within the 30S ribosomal subunit. Cleavage at this site causes removal of the region encompassing the anti-Shine-Dalgarno sequence and helix45, where the ribosomal protein S1 associates. These "specialised" ribosomes can no longer make an SD-aSD interaction to initiate canonical translation, and therefore are re-directed to translate the lmRNAs generated by MazF (Vesper et al., 2011). Therefore, components of the RNA decay machinery also have the potential to direct the selective translation of a subclass of transcripts.

### 1.1.4 Spatial and temporal organisation of RNA decay machinery

The reciprocal relationship between translation and RNA degradation raises the question of how these two processes can exist together in the cell and be so finely tuned. An interesting answer to this question could lie in the spatial organisation of the bacterial cytoplasm. The bacterial chromosome is condensed into a central region of the cell termed the 'nucleoid', which does not fill the entire cytoplasmic volume (Robinow and Kellenberger, 1994). Surrounding this 'nucleoid' region is the ribosome-rich region, which will be termed the 'ribosphere' throughout this work. It is generally believed that mRNA transgresses the nucleoid-ribosphere boundary as it is being transcribed, and therefore is translated by ribosomes as it is being synthesised by RNA polymerase. Indeed, transcripts with multiple translating ribosomes, termed 'polysomes', have been found tethered to DNA via RNA polymerase linkages (Miller et al., 1970, Brandt et al., 2009). In addition, evidence has been shown that RNA polymerase tends to be located at the edge of the nucleoid boundary, hence presenting mRNA to the ribosomes as soon as it begins transcribing (Durrenberger et al., 1988, Bakshi et al., 2012).

Surrounding the 'ribosphere' is the 'degradosphere', a region rich in RNA decay machinery that is localised to the inner membrane. Membrane localisation of the RNA decay machinery is dependent on a 20 residue amphipathic α-helix found within the C-terminal half of RNase E (Khemici et al., 2008). The remaining CTH-RNase E provides additional contacts for interactions with other components of the degradosome, a complex of proteins involved in the rapid degradation of mRNA. One such protein is RNA helicase B (Py et al., 1996, Chandran et al., 2007), which may assist in unwinding of double-stranded RNA and therefore providing accessible substrates for RNase E and another degradosomal protein PNPase, which is a major 3' exonuclease (Carpousis et al., 1994, Duran-Figueroa et al., 2006). Enolase is also present (Chandran and Luisi, 2006, Nurmohamed et al., 2010), which may provide localised phosphoenolpyruvate (PEP) for pyruvate kinase, a membrane associated protein whose activity can generate ATP for PNPase and RhlB.

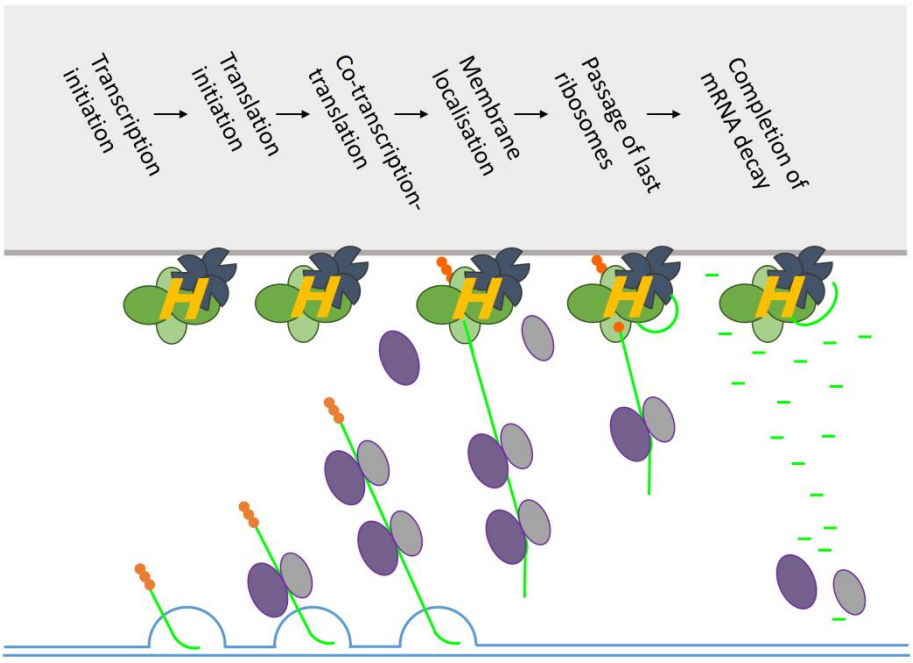


**Figure 1.1 Compartmentalisation of the protein components of the *E. coli* cytosol.** The mRNA (light green strand) is synthesised from its DNA template (light blue strand) by RNA polymerase. The 5' end becomes accessible to ribosomes (purple), which begin translation on the mRNA. As the mRNA diffuses away from the nucleoid, it comes in to contact with RNase E (dark green). Either due to direct blocking of the 5' UTR, or due to localisation away from the ribosome pool, translation of the mRNA is no longer initiated and the final ribosomes are allowed to finish. Endonucleolytic cleavage by RNase E initiates further degradation of the mRNA by the action of RhlB (yellow) and PNPase (dark blue).

The stoichiometry of the degradosome is complex given that the ratio of interactions provided by the native RNase E, RhlB, enolase and PNPase proteins could potentially be 4: 1: 1: 3, respectively. Therefore, the degradosome can form an intricate network around the inner membrane, organised

into a coiled structure by additional interactions with the cytoskeleton of *E. coli* (Taghbalout and Rothfield, 2007, Taghbalout and Rothfield, 2008). There is also evidence for RNase III, PAP I, RppH, oligoribonuclease and Hfq associating with the membrane at the same positions associated with the network of the degradosome (Taghbalout et al., 2014, Miczak et al., 1991, Carabetta et al., 2010). RNase II, although not associated with the degradosome, has also been shown to interact with the inner membrane via an amphipathic α-helix found at its N terminus. As found with the degradosome, RNase II can form a coiled network around the periphery of the cell (Lu and Taghbalout, 2013).

The isolation of the RNA degradative machinery to the inner membrane of the cell could provide several advantages, as shown in Figure 1.1. First of all, it would ensure that recently transcribed mRNAs enter the 'ribosophere' before they enter the 'degradosphere', giving all mRNAs the opportunity to be translated before they are degraded. Secondly, localisation of the RNA degradative machinery to the inner membrane also provides a temporal barrier between diffusion of the last ribosome from the transcript and the initial endonucleolytic cleavage. Although the *trans*-translation system does remove truncated proteins and rescue ribosomes from transcripts that are cleaved prematurely, such processes are still quite energetically wasteful. If the RNA decay machinery was diffused throughout the cytoplasm, premature cleavage of transcripts would be prevalent and therefore detrimental to cell survival. By sequestering the degradative machinery away from the pool of ribosomes, translation would be permitted to completion before endonucleolytic inactivation of the mRNA occurred. Thirdly, compartmentalisation of the RNA decay machinery also brings protein partners into close proximity that act simultaneously or sequentially during RNA degradation, ensuring rapid degradation of mRNA (Strahl et al., 2015).

### 1.1.5 Analogous processes in other bacteria and eukaryotes

A general model for mRNA turnover has been developed in *E. coli*. The initial step that is believed to commit a transcript to degradation is an endonucleolytic cleavage by the single strand-specific RNase E, or in some cases by the double strand-specific RNase III. Further degradation of the cleavage products is performed by the 3' to 5' exonucleases PNPase, RNase II and RNase R, with the assistance of accessory factors such as the RNA helicase RhlB or PAP I. Exonucleolytic degradation yields final products that are 4 nt long, which are substrates for the essential enzyme oligoribonuclease. RNase E is also believed to be stimulated in some cases by the presence of a monophosphate at the 5' end of a transcript, which is generated either by an initial endonucleolytic cleavage by RNase E or another endonuclease, or by RNA 5' pyrophosphohydrolase, the major decapping enzyme in *E. coli* that converts the 5' end from a triphosphate to a monosphosphate.

Further information on the general model of RNA decay can be found in several reviews (Carpousis et al., 2009, Mackie, 2013b, Andrade et al., 2009b) and in Section 1.3.

Given that RNase E and RNase G have a high sequence similarity (Wachi et al., 1997), similar enzymatic properties (Tock et al., 2000, Jourdan and McDowall, 2008), and that deficiency in RNase E can be complemented by RNase G overexpression (Wachi et al., 1997, Lee et al., 2002), it is generally assumed that the *rng* gene arose from a chromosomal duplication in the *rne* gene in the common ancestor of γ-proteobacteria. Therefore, homologues of RNase E and G in other bacteria are generally referred to as RNase E/G family members. RNase E/G family members are highly conserved amongst the α, β and γ subdivisions of the proteobacteria, as well as the chlamydiae family, although the C-terminal half of RNase E appears to be less well conserved (Condon and Putzer, 2002). Conservation amongst the gram-positive bacteria is less apparent, with only the high G+C family showing a significant conservation of the RNase E/G family. However, despite the low conservation of RNase E homologues, it is still believed that the general model of mRNA decay is similar in most bacterial species.

One of the most well studied gram-positive bacteria in the field of mRNA decay is *Bacillus subtilis*. Although *B. subtilis* has no apparent RNase E/G family member it does contain a functional homologue, known as RNase Y, which is involved in the degradation of a significant proportion of cellular mRNAs and can be stimulated by the presence of a 5' monophosphate (Shahbabian et al., 2009, Yao and Bechhofer, 2010, Durand et al., 2012, Laalami et al., 2013). *B. subtilis* also contains a homologue of RppH that could provide these 5'-monophosphorylated substrates for RNase Y (Richards et al., 2011). Like RNase E, RNase Y contains a highly structured N-terminal domain, which is essential for catalytic activity and an intrinsically disordered C- terminal domain, which could be involved in mediating protein-protein interactions (Lehnik-Habrink et al., 2011). Interestingly, there also appears to be a degradosome-like complex in *B. subtilis* that consists of RNase Y, J1, J2, the RhlB functional homologue CshA, PNPase, enolase and phosphofuctokinase, whereby RNase Y actually has the ability to contact 5 of these other proteins and therefore may provide the scaffold for the *B. subtilis* degradosome (Commichau et al., 2009, Lehnik-Habrink et al., 2010, Lehnik-Habrink et al., 2011). Indeed, mutations in RNase Y that prevent its localisation to the inner membrane actually result in cell death, suggesting that RNase Y-mediated compartmentalisation of the RNA decay machinery to the inner membrane may be an essential feature in gram-positive bacteria (Lehnik-Habrink et al., 2011).

*B. subtilis* also contains another major enzyme involved in mRNA decay called RNase J, an enzyme that has no functional homologue in *E. coli* (Condon and Putzer, 2002, Danchin, 2009). RNase J, of

which there are two forms, the more active J1 and the less important J2, was originally identified as having endonucleolytic activity (Even et al., 2005, Daou-Chabo and Condon, 2009). However, more recently it has been found that RNase J1 also exhibits significant 5' to 3' exonucleolytic activity (Mathy et al., 2007, Britton et al., 2007, Mathy et al., 2010), which is stimulated by the presence of a 5'-monophosphate group (de la Sierra-Gallay et al., 2008). Interestingly, this makes it the first example of a 5' exonuclease in bacteria. The 5'-monophosphorylated RNAs that are degraded by the exonucleolytic activity of RNase J1 may be generated by either the endonucleolytic activity of RNase J, which is not affected by the presence of a 5'-triphosphate group (Daou-Chabo and Condon, 2009), or by the *B. subtilis* RppH homologue (Richards et al., 2011). In addition, RNase Y may provide many substrates for RNase J1 as part of the *B. subtilis* degradosome complex.

The general model for mRNA decay is very different in eukaryotes. During transcription, the capping enzyme complex (CEC), which consists of three enzymes, associates with RNA polymerase II in the nucleus of the cell (Cho et al., 1997, Fabrega et al., 2003). The first enzyme, RNA terminal phosphatase, removes the γ phosphate from the 5' triphosphate of the mRNA, producing a 5'-biphosphorylated substrate (Tutas and Paoletti, 1977, Venkatesan et al., 1980). The second enzyme, mRNA guanylyltransferase, then adds a guanosine monophosphate onto the two terminal phosphates, forming a 5' to 5' triphosphate bridge, as shown in Figure 1.2A. The orientation of this cap gives the modified transcript a "pseudo" 3' end, providing significant resistance to attack by 5'-dependent exonucleases. The last component of CEC, an RNA methyltransferase, then transfers a methyl group on to the carbon at position 7 on the guanine base (Martin et al., 1975, Shatkin, 1976). Further methylation can occur on the 2' oxygen atoms of the first two nucleotides (Barbosa and Moss, 1978).

The final 5'-7 methylguanylate ($m^7G$) cap interacts with the cap binding complex (CBC), which in turn is recognised by the nuclear pore complex, resulting in exportation of the capped transcript out into the cytoplasm (Izaurralde et al., 1995, Visa et al., 1996). In the cytoplasm, the CBC is replaced by the trimeric eukaryotic translation initiation factor eIF-4F. This complex consists of eIF-4E, which recognises the 7-methyl group on the $m^7G$ cap of the mRNA (Marcotrigiano et al., 1997a, Marcotrigiano et al., 1997b); eIF-4A, a DEAD-box RNA helicase involved in unwinding secondary structure at the 5' end of the RNA (Svitkin et al., 2001); and eIF-4G, which contains binding sites for these two other factors and for the mRNA (Lamphear et al., 1995, Tarun and Sachs, 1996). This complex promotes ribosomal binding to the mRNA and restricts access of the decapping enzymes (Shatkin, 1976).

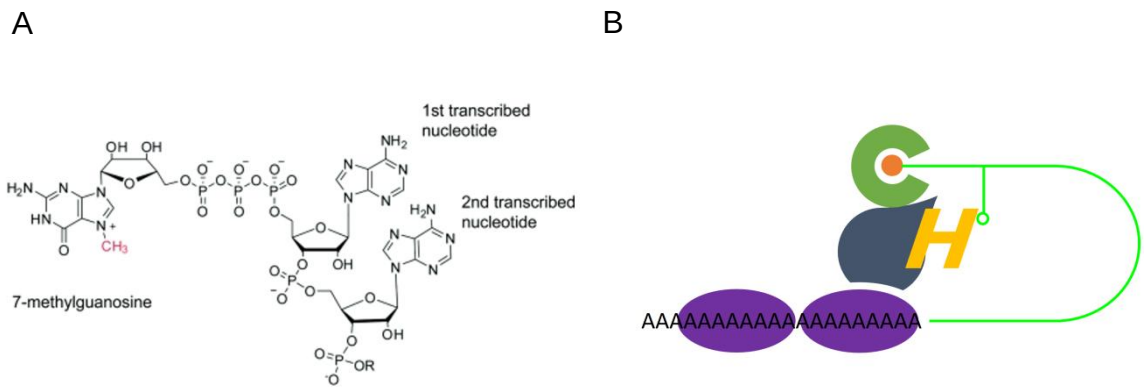


**Figure 1.2 The 5' 7 methylguanylate cap of eukaryotic mRNA.** Panel A shows the molecular representation of the 5'-7 methylguanylate cap. The 7-methyl group is shown in red. Figure taken from previous study (Cowling, 2010). Panel B shows a schematic of the lariat mRNA complexed with the eIF-4F factor. RNA is shown as a green line, the $m^7G$ cap is shown as an orange circle, eIF-4E is shown in dark green, eIF-4A is shown in yellow, eIF-4G is shown in dark blue and PAPB proteins are shown in purple.

In addition to protection at the 5' end, the mRNA can also be protected at the 3' end by the action of poly(A) polymerase. In the cytoplasm of eukaryotes, the polyadenyl tails formed by PAP activity have been shown to increase the half-life of mRNA by preventing accessibility of the exonucleolytic machinery (Ford et al., 1997), the exact opposite function to PAP I in bacteria (Mohanty and Kushner, 1999). The long poly(A) tails produced by PAP are bound by poly(A)-binding proteins (PAPBs), which hinder the access of 3' exonucleases (Coller et al., 1998). PAPB also interacts with the eIF-4E and 4G factors bound to the 5' end, forming an inaccessible lariat-like structure in the mRNA further stabilising the transcript and promoting translation, as shown in Figure 1.2B (Preiss and Hentze, 1998, Tarun and Sachs, 1996). However, PAP can also form pol(A) tails in the nucleus of the cell, where there is an absence of the various stabilising proteins present in the cytoplasm. The poly(A) tails in the nucleus perform a similar function to the oligo(A) tails in prokaryotes, providing a region onto which the exosome, a 3'-exonucleolytic complex of the RNB family (Mitchell et al., 1997), can bind and degrade the mRNA (LaCava et al., 2005, Vanacova et al., 2005).

Like bacteria, eukaryotes contain a 5'-end decapping enzyme, called Dcp2. The bacterial RNA-decapping enzyme RppH and Dcp2 both belong to the Nudix family and so appear to have evolved from a common ancestor. Dcp2 cleaves the triphosphate bridge of the $m^7G$ cap to produce a 5'-monophosphorylated transcript (Dunckley and Parker, 1999, Dunckley et al., 2001), which can be degraded by the 5' monophosphate-dependent 5' to 3' exonuclease Xrnl (Muhlrad et al., 1994). This mechanism bears a resemblance to RppH-initiated RNase E cleavage and RNase J degradation in *E. coli* and *B. subtilis*, respectively. Conservation of function between the decapping enzymes is therefore apparent, despite considerable differences in bacterial and eukaryotic mRNA structure.

## 1.2 Stable RNA processing

Stable RNAs, which consist mainly of the transfer and ribosomal RNAs, are not degraded or translated during exponential growth. Instead, they form functional molecules that have significant biological roles. However, most if not all stable RNAs are transcribed as precursors and therefore must undergo processing to yield their mature forms. This usually involves separation of the individual RNA units, followed by trimming of excess RNA sequences from the 5' and 3' ends. Both of these steps require the concordant action of endo- and exonucleases.

### 1.2.1 Ribosomal RNA maturation

In prokaryotes, the 70S ribosome is composed of a 50S and a 30S subunit. The smaller 30S subunit contains a 16S rRNA molecule complexed with 21 ribosomal proteins, while the larger 50S subunit is composed of a 23S rRNA and 5S rRNA complexed with 33 proteins. Studies of the complex process, which requires the correct ordering and assembly or these various molecules, have been reviewed (Williamson, 2003, Britton, 2009). Before the assembly of the ribosomal proteins, the precursor RNAs must undergo nucleolytic processing to generate the mature rRNAs.

As shown in Figure 1.3A, the three rRNAs are transcribed as one strand, probably to ensure stoichiometric levels are maintained within the cell. Due to the presence of complementary sequences in the rRNA, the precursors form double-stranded regions as the RNA is transcribed. These regions contain sites that can be cleaved by RNase III, separating the three precursors (Young and Steitz, 1978). The 16S rRNA precursor, which is known as 17S RNA, is cleaved by RNase E at a position 66 nt upstream of the start of the functional unit, as shown in Figure 1.3B (left) (Li et al., 1999c, Wachi et al., 1999). This cleavage exposes a 33 nucleotide fragment at the 3' end of the functional unit, which is removed by the combined action of the endonuclease YbeY and several exonucleases (Davies et al., 2010, Sulthana and Deutscher, 2013). The final 66 nt at the 5' end of the resulting precursor, known as the 16.3S RNA, is removed by RNase G, producing the final mature 16S rRNA (Li et al., 1999c, Wachi et al., 1999).

The 23S rRNA precursor, also known as p23 RNA, is cleaved by RNase III again within a double-stranded region that sequesters the 5' and 3' end of the RNA, as shown in Figure 1.3B (middle) (Bram et al., 1980). The resulting cleavage produces a 23S rRNA precursor with only a 3 nt region present at the 5' end of the functional unit, which is removed via an unknown ribonuclease. Maturation at the 5' end releases the 7 nt region downstream of the 3' end of the functional 23S rRNA unit, which is degraded by the exonuclease RNase T. However, RNase T is more active on the

23S rRNA precursor when it is associated with the ribosome, meaning that the maturation of the 3' end of 23S rRNA does not occur until during ribosome assembly (Li et al., 1999b).

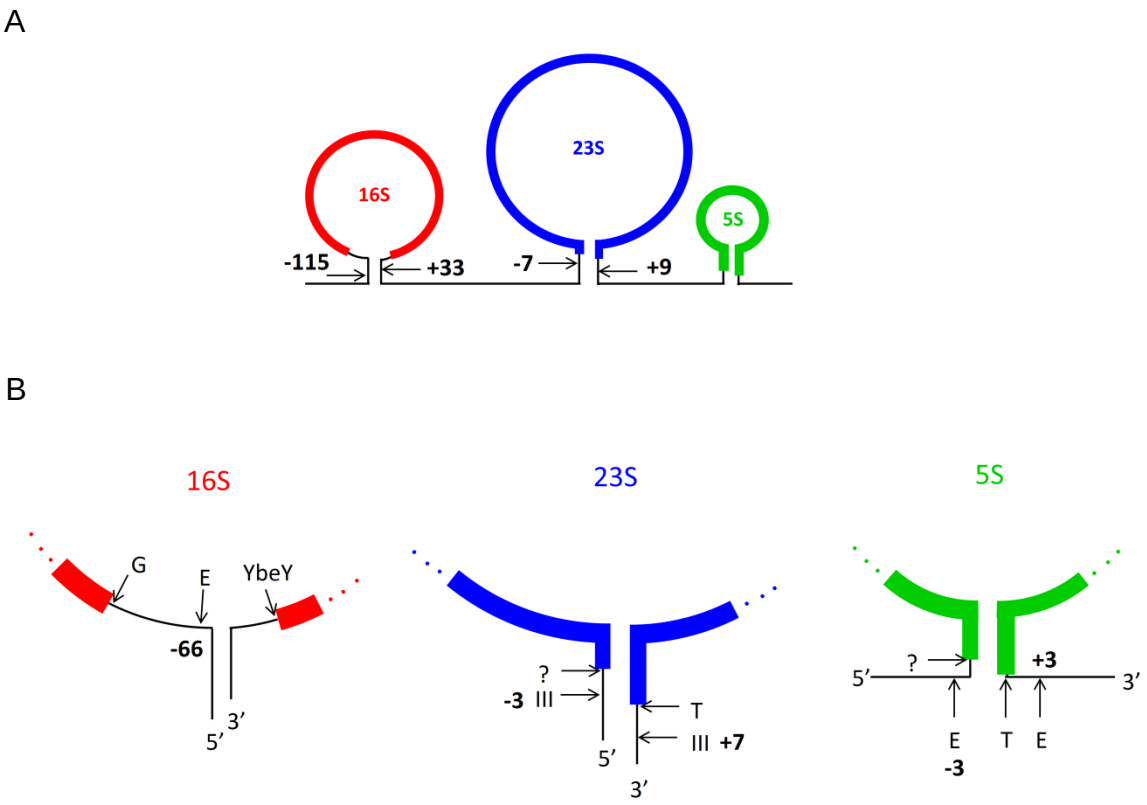


**Figure 1.3. A schematic highlighting the processing sites during rRNA maturation.** Panel A shows the general layout of the 16S-23S-5S precursor, which is transcribed from a single operon. Separation of the three precursors is performed by initial RNase III cleavages, which are highlighted as arrows. Numbers are the nt positions where RNase III cleavage occurs with respect to the nearest end of the functional rRNA unit, which is highlighted as a coloured bar. Panel B shows the individual 16S, 23S and 5S precursors on the left, middle and right, respectively. Cleavage sites by various enzymes are highlighted with an arrow. In bold are numbers that correspond to the nt positions of the cleavage sites with respect to the nearest end of the functional rRNA unit. Figures are adapted from a previous review (Deutscher, 2009).

The 5S precursor, known as 9S RNA, is cleaved by RNase E at positions 3 nt upstream and downstream of the 5' end and 3' end of the functional unit, respectively, as shown in Figure 1.3B (right) (Ghora and Apirion, 1978, Misra and Apirion, 1979). Removal of the last 3 nt at the 3' end of the functional 5S rRNA unit is performed by RNase T (Li and Deutscher, 1995). The final maturation at the 5' end of 5S rRNA is performed by an unknown enzyme.

### 1.2.2 Transfer RNA maturation

In prokaryotes, many tRNAs are transcribed together as a single polycistronic precursor connected by regions known as flanking sequences. In order for mature transfer RNAs to function correctly, all potentially interfering nucleotides that are not part of the functional unit must be removed. In *E. coli*, endonucleolytic cleavages are performed by RNase E within the 3'-trailer sequences of the tRNA precursors to separate the immature tRNAs for further processing (Ow and Kushner, 2002, Li and Deutscher, 2002, Soderbom et al., 2005, Perwez et al., 2008). Truncation of the 3' trailer by RNase E allows generates a preferable substrate for RNase P, which then cleaves the phosphodiester bond between the last nucleotide of the 5' leader and the first nucleotide of the tRNA unit, generating a mature 5' end (Shiraishi and Shimura, 1995, Li and Deutscher, 2002).

Due to the fact that all tRNA units in *E. coli* have an encoded CCA motif (Marck and Grosjean, 2002) following the discriminator nucleotide, *i.e.* the first nucleotide at the 3' end of the tRNA precursor that remains unpaired, 3' end maturation usually occurs by the "exonucleolytic" pathway, as shown in Figure 1.4A (Redko et al., 2007).

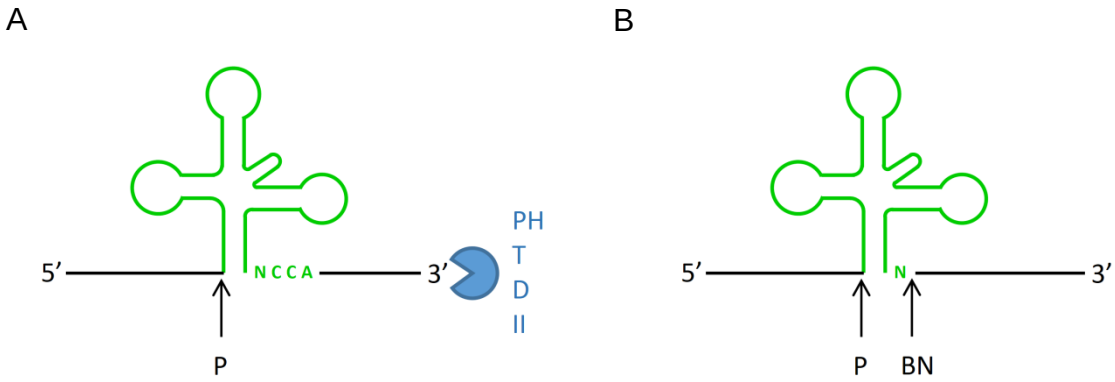


**Figure 1.4 The pathway for maturation of transfer RNAs in prokaryotes.** Panel A shows a schematic with the "exonucleolytic" pathway of 3' maturation. An endonucleolytic cleavage by RNase E exposes 3' ends for various 3' exonucleases (blue). Exonucleases degrade the 3'-trailer sequence until they reach the CCA motif at which point they dissociate from the substrate. Panel B shows a schematic with the "endonucleolytic" pathway of 3' maturation. In the absence of the CCA motif, the endonuclease RNase BN cleaves the 3'-trailer sequence after the discriminator nucleotide (N) and further CCA addition occurs to generate mature tRNA. In both panels, the site of RNase P cleavage to remove the 5'-leader sequence is highlighted. The tRNA unit is shown in green. Image adapted from a previous review (Redko et al., 2007).

Much of the initial processing of the 3' trailer is performed by RNase PH, a member of the PDX family related to PNPase. However, as RNase PH approaches the double-stranded region of the tRNA unit, it dissociates leaving a short stretch of nucleotides at the 3' end (Li and Deutscher, 1996). Final

maturation of the 3' end of the tRNA unit is performed by the single strand-specific exonuclease RNase T (Deutscher et al., 1984, Li et al., 1998a), which can cut close to the secondary structure of the precursor without unwinding the RNA duplex (Li et al., 1998a, Zuo et al., 2007). RNase T is released when it comes into contact with the cytosine residues on the CCA motif (Zuo and Deutscher, 2002a, Zuo and Deutscher, 2002b). Preservation of the CCA sequence at the 3' end of the tRNA is important as this is the site at which aminoacylation will occur (Sprinzl and Cramer, 1979).

The 3' end of tRNAs can also be processed by the "endonucleolytic" pathway, as shown in Figure 1.4B. This pathway involves recognition of the 3' trailer by an endonuclease called RNase BN, also known as RNase Z in other bacteria (Ezraty et al., 2005). However, RNase BN is sterically hindered by the amino group present on cytosine residues of the CCA motif; this prevents the removal of CCA from mature tRNAs or tRNA precursors that encode this sequence (Pellegrini et al., 2003, de la Sierra-Gallay et al., 2005). Because all *E. coli* tRNAs contain a CCA motif at the 3' end (Marck and Grosjean, 2002), the importance of RNase BN in tRNA maturation is uncertain. However, in organisms that encode tRNAs with and without CCA motifs, such as *Bacillus* subtilis, RNase Z is an important enzyme for tRNA maturation. Cleavage by RNase Z occurs on the phosphodiester bond between the discriminator nucleotide and the first nucleotide in the 3' trailer region, as shown in Figure 1.3B (Castano et al., 1985, Frendewey et al., 1985). The discriminator nucleotide is then exposed to tRNA nucleotidyltransferase, which catalyses addition of the CCA motif onto the 3' end (Schmidt, 1975, Xiong and Steitz, 2004).

RNase BN is essential in *E. coli* strains that have mutations in the enzymes involved in the "exonucleolytic" pathway of tRNA maturation (Kelly and Deutscher, 1992, Kelly et al., 1992, Dutta and Deutscher, 2010). Further analyses have found that RNase BN does not perform an endonucleolytic cleavage following the discriminator nucleotide, and in fact can adopt a 3'-exonucleolytic activity to allow it to remove the 3' trailer (Dutta and Deutscher, 2009, Dutta and Deutscher, 2010, Dutta et al., 2012). The conserved endonucleolytic activity of RNase BN could allow it to recognise and remove mutated CCA motifs in defective tRNAs, which could then be restored by the action of tRNA nucleotidlytransferase (Deutscher et al., 1977, Zhu and Deutscher, 1987).

## 1.3 Components of RNA decay machinery in *E. coli*

Around 18 ribonucleases are known to be involved in RNA degradation and processing in *E. coli*. Most of these nucleases require a divalent metal ion, such as magnesium, to help coordinate the attack of the sugar-phosphate backbone. The divalent cation assists in the formation of a nucleophilic species, which can then attack the scissile phosphodiester bond on the sugar-phosphate

backbone of the RNA, resulting in cleavage. Phosphodiesterases, which use water to generate hydroxyl ions as the nucleophile, produce downstream products with a 5'-monophosphate group. Phosphotransferases, which use ATP to generate orthophosphate as the nucleophile, produce downstream products with a 5'-biphosphorylated end. Both mechanisms generate upstream products with a 3'-hydroxyl group (Deutscher and Reuven, 1991).

### 1.3.1 Exonucleases

Exonucleases perform the bulk of mRNA degradation; by cleaving off the terminal nucleotides from mRNA sequentially, they replenish the nucleotide pool for further transcription. Exonucleases can be either: processive, whereby the enzyme remains bound to the substrate throughout the reaction and removes the terminal nucleotides repeatedly; or distributive, whereby the enzyme releases the substrate after cleaving one nucleotide from the end and has to re-associate with the substrate (Carpousis et al., 2009). The only exonucleases found in *E. coli* are all 3' to 5' in directionality (Deana and Belasco, 2005, de la Sierra-Gallay et al., 2008, Andrade et al., 2009b, Deutscher, 2006).

#### 1.3.1.1 PNPase

Polynucleotide phosphorylase (PNPase) is a 3' to 5' exonuclease with phosphotransferase activity (Zuo and Deutscher, 2001). The monomer of PNPase is structurally related to the tRNA processing enzyme RNase PH (Symmons et al., 2000), and self-associates into a trimer with structural similarity to the exosome, which is found in other bacteria and higher organisms (Symmons et al., 2002). PNPase is less sensitive to RNA secondary structure than the exoribonuclease RNase II, allowing it to cleave double-stranded RNA, albeit at a reduced rate than single-stranded RNA (Guarneros and Portier, 1991, McLaren et al., 1991). However, PNPase does require a 3' overhang of 10 unpaired nucleotides to associate with its substrate (Coburn and Mackie, 1996a).

Unlike other exonucleases, the processing of RNA by PNPase results in the accumulation of nucleotide diphosphates (NDPs) instead of nucleotide monophosphates (NMPs). Because NDPs contain two phosphates, under conditions of low orthophosphate concentration, PNPase can catalyse the reverse reaction, causing oligomerisation of NDPs on to the 3' end of the RNA (Ost and Deutscher, 1990). The addition of small single-stranded tails onto the 3' end of highly-structured RNAs may provide a binding site for other ribonucleases, such as RNase II, that require overhangs to associate with the RNA, but do not require orthophosphate for activity (Mohanty and Kushner, 2000). In this way, mRNA decay levels could be maintained under low-energy conditions. However, it should be noted that NDPs, produced by PNPase activity, only require one high-energy phosphate donor to be recycled to nucleotide triphosphates (NTPs) for further rounds of transcriptions,

whereas NMPs, produced by RNase II activity, require two high-energy phosphate donors. Therefore the interplay between hydrolytic and phosphoryltic activity may be much more tightly regulated based on the interplay between transcription and central metabolism.

The complementation of phosphorlytic and hydrolytic exonucleases is reflected in the fact that mutation in either *pnp*, the gene that encodes PNPase, or *rnb*, the gene that encodes RNase II, only slows growth, but mutation in both genes is lethal (Donovan and Kushner, 1986, Zilhao et al., 1996);. In addition, mutation in *rnb* results in over production of PNPase and mutation in *pnp* results in overproduction of RNase II (Zilhao et al., 1996).

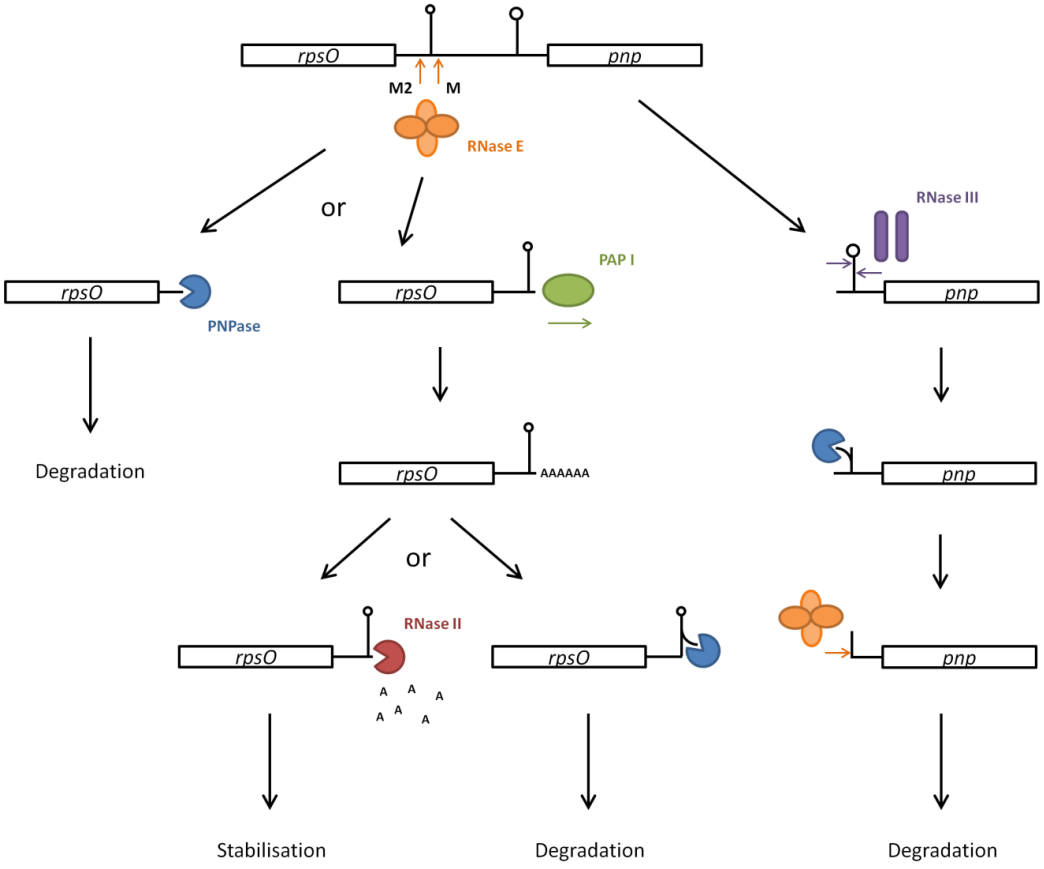


**Figure 1.5 Concordant action of endo- and exonucleases in the degradation of the *rpsO-pnp* mRNA.** The *rpsO* and *pnp* RNA units are transcribed as one mRNA. The separation of the two units occurs due to an initial cleavage by RNase E (orange) at site M2 or M. Cleavage at site M2 also removes a hairpin 3' to *rpsO*, allowing access for PNPase (blue). Cleavage at site M retains the hairpin at the 3' end of *rpsO* mRNA. PAP I (green) extends a 5 nt unpaired region at the 3' end of *rpsO* producing an oligo(A) tail. This tail provides access for PNPase, which can then slowly degrade the hairpin and then subsequently the rest of *rpsO*. The tail also provides access for RNase II (red), which degrades the 3' end up until the 3' hairpin, therefore stabilising *rpsO*. The *pnp* transcript is cleaved by RNase III (purple) within a hairpin at the 5' end. This produces a 37 nt fragment, with a 10 nt unpaired region at the 3' end, hybridised to the 5' UTR of *pnp*. PNPase binds to this overhang and slowly degrades the 37 nt fragment, releasing the 5' UTR of *pnp*. RNase E can then make subsequent cleavages within *pnp,* therefore initiating its degradation.

The homotrimeric ring structure of PNPase forms a central pore into which the 3' end of single-stranded RNA can thread through and contact one of the three hidden active sites (Shi et al., 2008, Nurmohamed et al., 2009). More recent studies have shown that metal-chelated citrate can also accommodate the active site, blocking mRNA access and therefore inhibiting PNPase. Conversely, metal-free citrate can bind to a vestigial site on PNPase and cause allosteric activation of the enzyme. The involvement of citrate, a metabolite of the Krebs cycle, in both PNPase activation and inhibition suggests that cellular metabolism and RNA degradation may be interlinked via a feedback network (Nurmohamed et al., 2011).

The *rpsO-pnp* mRNA, which encodes the ribosomal protein S10 and PNPase protein respectively, is one of the most well studied PNPase targets (Robert-Le meur and Portier, 1994). The *pnp* transcript contains a stem loop in the 5' UTR, which is cleaved by RNase III, producing a RNA37-*pnp* duplex with a 3' overhang, as shown in Figure 1.5. PNPase binds to this 3' overhang and slowly degrades RNA37, allowing RNase E to interact with the 5' monophosphate of the *pnp* transcript and initiateits degradation (Jarrige et al., 2001, Carzaniga et al., 2009). Mutations that inactivate PNPase result in stabilisation of the *pnp* mRNA (Robert-Le meur and Portier, 1994). Further mutations that result in removal of the *rpsO* and RNA37 regions of the transcript restore the lability of *pnp*, confirming that PNPase activity is only required to remove the stabilising RNA37 fragment and expose *pnp* to further degradation (Jarrige et al., 2001). Interestingly, the mechanism of *pnp* degradation suggests a role reversal in the general model of mRNA decay; an exonuclease initiates degradation by removing a stabilising feature on the transcript, allowing access for an endonuclease.

PNPase is also involved in regulating the expression of the upstream *rpsO*, as shown in Figure 1.5. An initial cleavage by RNase E is performed on the 3' UTR, either at site M or M2. Cleavage at site M2 occurs before a stem-loop structure, removing this stabilising feature and allowing access for PNPase (Regnier and Hajnsdorf, 1991, Braun et al., 1996). Cleavage at M2 provides a good example of the standard model of RNase E-mediated mRNA degradation. Cleavage at site M occurs after the stem-loop structure, producing a more stable *rpsO* with a 3'-end tail of only 5 nt (Braun et al., 1996). However, poly(A) polymerase I (PAP I) catalyses the addition of oligo-adenosine monophosphate extensions to this 3' tail, providing a foothold for PNPase and hence enhancing the degradation of stable *rpsO* (Hajnsdorf et al., 1995).

#### 1.3.1.2 RNase II

RNase II is a single-strand specific 3' exonuclease that displays phosphodiesterase activity. RNase II contains a single-stranded RNA binding channel that can accommodate 10 nucleotides, similar to

PNPase. Occupancy into the channel favours processive degradation (Frazao et al., 2006). However, unlike PNPase, RNA fragments below 10 nucleotides can still be cleaved, albeit in a distributive manner until 4 nucleotides remain, at which point cleavage by RNase II ceases (Frazao et al., 2006, Zuo et al., 2006, Barbas et al., 2008).

Along with PNPase, RNase II also plays a role in the regulation of *rpsO* mRNA stability, as shown in Figure 1.5. However, unlike with PNPase, studies have shown that mutations in *rnb* actually result in destabilisation of *rpsO*. As described above, RNase E cleavage at site M produces a stable 3' end consisting of a hairpin followed by 5 unpaired nucleotides. PAP I increases the length of this 3' end by sequential addition of adenosine monophosphates, providing a foothold for PNPase that can then slowly degrade the 3' hairpin. The oligo(A) tail produced by PAP I is also bound by RNase II. RNase II degrades the oligo(A) tail in a distributive manner until it reaches the 3' hairpin, which causes RNase II to dissociate. This produces an even shorter unpaired strand of nucleotides, causing stabilisation of the 3' end of *rpsO* by impairing the access of PNPase (Hajnsdorf et al., 1994b, Marujo et al., 2000). In addition, RNase II also renders the stabilisation of *rpsO* as irreversible, by shortening the initial 3' end and therefore preventing PAP I from re-binding and re-extending the 3' tail (Yehudai-Resheff and Schuster, 2000). Further studies have found that RNase II-mediated stabilisation of mRNA is not limited to the *rpsO* transcript (Coburn and Mackie, 1996b, Mohanty and Kushner, 2003). Around 31% of transcripts were actually destabilised when RNase II was inactivated *in vivo*, whereas only 7.3% of transcripts were stabilised in the same mutant (Mohanty and Kushner, 2003).

Alterations of the structure of RNase II have also shed new insights into RNase II specificity. One study has shown that mutation of a glutamate residue at position 542, which was originally believed to assist in release of the "leaving" nucleotide at the 3' end of RNA following cleavage, to an alanine actually resulted in RNase II gaining "super" activity. The E542A mutant showed over 110-fold increase in cleavage rate and a 10 to 20-fold increase in affinity for RNA, caused by subtle conformational changes that allowed increased stacking of the RNA into the RNA-binding channel (Barbas et al., 2008). Another study has shown that by swapping the S1 domain of RNase II with the S1 domain of RNase R, a structural analogue of RNase II that can degrade double-stranded RNA, RNase II can bypass its sensitivity to double-stranded structures by unwinding the RNA before it enters the RNA-binding channel (Matos et al., 2011).

#### 1.3.1.3 RNase R

RNase R was originally discovered as a residual exonuclease activity present in strains lacking RNase II (Gupta et al., 1977). More recently, RNase R has been shown to be a structural analogue of RNase

II (Zuo and Deutscher, 2001), with additional basic motifs present near the entrance of the RNA-binding channel (Matos et al., 2009). The positive residues on these motifs form electrostatic interactions with the negative phosphate groups on both strands of a RNA duplex. These interactions force the secondary structure of the RNA to unwind as the RNase R catalytic site approaches, feeding the 3' end into the RNA-binding channel (Awano et al., 2010). However, in order for RNase R to make an initial interaction with RNA, there must be a single-stranded region of at least 7 nt at the 3' end (Vincent and Deutscher, 2006). The ability of RNase R to process double-stranded structures is utilised in the degradation of defective tRNA (Li et al., 2002) and rRNA (Cheng and Deutscher, 2003).

RNase R is another enzyme involved in the regulation of *rpsO* mRNA stability, particularly following RNase E cleavage at site M (Andrade et al., 2009a). Like PNPase, RNase R would require a 3' overhang of around 10 nt for tight binding to *rpsO* (Vincent and Deutscher, 2006) (Vincent and Deutscher, 2006), which could be provided by the activity of PAP I. However, unlike PNPase, RNase R cleavage rate is unaffected by the secondary structure once it is bound (Cheng and Deutscher, 2002) (Cheng and Deutscher, 2002), and therefore RNase R can degrade the *rpsO* 3' hairpin rapidly. Given that RNase R still requires a foothold, RNase II activity would still stabilise the *rpsO* transcript (Andrade et al., 2009a).

More recently it has been shown that RNase R may provide some of the hydrolytic activity believed to be caused by RNase II alone. Strains with a disruption in both *rnb* and the gene encoding RNase R (*rnr*) are still viable, showing no major functional overlap between RNase II and RNase R enzymes, despite their similarities in structure (Cheng and Deutscher, 2002). However, disruption in both the *pnp* and *rnr* genes was found to cause inviability, suggesting PNPase and RNase R may overlap (Cheng et al., 1998). Further studies have suggested that PNPase and RNase R may be able to substitute for one another during defective rRNA degradation (Cheng and Deutscher, 2003). In addition, given that only 7.3% of transcripts appear to be degraded by RNase II (Mohanty and Kushner, 2003), perhaps RNase R plays more of the role in hydrolytic degradation. This would explain why RNase II is one of the few RNases not associated with the degradosome, as its function in the cell may be to stabilise transcripts (see Section 1.1.4).

#### 1.3.1.4 Orn

The remaining 4 nt fragments produced from exonucleolytic activity are degraded by oligoribonuclease (Orn) (Ghosh and Deutscher, 1999). The activity of Orn is important in replenishing

the mononucleotide pool. This is confirmed as it is the only exoribonuclease whose deletion results in a lethal phenotype in *E. coli* (Zhang et al., 1998, Ghosh and Deutscher, 1999).

### 1.3.2 Endonucleases

Theoretically, mRNA could be degraded exclusively by exonucleases. However in reality, most exonucleases are hindered by stabilising features within the nascent transcripts (Chen et al., 1988, Mott et al., 1985, Newbury et al., 1987) *e.g.* stem loops present at the 3' end as a by-product of Rho-independent transcriptional termination (Farnham and Platt, 1981). Endonucleases accelerate the turnover of mRNA by removing these features within the transcript, presenting a more accessible 3' end to the 3'-5' exonucleases. Cleavage by endonucleases also produces shorter RNA species, which can be degraded by exonucleases more rapidly. Endonucleolytic cleavage at the 5' end of a transcript can also inactivate translation of the mRNA, removing ribosomes that could potentially clash with exonucleases working in the opposite direction as well as committing the mRNA to degradation. Due to the initiating role endonucleases play in RNA degradation and processing, these enzymes present an important target for studying gene regulation in prokaryotes (Carpousis et al., 2009).

#### 1.3.2.1 RNase III

One of the first major endonucleases discovered in *E. coli* was RNase III, an enzyme that cleaves double-stranded RNA (Robertson et al., 1967, Robertson et al., 1968). RNase III is important in the processing of stable RNAs such as the ribosomal RNA precursors, cutting within stem-loop structures (Dunn and Studier, 1973). Disruption of the corresponding gene for RNase III (*rnc*), while affecting the path of rRNA processing, only slows the degradation of a few mRNAs (Apirion et al., 1976a, Babitzke et al., 1993, Gegenheimer et al., 1977) and does not show a lethal phenotype (Apirion et al., 1976a, Apirion et al., 1976b). Nevertheless, mutations in *rnc* result in a reduced growth rate, possibly due to decreased protein synthesis (Apirion et al., 1976a, Talkad et al., 1978) as a result of incomplete 23S rRNA maturation and hence defective 50S subunits (King et al., 1984).

One of the mRNA targets for RNase III is the *rpsO-pnp* operon, as shown in Figure 1.5. The *pnp* transcript is stabilised *in vivo* by the disruption of the *rnc* gene (Takata et al., 1987). RNase III cleaves towards the top of a stem loop on the 5' UTR of *pnp* (Portier et al., 1987, Regnier and Portier, 1986), producing an RNA37 fragment, with a 3' overhang, base paired to the remaining 5' UTR. PNPase is able to access this 3' overhang and degrade the RNA37 fragment (Jarrige et al., 2001), exposing a single-stranded 5'-monophosphorylated end on the *pnp* transcript which can then be accessed by RNase E (Hajnsdorf et al., 1994a, Carzaniga et al., 2009). Destabilising cleavages by RNase III are

found in stem-loop structures within the *rnc-era-recO* and *metY-nusA-infB* operons, suggesting that the concordant action of RNase III and other ribonucleases, such as PNPase and RNase E, is not limited to *rpsO-pnp* (Regnier and Grunberg-Manago, 1990).

The *adhE* transcript, which encodes alcohol dehydrogenase, is another target of RNase III cleavage. However, cells lacking functional RNase III have a significantly decreased population of alcohol dehydrogenase. The ribosome binding site (RBS) of *adhE* is occluded within a double-stranded region of the 5' UTR. RNase III cleavage within this stem-loop structure exposes the RBS of *adhE*, allowing access for the 30S ribosomal subunit and hence promoting translation (Aristarkhov et al., 1996). The resulting 5' end folds into a small stem loop structure, occluding the 5' monophosphate from interacting with endonucleases that have 5' monophosphate-dependent activity, such as RNase E (Ito et al., 2013). It is interesting to note that the *adhE* transcript also serves as a substrate for RNase G, whose activity destabilises the transcript (Umitsuki et al., 2001, Wachi et al., 2001). RNase G cleavage occurs further downstream than the RNase III cleavage, and occurs independently of RNase III activity. The resulting 5' end caused by RNase G cleavage does not contain the small stem loop found after RNase III cleavage and is therefore exposed to further attack (Ito et al., 2013). Therefore it seems that there is competition between RNase III and RNase G to promote translation and degradation of *adhE*, respectively.

The *adhE* mRNA is by no means the only example of a substrate whereby RNase III cleavage can promote translation. The *rpoS* mRNA, which encodes the stationary-phase sigma factor ($\sigma^S$), contains a stem loop structure within the 5' UTR that occludes the RBS and prevents translation (Hengge-Aronis, 2002). This stem loop is cleaved 3 nt upstream of the start of the RBS by RNase III. However, evidence shows that this cleavage does not release the RBS and that *in vivo* this cleavage also results in destabilisation of *rpoS* (Resch et al., 2008). However, DsrA, a small RNA that hybridises to a complementary region in the 5' UTR of *rpoS*, disrupts the inhibitory stem-loop structure (Lease and Woodson, 2004). Not only is the RBS freed from the stem loop, hence permitting ribosomal loading (Lease and Belfort, 2000), but also the RNase III cleavage is redirected to the DsrA-*rpoS* hybrid, removing the upstream region of the *rpoS* 5' UTR and so preventing it from reannealing to the downstream region where the RBS is located (Resch et al., 2008).

Recent microarray based studies have shown that only 12% of transcripts are stabilised in the absence of RNase III in *E. coli*, highlighting a significant, albeit not essential, role for RNase III in mRNA decay. For example, the stability of transcripts involved in cysteine metabolism was decreased in the absence of RNase III *e.g. cysP* involved in sulphate uptake and *cysD* involved in cysteine biosynthesis (Stead et al., 2011). In addition, a population of mRNAs were identified that

were actually destabilised in the absence of RNase III, which could be due to reduced translation as a consequence of defective ribosomes (Talkad et al., 1978); RNase III having a major role in destabilising regulatory sRNAs (Stead et al., 2011, Viegas and Arraiano, 2008); and RNase III cleavages in some mRNAs that result in increased translation and stability (Aristarkhov et al., 1996).

#### 1.3.2.2 RNase E

Ribonuclease E was originally identified as an endonuclease that is involved in processing of the 9S rRNA precursor (Ghora and Apirion, 1978, Misra and Apirion, 1979) and loss of this activity was believed to cause the lethal phenotype in *rne* mutants of *E. coli* (Apirion and Lassar, 1978). However, genetic mapping of one of the temperature-sensitive mutations (*rne*-3071) found that the mutation was located on the same protein-coding gene as a mutation that was previously found to affect bulk mRNA stability (Mudd et al., 1990, Melefors and von Gabain, 1991, Babitzke and Kushner, 1991, Taraseviciene et al., 1991). This mutation, termed altered mRNA stability (*ams*-1), was originally found to increase the stability of the majority of transcripts in *E. coli* at a non-permissive temperature (Kuwano et al., 1977, Ono and Kuwano, 1979). The role of RNase E in the degradation of most transcripts has been confirmed using microarrays (Lee et al., 2002, Stead et al., 2011). Therefore, not only does the function of RNase E extend far beyond the processing of ribosomal RNA, but also its role in initiating mRNA decay may be source of its essentiality in *E. coli*.

One of the most well studied substrates of RNase E cleavage is the *rpsO-pnp* transcript, whereby multiple cleavages performed by RNase E initiates the decay of both mRNAs, as shown in Figure 1.5 (Braun et al., 1996, Braun et al., 1998, Hajnsdorf et al., 1994a, Hajnsdorf et al., 1994b). RNase E has also been shown to be important in the decay of many other transcripts including *rpsT*, which encodes ribosomal protein S20 (Mackie, 1991); *dnaG*, which encodes a DNA primase (Yajnik and Godson, 1993); the *unc* operon, which encodes components of the bacterial ATPase (Patel and Dunn, 1992, Patel and Dunn, 1995); and the *epd-pgk* operon, which encodes proteins involved in metabolic pathways (Bardey et al., 2005). RNase E has also been shown to be important in the processing of several stable RNAs in addition to rRNAs and tRNAs (see Sections 1.2.1 and 1.2.2, respectively), such as tmRNA (Lin-Chao et al., 1999), 6S RNA (Kim and Lee, 2004), and M1 RNA (Gurevitz et al., 1983, Kim et al., 1999). Finally, RNase E activity has been implicated in numerous cellular pathways including stress response (Manasherob et al., 2012), regulation of mobile genetic elements (Lin-Chao and Cohen, 1991, Jerome et al., 1999), and virulence (Yang et al., 2008, Pichon et al., 2013, Viegas et al., 2013).

The smallest detectable upstream and downstream products obtained from RNase E cleavage are 8 and 3 nt, respectively. This suggests RNase E cleaves at least 8 nt from the 5' end or 3 nt from the 3' end (Walsh et al., 2001). RNase E has strong preference for single-stranded regions (Cormack and Mackie, 1992, Mackie, 1992, Mackie et al., 1997), which reflects its low sequence specificity for regions rich in A and U nucleotides (McDowall et al., 1994, Kaberdin, 2003), sequences also associated with low secondary structure. Further studies of oligonucleotide substrates has revealed some specific sequence bias; in particular, the presence of a guanine nucleotide has been shown to stimulate cleavage two nt downstream (Kaberdin, 2003, Redko et al., 2003).

RNase E auto-regulates its own synthesis by binding to and initiating degradation of the *rne* transcript (Jain and Belasco, 1995). Removal of 2 hairpins in the 5' UTR results in stabilisation and increased expression of *rne in vivo* (Diwa et al., 2000). Because RNase E recognises single-stranded regions, it is believed to bind to unpaired "bulge" regions within these hair pins (Diwa and Belasco, 2002, Schuck et al., 2009), providing evidence that RNase E possesses flexibility with regard to the spatial organisation of the single-stranded regions it can interact with. Furthermore, one of these bulge regions interacts with a residue situated away from the RNA-binding channel of RNase E (Schuck et al., 2009), suggesting that additional residues besides those associated with the active site can contribute to RNase E interactions. Further details on the structure and mechanism of cleavage by RNase E are discussed later on in this chapter.

#### 1.3.2.3 RNase G (CafA)

RNase G, originally known as CafA, was originally identified as a protein involved in the regulation of cell division and/or chromosome partitioning (Okada et al., 1994). However, subsequent studies discovered that RNase G displayed endonucleolytic activity involved in the processing of the 5' end of the 16S rRNA precursor (Wachi et al., 1999, Li et al., 1999a, Li et al., 1999c). Further characterisation *in vitro* confirmed that the primary function of RNase G is an endonuclease (Tock et al., 2000). Interestingly, RNase G and RNase E share a high sequence similarity (McDowall et al., 1993, Wachi et al., 1997), and disruption of the *rng* gene (gene encoding RNase G) enhanced the temperature sensitivity of the *ams*-1 mutant (Wachi et al., 1997), suggesting that there may be significant overlap between the functions of both enzymes. Furthermore, overexpression of RNase G reduced temperature sensitivity in *ams*-1 mutants and even cell lethality in *rne* disruption mutants (Wachi et al., 1997, Lee et al., 2002). However, RNase G cannot compensate for RNase E in the processing of stable RNAs such as 9S and the M1 precursor. Therefore it appears that RNase E processing of stable RNAs is dispensible for cell viability. In regards to mRNA decay, only 100 transcripts that were stabilised as a consequence of *rne* disruption displayed normal half-lives when

*rng* was over-expressed. Most of these transcripts were implicated in metabolic pathways (Lee et al., 2002). Therefore, these 100 mRNAs represent targets whose degradation is the basis for the essentiality of RNase E. Because over-expression of *rng* in an *rne* mutant can compensate for cleavage of this subset of mRNAs, while retaining the stabilisation of bulk mRNA, RNase G may be a potential target for improving *E. coli* expression systems.

Although RNase G is not required for cell viability (Wachi et al., 1999, Li et al., 1999c) and does not play a broad role in mRNA decay (Lee et al., 2002, Ow et al., 2003), it does initiate the degradation of several specific mRNA targets. One such example is *adhE*, which encodes an alcohol dehydrogenase involved in the anaerobic fermentation of glucose. Mutations in *rng* result in overproduction of the AdhE protein (Umitsuki et al., 2001, Wachi et al., 2001). Interestingly, RNase G cleaves within the 5' UTR of *adhE* at a position only 14 nt downstream from an RNase III cleavage site (Aristarkhov et al., 1996). It is believed that RNase G and RNase III compete for cleavage of the 5' UTR of *adhE*, whereby the fate of the mRNA is determined by whichever of these endonucleases makes the initial cleavage (Ito et al., 2013). In addition to alcohol dehydrogenase, another protein that has been shown to accumulate in the absence of RNase G is enolase, a major glycolytic enzyme in *E. coli*. The half-life of *eno* mRNA was subsequently shown to be 3-fold higher in an *rng* mutant compared to wild-type cells (Kaga et al., 2002). Mutations in *rng* result in the stabilisation of several mRNAs that encode proteins associated with central metabolism, including, in addition to the examples mentioned above, *pgi, glk, and tpiA* (Lee et al., 2002). These same mutations also result in increased cellular levels of pyruvic acid. Taken together, these findings suggest that RNase G has a major role in the regulation of central metabolism (Sakai et al., 2007).

1.3.2.4 Other endonucleases

The RNase H family are a set of endonucleases that can be found in nearly all organisms (Nicholson, 1999) and has the unique ability to only cleave RNA that is present in a DNA-RNA hybrid. RNase H is important during DNA replication, whereby it degrades the RNA primers after the newly synthesized DNA strand is formed and hence promotes completion of DNA synthesis (Champoux and Schultz, 2009). Given the specific requirements for RNase H cleavage, it has been assumed that RNase H does not play a major role in mRNA decay. However, more recently it has been shown that cells with lethal mutations in *rne* can remain viable when mutations were introduced in *rho*, the gene which encodes the transcriptional terminator Rho. Further analyses indicated that this restoration in viability was dependent on the activity of RNase H1. Theoretically, inactivation of Rho prevents the release of many of the mRNAs from the transcriptional complex after the DNA polymerase has stalled. The DNA-RNA hybrid between the DNA template and mRNA is therefore stabilised, and is

exposed to RNase H1. Cleavage by RNase H releases the mRNA and removes potential 3' stabilising elements, which promoting further degradation by 3' exonucleases (Anupama et al., 2011).

Other minor endonucleases in *E. coli* include RNase I, which was originally believed to be the major initiator of mRNA decay due to its broad substrate specificity (Spahr and Hollingworth, 1961). However, the majority of RNase I was located in the periplasm of *E. coli* (Neu and Heppel, 1964), and inactivation of the enzyme had little effect on mRNA stability *in vivo* (Kivity-Vogel and Elson, 1967). Another endonuclease with broad specificity, termed RNase M, was found in the cytoplasm of *E. coli* and was hypothesized as the major endonucleolytic activity in mRNA degradation (Cannistraro and Kennell, 1989). However, studies have shown that RNase M is actually just an altered form of RNase I, found in the *E. coli* strain MRE600 (Subbarayan and Deutscher, 2001).

### 1.3.3 Additional factors

Besides the large repertoire of ribonucleases, *E. coli* also contains several ancillary proteins that assist in RNA degradation.

#### 1.3.3.1 Poly(A) polymerase I

Poly(A) polymerase (PAP) is an enzyme that can be found in many organisms and catalyses the addition of adenosine monophosphates to the 3' end of transcripts (Hajnsdorf and Regnier, 2009). *E. coli* contains PAP I, which produces small oligoadenyl tails on the end of an RNA molecule that are usually around 7-10 nt long (Cao and Sarkar, 1992). These oligo(A) tails promote the degradation of many transcripts (Xu et al., 1993, O'Hara et al., 1995), in particular nascent transcripts and RNA decay intermediates whose 3' ends are confined to secondary structures (Blum et al., 1999), by providing a foothold for the 3' exonucleases RNase II, RNase R and PNPase (Mohanty and Kushner, 2002, Hajnsdorf et al., 1995, Coburn and Mackie, 1996a, Andrade et al., 2009a). In addition, oligo(A) tails have been shown to be cleaved by RNase E (Huang et al., 1998, Walsh et al., 2001). It has been estimated that over 90% of mRNAs are oligoadeylated at some point during their life cycle (Mohanty and Kushner, 2006). Oligadenylation at the 3' end is not restricted to mRNAs. Oligoadenylation occurs at the 3' end of stable RNA precursors to stimulate exonuclease-assisted maturation (Li et al., 1998b) and at the 3' end of defective tRNA and rRNAs to assist in their degradation (see Section 1.1.3).

#### 1.3.3.2 RNA helicase B

RNA helicase B (RhlB) is a member of the DEAD-box family of helicases, a group of ATP-dependent proteins responsible for unwinding RNA in a non-processive manner. Because of this distributive

activity, RhlB can only unwind short RNA duplexes that are no more than 2 helical turns, or 22 bp, in length (Cordin et al., 2006). The general structure of a DEAD box family member consists of two RecA-like domains that are connected by a flexible linker region (Caruthers and McKay, 2002). An interdomain groove is formed between the two RecA-like domains, whereby an ATP interacts with the conserved aspartate-glutamate-alanine-aspartate (D-E-A-D) residues (Cordin et al., 2006, Worrall et al., 2008). The negative charge of the phosphate backbone on the RNA strand interacts with a cationic exposed region present on both domains (Milner-White et al., 2010). The C-terminal RecA-like domain also contains a tail with additional cationic residues. These positively charged residues increase RNA affinity by making further contacts with the sugar-phosphate backbone of the substrate (Chandran et al., 2007, Worrall et al., 2008). Binding of ATP and RNA to RhlB has been shown to be highly cooperative. Upon binding of both substrates, ATP is hydrolysed, causing a conformational shift that separates the two RecA domains, unwinding the RNA strands (Polach and Uhlenbeck, 2002).

#### 1.3.3.3 RppH

RNA pyrophosphohydrolase (RppH) is a major decapping enzyme found in *E. coli* (Celesnik et al., 2007) and other bacteria (Richards et al., 2011), which removes a pyrophosphate from the 5'-triphosphate cap of nascent transcripts, producing a 5'-monophosphorylated end (Deana et al., 2008). These 5'-monophsophorylated substrates can then engage RNase E, which initiates their degradation (Mackie, 1998). In addition, the presence of a monophosphate at the 5' end has also been shown to enhance the activity of PAP I on some substrates (Feng and Cohen, 2000). The further importance of RppH in assisting RNase E-mediated degradation is discussed later on.

## 1.4 RNase E

In *E. coli,* RNase E is recognised as the major regulator of post-transcriptional gene expression. Therefore, understanding how RNase E can recognise and cleave substrates could lead to manipulation in overall gene expression. This could be particularly useful in improving *E. coli* protein expression systems by either introducing mutations in the *rne* gene (Lopez et al., 1999) or by production of decoy RNAs that could sequester RNase E activity (Makeyev et al., 2002, Marzi and Romby, 2012). This information could also have applications in synthetic biology, whereby the expression of multiple genes at coordinated levels could be finely tuned by modification of intergenic regions within polycistronic mRNA operons (Smolke and Keasling, 2002, Pfleger et al., 2006). RNase E also has huge potential as an antimicrobial target given that along with RNase P and Orn, RNase E is one of the few essential components of the RNA decay machinery in *E. coli* (Apirion

and Lassar, 1978, Ono and Kuwano, 1979, Li et al., 2003, Ghosh and Deutscher, 1999) and RNase E homologues are found widespread throughout the gram-negative bacteria. However, unlike RNase P and Orn, there are no known homologues of RNase E in humans (Condon and Putzer, 2002, Danchin, 2009). Recently, using a structure-based approach, several small molecules have been developed that appear to inhibit RNase E activity (Kime et al., 2015).

### 1.4.1 Structure

#### 1.4.1.1 N-terminal half

The RNase E protein is 118 kDa and composed of 1061 amino acids. The N-terminal half (NTH) consists of the first 529 amino acids of the RNase protomer. The NTH of RNase E contains the major endonucleolytic activity and is required for cell viability (McDowall and Cohen, 1996). The NTH of RNase E is also the site where the temperature sensitive mutations *ams*-1 and *rne*-131 are located (McDowall et al., 1993).

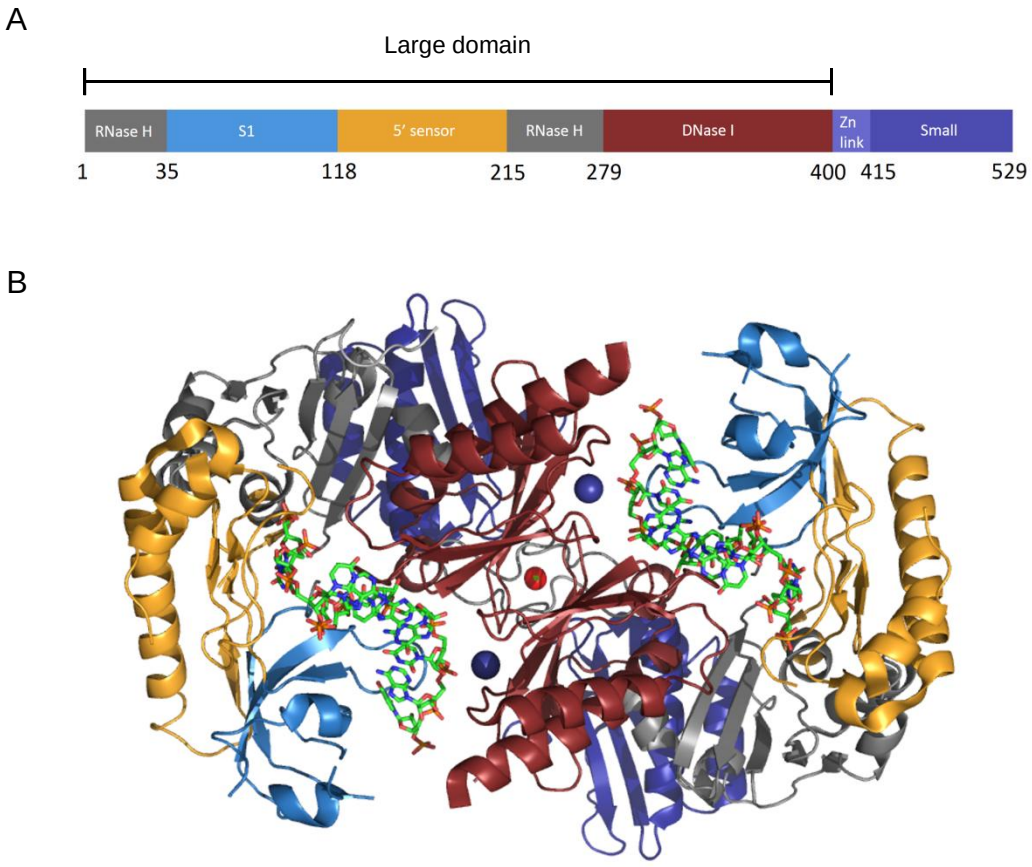


**Figure 1.6 Structure of the N-terminal half of RNase E.** Panel A shows a linear representation of the the first 529 amino acids of the RNase E protomer, whereby the domain boundaries are shown. Panel B shows the crystal structure of the NTH-RNase E principal dimer at 3.18 Å resolution (PMD ID: 2C0B) with the same colour coding as Panel A and the RNA shown in green (Callaghan et al., 2005a).

Each NTH is divided into 2 major domains, known as the large and small domains, connected by a link region. The large domain consists of the first 400 amino acids of the NTH of RNase E and is divided into 4 minor domains, each of which form independent structural motifs that are found to be conserved in several other proteins, as shown in Figure 1.6 (Schubert et al., 2004, Callaghan et al., 2005a). It is important to note that the RNase H-like domain is formed from two regions on the NTH.

#### 1.4.1.1.1 The S1-like domain

The S1-like domain is a highly conserved domain present in several RNA-binding proteins, including PNPase and RNase II (Bycroft et al., 1997). The S1-like domain of RNase E exists as an "arm" like structure that closes down onto the DNase I-like domain, producing an RNA-binding channel that can accommodate single-stranded RNA only (Callaghan et al., 2005a). However, due to the ability of the S1-like domain to swing out, it has been hypothesised that more structured RNA elements may be able to accommodate this region (Koslover et al., 2008).

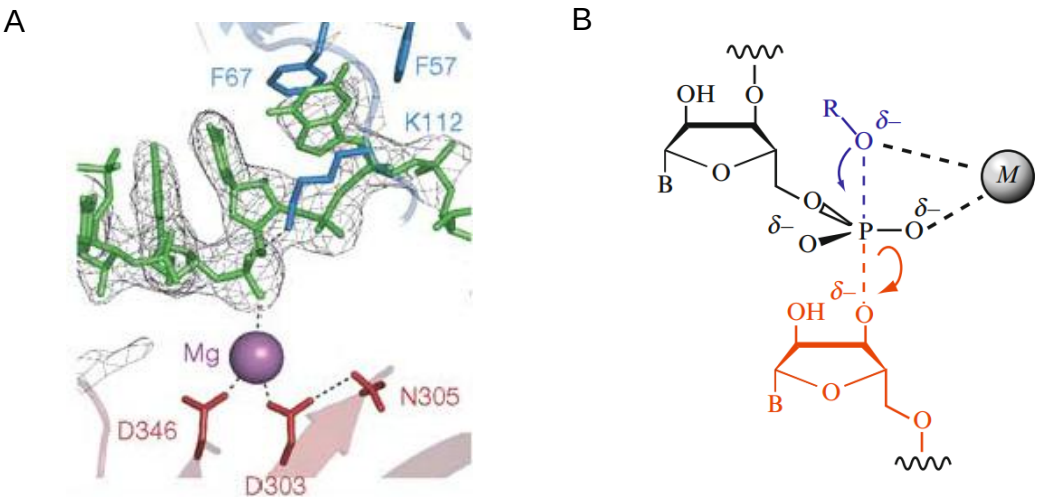


**Figure 1.7 Representation of the proposed catalytic site at the DNase I subdomain.** Panel A shows a three-dimensional model of the proposed catalytic site of RNase E. The residues Asp346 and Asp303 coordinate the divalent magnesium ion to the RNA backbone via their negative charge. The polar Asn305 residue supports the positioning of Asp303. The residues Phe67, Phe57 and the side chain of Lys112 form a hydrophobic pocket that can accommodate one of the RNA bases. The charged group at the end of the Lys112 residue promotes cleavage of the phosphodiester bond. Image taken from previous studies (Callaghan et al., 2005a). Panel B shows a schematic diagram that illustrates the basic divalent metal ion-dependent cleavage. The deprotonated nucleophile, in this case a hydroxyl ion, is coordinated by the divalent metal ion, in this case magnesium. The phosphorous atom undergoes an $S_N2$ reaction via attack from the nucleophile resulting in cleavage of the phosphodiester bond with the 3' oxygen. Image taken from a previous review (Forconi and Herschlag, 2009).

Two phenylalanine residues at positions 57 and 67 on the S1-like domain stack between the base two nt downstream of the site of cleavage within the RNA, as shown in Figure 1.7A. This hydrophobic "pocket" is supported by additional hydrophobic interactions contributed by the aliphatic side chain of the lysine residue at position 112 on the S1-like domain. Accommodation of the base into the hydrophobic "pocket" causes a distortion of the phosphodiester backbone that is in contact with the DNase I subdomain, possibly promoting cleavage (Diwa et al., 2002, Callaghan et al., 2005a). Substitution of one of these residues with alanine resulted in a 50-fold reduction in enzyme activity (Callaghan et al., 2005a). Even if double-stranded RNA could accommodate the RNA-binding channel, cleavage would be unlikely due to the fact that double-stranded RNA cannot present a base to the hydrophobic pocket.

The hydrophobic interaction between the aliphatic portion of the side chain of Lys112 and the RNA base re-orientates the positively-charged amino group at the end of the lysine residue to make contact with the scissile phosphate. This interaction is believed to support the charge of the phosphate bond built up during the transition state, reducing the energy barrier for product formation (Callaghan et al., 2005a).

Two temperature-sensitive mutations that have shown that RNase E is essential for cell viability and mRNA metabolism (Apirion and Lassar, 1978, Ono and Kuwano, 1979) have been located within the S1-like domain (Schubert et al., 2004). These mutations, which involve substitution of glycine and leucine to serine and phenylalanine at positions 66 and 68, respectively (McDowall et al., 1993), are buried deep within the S1-like domain directly beneath the hydrophobic "pocket" and may actually affect the stability of the region directly above (Diwa et al., 2002).

Another potential interaction of the S1-like domain with RNA is a hydrogen bond between the exocyclic oxygen on the base located 2 nt upstream from the scissile phosphate and the amino group of the lysine residue at position 106 (Callaghan et al., 2005a). This interaction explains the increased preference of RNase E for the presence of either a G or U residue at this position, which are the only bases that display an exocyclic oxygen (Kaberdin, 2003, Redko et al., 2003).

#### 1.4.1.1.2 The 5' monophosphate-sensing domain

Arguably the most distinguishing feature of RNase E and its family members is the 5'-monophosphate-sensing domain. The residues on several amino acids form a "horse shoe" of hydrogen bonds that can interact with a monophosphate at the 5' end of an RNA molecule, as shown in Figure 1.8A.

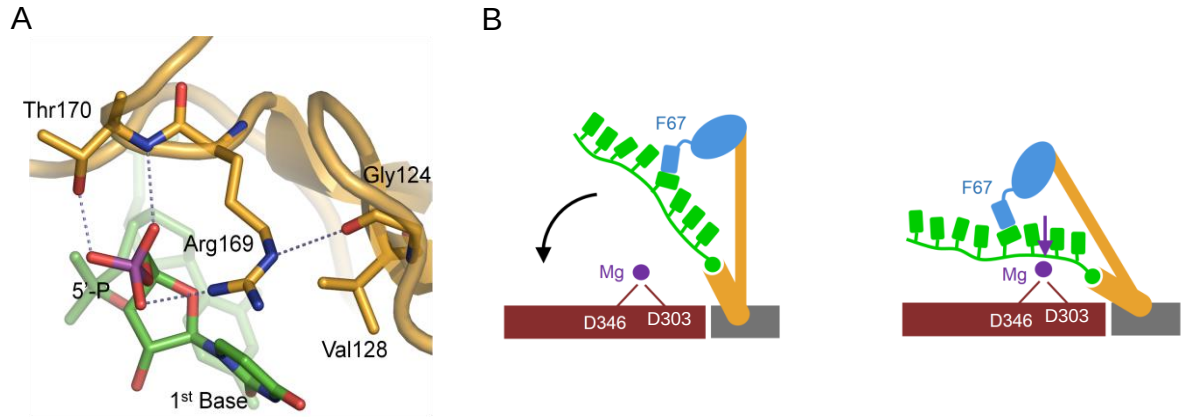


**Figure 1.8 The 5'-monophosphate sensor of RNase E.** Panel A shows a three-dimensional representation of the 5'-monophosphate-sensing pocket. The Thr170 and Arg169 residues make extensive hydrogen bonds with the three non-bridging oxygen atoms on the monophosphate (purple) present at the 5' end of the RNA (green). The large Arg169 residue is stabilised by hydrogen bonding with the Gly124 residue. Val128 provides a hydrophobic interaction with the base of the first nucleotide. Image taken from a previous study (Callaghan et al., 2005a). Panel B shows the proposed mechanism for the "mouse trap" model of RNase E activation. The RNA strand (green) approaches the enzyme and the monophosphate at the 5' end interacts with the 5'-monophosphate-sensing pocket (yellow). This causes the S1-like domain (blue) to clamp down onto the RNA, exposing it to the active site of the DNase I-like domain (red). Residues important for catalysis are highlighted. Image adapted from a previous study (Callaghan et al., 2005a).

The hydroxyl group of a threonine residue at position 170 provides a hydrogen bond to the double-bonded oxygen atom on the phosphate group. The positively-charged guanidinium group at the end of an arginine residue at position 169 provides another interaction with one of the single-bonded oxygen atoms. The final interaction is provided by the positively-charged amino portion of the peptide bond between the Arg169 and Thr170 residues. An interaction between the intra-chain amino group of Arg169 and the carbonyl portion of the peptide bond of glycine at position 124 supports the position of the long Arg169 residue. A valine residue at position 128 strengthens the binding of the 5' end by making a hydrophobic interaction with the base on the first nucleotide (Callaghan et al., 2005a).

The accommodation of the monophosphate into this 5'-sensing pocket explains why, in previous observations, 5'-triphosphorylated and -hydroxylated RNA strands are not cleaved as well (Mackie, 1998, Jiang and Belasco, 2004, Garrey et al., 2009, Kime et al., 2010). A triphosphate would be sterically unable to fit inside the pocket, due to the presence of the hydrophobic Val128 residue, whereas a hydroxyl group would not be able to make sufficient contacts with the Arg169 and Thr170 residues (Callaghan et al., 2005a). In addition, the interaction of the first base of the mRNA with

Val128 explains why certain mRNAs with stem loop structures at the 5' end are stabilised in *E. coli* (Emory and Belasco, 1990, Chen et al., 1991, Emory et al., 1992).

Further structural studies have found that, in the absence of RNA binding, the enzyme was shown to adopt a more "open" structure. Between the open and closed confirmations, the S1-like domain and the 5'-sensing domain move as one unit at an angle of around 55°. A hypothesis, termed the "mouse trap" model, was suggested whereby the 5' monophosphate interacts with the 5' monophosphate-sensing pocket, causing a conformational change in the 5'-sensing domain. This change results in the S1-like domain clamping on to the DNase I-like domain, distorting the sugar-phosphate backbone of the RNA and hence promoting cleavage, as shown in Figure 1.7B (Koslover et al., 2008).

However, kinetic studies have shown that addition of single-stranded regions on to RNase E substrates can promote bypass of 5'-monophosphate dependence (Baker and Mackie, 2003, Kime et al., 2010, Jourdan et al., 2010). In addition, early results have shown that a 5' monophosphate on oligonucleotides increases the affinity of interaction with RNase E (Jourdan and McDowall, 2008, Jourdan et al., 2010). Therefore, a second model has been proposed, whereby the interaction of the 5' monophosphate with the 5' monophosphate-sensing pocket increases the affinity of the substrate for RNase E, and the clamping down of the S1-like domain is largely independent of the interaction.

#### 1.4.1.1.3 The RNase H-like domain

Recently, several residues in the RNase H-like domain that are involved in RNA cleavage have been revealed. One of the most interesting residues is a glutamine at position 36, which when substituted for an arginine residue actually resulted in increased RNase E activity (Go et al., 2011). Several studies have found that the interaction of RNA with the Gln36 residue actually represents a form of uncompetitive regulation; the Q36R mutant shows increased binding of RNA to the active site, but less overall binding of the RNA (Go et al., 2011, Kim et al., 2014). Interestingly, another residue located at the same region of the RNase H-like domain, tyrosine at position 25, displayed the opposite effect when mutated to an alanine. This mutation led to a decrease in RNase E activity, but showed an increase in binding, specifically to an allosteric site found between residues 427 to 433 within the small domain, which may represent a form of allosteric regulation in RNase E (Kim et al., 2014).

Another interesting region within the RNase H-like domain was found during an analysis of RNase G. When mutations were introduced in RNase G that resulted in substitution of a valine to a phenylalanine or glutamate to a lysine at positions 219 and 248, respectively, viability was restored in RNase E-deficient cells (Chung et al., 2010). However, the equivalent residues in RNase E are

alanine and leucine at positions 217 and 247, which show little chemical similarity to either residue in the RNase G mutants. Therefore, it appears that the RNase H-like domain plays a key role in the differential activities found within the RNase E family.

#### 1.4.1.1.4 The DNase I-like domain

The DNase I-like domain houses the active site of RNase E, which contains a hydrated magnesium ion essential for catalysis. The magnesium ion is coordinated by the negatively-charged aspartate residues located at positions 303 and 346, as shown in Figure 1.7A. Substitution of these residues with asparagine, an amino acid with a similar special arrangement as aspartate but with a polar nature, had little to no effect on RNA binding, but decreased the catalytic activity by around 25 fold. The Asp303 residue is itself orientated by a nearby asparagine residue located at position 305 through hydrogen bonding interactions. Mutation of this residue to aspartate, which would disrupt the hydrogen bond interaction, caused a decrease in activity (Callaghan et al., 2005a).

Interestingly, substitution of aspartate at position 346 for a cysteine residue actually showed a similar level of activity to the wild-type RNase E, only when in the presence of manganese instead of magnesium. However, this mutation caused inviability *in vivo* even when $MnSO_4$ was supplemented in the media (Thompson et al., 2015).

The proposed mechanism for one metal ion-dependent cleavage is shown in Figure 1.7B. The divalent metal ion, which for RNase E is magnesium (Thompson et al., 2015), coordinates the phosphodiester bond of the RNA by interacting with the non-bridging oxygen atom on the phosphorous atom (Forconi and Herschlag, 2009). The positive charge of the magnesium decreases the p$K_a$ of one of the water molecules in its hydration shell, promoting formation of a hydroxyl ion nucleophile (Kirby, 1970, Forconi and Herschlag, 2009). The phosphate bond then undergoes an $S_N2$ mechanism with the nucleophile, whereby formation of a bond between the phosphorous and the nucleophile causes departure of the 3'-hydroxyl group of the upstream nucleotide from the phosphorous atom. Therefore, the final upstream and downstream products are 3' hydroxylated and 5' monophosphorylated, respectively (Burgers and Eckstein, 1979, McSwiggen and Cech, 1989).

Several other residues in the DNase I-like domain have roles in interacting with the RNA substrates. An arginine residue located at position 373 provides a positive charge for interaction with the negatively-charged phosphodiester backbone of RNA. This interaction organises the substrate so that it can make contact with the 5' monophosphate-sensing pocket and the active site simultaneously (Callaghan et al., 2005a). An asparagine residue located at position 323 has also been found to make interactions with some substrates, specifically with uracil residues found on "bulge"

regions of RNA hairpins. However, this residue is not found within the RNA-binding channel and likely plays a role in recognition of a specific population of RNAs (Diwa and Belasco, 2002, Schuck et al., 2009).

Along one side of the DNase I-like domain exists a patch of hydrophobic residues, which allows the RNase E protomer to self-associate and form a dimer with two RNA-binding channels, as shown in Figure 1.6B. The dimer is the minimal functional unit of RNase E, due to the fact that formation of each RNA-binding channel occurs between the S1-like domain from one protomer and the DNase I-like domain from the other protomer. This gives the RNase E principle dimer a "scissor like" structure (Caruthers et al., 2006, Callaghan et al., 2005b).

#### 1.4.1.1.5 The Zinc link and the small domains

The principle dimer self-associates to form a homotetramer, also termed a "dimer of dimers" (Callaghan et al., 2003). Each of the RNase E protomers contains two cysteine residues found at positions 401 and 411, which has been termed the "Zn link". The four cysteine residues in the dimer are coordinated by a zinc ion, orientating the two small domains at the C terminus of each protomer so that they can make sufficient contact with two small domains of another dimer. A mutation in either of the cysteine residues results in accumulation of the principle dimer and a significant reduction in catalytic activity, suggesting that formation of the homotetramer is required for maximum catalytic activity of RNase E (Callaghan et al., 2005b, Caruthers et al., 2006). Changes in the confirmation of the small domains has been observed between the "open" and "closed" forms of RNase E, possibly indicating that "cross talk" between the dimer-dimer interface could exist. This could explain why RNase E is most active as a homotetramer (Koslover et al., 2008, Bandyra et al., 2013).

### 1.4.1.2 The C-terminal half

The C-terminal half (CTH) of RNase E is much less conserved amongst bacteria than the NTH, showing large variation even within the *γ*-proteobacteria group (Condon and Putzer, 2002, Marcaida et al., 2006). In *E.* coli, the CTH of RNase E encompasses the region from amino acid at position 530 up to the end of the RNase E protein at position 1061. Although the CTH does provide a selective advantage for growth (Leroy et al., 2002), it is not essential for cell viability (Kido et al., 1996, Vanzo et al., 1998). The CTH does contribute significantly to mRNA decay (Bernstein et al., 2004), but is not instrumental for rRNA maturation *in vivo* (Lopez et al., 1999).

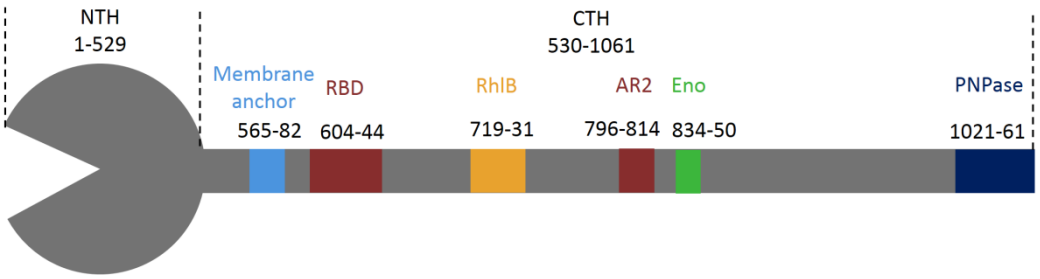


**Figure 1.9 A diagrammatic representation of the RNase E CTH.** The regions involved in protein, RNA and membrane interactions are highlighted. Image adapted from a previous study (Bandyra et al., 2013).

The main function of the CTH is to provide a scaffold for assembly of the RNA degradosome, a protein complex involved in degradation of cellular RNA (Vanzo et al., 1998). The three major components of this complex are the RNA helicase RhlB (Py et al., 1996), the glycolytic enzyme enolase (Miczak et al., 1996), and PNPase (Carpousis et al., 1994). The function of the domains found in the CTH of RNase E, as shown in Figure 1.9, will be discussed below.

#### 1.4.1.2.1 Membrane anchor

RNase E has been confirmed as a membrane binding protein (Miczak et al., 1991, Liou et al., 2001). The CTH of RNase E consists of an amphipathic helix, also known as Segment A, located between amino acids at positions 565-585, as shown in Figure 1.9. This helix contains an organisation of hydrophobic residues on one side, which can be embedded into the hydrophobic core of the lipid bilayer, and polar residues on the other, which can be exposed to the cytoplasm. The boundary between these two sides consists of positively-charged arginine and lysine residues that have been hypothesized to interact with the negatively charged heads of the phospholipids. This segment of the CTH can bind strongly, and therefore localise the degradosome, to the inner membrane (Khemici et al., 2008). The organisation of the degradosome along the inner membrane is believed to form filament like structures that are associated with the cytoskeleton (Taghbalout and Rothfield, 2007, Taghbalout and Rothfield, 2008). More recent studies have suggested that association of the RNase E to the membrane can also induce conformational changes that increase the catalytic rate of the NTH (Murashko et al., 2012).

#### 1.4.1.2.2 Arginine-rich regions

The CTH of RNase E contains two RNA-binding regions known as the primary RNA-binding domain (RBD), located at amino acid positions 604-644, and the arginine-rich region (AR2), located at amino acid positions 796-814. The RBD has been shown to form a coiled-coil domain when interacting with RNA (Callaghan et al., 2004). Both RNA-binding domains enhance the cleavage of the 9S precursor *in vitro* (Kaberdin et al., 2000) and are involved in the degradation of several transcripts (Leroy et al., 2002, Lopez et al., 1999, Ow et al., 2000). Because both RNA-binding regions are found flanking RhlB (see next section), they could provide anchors for the two single-stranded RNA regions produced by the distributive activity of RhlB, allowing it to re-associate and facilitate further unwinding. RhlB is usually limited to RNA duplexes that are around 22 bp in length (Cordin et al., 2006), but with the localised RBD and AR2, could adopt a processive activity.

#### 1.4.1.2.3 RhlB-binding site

The C-terminal RecA-like domain of RNA helicase B interacts with the region located between amino acids 719-731 on the CTH of RNase E (Chandran et al., 2004, Chandran et al., 2007), as shown in Figure 1.9. The stoichiometry of binding of RNase E (monomer) to RhlB is 1:1 (Callaghan et al., 2004), and binding is required for ATPase activity of RhlB (Worrall et al., 2008). Therefore, it is not surprising that most of the cellular RhlB is recruited to the degradosome (Khemici et al., 2004, Khemici et al., 2005).

The position of RhlB on the CTH is such that its positively-charged C-terminal tail is presented towards the arginine-rich region (AR2). The arginine residues of AR2 interact with the target RNA and present the 5’ end to the C-terminal tail of RhlB. Binding of ATP into the interdomain groove of RhlB causes changes in the relative positioning of the two RecA-like domains so that the C-terminal tail can then present the 5’ end of the RNA to the N-terminal RecA-like domain. The ATP is then hydrolysed, causing the two Rec-A domains to reposition, unwinding the double-stranded region of the RNA and presenting a 5’ single-stranded end to RNase E for hydrolytic cleavage and a 3’ single-stranded end to PNPase for phosphorylytic degradation (Khemici et al., 2005, Chandran et al., 2007).

Studies have found that the CTH is essential only when there are mutations in the 5’ sensor of RNase E (Garrey and Mackie, 2011, Anupama et al., 2011). However, viability is restored in CTH truncations that retain the RhlB-binding site, suggesting an essential role for RhlB in 5’ end-independent cleavage by RNase E *in vivo* (Garrey and Mackie, 2011). In addition, microarray analyses have confirmed that RhlB is required for normal mRNA decay (Bernstein et al., 2004).

Apart from RhlB, several other RNA helicases have been found to associate with the RNA degradosome (Khemici et al., 2004, Carabetta et al., 2010). In addition, under conditions of low temperature, RhlB has been shown to be displaced by the cold-shock RNA helicase CsdA (Prud'homme-Genereux et al., 2004).

#### 1.4.1.2.4 Enolase-binding site

Unlike RhlB, only around 10% of cellular enolase is incorporated into the degradosome (Py et al., 1994). Enolase contains an inter-protomer groove at the top of the dimer that can accommodate a small α helix consisting of amino acids located between 834-850 from the CTH of RNase E, as shown in Figure 1.9 (Nurmohamed et al., 2010, Chandran and Luisi, 2006). The binding stoichiometry of the RNase E monomer and enolase dimer is 1:1. Upon binding, there is no conformational change in the enolase enzyme and its activity is not affected by recruitment to the degradosome (Callaghan et al., 2004).

The presence of enolase in the degradosome is still not fully understood, but its ability to catalyse the production of phosphoenolpyruvate (PEP), an important phosphate donor in the cell, has led to a theory that enolase is important in localised phosphotransfer reactions. The formation of PEP by enolase would be readily available to the membrane-bound protein pyruvate kinase (Lasserre et al., 2006) due to the close proximity of the degradosome. Pyruvate kinase catalyses the production of pyruvate by transferring the phosphate group on PEP to an ADP molecule, generating membrane-localised ATP for the degradosomal components RhlB and PNPase (Bandyra et al., 2013), as well as nearby enzymes such as PAP I (Carabetta et al., 2010).

The production of PEP by enolase may also have other roles in RNA decay. Mutations that prevent recruitment of enolase to the degradosome have been found to increase the stability of several transcripts associated with metabolism (Morita et al., 2004, Bernstein et al., 2004). One model that has been proposed is that localised PEP levels mediated by enolase may regulate the production of sRNAs, which ultimately target mRNAs that encode the components of metabolic pathways (Vanderpool, 2007). This is interesting, since the basis for RNase E essentiality in *E. coli* is believed to be based on the cleavage of mRNAs that encode protein components involved in similar pathways (Lee et al., 2002). Although the association of enolase with the degradosome is not essential in *E. coli* (Callaghan et al., 2004, Chandran and Luisi, 2006), perhaps its localised activity provides a form of selectivity in the RNase E-initiated degradation of this specific pool of mRNAs.

#### 1.4.1.2.5 PNPase-binding site

PNPase interacts with the CTH of RNase E at a region known as Segment D, which encompasses the amino acids at positions 1021-1061, as shown in Figure 1.9 (Callaghan et al., 2004). Segment D adopts a β-sheet conformation that forms extensive hydrogen bonds with the terminal β-sheet present within the inter-protomer groove on the surface of the PNPase enzyme. Therefore, each PNPase has the capacity to interact with up to three CTH-RNase E tails (Nurmohamed et al., 2009). Around 20% of cellular PNPase is associated with the degradosome (Liou et al., 2001).

PNPase in the degradosome degrades the majority of products produced by RNase E. In addition, the association of PNPase on to the degradosome is believed to be required for the degradation of structured mRNAs in coordination with RhlB (Coburn et al., 1999, Khemici and Carpousis, 2004). In fact, even when the CTH of RNase E is deleted in *E. coli*, RhlB and PNPase are still found to associate (Liou et al., 2002).

### 1.4.2 Mechanism of RNase E cleavage

#### 1.4.2.1 5’ monophosphate-dependent cleavage

RNase E can initiate mRNA degradation by performing an endonucleolytic cleavage on the transcript, producing an upstream fragment with an exposed 3’ end susceptible to degradation by exonucleases. The resulting downstream fragment would also present a 5’-monophosphorylated end, which would make an ideal substrate for further endonucleolytic cleavage by RNase E or RNase G by engaging the 5’-sensing pocket (Mackie, 1998, Callaghan et al., 2005a). However, because RNase E is stimulated by the presence of a monophosphate on the 5’ terminus of a transcript (Mackie, 1998, Mackie, 2000, Jiang and Belasco, 2004, Garrey et al., 2009), the 5’-triphosphate cap on nascent transcripts effectively protects mRNA from degradation (Celesnik et al., 2007).

Another enzyme was identified in *E. coli* that removes a pyrophosphate from the 5’ end of a nascent transcript, producing these 5’-monophosphorylated substrate for RNase E (Celesnik et al., 2007, Deana et al., 2008). This enzyme, termed RNA pyrophosphohydrolase (RppH), was considered the initiator of mRNA decay in *E. coli* (Celesnik et al., 2007, Richards et al., 2012). It is believed that the production of 5’-monophosphorylated ends by RppH could provide a foothold for RNase E to bind to transcripts with high secondary structure (Mackie, 2013a) or that are highly translated (Richards et al., 2012), factors that would both reduce the ability of RNase E to access single-stranded regions. RppH activity has also been implemented in the 5’ monophosphorylation of sRNAs, which could provide selective anchors for RNase E to degrade target mRNAs (Bandyra et al., 2012, Mackie, 2013a). Finally, RppH could play a role in committing mRNAs to a “decapped” step. Recently, several

RNAs in *E. coli* have been found to contain an NAD cap on their 5’ ends, similar to the $m^7G$ cap of eukaryotic mRNA (Chen et al., 2009, Cahova et al., 2015). The 5’-monophosphorylated ends produced by RppH would not be able to provide a leaving group during the NAD capping step, and therefore would be permanently “decapped”.

#### 1.4.2.2 Direct entry

Interestingly, disruption of the *rppH* gene, which encodes RppH, was found to slow the turnover of only 25% of transcripts whose degradation is thought to be dependent on RNase E (Deana et al., 2008). One suggestion is that a 5’ monophosphate could be generated by another enzyme in *E. coli*. However, overexpression of RppH, which results in an increase in the proportion of mRNAs that are monophosphorylated at the 5’ end, does not enhance the rate of mRNA decay (Luciano et al., 2012). This suggests that either: the degradation of many transcripts might be dependent on RNase E, but not require it to be cleaved (and thus not require decapping); or RNase E can initiate the degradation of many transcripts without requiring decapping. Biochemical evidence for the latter has been shown (Hankins et al., 2007, Kime et al., 2010). Other studies have also confirmed *in vivo* that RNase E can cleave substrates without having to engage a 5’-monophosphorylated end (Garrey and Mackie, 2011, Anupama et al., 2011).

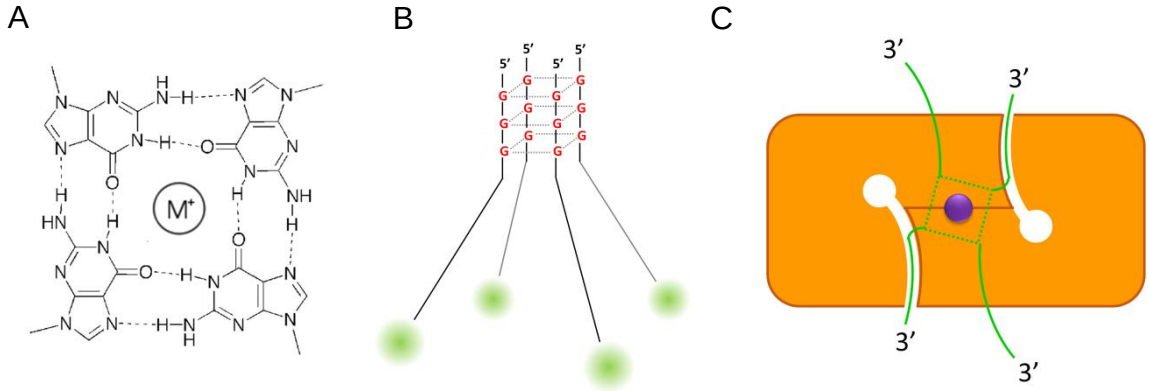


**Figure 1.10 Oligonucleotide quadruplexes enhance binding to NTH-RNase E.** Panel A shows a molecular schematic of the G quartet. Hydrogen bonding within a plane occurs via Hoogsteen and Watson-Crick faces of the guanine bases, stabilized by the interaction between the oxygen groups on carbon 6 of each base with a monovalent ion, preferably potassium, in the centre (Parkinson, 2006). Image was taken from previous work (Burge et al., 2006). Panel B shows the hydrophobic stacking of G-quartets in a planar arrangement. RNA downstream of the 5’ GGG sequence is shown as a line. Fluorescein is shown as a green circle. Image adapted from a previous study (Kime et al., 2010). Panel C shows a schematic of the principal dimer (orange) interacting with the quadruplex oligonucleotide (green). Each protomer is separated by a dark orange boundary and contains an RNA binding channel (white line) ending with a 5’ monophosphate-binding pocket (white circle). The oligonucleotide quadruplex is bound to the dimer, with the guanosine quartet represented as a green dotted square and a potassium ion within (purple). Images were adapted from a previous study (Kime et al., 2010).

In one study, it was found serendipitously that an 13 nt long oligonucleotide, termed BR13, with a 5'-hydroxylated end could be cleaved rapidly by RNase E, provided the substrate had been stored on ice immediately prior to starting the reaction. Further circular dichroism analyses revealed that the 5'-GGG sequence of BR13 formed intermolecular quadruplexes at low temperatures, in effect creating a substrate that presents four single-stranded segments of the oligonucleotide, as shown in Figure 1.10 (Kime et al., 2010). Moreover, modelling studies revealed that two single-stranded segments on RNA could interact simultaneously with two RNA-binding channels found on the principal dimer of NTH-RNase E (Kime et al., 2010). Thus, the simultaneous recognition of more than one single-stranded region could facilitate rapid cleavage in the absence of 5'-end recognition. Modified substrates have been produced that confirm this model (Baker and Mackie, 2003, Jourdan et al., 2010). Cooperative interactions of this nature are common in various systems, *e.g.* the recognition of operators by the *lac* repressor (Chen and Matthews, 1994, Vossen et al., 1996).

Given the prevalence of single-stranded regions in mRNA, this type of RNase E cleavage, which has been referred to as 'direct entry', may be another means by which mRNA degradation is initiated. It would offer a simple explanation for the observed interplay between translation and mRNA degradation, whereby the passage of ribosomes limits RNase E access to single-stranded sites (see Section 1.1.3). Given also that mutations in the 5'-sensing pocket of RNase E or in RppH do not have a significant effect on cell viability or cellular mRNA levels (Garrey and Mackie, 2011, Deana et al., 2008, Anupama et al., 2011), but mutations in RNase E activity do (Apirion and Lassar, 1978, Ono and Kuwano, 1979, Garrey and Mackie, 2011), direct entry may play the major role in initiating mRNA decay.

The 5' monophosphate-dependent pathway is not exclusive with direct entry, and may actually be an important pathway for further cleavage of direct entry products. Physical separation of multiple single-stranded regions of RNA, as a result of endonucleolytic cleavage, would result in a reduction in the single-stranded character of the products required for direct entry. However, the downstream products would have a 5'-monophosphate group to assist in binding to RNase E. Previous kinetic analyses have suggested that the 5'-monophosphate group enhances the catalytic activity of RNase E without affecting the affinity, potentially contradicting this model (Jiang and Belasco, 2004). However, the findings presented previously were derived from heavily extrapolated data. Therefore, a kinetic analysis of the 5' monophosphate-dependent pathway will have to be reinvestigated.

The broad objective of this thesis is to understand in greater detail the initiation of mRNA degradation by RNase E in *E. coli*. The specific aims are to (1) confirm the molecular recognition by which the catalytic domain of RNase E can cleave transcripts rapidly without requiring recognition of

a 5’-monophosphorylated end; (2) establish the importance of ‘direct’ entry in the degradation of the mRNA pool; and (3) investigate the possible contributions of other regions of RNase E to the initiation of mRNA degradation.

# Chapter 2

# Materials and Methods

## 2.1 Materials

### 2.1.1 Growth and maintenance of bacteria

2.1.1.1 Media

LB (Luria Bertani) media consisted of 10 g/l Bacto-tryptone, 5 g/l Bacto-yeast extract (Oxoid) and 10 g/l NaCl and was purchased as tablets from Sigma Aldrich (UK). Tablets for solid media consisted of 15 g/l agar in addition to the components above.

2.1.1.2 Sterilisation

All media were sterilised at 121°C for 20 min. Heat-sensitive supplements, such as antibiotics and IPTG, were sterilised by filtration through 0.2 µM filters (Sarstedt GmbH, Germany), or through vacuum-driven Durapore 0.22 µm filters (Millipore Corporation, Massachusetts, USA) for volumes larger than 20 ml.

2.1.1.3 Bacterial strains

| ***E. coli* strain** | **Genotype** |
|---|---|
| BW25113 | $F^-$, $\lambda^-$, *ΔlacZ4787*(::*rrnB-3*), *hsdR514, Δ(araBAD)567, Δ(rhaBAD)568, rph-1* (Baba et al., 2006). |
| BL21 (DE3) | $F^-$, *hsdS*($r_B^-m_B^-$), *gal, ompT, lon,* $\lambda$ *(cI857, ind-1, nin-5, sam-7, lacI, lacUV5-T7 gene 1*). Purchased from Agilent Technologies. |
| DH5α | *fhuA2, ΔlacU169, phoA, glnV44, Φ80', ΔlacZM15, gyrA96, recA1, relA1, endA1, thi-1, hsdR17*. Purchased from Invitrogen. |
| MG1655 | $F^-$, $\lambda^-$, *ilvG-*, *rfb*-50, *rph*$^-$. Obtained from *E. coli* Genetic Stock Center (Yale, USA). |
| N3433 | Hfr, *lacZ43*(Fs), $\lambda^-$, *elA, spoT1*, *thiE1*. Laboratory stock. |
| N3431 | Same as above with *rne*-3071 (ts) mutation. |
| SDF204 | $F^-$, $\lambda^-$, IN(*rrnD-rrnE*)1, *rph*-1, *rnc+, TD1-17::*ΔTn10. Laboratory stock. |
| SDF205 | Same as above with *rnc*-105 mutation. |
| MC1061 | $F^-$, *Δ*(*ara-leu*)7697, [*araD*139]$_{B/r}$, *Δ*(*codB-lacI*)3, *galK*16, *galE*15(GalS), $\lambda^-$, e14$^-$, *mcrA*0, *relA*1, |

| | |
|---|---|
| | *rpsL*150(*strR*), *spoT*1, *mcrB*1, *hsdR*2($r^-m^+$) (Casadaban and Cohen, 1980). |
| GM11 | Same as above with *rng::cat* mutation (Umitsuki et al., 2001). |

Glycerol stocks were made as described previously (Sambrook and Russell, 2001).

2.1.1.4 Plasmids

| **Plasmid** | **Description** |
|---|---|
| pET16b | Contains hexahistidine-encoding sequence for tagging recombinant proteins. Also contains T7 *lac* promoter to drive transcription. Confers ampicillin resistance. |
| pRne529N | Based on pET16b, contains insert encoding first 529 amino acids of *rne* from *E. coli*, after hexahistidine-encoding sequence. |
| pRneD346N | As above with RneD346N mutation. |
| pRNAI | Based on pUC18, containing insert for RNAI gene from pBR322. |

### 2.1.2 Buffers and solutions

Buffers were either purchased from Sigma-Aldrich (unless otherwise stated) or prepared as described previously (Sambrook and Russell, 2001).

**Acrylamide stock solutions** of 30% (w/v; 29:1 acrylamide: *bis*-acrylamide) and 40% (w/v; 19:1 acrylamide: *bis*-acrylamide) were purchased from Severn Biotech Ltd (UK). Denaturing PAGE stocks consisted of 20% (w/v) acrylamide, 7 M urea, 1x TBE. All acrylamide solutions were stored at -4°C.

**Tris-EDTA (TE) buffer** consisted of 10 mM Tris-HCl (pH 8.0), 1 mM EDTA.

**10x SDS running buffer** consisted of 250 mM Tris-HCl (pH 8.3), 1.9 M glycine, 1% (w/v) SDS.

**10x Tris-Acetate-EDTA (TAE)** running buffer consisted of 890 mM Tris-HCl (pH 8.0), 890 mM acetic acid and 0.25 mM EDTA.

**10x Tris-Borate-EDTA (TBE)** running buffer was purchased from Severn Biotech Ltd (UK) and consisted of 890 mM Tris (pH 8.3), 890 mM boric acid and 0.25 mM EDTA.

**6x DNA loading dye** was purchased from Thermo Scientific and consisted of 10 mM Tris-HCl (pH 7.6), 0.03% (w/v) BPB, 0.03% (w/v) XyCy, 60% (v/v) glycerol and 60 mM EDTA.

**2x RNA loading dye** was purchased from Ambion (Life Technologies, USA) and consisted of 95% (v/v) formamide, 18 mM EDTA, 0.025% (w/v) BPB, 0.025% (w/v) XyCy and 0.025% (w/v) SDS.
**2x SDS loading dye** consisted of 100 mM Tris-HCl (pH 6.8), 4% (w/v) SDS, 0.2% (w/v) bromophenol blue, 20% (v/v) glycerol and 200 mM β-mercaptoethanol. All loading dyes were stored at -20°C.

## 2.2 General RNA Methods

### 2.2.1 RNase decontamination

To prepare ribonuclease-free solutions, diethylpyrocarbonate (DEPC; Sigma, UK) was added at a final concentration of 0.1% (v/v) and then incubated overnight at 37°C. The solutions were then autoclaved at 121°C for 20 min to inactivate the DEPC. Solutions that were reactive to DEPC (such as Tris) or sensitive to heating (imidazole) were purchased from Sigma Aldrich guaranteed RNase free. Equipment was decontaminated by treatment with RNase*ZAP*® RNase decontamination solution (Ambion, USA).

### 2.2.2 Total RNA methods

2.2.2.1 Isolation of bacterial RNA

*E. coli* cells were grown in 50 ml of LB broth at 37°C, 200 rpm to an $OD_{600}$ of 0.6. Cell metabolism was quenched by adding 6.25 ml stop solution (5% [v/v] phenol in absolute ethanol) to the culture and cells were harvested by centrifugation at 4,300 x *g*, 4°C for 10 min in a Sorvall RC-5B Superspeed centrifuge (SS-34 rotor). Cell pellets were resuspended in 5 ml of TE buffer and lysed by adding 5 ml of preheated (95°C) 2x Lysis buffer (20 mM Tris-HCl pH 8, 40 mM EDTA, 0.3 M NaCl, 0.5% w/v SDS). The mixture was incubated in a boiling water bath for 30 s. Cell lysate was then mixed with 10 ml of phenol saturated with 100 mM citrate buffer (pH 4.3) by inversion. Phases were separated by centrifugation under the same conditions as above. The aqueous phase was transferred to a 50-ml Falcon tube and mixed with 2.5 volumes of absolute ethanol. The nucleic acid precipitate was pelleted by centrifugation at 4,300 x *g*, 4°C for 20 min. Pellets were washed twice with 2 ml of 70% (v/v) ethanol and resuspended in 100 µl of DEPC-treated water.

2.2.2.2. DNase I treatment

Amounts of RNA less than 100 µg of RNA were incubated with 2 U of DNase I (Promega, UK) at 37°C for 60 min. The volume was made up to 400 µl with DEPC-treated water and the total RNA was extracted with an equal volume of acidic phenol: chloroform: isoamyl alcohol (25: 24: 1). The aqueous phase was separated from the organic phase by centrifugation at 4,300x *g*, 4°C for 10 min

using an Eppendorf 5415-R benchtop centrifuge and transferred to a 1.5 ml Eppendorf tube. The RNA was precipitated by addition of 0.1 volumes of 5 M NaCl and 2.5 volumes of absolute ethanol and pelleted by centrifugation at 16,100 x *g*, 4°C for 20 min. The pellet was washed twice using 70% (v/v) ethanol and resuspended in 50 µl of DEPC-treated water.

2.2.2.3 Quantitation of RNA

The concentration of RNA in the final samples was determined using the Beer-Lambert law as shown in Equation 1:

$$A = \varepsilon cl \qquad \textbf{Equation 1.}$$

Where A is the absorbance, c is the concentration (g/l), l is the cell path length (in cm) and ε is the extinction coefficient. By treating nucleic acid solutions as a mixture of mononucleotides, the formula of $A_{260}$ of 1.0 ≈ 40 ng/µL was used to determine the concentration of total RNA. Around 1 µl of the sample was mixed with 99 µl of water before measuring to ensure the reading was in the linear range of absorbance. The 260: 280 ratio was also calculated to ensure the purity of the sample, which for RNA should be ~2. These values were confirmed by measuring the concentration of the samples using a NanoDrop 1000 spectrophotometer.

2.2.2.4 Agarose gel electrophoresis

Agarose gels were made by melting 0.5 g of agarose (Melford Laboratories Ltd, UK) in 50 ml of 1x TBE using an 800 W microwave at the highest power setting and 20 s incubations until completely dissolved. Ethidium bromide (Sigma-Aldrich, UK) was added to a final concentration of 1 µg/ml when the agarose mixture had cooled to 55°C. Gels were cast and placed in an electrophoresis tank (Bio-Rad, UK) and topped with 1x TBE buffer. Around 10 µg of RNA was mixed with 2x RNA loading dye before loading onto the gel. The gel was run at 10 V/cm for 30 min. Gels were imaged at 310 nm using a Transilluminator (Syngene, UK) to determine the integrity of the sample.

2.2.2.5 RNA ligase-mediated reverse-transcription polymerase chain reaction (RLMRTPCR)

A) RNA ligation

To confirm the genotype of the N3433 and N3431 cells, 1.2 µg of total RNA extracted from both strains was incubated with 5 U of T4 RNA ligase 1 (New England Biolabs, USA), 20 µM S4 RNA oligonucleotide (Dharmacon, USA), 20 U RNaseOUT$^{TM}$ (Invitrogen, USA) and 1 mM ATP in 1x T4 ligase buffer at 37°C for 1 h. S4 oligonucleotide had the following sequence: 5'-ACAUGAGGAUUACCCAUGUCGAAGACAACAAAGAAGUUCAACUCUUUAUGUAUU-3'.

B) Reverse transcription

The reverse transcription reaction was carried out by addition of 50 ng of random hexamers (Invitrogen, USA) to 5 µl of ligated RNA at a final volume of 20 µl. The reactions were heated to 65°C for 5 min and then chilled on ice immediately. The RNA mixture was then incubated with 200 U of M-MLV RNase H minus Reverse transcriptase (Promega, UK), 1 mM dNTPs (Invitrogen, USA), and 80 U RNaseOUT™ in 1x RT buffer at 25°C for 15 min, 42°C for 60 min and 70°C for 15 min. Following addition of 80 µl of 10 ng/ml yeast tRNA (Ambion, USA), tubes were then stored at -20°C for 1 h.

C) PCR

PCRs consisted of 2 µl of RT reaction mix, 2 µM FW RLM primer, 2 µM Eno RLM2 primer, 3 mM $MgCl_2$ (Promega, UK), 800 µM dNTPs, and 0.8 U of GoTaq® DNA polymerase (Promega, UK). The sequences for the PCR primers were as follows: FW RLM (5'-CATGAGGATTACCCATGTCG-3') and Eno RLM2 (5'-GTCAATGCCAGCCTGATCTT-3'). The program for the thermal cycler was as follows: initial denaturation at 95°C for 5 min followed by 35 cycles of 95°C for 30 s, 50°C for 30 s, 72°C for 1 min, before a final extension of 72°C for 7 min. Samples were analysed using a 1.2% (w/v) agarose gel as described (Section 2.2.2.4) and phenotypes were confirmed by the presence/absence of a 335-bp amplicon.

2.2.2.6 Differential RNA sequencing

Total RNA for *in vitro* studies was depleted of rRNA using *MICROBE*xpress™-Bacteria beads as per manufacturer's instructions (Ambion, USA). Total RNA for *in vivo* studies was depleted of rRNA by Vertis Biotechnologie AG (Germany) prior to sequencing. The 5'-sequencing adaptor was ligated to transcripts, followed by fragmentation using a Bioruptor® Next Gen UCD-300™ sonication system (Diagenode, Belgium) to allow ends of both long and short transcripts to be detected. RNA was then tailed at the 3' end using poly(A) polymerase (New England Biolabs, USA). The cDNA libraries were then constructed by reverse transcription using RNase H-minus M-MLV reverse transcriptase (Agilent Technologies, UK) and an oligo(T) deoxynucleotide primer, amplification by PCR and fractionation using gel electrophoresis. Fragments of 250-400 bp were selected and sequenced on an Illumina HiSeq platform (single end, read length of 50 bp). The determined sequences were then aligned to the *E. coli* K12 substrate MG1655 genome, which was retrieved from NCBI (accession number U00096.2). For each chromosome position, a score was given based on the frequency this nucleotide was the first nucleotide in a sequence. These data were then viewed as peaks on the UCSC Microbial Genome browser (UCSC, USA). Each of the datasets was compared using M-A (ratio-

intensity) scatter plots and populations of cleavage candidates were selected having M values of greater than or equal to 5 and 3.4 for the *in vivo* and *in vitro* dataset, respectively.

### 2.2.3 Synthesised RNA methods

#### 2.2.3.1 T7 *in vitro* transcription

RNase E substrates were transcribed *in vitro* by incubating 100 nM template cDNA with 100 U of T7 RNA polymerase, 5 mM DTT, 2.5 mM of each NTP, 80 U RNaseOUT™ (all from Invitrogen, USA), and 1 U of inorganic pyrophosphatase from *Saccharomyces cerevisiae* (Sigma, UK) in 1x T7 buffer at 37°C for 3 h. Reactions were stopped by adding 2 U of DNase I and 40 U of RNaseOUT™ followed by incubation at 37°C for 1 h. Transcripts were purified by extraction with acidic phenol: chloroform: isoamyl alcohol (25:24:1) as described previously (Section 2.2.2.2). The aqueous phase was transferred to a fresh tube and the RNA was precipitated by adding 0.1 volumes of 3 M sodium acetate (pH 5.2) and 2.5 volumes of absolute ethanol. The precipitate was pelleted by centrifugation at 16,100 x *g*, 4°C for 20 min and washed with 0.5 ml of 70% (v/v) ethanol. The pellet was resuspended in 40 µl of DEPC-treated water. Quantification of the RNA was performed as described (Section 2.2.2.3).

#### 2.2.3.2 Denaturing polyacrylamide gel electrophoresis

Polyacrylamide gels were made at a final concentrations of 8% by mixing 4 ml of 20% (w/v; 19:1 acrylamide: *bis*-acrylamide) acrylamide, 7 M urea, 1x TBE stock solution and 6 ml of 7 M urea, 1x TBE stock solution. Polymerisation was catalysed by adding 100 µl of 10% (w/v) APS and 10 µl of TEMED, followed by thorough mixing. The gel was set in a vertical PAGE gel cast and placed into a PAGE tank (Bio-Rad) topped with 1x TBE. Wells were washed using 1x TBE and gels were pre-run at 25 mA for 20 min. Samples were prepared by addition of 1 µl of the transcription reaction to 4 µl of DEPC-treated water and 5 µl of 2x RNA loading dye and denatured at 95°C for 3 min, before being loaded onto the gel. The gels were run for 40 min at 25 mA, stained in 1x TBE containing ethidium bromide (final concentration of 1 µg/ml) for 5 min, and viewed using the Transilluminator as described (Section 2.2.2.4).

#### 2.2.3.3 Gel purification of transcripts

Transcripts preparation contains easily observable contaminants. Products were purified further using D-tube dialyzers with a 3.5-kDa Molecular weight cut off (Novagen, USA). Transcription reactions were mixed with an equal volume of 2x RNA loading dye and separated via denaturing PAGE as described (Section 2.2.3.2) using a 30-ml gel. Gels were stained as before and slabs

containing the transcript expected to be full-length were excised under a UV box and diced. The diced gel pieces were placed in pre-hydrated D-tube dialyzers, which were then filled with RNase-free 1x TBE. The dialyzers were then placed in a horizontal electrophoresis tank (Bio-Rad) and the RNA was eluted at 8 $Vcm^{-1}$ for 20 min. The eluate was transferred to 0.5 ml Eppendorf tubes and immediately extracted with equal volumes of acidic phenol: chloroform: isoamyl alcohol and precipitated as described previously (Section 2.2.3.1.). D-tube dialyzers were filled with fresh RNase-free 1x TBE and RNA was eluted again as described before. This was repeated until the majority of RNA was eluted, as determined by exposing fragments to the UV box. On the final elution, polarity of the electrical current was reversed to ensure all RNA was resuspended. Final purified transcripts were analysed for purity and integrity via denaturing PAGE and were quantified as described previously (Sections 2.2.3.2 and 2.2.2.3, respectively).

2.2.3.4 Discontinuous cleavage assay of RNase E

Each reaction consisted of 20 nM NTH-RNase E (wild-type or T170V) pre-incubated with 32 U of RNaseOUT™ in 25 mM *bis*-Tris-propane-HCl pH 8.3 (Sigma, UK), 100 mM NaCl, 15 mM $MgCl_2$, 0.1% (v/v) Triton X-100 and 1 mM DTT at 37°C for 20 min. Pre-warmed (37°C) transcripts were added and mixed to a final concentration of 180 nM to start the reaction. Immediately upon mixing, a 10 µl aliquot of the reaction was quenched with 10 µl of 2x RNA loading dye. Further aliquots were taken at 5, 15, 30 and 60 min following the start of the reaction, unless otherwise stated in the figure legends.

2.2.3.5 Electrophoresis and quantitation of cleavage products

Samples were separated on 30-ml, 8% (v/v) polyacrylamide, 7 M urea, 1x TBE gels, which were stained and imaged as described (Section 2.2.3.2). Gel images were exported as TIFF images and imported to AIDA v4.22 software. Bands were quantified via 2D densitometry and data was transferred to Microsoft Excel for background subtraction and normalization.

2.2.3.6 Tobacco Acid Pyrophosphatase and Terminator Exonuclease treatment

A) TAP treatment

Transcripts synthesised *in vitro* were incubated with Tobacco Acid Pyrophosphatase (TAP; Epicentre, USA) at a ratio of 8 µg of RNA to 25 U of TAP with 100 U of RNaseOUT™ in 1x TAP buffer at 37°C for 2 h. After incubation, DEPC-treated water was added to a final volume of 200 µl and the solution was phenol extracted as described (Section 2.2.2.2). The aqueous phase was transferred to a new 1.5-ml Eppendorf tube and mixed with 0.1 volumes of sodium acetate, 0.02 volumes of 5 mg/ml glycogen

(Ambion, USA) and 2.5 volumes of absolute ethanol. Nucleic acid was allowed to precipitate at -20°C for 1 h. Precipitate was then pelleted by centrifugation at 16,100 x *g*, 4°C for 30 min, washed with 70% (v/v) ethanol and resuspended in 50 µl of DEPC-treated water.

B) TEX treatment

Reactions consisted of 300 ng of TAP-treated and -untreated transcripts (in separate reactions) incubated with 0.3 U of Terminator™ 5'-phosphate-dependent Exonuclease (TEX; Epicentre, USA) and 40 U of RNaseOUT™ in 1x TEX buffer B at 42°C for 30 min in a final reaction volume of 20 µl. After incubation, 180 µl of DEPC-treated water was added and the solution was phenol extracted and ethanol precipitated as described above. The pellets were resuspended in 10 µl of 1x RNA loading dye and analysed by denaturing PAGE as described (Section 2.2.3.2).

2.2.3.7 Hybridising with DNA oligonucleotides

A) Oligonucleotide hybridisation

80 pmol of RNA was incubated at 95°C for 3 min before addition of 240 pmol of complementary DNA oligonucleotide. The mixture was then incubated at 65°C for 5 min, 35°C for 5 min, and 4°C for 5 min. Oligonucleotide sequences are shown in Table 2.1.

| **Oligo name** | **Sequence** |
|---|---|
| a1 | 5'- ATCTTTTTTTTCGCGATACCT TATCGGCGT TGC -3' |
| b1 | 5'- AGATTGTTTCTTCGAAGG -3' |
| b2 | 5'- ACAAATTGGTTTTGAATTTGCCGAACATATTCGATACATTCAGAATT -3' |
| b3 | 5'- ACAAATTGGTTTTGAATTTGCCGAACATATTCGATAC -3' |
| b4 | 5'- TTGGGTGGTCTGTGCCTTACAGCACTTTCAAATTT -3' |
| b5 | 5'- ACAGCACTTTCAAATTTTGG -3' |
| b6 | 5'- TTGGGTGGTCTGTGCCTTA -3' |
| b7 | 5'- GCGTCGCTGTGGATATTTTATTGAGAGAAGAATT -3' |
| b8 | 5'- GCGTCGCTGTGGATATTTTATTGAG -3' |
| b9 | 5'- TCGGTTCAATGCGGGTGATT -3' |
| b10 | 5'- CGT TCA GCG CCG TAA TCA AC -3' |
| b11 | 5'- TCTTTTAATTCGGTACGGTC -3' |
| b12 | 5'- CGGAAGCTTAAATCCCATTG -3' |

**Table 2.1 Hybridisation oligonucleotides.** All DNA oligonucleotides had a $T_m$ greater than 50°C and named according to the region in the RNA to which they hybridised.

B) RNase H treatment

RNase H reactions consisted of 1 pmol of RNA:DNA hybrid incubated with 2.5 U of RNase H (Thermo Scientific, USA) and 20 U of RNaseOUT™ in 1x RNase H buffer at 37°C for 1 h in a final reaction volume of 20 µl. Reactions were stopped by addition of 20 µl of 2x RNA loading dye. Results were analysed by loading 10 µl of each sample on to denaturing polyacrylamide gels as described (Section 2.2.3.2).

### 2.2.4 RNA oligonucleotide methods

2.2.4.1 Synthesis of oligonucleotides

Two derivatives of LU13 (5'-GAGACAGUAUUUG-3') were used in these assays. One was synthesised with a 5'-monophosphate group and the other with an unmodified 5'-hydroxyl group. Both were purchased from Eurogentec (Kaneka, Germany). A third oligonucleotide, BR15 (5'-GGGGG*ACAGUAUUG*-3') was synthesised as a chimera (RNA and 2'-*O*-methylated RNA shown in normal and italic typeface, respectively) by MWG operon (Eurofins, Germany). The 5' end was unmodified, *i.e.* hydroxylated. All oligonucleotides were synthesised with a 3' fluorescein to aid detection on denaturing polyacrylamide gels. Derivatives of LU13 and BR15 were stored at -80°C in RNase-free water containing 100 mM KCl, respectively.

2.2.4.2 Gel purification of oligonucleotides

Oligonucleotides were purified due to presence of minor contaminants. LU13 and BR15 solutions were mixed with an equal volume of 2x RNA loading dye and 0.2 volumes of 6x DNA loading dye, respectively. LU13 samples were separated on 30-ml, 20% (v/v) polyacrylamide, 7 M urea, 1x TBE gels. BR15 samples were separated on 30 ml 20% (v/v) polyacrylamide, 1x TBE gels. Bands were viewed via UV shadowing on Thin-Layer chromatography (TLC) plates. Gel slabs containing bands corresponding to the expected sizes of intact oligonucleotides were excised and diced. The gel pieces were crushed by centrifugation at 16,100 x *g* for 5 min through restricted holes in 0.5-ml Eppendorf tubes and collected in 2 ml Eppendorf tubes. The crushed pieces were then soaked in 0.5 ml of elution buffer (500 mM ammonium acetate, 10 mM magnesium acetate, 1 mM EDTA, 0.1% [w/v] SDS). The mixture was frozen at -80°C for 30 min and then incubated in a water bath set to 85°C for 5 min. The oligonucleotides were then left to elute overnight at 37°C with gentle shaking (200 rpm). The crushed gel pieces were pelleted by centrifugation at 16,100 x *g* for 10 min and the

eluate was transferred to a fresh 2-ml Eppendorf tube. The crushed gel fragments were soaked with fresh elution buffer and oligonucleotides were allowed to elute as before. This process was repeated until the majority of nucleic acid was eluted, as determined by minimum shadowing on TLC plates under a UV light. The eluate was phenol extracted as described (Section 2.2.3.3). Oligonucleotides were precipitated and pelleted as described (Section 2.2.3.6), and resuspended in 100 µl of DEPC-treated water or 100 mM KCl for LU13 or BR15, respectively.

2.2.4.3 Discontinuous cleavage of oligonucleotides

Reactions were performed under similar conditions as described previously (Section 2.2.3.4). Reactions were also performed with substitutions of NaCl for KCl and/or $MgCl_2$ for $CaCl_2$ at the same concentrations. The final concentration of oligonucleotide and enzyme in the reactions was 250 nM and 5 nM, respectively. Samples were taken at: 0, 2, 5, 15, 60, 120 and 180 min for 5'-monophosphorylated LU13 and BR15, and 0, 15, 60, 120, 180, and 330 min for 5'-hydroxylated LU13.

2.2.4.4 Electrophoresis and quantitation of oligonucleotide cleavage

Samples were separated on 30-ml, 20% (v/v) polyacrylamide, 7 M urea, 1x TBE gels. Gels were then imaged using a Fujifilm FLA 5000 scanner with the laser set to 473 nm and a Y510 (510 nm) filter. Images were converted to TIFF files and imported to AIDA v4.22 software for band intensity quantification as described (Section 2.2.3.5).

2.2.4.5 Michaelis-Menten analysis of LU13

Reactions were performed under similar conditions as described (Section 2.2.4.3) except that 16 U RNaseOUT™ was used to minimise the reaction volumes. The final concentration of wild-type NTH-RNase E was reduced to 1 nM. The reaction was started by addition of LU13. Final substrate concentrations were: 0, 0.5, 1, 2, 4, 6, 8, 10, 12 and 14 µM for 5'-monophosphorylated LU13 and 0, 10, 25, 50, 100, 250, 500, 750, 1000 µM for 5'-hydroxylated LU13. Samples were taken after 0, 2 and 5 min and quenched with an equal volume of 2x RNA loading dye. Samples were separated and analysed by denaturing PAGE as described (Section 2.2.4.4), alongside a series of dilutions of LU13 at concentrations of: 0, 0.05, 0.1, 0.5, 1, 5, 10, 20, 40, 80 and 120 nM. Initial rates of product formation were calculated using the calibration curve of the serial dilutions and were fitted by non-linear regression, using OriginPro 8.6, to the Michaelis-Menten equation as shown in Equation 2:

$$\frac{v}{[E]} = \frac{k_{\mathrm{cat}}[S]}{K_{\mathrm{M}} + [S]} \qquad \textbf{Equation 2.}$$

Where *v* is the initial rate, [*E*] is the total enzyme concentration, $k_{cat}$ is the enzyme turnover number, [*S*] is the initial substrate concentration and $K_M$ is the Michaelis constant.

2.2.4.6 Inhibition assays of RNase E

To screen for transcripts that bind to RNase E, inhibition assays were performed using 5'-monophosphorylated LU13 as the reporter ligand due to the high rate of cleavage at low concentrations. Assays were performed under similar conditions as described (Section 2.2.4.3) with fixed concentrations of wild-type NTH-RNase E and 5'-monophosphorylated LU13 at 5 nM and 75 nM, respectively. Samples were quenched and separated by denaturing PAGE as described (Section 2.2.4.4). Gels were quantified as above and initial rates were calculated using Excel as described (Section 2.2.4.4).

2.2.4.7 Circular Dichroism of BR15

5'-hydroxylated LU13 and BR15 were diluted to a concentration of 7.5 µM in 25 mM *bis*-Tris-propane (pH 8.3), 100 mM KCl, 15 mM $MgCl_2$, 0.1% (v/v) Triton X-100 in a final volume of 240 µl. The solutions were placed in a quartz cuvette with path length of 1 mm. The cuvettes were placed into a Jasco J-715 spectropolarimeter and allowed to equilibrate to 37°C for 10 min. Two CD scans were performed at 50 nm/min over a range of 220-320 nm with a 2 s response time, 1 nm pitch and 1 nm bandwidth. The sensitivity was set to 10 mHg and slit width was set to 1000 µm. The CD spectrum of the buffer was taken first and was subtracted from the average spectrum of each oligonucleotide. Molar ellipticity was then calculated using the near UV equation as shown in Equation 3:

$$[\theta] = \frac{\theta}{10cl} \qquad \textbf{Equation 3.}$$

Where $[\theta]$ is the molar ellipticity, $\theta$ is the ellipticity measured, *c* is the molarity and l is the path length of the cuvette. Data was then zero-corrected at 320 nm. High tension values remained below 450 mV for all experiments indicating a high signal to noise ratio.

2.2.4.8 Dilutions of BR15

An aliquot of the BR15 sample from the CD analysis was diluted to concentrations of 300, 250, 200, 150, 100, 75, 50, 25, 10, 5, and 1 nM using 25 mM *bis*-Tris-propane (pH 8.3), 100 mM KCl, 15 mM $MgCl_2$, 0.1% (v/v) Triton X-100, 20% (v/v) glycerol. These samples were then separated on 1% (w/v) agarose, 1x TBE gels. The gels were imaged as described (Section 2.2.4.4). A minimum concentration of 7.5 nM of BR15 was then determined for the binding assays.

2.2.4.9 Electrophoretic mobility shift assays of BR15 binding with NTH-RNase E

NTH-RNase E samples were dialysed on MF-Millipore 0.025 µm membrane filters (Merck, USA) floating on 10 ml of 25 mM *bis*-Tris-propane (pH 8.3), 100 mM KCl, 15 mM $CaCl_2$, 0.1% (v/v) Triton X-100, 20% (v/v) glycerol, and 1 mM DTT for 30 min at room temperature. Protein dilutions of NTH-RNase E at 18 µl volumes were prepared in 25 mM *bis*-Tris-propane (pH 8.3), 100 mM KCl, 15 mM $CaCl_2$, 0.1% (v/v) Triton X-100, 20% (v/v) glycerol, and 1 mM DTT as follows: 10, 5, 2.5, and 1.25 µM, 620, 312, 156, 78, 39, 19.5, 9.5, 4.8, 2.4, 1.2, 0.6, 0.3 and 0 nM. To each of these volumes, 2 µl of 75 nM BR15 was added. A control was prepared of 10 µM NTH-RNase E without BR15. Reactions were incubated at 37°C for 20 min, cleared by centrifugation at 16,100 x *g* for 1 min, and separated on 1% (w/v) agarose gels for 35 min. Gels were imaged as described previously (Section 2.2.4.4). Bands were quantified via 2D densitometry using AIDA v4.22 software. The proportion of bound to unbound BR15, represented as shifted and non-shifted bands respectively, was calculated from these values and plotted as a function of protein concentration. From this graph, the $K_d$ value was calculated as the concentration of protein at which the binding of BR15 was 50% of the maximum. This analysis was re-performed with buffer containing substitution of $CaCl_2$ for $MgCl_2$ to determine the effect of divalent cation composition on ligand-protein interaction.

2.2.4.10 Competition binding assays

Dilutions of competitor RNAs at 16 µl volumes were prepared in the same binding buffer as described above (Section 2.2.4.9). Final competitor RNA concentrations are detailed in the figure legends. To each of these volumes, 2 µl of 75 nM BR15 and 2 µl of 200 nM NTH-RNase E were added. Samples were set up and analysed as described above. The proportion of bound to unbound BR15 was calculated from the band intensity values, and plotted as a function of competitor RNA concentration. From this graph, $IC_{50}$ values were calculated as the concentration of competitor RNA at which the dissociation of the BR15-NTH complex was 50% maximum (restored).

## 2.3 General DNA Methods

### 2.3.1 DNase decontamination

To ensure solutions contained no DNase contaminants, all solutions were autoclaved at 121°C for 20 min. All DNA samples were stored at -20°C.

### 2.3.2 Genomic DNA methods

2.3.2.1 Isolation of bacterial genomic DNA

Genomic DNA was extracted from MG1655 cells in a similar method as described previously (Section 2.2.2.1). However, phenol solutions were saturated with 10 mM Tris-HCl (pH 8.0). The pellet produced towards the end was further resuspended in 0.4 ml of TE buffer and then mixed with 12.5 µl of 5 M NaCl and 1 ml of absolute ethanol. The genomic clump of DNA that formed was then transferred to a new 1.5-ml Eppendorf tube, resuspended in 0.4 ml of TE buffer and extracted with basic phenol (pH 8.0), followed by 3 rounds of basic phenol: chloroform: isoamyl alcohol (25:24:1) and finally chloroform: isoamyl alcohol (49:1) as described (Section 2.2.2.1). The aqueous phase was transferred to a new tube and the nucleic acid precipitated by adding 0.1 volumes of 5 M NaCl and 2.5 volumes of absolute ethanol, pelleted via centrifugation at 16, 100 x *g*, 4°C for 15 min and washed with 70% (v/v) ethanol before being resuspended in 200 µl of sterile water.

2.3.2.2. Quantification of DNA

The concentration of DNA in the sample was calculated in a similar fashion as described previously (Section 2.2.2.3). For double-stranded DNA, an $A_{260}$ of 1 corresponds to ~50 ng/µl. The 260: 280 absorbance ratio for pure DNA was ~1.8.

2.3.2.3 Design of PCR primers

All deoxyribonucleotide primers in this work were synthesised by MWG operon (Eurofins, Germany). Primers were designed using the Primer3Plus software (Rozen and Skaletsky, 2000) with the following criteria: $T_m$ (°C) range of 57 to 63°C; GC (%) range of 40 to 60%; maximum 3' self complementarity of 3; and maximum Poly-X of 5. Forward and reverse primers were designed to start at the 5' and 3' end of the known transcriptional unit, respectively, using information from EcoCyc (Keseler et al., 2013). Primers are detailed in Table 2.2.

| **Product name** | **Product size** | **Sequence** |
|---|---|---|
| cspA | 420 | FOR 5'-TTTGACGTACAGACC-3' |
| | | REV 5'- AAAATCCCCGCCAAATGGCAGGG-3' |
| rrfB | 269 | FOR 5'-AAGCTGTTTTGGCGGATGAG-3' |
| | | REV 5'- ACGAAAGGCCCAGTCTTTC-3' |
| argX | 481 | FOR 5'-AACGGCGCTAAGCGCCCG-3' |
| | | REV 5'-AAAAAACCCCGCCGAAGCGG-3' |

| | | |
|---|---|---|
| m793 | 793 | FOR 5’-CGCAACGCCGATAAGGTA-3’ |
| | | REV 5’-ATTGAATGAACGCAGAAAAGC-3’ |
| g386 | 386 | FOR 5’-CCGTAACGACGCAGAAATG-3’ |
| | | REV 5’-GCGTCGCTGTGGATATTTTATT-3’ |
| cspC | 781 | FOR 5’-ACGCCAGTTTAAGTATCTGCC-3’ |
| | | REV 5’-TTCACGCGAAAGAGGCT-3’ |
| rnc | 871 | FOR 5’-GAAGTTTAAGGTTGGCAC-3’ |
| | | REV 5’-TAAATCCGCAGTAACTTTTATCG-3’ |
| uspG | 525 | FOR 5’-GCGAATGATTTGTTCATGATT-3’ |
| | | REV 5’-ATTAAAAAGCCCCGCCG-3’ |
| ftsI | 350 | FOR 5’-TGGCGCTACCAGGCG-3’ |
| | | REV 5’-TTACGATCTGCCACCTGTCC T-3’ |
| envZ | 193 | FOR 5’-ATGTTGATGACCGACAAACTG-3’ |
| | | REV 5’-GGCCGCCCAGTTGCT-3’ |
| rng cat | 165 | FOR 5’-AATGTGTGGCGGGTGAAG-3 |
| | (MC1061)/1492 | REV 5’-TAAACACCAGATAGCGAGAAGG-3’ |
| | (GM11) | |

**Table 2.2 Sequences, product sizes and annealing temperatures of primers used to make cDNA templates for generation of ‘direct’ entry candidates and controls.** All forward primers contained additional start sequence (5’-ATCCTAATACGACTCACTATAGGG-3’) where the T7 promoter sequence is underlined. Primers for further dissections have not been provided and instead schematics are shown in appropriate figures with the boundaries of each substrate.

For cDNA targets to be used as templates for *in vitro* transcription, a T7 promoter (5’-ATCCTAATACGACTCACTATAGGG-3’) was integrated into the 5’ end of the forward primer.

2.3.2.4 Polymerase chain reaction

Standard PCR reactions consisted of 100 ng of genomic DNA incubated with 2 U of GoTaq® DNA polymerase, 4.5 mM $MgCl_2$, 0.8 mM dNTPs, 500 nM forward primer, 500 nM reverse primer, and 5% (v/v) DMSO in 1x Gotaq Flexi colourless buffer. PCR reagents were purchased from Promega (UK) except for DMSO and dNTPs, which were purchased from Sigma Aldrich and Invitrogen, respectively. The standard thermal cycle programme used was 95°C for 5 min, followed by 30 cycles of 95°C for 30 s, 58-62°C for 30 s and 72°C for 60 s. After 30 cycles, the reaction was held for a final extension of 72°C for 7 min. A 2 µl sample of the PCR products was mixed with 1 µl of 6x DNA loading dye and 3 µl

of sterile water and separated on a 1.2% (w/v) agarose gel alongside a Generuler$^{TM}$ 100 bp DNA ladder (Thermo Scientific, USA).

2.3.2.5 PCR purification

PCR amplicons that contained no contaminating bands were purified using the QIAquick PCR purification kit (Qiagen, ND). For PCR products that contained high levels of contamination, a gel extraction was performed. The PCR product solution was mixed with 0.2 volumes of 6x DNA loading dye and separated on 100 ml 1.2% (w/v) agarose gels with 50 mm wide wells prepared as described (Section 2.2.2.4). The bands corresponding to the correct sized PCR product were excised and placed into 2-ml Eppendorf tubes. The rest of the protocol was completed using the QIAquick gel extraction kit (Qiagen, ND) as per the manufacturer's instruction using a benchtop centrifuge. Purified cDNA was then quantified as described (Section 2.3.2.2).

**2.3.3 Plasmid DNA methods**

2.3.3.1 Introduction of plasmid by transformation

Aliquots of BL21 (DE3) or DH5α competent cells at a volume of 25 µl were incubated with 1 µl of plasmid solution on ice for 30 min. Cells were then heat shocked at 42°C for 45 s before being immediately placed back on ice for 2 min. Cells were mixed with 475 µl of LB broth and incubated at 37°C for 1 h with shaking (200 rpm). Cell cultures were spread on LB agar plates containing the appropriate antibiotic for plasmid selection (e.g. 100 µg/ml carbenicillin for pET16b-based constructs) and incubated overnight at 37°C. Well isolated colonies were picked and plasmids were purified and sequenced as described below (Section 2.3.3.2).

2.3.3.2 Purification of plasmid DNA from bacteria

*E. coli* strains containing plasmids were spread onto LB agar plates containing appropriate antibiotics and incubated overnight at 37°C. Well isolated colonies were picked and used to inoculate 10 ml of LB broth (with appropriate antibiotic) in 50-ml Falcon tubes (Starlab, Germany). Cultures were incubated at 37°C with shaking (200 rpm) for 12-16 h. Cells were harvested by centrifugation at 3,300 x *g*, 4°C for 10 min and the supernatant was discarded. Plasmid DNA was purified using a Wizard SV plasmid preparation kit (Promega, USA) as per the manufacturer's instructions. Plasmid integrity was confirmed by DNA sequencing (GATC biotech, Germany) using the primers detailed in Table 2.3 below.

| Primer name | Sequence | Suitable range on *rne* |
|---|---|---|
| T7 prom | 5'-TAATACGACTCACTATAGGG-3' | <1 (-150) |
| pRne1 | 5'-ATGAAAAGAATGTTAATCAACGCAA-3' | 1-190 |
| pRne2 | 5'-GTCACGGTTTCCTCCCACTA-3' | 191-367 |
| pRne3 | 5'-CGGGTAGCTATCTGGTTCTGATG-3' | 368-550 |
| pRne4 | 5'-TAAGCTTCCGTCTGAAACACTG-3' | 551-790 |
| pRne5 | 5'-CGAGATCCCGCTGTTCAG-3' | 791-980 |
| pRne6 | 5'-CGATGAGATTGCTCGTCAGC-3' | 981-1151 |
| pRne7 | 5'-GCTGGAAATGTCCCGTCA-3' | 1152-1380 |
| pRne8 | 5'-GCCATTGAAACTCGTCAGGA-3' | 1381-1587 |
| T7 term | 5'-GCTAGTTATTGCTCAGCGG-3' | >1587 (+64) |

**Table 2.3 Sequences and annealing positions of primers used to sequence *rne* insert in pRne529N.**

## 2.4 General Protein Methods

### 2.4.1 Overexpression of hexahistidine-tagged NTH-RNase E in *E. coli*

BL21 (DE3) cells transformed with pRne529N, as described above (Section 2.3.3.1), were plated, picked and cultured as described (Section 2.3.3.2) with media containing 100 µg/ml carbenicillin. Overnight cultures at a volume of 8 ml were used to inoculate 800 ml of LB broth.. Expression of the chromosomal T7 RNA polymerase gene was induced by adding IPTG to a final concentration of 1 mM when cultures reached an $OD_{600}$ ~ 0.8. Induced cultures were incubated under the same conditions for 3 h to allow production of the pRne529N product.

### 2.4.2 Purification of hexahistidine-tagged NTH-RNase E

2.4.2.1 Preparation of cleared extract from cell lysate

Cells were harvested by centrifugation at 3,300 x *g*, 4°C for 30 min using a SH-3000 swing bucket rotor (Sorvall, Germany). Cells pellets were washed by resuspension in 20 ml of ice-cold wash buffer (20 mM Tris-HCl [pH 7.6], 0.5 M NaCl, 50 mM imidazole) and re-pelleted as before. Cell pellets were resuspended in 10 ml of wash buffer with 1 cOmplete Mini EDTA-free protease inhibitor cocktail tablets (Roche, Germany). Cells were then lysed at 15,000 psi in a Z-plus 1.1kW Constant systems cell disruptor with a one shot head (Constant systems Ltd, UK). Cell lysate was diluted in wash buffer to a final volume of around 30 ml and cleared by ultracentrifugation at 100,000 x *g*, 4°C for 30 min using a Beckman Optima™ XPN ultracentrifuge (SW32 Ti rotor). The supernatant was passed through a 0.45 µm syringe filter (Sartorius, Germany) to remove residual precipitants.

2.4.2.2 Nickel affinity chromatography

Protein was purified using an ÄKTA Explorer FPLC system (GE healthcare, USA). All buffers used during this process were filtered through 0.2 µm Vacuum driven Stericups (Millipore, USA) and degassed on a magnetic stirrer for 30 min. Both pumps were washed with deionised water, followed by wash buffer (20 mM Tris-HCl [pH 7.6], 0.5 M NaCl, 50 mM imidazole) through inlet A11, and then elution buffer (20 mM Tris-HCl [pH 7.6], 0.5 M NaCl, 1 M imidazole) through inlet B1. A 1-ml HiTrap Nickel chelating HP column (GE healthcare, USA) was washed with 10 ml of deionised water, followed by charging with 1 ml of 0.5 M $NiCl_2$ and further washing with 10 ml of deionised water at a flow rate of 1 ml/min. The column was equilibrated with 5 ml of wash buffer (prepared as described above) and the lysate was loaded onto the column at a flow rate of 0.7 ml/min using an external peristaltic pump. The flow through was retained for SDS-PAGE. The column was then attached to the ÄKTA system at valve 2. The programme for the purification was as follows: 4 column volumes 0% B1 (Using A11 as diluent), 10 column volumes B1 gradient 0-10%, 10 column volumes B1 gradient 10-100%, 10 column volumes 100% B1, 10 column volumes 0% B1. Samples were collected in 1.5-ml volumes at a flow rate of 1 ml/min. To each fraction, 15 µl of 1 M DTT, 15 µl of 1 M $MgCl_2$, 1.5 µl of 0.5 M EDTA, and 75 µl of 100% (v/v) glycerol were added. Peak fractions were pooled and desalted at 4°C in PD-10 Sephadex G25 10 ml desalting columns (GE healthcare, UK) equilibrated with 20 mM Tris-HCl (pH 7.6), 0.5 M NaCl, 10 mM $MgCl_2$, 10 mM DTT, 0.5 mM EDTA, 5% (v/v) glycerol. Protein samples were then concentrated in Corning spin-X UF 20 ml concentrators 50,000 MWCO (Corning International, Japan) by centrifugation in a SH-3000 swing bucket rotor at 3,300 x *g*, 4°C for 10 min.

**2.4.3 SDS-polyacrylamide gel electrophoresis**

Resolving gel solutions were produced at a concentration of 15% by mixing 7.5 ml of 30% (w/v; 29:1 acrylamide: *bis*-acrylamide) acrylamide, 3.8 ml of 1.5 M Tris-HCl (pH 8.8), 75 µl of 20% (w/v) SDS together to a final volume of 15 ml. Polymerisation was catalysed by adding 150 µl of 10% (w/v) APS and 15 µl of TEMED, followed by thorough mixing. The resolving gel was set in a vertical PAGE gel cast under a layer of absolute ethanol. Stacking gel solutions were produced at a concentration of 5% by mixing 0.8 ml of 30% (w/v; 29:1 acrylamide: *bis*-acrylamide) acrylamide, 0.63 ml of 1 M Tris-HCl (pH 6.8), 25 µl of 20% (w/v) SDS together to a final volume of 5 ml. Polymerisation was catalysed by adding 50 µl of 10% (w/v) APS and 5 µl of TEMED, followed by thorough mixing. The stacking gel was set on top of the resolving gel with 1-mm thick gel combs. After polymerisation, the whole gel was placed into a PAGE tank (Bio-Rad) topped with 1x SDS running buffer. Samples were prepared by addition of 5 µl of 2x SDS running buffer to 5 µl of protein solution. Samples were denatured by incubation at 99°C for 5 min and separated on the gel at 25 mA for 1 h.

### 2.4.4 Staining of protein

After separation, stacking gels were cut from the resolving gels using a clean razor and discarded. Resolving gels were placed in a plastic container containing 200 ml of Coomassie solution (0.25% w/v Coomassie Brilliant Blue R-250, 40% [v/v] methanol, 10% [v/v] glacial acetic acid) and placed in a microwave at full power for 10-20 s. Gels were left to stain in containers for at least 4 h with gentle rocking. Coomassie stain was removed from the contained and gels were destained in 200 ml of destain solution (40% [v/v] methanol, 10% [v/v] glacial acetic acid) for 2 h with gentle rocking, replacing older solution with fresh destain every 10-20 min. Destained gels were imaged under white light from above in a Transilluminator (Syngene).

### 2.4.5 Quantitation of NTH-RNase E

Protein concentrations were determined using Bradford assays. A standard curve was produced using 0, 5, 10, 15, 20, 25 and 30 µg of BSA at volumes of 20 µl. Protein samples were made at similar volumes with several dilutions. Bradford dye concentrate (Bio-Rad) was diluted 1 part in 4 parts distilled water and 1 ml was mixed with each of the protein solutions. Samples were left to incubate at room temperature for 5 min. Absorbance values were measured at 595 nm and concentrations of protein in the samples were determined. Concentrations were confirmed by running dilutions of protein sample on SDS-PAGE gels as described (Section 2.4.3), against a dilution series of BSA followed by Coomassie staining of the gels as described (Section 2.4.4), and quantification of bands (Section 2.2.3.5).

# Chapter 3

# Biochemical characterisation of RNase E cleavage

## 3.1 Introduction

The RNase E protein consists of a 1061 amino acid chain that has two function halves. The first 529 amino acids make up the N-terminal half, a highly-structured region that displays the main endonucleolytic activity and is required for cell viability (McDowall and Cohen, 1996, Redko et al., 2003). The NTH self-associates to form a functional dimer with two symmetrical active sites each set within a single-stranded-RNA-binding channel (Callaghan et al., 2005a, Caruthers et al., 2006). The dimers then associate to form a homotetramer, which shows greatly enhanced activity (Callaghan et al., 2003, Caruthers et al., 2006). The remaining 532 amino acids make up the C-terminal half, which has very little tertiary structure (Callaghan et al., 2004) and is dispensable for cell viability (Kido et al., 1996, Leroy et al., 2002). The main roles of the CTH are to provide a scaffold for components of the RNA degradosome (Vanzo et al., 1998), provide ancillary RNA-binding regions (McDowall and Cohen, 1996, Kaberdin et al., 2000, Taraseviciene et al., 1995), and locate RNase E to the inner surface of the cytoplasmic membrane (Khemici et al., 2008).

One of the most characterised substrates for RNase E is a single-stranded oligonucleotide called BR13, which is derived from the first 10 nt of RNAI, a repressor of ColE1-type plasmid replication (McDowall et al., 1995). Using this oligonucleotide it has been found that RNase E cleaves RNA within single-stranded regions (McDowall et al., 1995, Redko et al., 2003), with particular preference for regions rich in adenine and uridine residues (McDowall et al., 1994, Kaberdin, 2003). As expected with an endonuclease that cleaves at single-stranded regions, studies of RNase E activity have found that adjacent stem loops tend to inhibit cleavage (McDowall et al., 1995, Belasco et al., 1986, Bricker and Belasco, 1999, Bouvet and Belasco, 1992, Arnold et al., 1998). However, other studies have found that some stem loops actually enhance cleavage by RNase E (Ehretsmann et al., 1992, Cormack and Mackie, 1992, Mackie and Genereaux, 1993, Diwa et al., 2000), suggesting that the location and conformational context of paired and unpaired regions of RNA are the major determinants of RNase E activity (Cormack and Mackie, 1992).

More recently, certain substrates have been shown to be cleaved more rapidly if they contain a monophosphate group at the 5’ end compared to a triphosphate or hydroxyl group (Mackie, 1998, Redko et al., 2003, Garrey et al., 2009, Mackie, 2013a). In addition, this 5’-monophosphate-dependent pathway has been confirmed *in vivo* (Mackie, 2000, Luciano et al., 2012, Garrey and Mackie, 2011), particularly in substrates that have been circularised to prevent access of RNase E to the 5’ end (Mackie, 2000). The physiological significance of this mechanism was confirmed when an RNA 5’ pyrophosphohydrolase (RppH) was discovered in *E. coli*, that converts 5'-triphosphate groups on nascent transcripts to monophosphates (Celesnik et al., 2007). Inactivation of RppH does

not affect cell viability, but it does cause the stabilisation of around 25% of transcripts, suggesting that pyrophosphate removal does play an important, albeit not essential, role in the degradation of several transcripts in *E. coli* (Deana et al., 2008).

Initially it was believed that a 5'-monophosphate group might stimulate cleavage by RNase E by catalytically activating the enzyme (Jiang and Belasco, 2004). The crystal structure of NTH-RNase E with RNA oligonucleotides has shown that the monophosphate of the substrates engages the 5' sensor, and that engagement may trigger a conformational change in RNase E (Callaghan et al., 2005a, Koslover et al., 2008). However, more recently it has been shown that 5'-hydroxlated oligonucleotides can be cleaved rapidly by RNase E when they are pre-incubated at lower temperatures to promote the formation of quadruplexes. These structures present multiple single-stranded regions that can then provide additional contacts with RNase E, hence increasing the overall affinity of the interaction (Kime et al., 2010). Cleavages that occur in this manner have been termed 'direct' entry cleavages (Coburn and Mackie, 1999). Moreover, the model that proposes that a 5' monophosphate catalytically activates RNase E fails to explain the presence of substrates that are cleaved by RNase E regardless of the 5'-end status (Hankins et al., 2007, Garrey and Mackie, 2011). Therefore, it is more likely that a 5'-monophosphate group increases the affinity of the substrate for RNase E, and that absence of 5'-monophosphate binding may not present a catalytic barrier, providing that the substrate can make suitable contacts by direct entry.

Most direct entry sites that have been identified so far are located within the trailer sequences of tRNA precursors (Garrey and Mackie, 2011). Indeed, RNase E has been shown to initiate the maturation of tRNAs, by making endonucleolytic cleavages within 3'-trailer sequences (Li and Deutscher, 2002, Ow and Kushner, 2002, Soderbom et al., 2005, Perwez et al., 2008), providing access for 3' exonucleases that remove the remaining 3' trailer in a pathway that has been termed the "exonucleolytic pathway" of tRNA maturation (Li and Deutscher, 1996, Hartmann et al., 2009). In addition, RNase E cleavage within tRNA precursors also provides access for RNase P, which removes the 5'-leader sequence by a single endonucleolytic cleavage (Altman et al., 1987, Li and Deutscher, 2002). *E. coli* also contains RNase BN, a homologue of tRNase Z that can make an endonucleolytic cleavage within the precursor at the 3' end of the tRNA unit (Ezraty et al., 2005). This cleavage results in the entire removal of the 3' trailer in a single-step that has been termed the "endonucleolytic pathway" of maturation (Pellegrini et al., 2003). However, all *E. coli* tRNAs contain an encoded CCA motif at the 3' end (Marck and Grosjean, 2002), which prevents access of RNase BN (Callahan et al., 2000, Pellegrini et al., 2003), hence further establishing the importance for RNase E in maturation at the 3' end of tRNAs. If direct entry plays a major role in tRNA maturation, which is

very likely given the similar structural arrangements of the tRNA precursors compared to quadruplexed oligonucleotides, then tRNA precursors will make ideal substrates for biochemical characterisation of this pathway.

## 3.2 Results

In this chapter, the general model for direct entry was tested *i.e.* that multiple single-stranded regions within RNA promote cleavage by RNase E in the absence of a 5' monophosphate. Two different forms of the NTH-RNase E were used for these studies, the wild-type form, which was purified using immobilised metal affinity chromatography (IMAC) as part of this study, and the T170V mutant (5' sensing mutant), which was purified in a similar manner by Louise Kime from a previous study.

### 3.2.1 Characterising a mutant deficient in 5' sensing

In order to confirm the activity of both enzymes, a discontinuous cleavage assay was performed using the model single-stranded substrate LU13. This RNA oligonucleotide is 13 nt long and contains a fluorescein label at the 3' end. Upon cleavage a downstream product is produced that is 5 nt in length, which can be separated from the full length substrate by denaturing PAGE as shown in Figure 3.1.

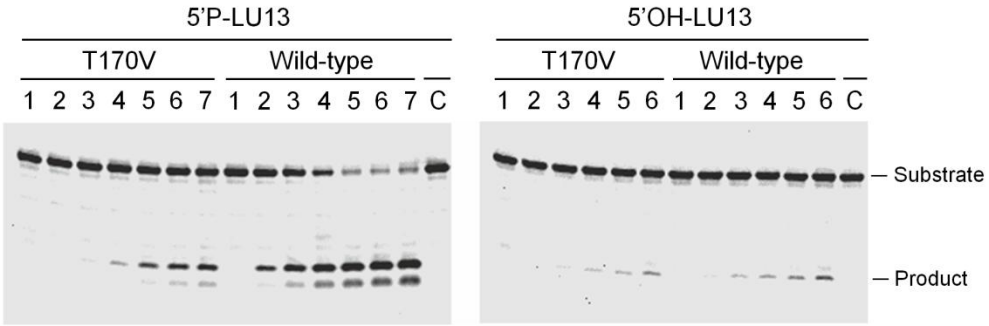


**Figure 3.1 Cleavage of defined oligonucleotide substrates by RNase E.** The 5'-monophosphorylated and -hydroxylated LU13 substrates were synthesised by MWG operons (Eurofins, Germany). Final substrate and enzyme concentrations were 250 nM and 5 nM, respectively. Identities of the substrate and enzyme are shown at the top of each image. Samples were taken after various time points upon incubation, quenched in 2x RNA loading dye, denatured at 95°C, separated on 20% polyacrylamide gels, and scanned at 473 nm. For 5'P-LU13 (left), lanes 1-7 contain samples taken at 0, 2, 5, 15, 30, 60, 120 and 180 min after incubation of substrate with enzyme. For 5'OH-LU13 (right), lanes 1-6 contain samples taken at 0, 15, 30, 60, 120, and 180 min after incubation of substrate with enzyme. Lane C contains substrate incubated without enzyme for 180 min. The identities of the substrates and cleavage products are shown at the right of each image.

The first substrate used to compare activities of T170V with the wild-type NTH-RNase E was modified to contain a 5'-monophosphorylated end. As expected, T170V displays a significant reduction in its ability to cleave this substrate compared to the wild type, given that the hydrophilic interaction between threonine at position 170 and the phosphoryl-oxygen group on the 5' monophosphate is disrupted (Callaghan et al., 2005a). The second substrate used was LU13 with a 5'-hydroxylated end, which appears to be cleaved very slowly by both enzymes. This again is expected, as this 5'-hydroxyl group does not contain a charged oxygen species that can provide an electrostatic interaction with the positively-charged arginine at position 169 in both enzymes (Callaghan et al., 2005a). However, it is important to note that both enzymes appear to cleave 5'-hydroxylated LU13 at a similar rate, suggesting that the T170V mutant retains its "basal" activity (5'-end-independent) and therefore making it an appropriate choice for further analyses of direct entry substrates.

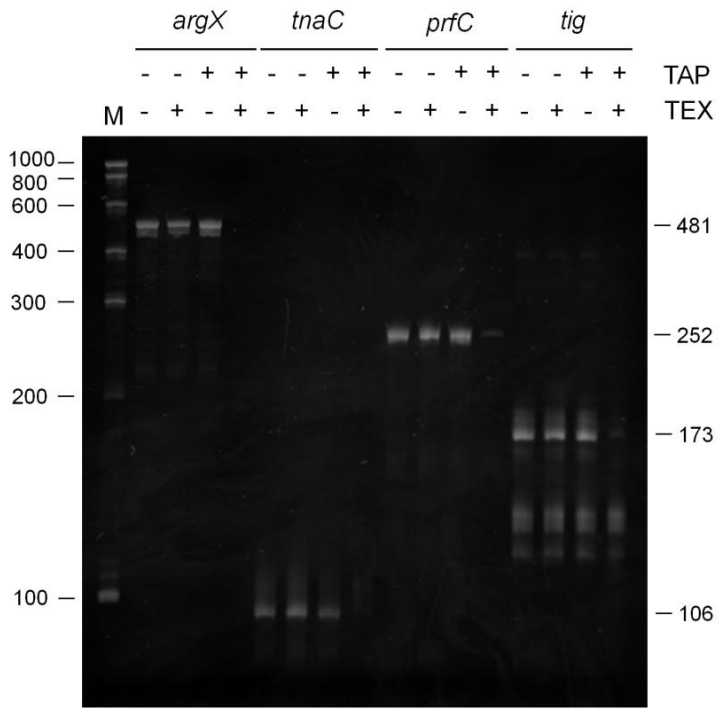


**Figure 3.2 Confirmation of TAP activity using TEX.** The 5'-triphosphorylated transcripts were generated by *in vitro* transcription. Nascent 5'-triphosphorylated ends were converted to 5' monophosphates by incubating transcripts with tobacco acid pyrophosphatase (TAP). The 5'-phosphorylation status was confirmed by incubating these transcripts with Terminator™ 5'-phosphate-dependent exonuclease (TEX). Samples were separated on 8% polyacrylamide gels, which were stained with ethidium bromide and analysed. The substrates and enzymes used are shown at the top of the image. Lane M contains a RiboRuler™ low range RNA ladder with sizes in nt indicated at the left of each image. The sizes in nt of the substrates are shown at the right of the image.

Given that the T170V mutation results in inactivation of the 5' sensor, the next analysis with T170V was performed using the *argX-hisR-leuT-proM* tRNA precursor (simplified as *argX*), a confirmed direct entry substrate (Garrey and Mackie, 2011). The goal of this analysis was to show that rapid cleavage by direct entry can be achieved independent of the 5'-end status of the substrate or 5' sensing by RNase E *in vitro*. However, in order to fully achieve this goal, *argX* with a 5'-monophosphorylated end had to be synthesised as a control. RNA was synthesised *in vitro* from DNA templates using T7 RNA polymerase and consequently had a 5'-triphosphate group. This transcript was "decapped" using tobacco acid pyrophosphatase (TAP) to produce 5'-monophosphorylated transcripts. The 5'-end status was confirmed using Terminator™ 5'-phosphate-dependent exonuclease (TEX), which degrades RNA with a 5'-monophosphate group preferentially, as shown in Figure 3.2. Both *argX* and *tnaC* appear to have been completely degraded, confirming that they are both completely 5' monophosphorylated. However, the degradation of *prfC* and *tig* is incomplete, possibly due to less accessibility of TAP or TEX to the 5' end of these transcripts, which could be occluded by secondary structure.

The 5'-triphosphorylated and -monophosphorylated forms of *argX* were incubated with T170V and wild-type NTH-RNase E and samples taken at various time points were analysed by denaturing PAGE, as shown in Figure 3.3. Efficiency of the initial cleavage(s), as determined by the reduction in the intensity of the band associated with full-length *argX*, was not reduced significantly when the 5'-monophosphorylated substrate was incubated with T170V compared to the wild-type enzyme (compare both assays in the left image of Figure 3.3B), or when the substrates 5' end was triphosphorylated compared to monophosphorylated (compare first assay in left image to first assay in right image).

However, it is important to note that 5' monophosphate-dependent cleavage also plays a role in the maturation of the *argX* tRNA precursor, as evidenced by the cleavage of the 138-nt product to produce the 108-nt and 29-nt products only found in the wild-type NTH-RNase E compared to the T170V assays. This substrate consists of the *proM* tRNA unit with a 5' and 3' flanking region of 4 and 30 nt respectively. This 138-nt substrate lacks numerous single-stranded regions compared to the full length precursor, and therefore it is likely that a 5' monophosphate could provide additional contacts required for subsequent cleavage.

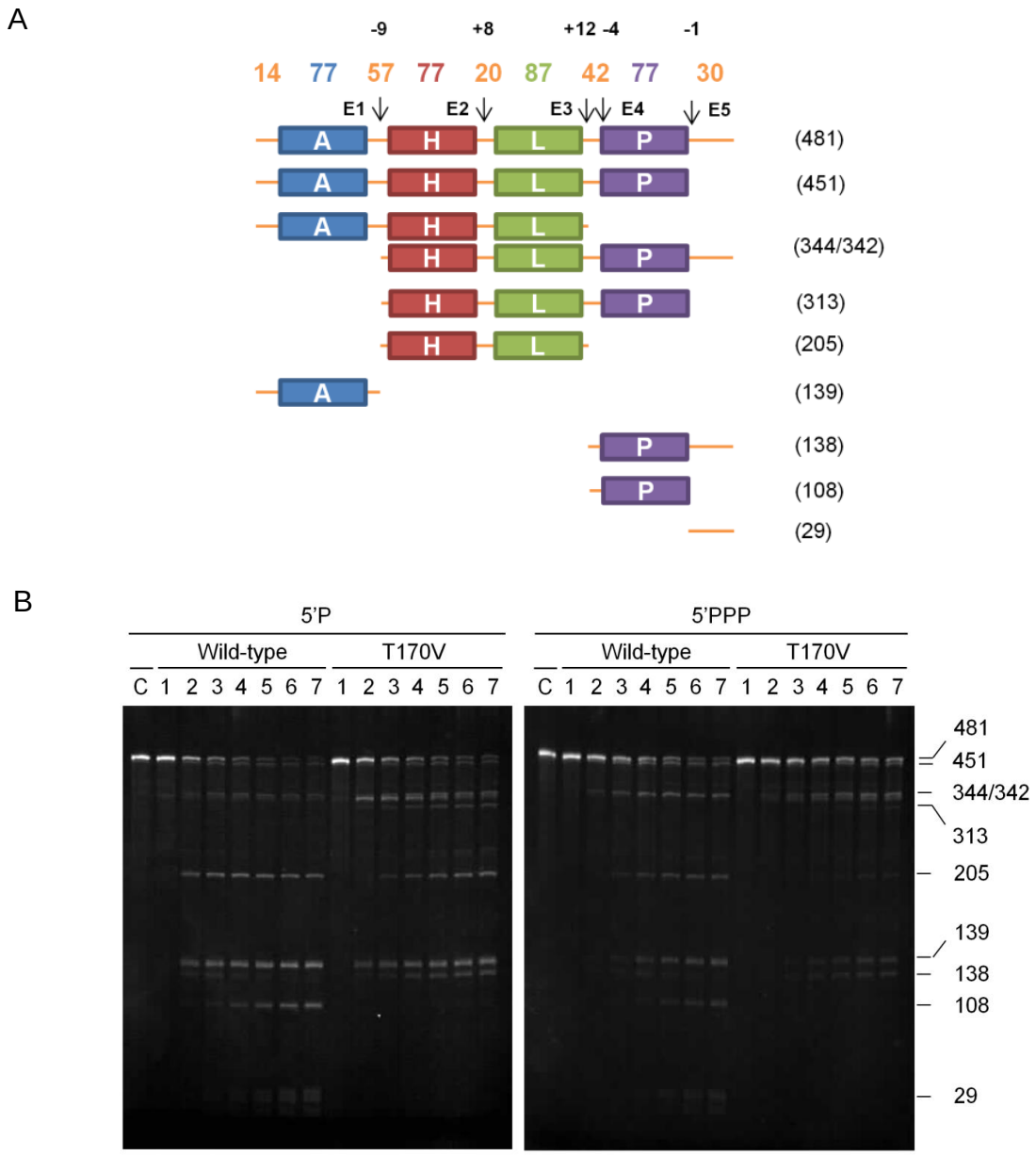


**Figure 3.3 Cleavage of the *argX-hisR-leuT-proM* tRNA precursor by direct entry.** The 5'-triphosphorylated transcripts were generated by *in vitro* transcription and incubated with TAP to produce 5'-monophosphorylated ends as described in Figure 3.2. Panel A shows a schematic of the *argX-hisR-leuT-proM* tRNA precursor with the identities of the various cleavage products. Sizes of the expected products (in nt) are shown on the right. Known RNase E cleavage sites are shown as vertical arrows and were calculated using information from previous studies (Li and Deutscher, 2002, Ow and Kushner, 2002). For Panel B, the 5'-phosphorylation status of the substrate and the enzymes' identity are shown at the top of each image. Final substrate and enzyme concentrations were 180 nM and 5 nM, respectively. Samples were taken after various time points upon incubation, quenched in 2x RNA loading dye, denatured at 95°C, separated on 8% polyacrylamide gels, and stained with ethidium bromide as described in Chapter 2. Lanes 1-7 contain samples taken at 0, 5, 15, 30, 60, 120 and 180 min after incubation of substrate with enzyme. Lane C contains substrate incubated without enzyme for 180 min. The sizes in nt of the substrates and cleavage products are shown at the right of the image.

### 3.2.2 Single-stranded regions promote bypass of the 5'-sensing mechanism

Despite the reduced cleavage of 5'-monophosphorylated LU13, the NTH-RNase E T170V mutant still retains the ability to cleave larger RNA substrates such as *argX* via direct entry. Theoretically, larger transcripts present single-stranded regions that are adjacent, but not contiguous, to sites of cleavage, allowing the RNA to interact in a cooperative manner with the homotetrameric enzyme (Kime et al., 2010). Direct entry has been mainly observed in tRNA precursors, possibly due to the stable tRNA units being able to present the flanking single-stranded regions in the correct confirmation that can engage two adjacent RNA-binding channels on RNase E (Garrey and Mackie, 2011). This additional interaction could cause an increase in affinity of the substrate to RNase E and hence negate the requirement for a 5'-monophosphate group or functional 5' sensor. To confirm this model, two tRNA precursors that contain only one direct entry site were truncated and hybridised with complementary oligonucleotides in order to map the regions that interact with RNase E.

The first substrate to be characterised using NTH-RNase E T170V was the *metT-leuW-glnU-glnW-metU-glnV-glnX* tRNA precursor, as shown in Figure 3.4. Interestingly, cleavage of the major site at position +2 nt downstream of the *metU* functional unit was unaffected by removal of the upstream *metT-leuW-glnU* regions (as shown by cleavage of *m*456), but was almost completely reduced with the subsequent removal of *glnW* (shown as *m*381). Removal of the downstream *glnV-glnX* regions had some effect, although cleavage is still apparent (as shown by cleavage of *m*329, *m*292 and *m*217). This suggests that upstream structural regions that are adjacent to, but not contiguous with, the cleavage site may also play a role in 5'-end-independent cleavage.

**Figure 3.4 Determining the minimal substrate for direct entry cleavage in the *metT-leuW-glnU-glnW-metU-glnV-glnX* tRNA precursor.** The transcripts were generated by *in vitro* transcription as described in Figure 3.2. Panel A shows a schematic of the *metT-leuW-glnU-glnW-metU-glnV-glnX* tRNA precursor with the identities of the various cleavage products. Sizes of the expected products (in nt) are shown on the right. Known RNase E cleavage sites are shown as vertical arrows. Below this schematic the relative positions of the 5' and 3' ends of the truncated substrates are shown relative to the full length precursor. The identities of these truncations are shown at the right. Fragments shown in black and grey are those that were and were not cleaved, respectively. For Panel B, the identity of each truncation is shown at the top of each image. Final substrate and NTH-RNase E T170V concentrations were 180 and 20 nM, respectively. Samples were taken at various time points and analysed as described in Figure 3.3. Lanes 1-5 contain samples taken at 0, 5, 15, 30 and 60 min after incubation with T170V. Lane C contains substrate incubated without enzyme for 60 min. Lane M contains a RiboRuler$^{TM}$ low range RNA ladder with sizes in nt indicated at the left of each image. The sizes in nt of the substrates and cleavage products are shown at the right of the image.

A

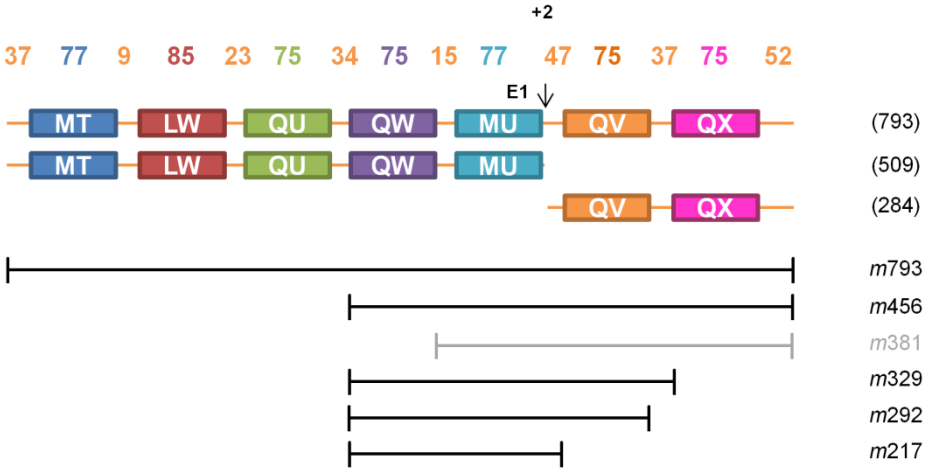
+2
37 77 9 85 23 75 34 75 15 77 47 75 37 75 52
E1
MT LW QU QW MU QV QX
(793)
MT LW QU QW MU
(509)
QV QX
(284)
m793
m456
m381
m329
m292
m217

B

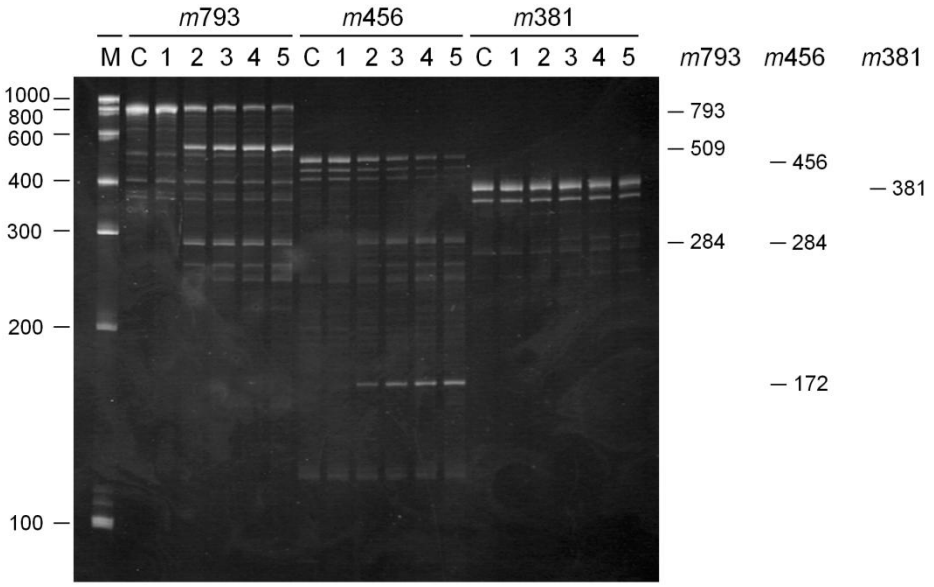
m793 m456 m381
M C 1 2 3 4 5 C 1 2 3 4 5 C 1 2 3 4 5
m793 m456 m381
1000
800
600
400
300
200
100
793
509
456
381
284
172

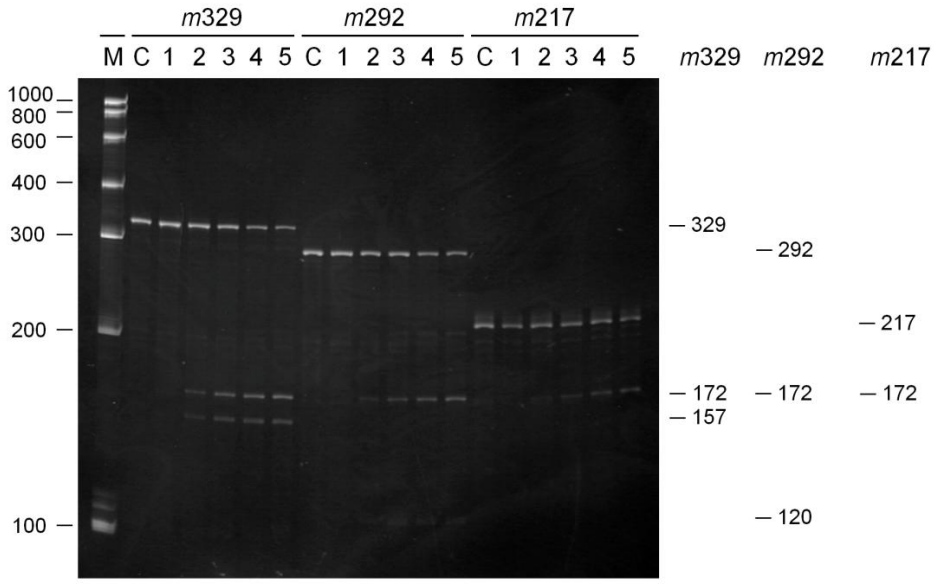
m329 m292 m217
M C 1 2 3 4 5 C 1 2 3 4 5 C 1 2 3 4 5
m329 m292 m217
1000
800
600
400
300
200
100
329
292
217
172
157
172
172
120

In order to confirm that an adjacent single-stranded region is also required for direct entry cleavage, DNA oligonucleotides were hybridised to complementary regions within the RNA fragment *m*292 (see Figure 3.5A for details). In order to confirm the position and extent of hybridisation, RNase H digests were performed as shown in Figure 3.5B.

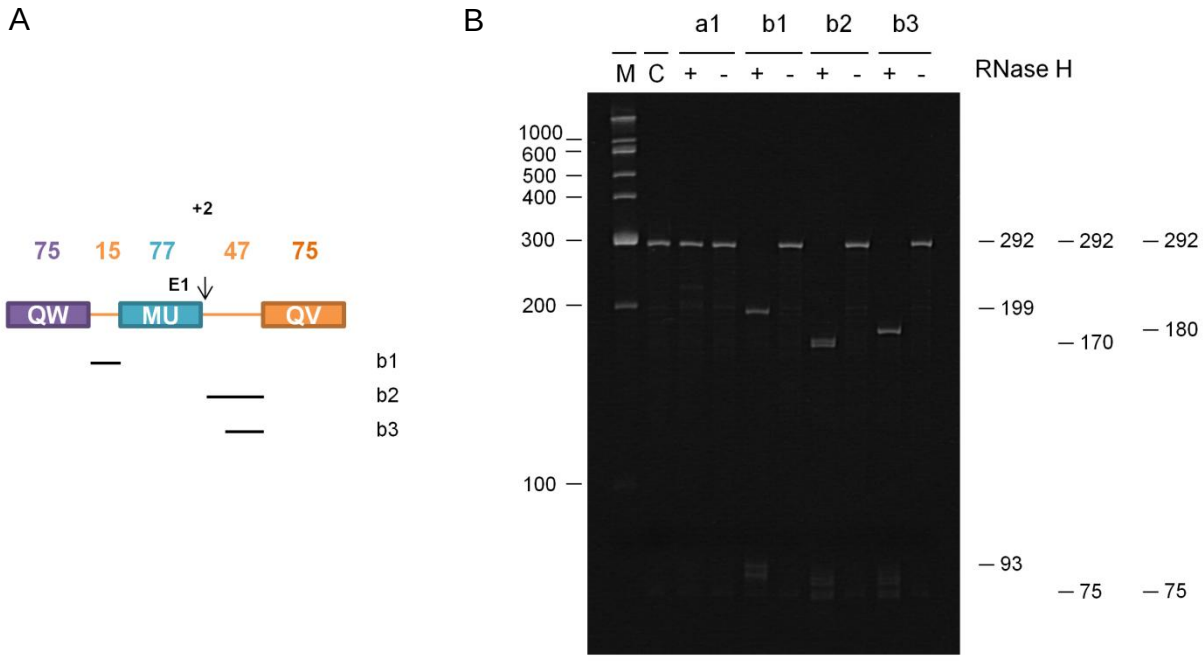


**Figure 3.5 Confirmation of oligonucleotide hybridisation to *m*292 using RNase H.** Panel A shows a schematic of the *m*292 fragment with the relative positions of hybridisation of the DNA oligonucleotides. Panel B shows the conformational RNase H digest results for DNA hybridisation. Several complementary DNA oligonucleotides were hybridised separately to the *m*292 RNA. The RNA was then incubated with RNase H to confirm the position and extent of hybridisation. The results of this diagnosis were analysed on 8% polyacrylamide gels, which were stained with ethidium bromide and analysed. The DNA oligonucleotides used are shown at the top of the image. Lane M contains a 0.1-2 k RNA ladder (Life Techonolgies, USA) with sizes in nt indicated at the left of each image. The sizes in nt of the substrates and products are shown at the right of the image.

Cleavages assays were then performed on these DNA-RNA hybrids and analysed as before. As shown in Figure 3.6, blocking of the 15-nt, single-stranded region between *glnW* and *metU* (labelled as b1) reduced cleavage to a level comparable to blocking of the site itself downstream of *metU* (labelled as b2). Blocking of the single-stranded region up to 8 nt downstream of the major cleavage site (labelled as b3) had little effect on the cleavage rate.

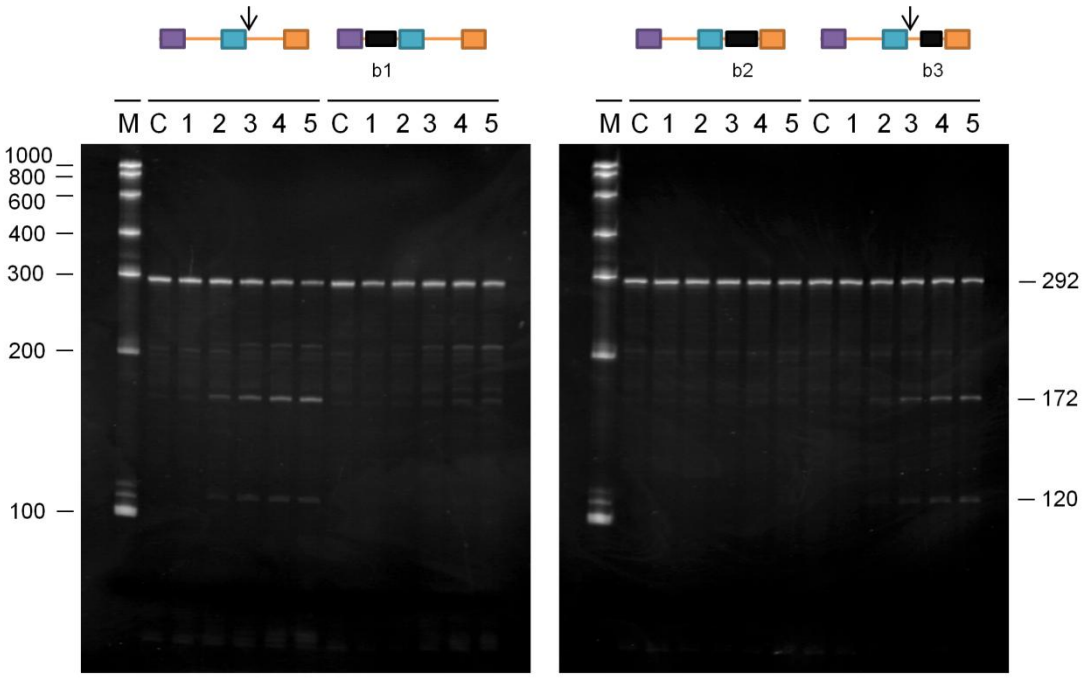


**Figure 3.6 Analysis of direct entry in the *metT* tRNA precursor.** The *m*292 transcript was hybridised with DNA oligonucleotides as described in Figure 3.5. A schematic of the RNA fragment with the positions of the direct entry sites (shown as vertical arrows) and binding of complementary oligonucleotides (shown as black boxes) is shown above each image. Labelling is as described in Figure 3.4B.

These findings indicate that simultaneous interaction of the regions upstream and downstream of *metU* with NTH-RNase E is required for direct entry cleavage of the *metT* tRNA precursor. Assuming the tRNA units fold in a similar manner as the mature tRNAs, the flanking single-stranded regions will be close in space and anti-parallel. The anti-parallel arrangement of these two single-stranded regions mirrors the similar arrangement of the two RNA-binding channels in the RNase E principal dimer. In fact, initial studies into direct entry found that oligonucleotide substrates in a quadruplex conformation can provide similar interactions with NTH-RNase E (Kime et al., 2010). It appears therefore that although the requirements for direct entry, *i.e.* interaction with two or more single-stranded regions, are relatively simple, preference for localised secondary structure that provides the conformational context may increase the selectivity of cleavage.

The second substrate to be characterised was the *glyV-glyX-glyY* tRNA precursor as shown in Figure 3.7. Cleavage at the major site 1 nt downstream of the *glyY* functional unit was unaffected by removal of the *glyV* region (as shown by cleavage of *g*224), but was reduced completely following subsequent removal of *glyX* (shown as *g*148). Just as with the *metT* tRNA precursor, 5'-end-independent cleavage of the *glyV* tRNA precursor is dependent on the presence of adjacent tRNA units found upstream of the cleavage site.

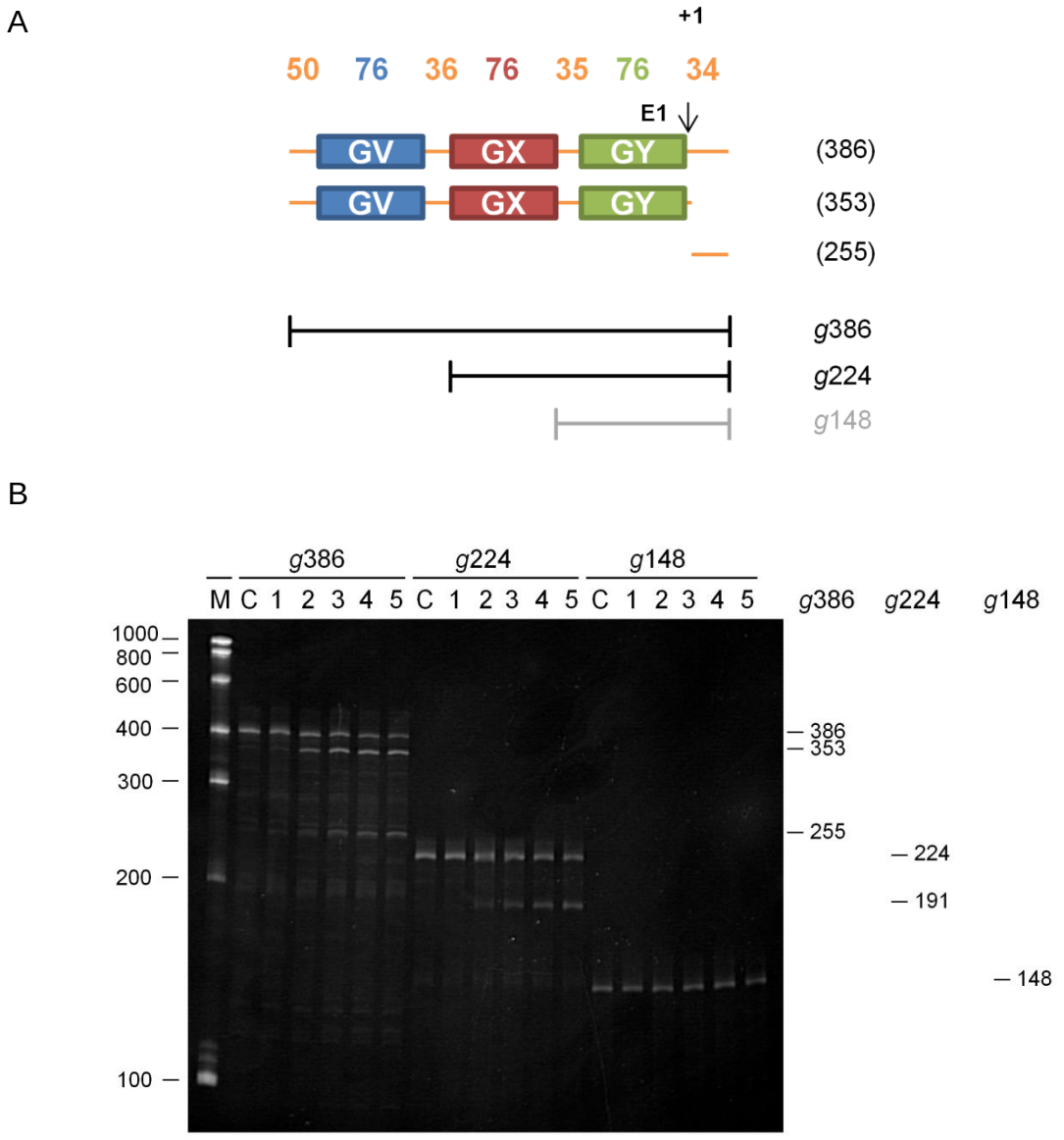


**Figure 3.7 Determining the minimal substrate for direct entry cleavage in the *glyV-glyX-glyY* tRNA precursor.** Panel A shows a schematic of the *glyV-glyX-glyY* tRNA precursor with the identities of the various cleavage products. Labelling is as Figure 3.4A. For Panel B, labelling is as described in Figure 3.4B.

Again, several single-stranded regions within the *g*224 fragment were hybridised with complementary DNA oligonucleotides and digested using RNase H as shown in Figure 3.8.

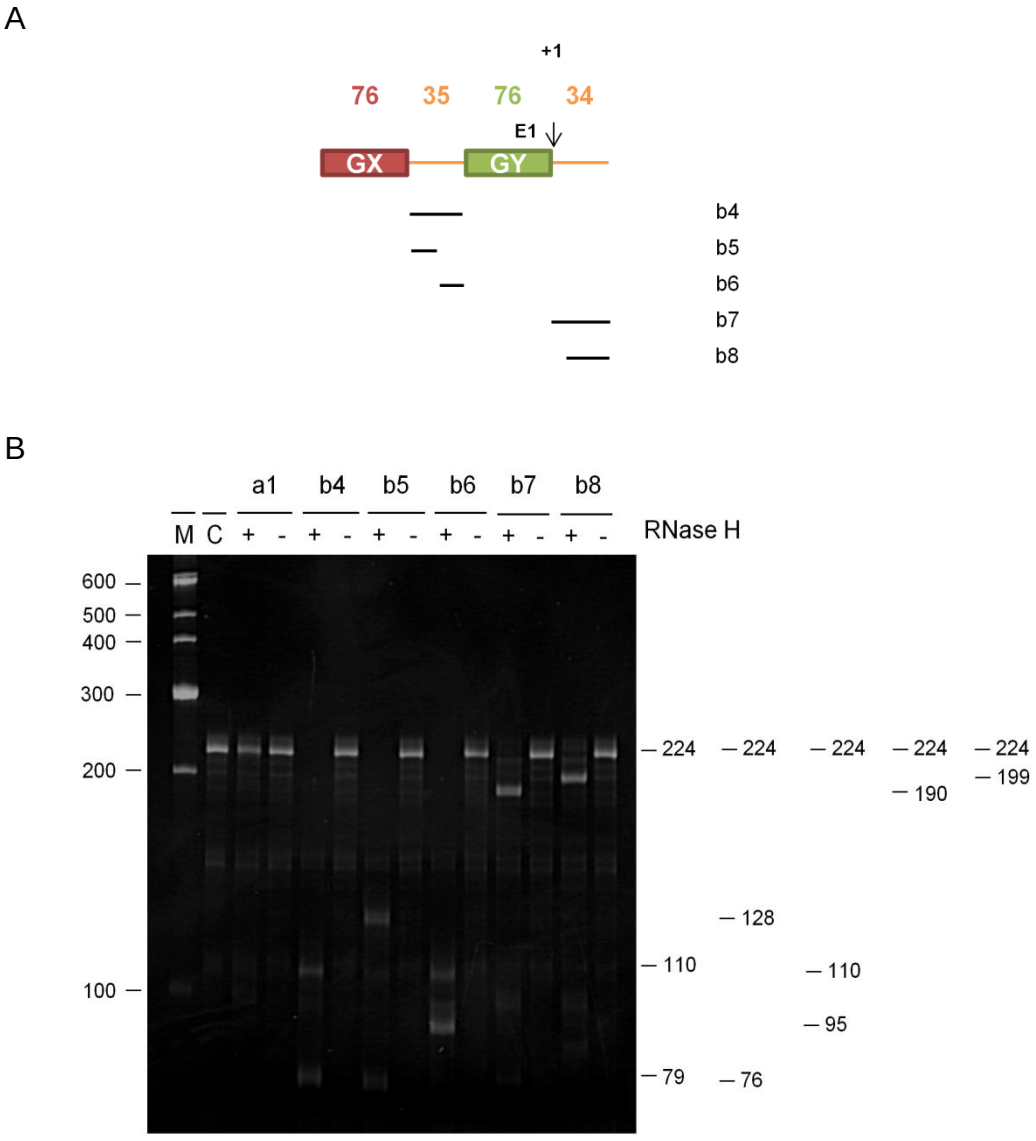


**Figure 3.8 Confirmation of oligonucleotide hybridisation to *g*224 using RNase H.** Several complementary DNA oligonucleotides were hybridised separately to the *g*224 RNA. Labelling is as described in Figure 3.5.

Cleavage assays were performed on these DNA-RNA hybrids as shown in Figure 3.9. As with the *metT* tRNA precursor, blocking of the single-stranded region on the opposite side of the functional tRNA unit relative to the cleavage site (labelled as b4) reduced cleavage substantially. Additionally, blocking of the 5' half of this region (labelled as b5) seems to have minimal effect on cleavage compared to blocking of the 3' half of this region (labelled as b6), which showed similar levels of reduction as b3. Therefore, it appears that RNase E must interact with regions less than 20 nt upstream and downstream of *glyY* for efficient direct-entry cleavage of the *glyV* tRNA precursor.

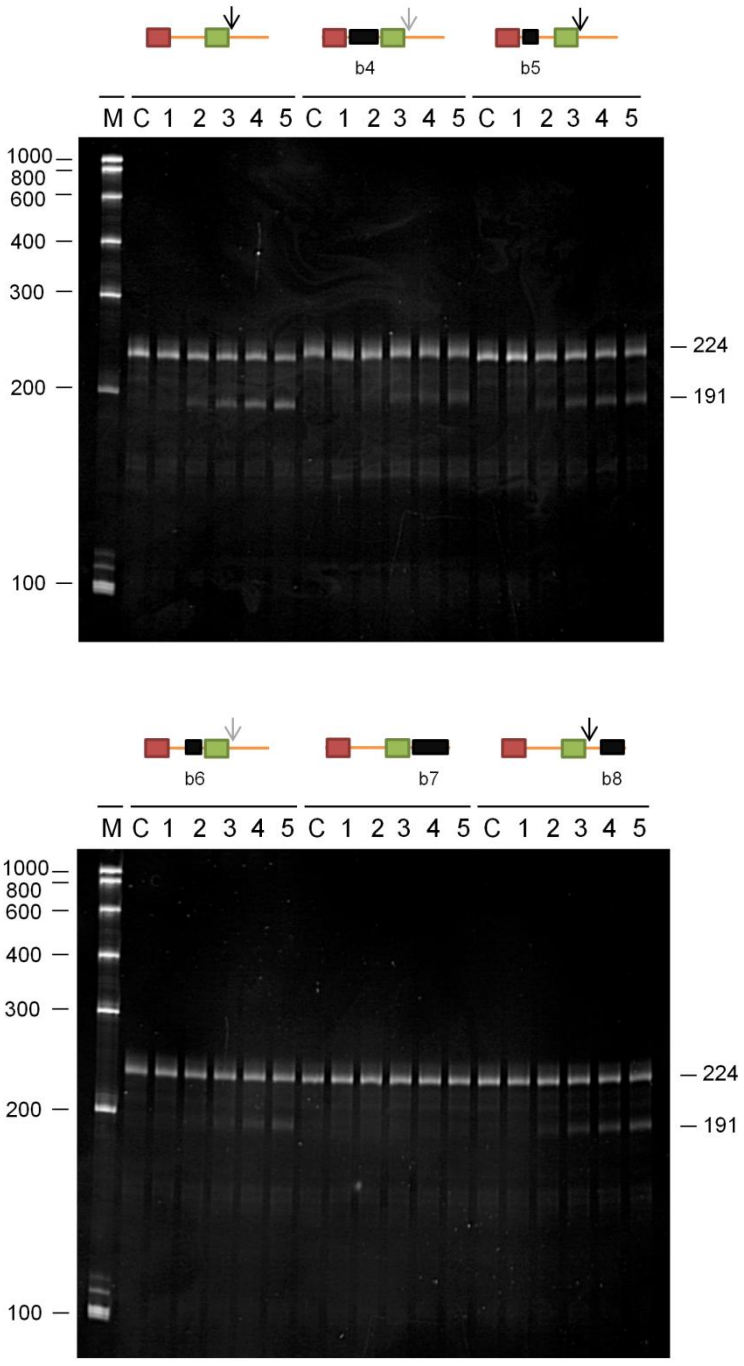


**Figure 3.9 Analysis of direct entry in the *glyV* tRNA precursor.** The *g*224 transcript was hybridised with DNA oligonucleotides as described in Figure 3.5. Labelling is as described in Figure 3.6. Grey arrows represent cleavages that were reduced significantly, but not necessarily abolished.

The two flanking single-stranded regions could be presented in an anti-parallel orientation by intervening structural units, restricting the number of single-stranded regions in the *E. coli* transcriptome that are susceptible to direct entry cleavage by RNase E. In fact, it may be the case that structural elements are the promoters of efficient cleavage by this single strand-specific endonuclease. This finding would complement previous work that has found that denatured

substrates or those that are modified to remove structural elements are less susceptible to cleavage by RNase E (Mackie, 1992, Ehretsmann et al., 1992).

### 3.2.3 The role of a 5' monophosphate in RNase E cleavage

Previously it has been suggested that the engagement of a 5'-monophosphate group into the 5' sensor enhances the catalytic activity of the enzyme in an allosteric manner (Jiang and Belasco, 2004, Koslover et al., 2008, Garrey et al., 2009). However, this model cannot account for transcripts that can be cleaved as efficiently by RNase E in the absence of a 5' monophosphate or functional 5' sensor, as shown in this work. Much of the evidence for the allosteric activation model is derived from Michaelis-Menten analyses comparing the cleavage of 5'-monophosphorylated and -hydroxylated oligonucleotide substrates (Jiang and Belasco, 2004, Garrey et al., 2009). However, because of the slow rate of cleavage of 5'-hydroxylated oligonucleotides, as can be seen in Figure 3.1, concentrations of substrate required to achieve saturation of the enzyme were not reached and hence Michaelis-Menten parameters were derived from heavily extrapolated data. Therefore, a reinvestigation using a higher concentration range of 5'-hydroxylated LU13 was performed (Figure 3.10).

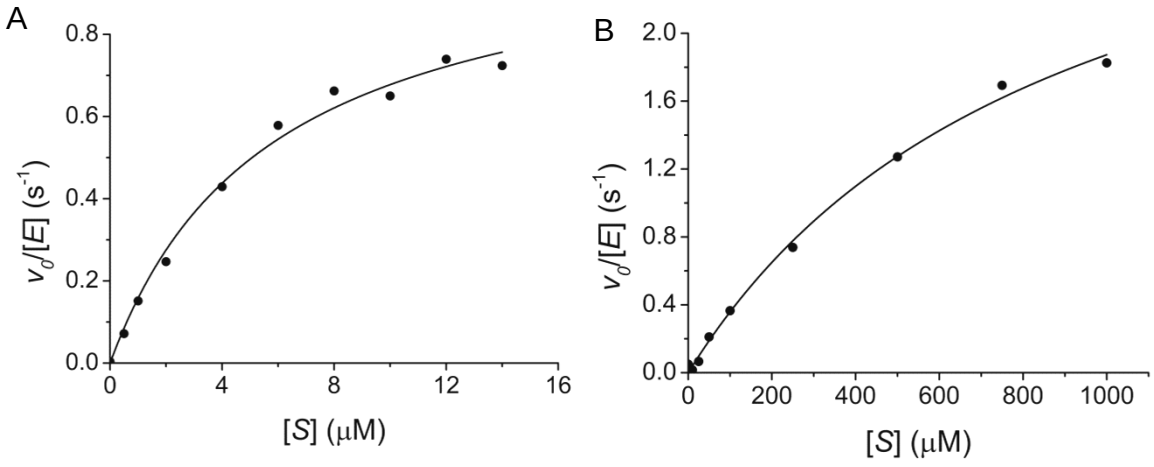


**Figure 3.10 Michaelis-Menten analyses of oligonucleotide substrates of RNase E.** Panels A and B show Michaelis-Menten graphs for the cleavage of 5'-monophosphorylated and –hydroxylated LU13, respectively. The concentration of NTH-RNase E (monomer) in each reaction was 4 nM. Rates normalised against enzyme concentration ($v_0/[E]$) were calculated as described in Materials and Methods, plotted against substrate concentration ([*S*]), and were fitted to the Michaelis-Menten equation.

For the 5'-monophosphorylated LU13, values of 5.7 μM and 1.1 $s^{-1}$ were obtained for the $K_M$ and $k_{cat}$, respectively, which is in agreement with previous findings (Redko et al., 2003, Kime et al., 2010). For the 5'-hydroxylated LU13, values of 0.9 mM and 3.5 $s^{-1}$ were obtained for the $K_M$ and $k_{cat}$, respectively. In contrast to previous studies (Jiang and Belasco, 2004, Garrey et al., 2009), the value

of the turnover number ($k_{cat}$) is not reduced in the absence of a 5'-monophosphate group, indicating that engagement with the 5' sensor does not enhance the catalytic step of RNase E. In fact, it appears that in the absence of a 5'-monophosphate, the turnover number is around 3-fold higher; upstream products of 5'-monophosphorylated LU13 cleavage could remain more tightly associated with the 5' sensor and hence limit the maximum rate of cleavage by RNase E. The significant decrease of the $K_M$ by 156-fold in the when there is a monophosphate group present at the 5' end compared to a 5'-hydroxyl group is also consistent with an apparent increase in the affinity of 5'-monophosphorylated oligonucleotides for RNase E.

It is worth noting that the mechanism of 5'-dependent cleavage proposed above is compatible with the direct entry model. Some transcripts may be able to present multiple single-stranded regions that interact with RNase E in a cooperative manner (for further information see Section 3.2.4); substrates that lack these direct entry requirements may be able to overcome this barrier by presenting a 5' monophosphate, which could provide alternative interactions with RNase E by engaging the 5' sensor. To examine this further, an assay was constructed whereby the cleavage of 5'-monophosphorylated LU13 was monitored in the presence of potentially competing 5'-triphosphorylated and -monophosphorylated transcripts that are not cleaved by RNase E, as shown in Figure 3.11. The 5'-monophosphorylated transcripts were produced and confirmed using TAP and TEX, respectively (Figure 3.2).

The rate of cleavage of 5'-monophosphorylated LU13, which acts as the reporter substrate, is reduced only marginally when the NTH-RNase E is pre-incubated with the 5'-triphosphorylated transcripts, suggesting that these substrates cannot bind to the RNA-binding channel of RNase E to compete with LU13. However, the rate of cleavage of the LU13 reporter is reduced by 5.4- and 3.3-fold when NTH-RNase E is pre-incubated with 5'-monophosphorylated *prfC* and *tig* mRNA, respectively, in comparison to the 5'-triphosphorylated forms. The additional interactions of the 5'-monophosphate group with the 5' sensor allows these two transcripts to bind to and occlude the active site of the enzyme effectively inhibiting the cleavage of 5'-monophosphorylated LU13.

In contrast, *tnaC* mRNA does not seem to inhibit the reaction significantly regardless of its 5'-phosphorylation status. This is probably due to the size and/or conformation of this transcript, suggesting that a 5'-monophosphate alone is not sufficient for interacting with RNase E and that the major requirements for the interaction are single-stranded regions. The control assay, using yeast tRNA as a competitor, provides confirmation of this finding, as mature tRNA, although presenting a monophosphate at the 5' end, remains highly structured and hence cannot access RNase E within the RNA-binding channel.

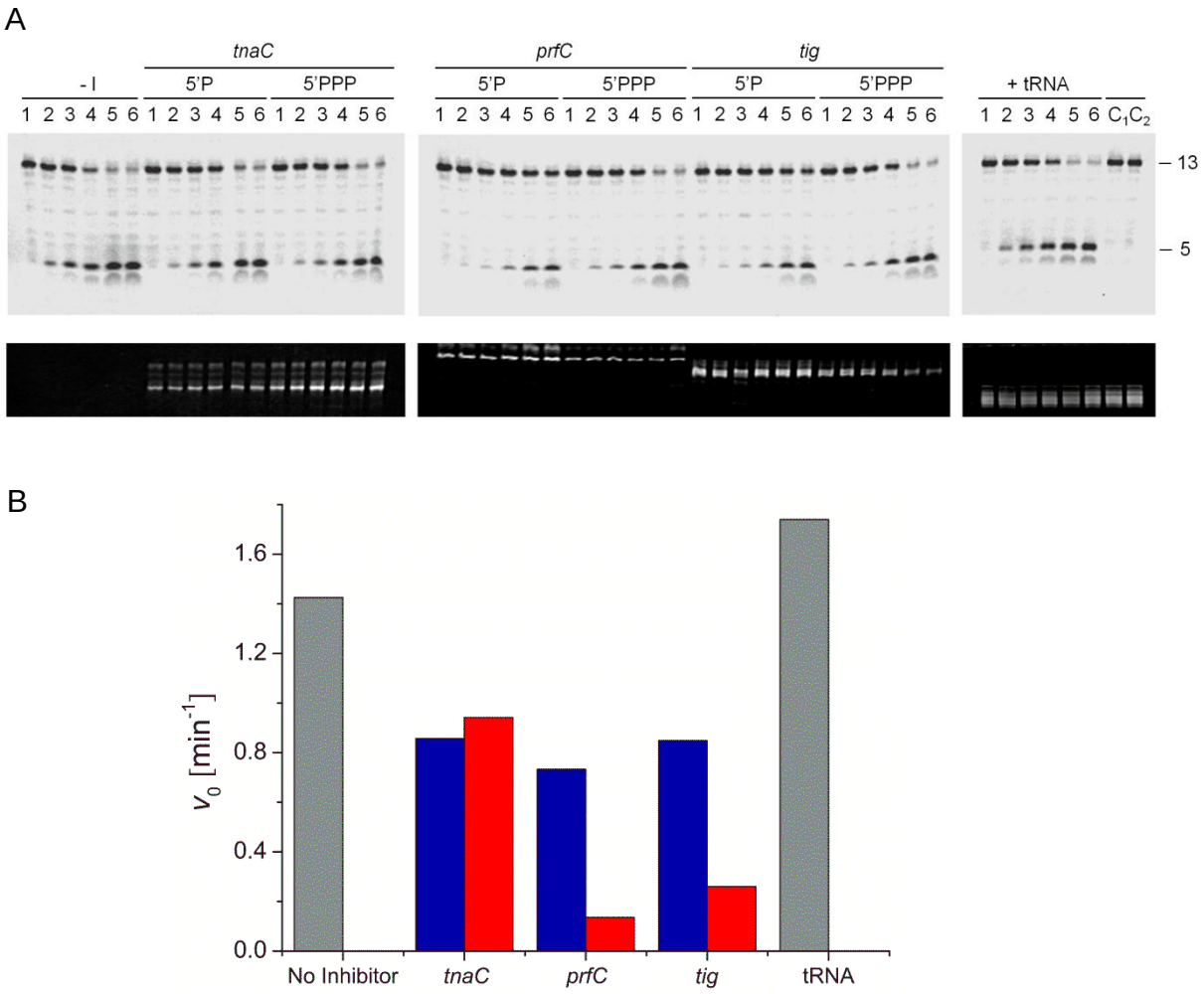


**Figure 3.11 Inhibition of 5'-monophosphorylated LU13 cleavage by 5'-monophosphorylated transcripts.** The transcripts were generated and modified at the 5' end as described in Figure 3.2. As a negative control, yeast tRNA was incubated with T7 RNA polymerase and purified under the same conditions. Panel A shows discontinuous cleavage assays of 5'-monophosphorylated LU13 in the presence of various transcripts. NTH-RNase E was pre-incubated with transcripts for 10 min before addition of 5'-monophosphorylated LU13 substrate. The final substrate, transcript and enzyme concentrations were 75 nM, 1 µM and 5 nM, respectively. Samples taken after various time points were analysed for cleavage of 5'-monophosphorylated LU13 as described in Figure 3.1, shown in the higher panel. Gels were also stained with ethidium bromide to image transcript bands as described in Figure 3.2, shown in the lower panel. Lanes 1-6 contain samples taken at 0, 2, 5, 15, 60 and 120 min after the start of the reaction. Lanes $C_1$ and $C_2$ contain samples after 0 and 120 min incubation without enzyme, respectively. The 5'-phosphorylation status and transcript identities are labelled at the top of each image. The sizes in nt of the substrate and product of 5'-monophosphorylated LU13 cleavage are shown at the right of the image. Panel B shows the initial rates of 5-monophosphorylated LU13 cleavage by RNase E in the presence of various transcripts. Initial rates of cleavage of 5'-monophosphorylated LU13 were calculated by 2D densitometry, whereby intensities of product bands, normalised against the intensity of substrate bands, were compared between Lanes 1 and 3 for each reaction. A bar chart was constructed using this information. Identities of the additional transcripts are shown at the bottom of the chart. Bars coloured blue and red represent values obtained from assays using transcripts before and after incubation with TAP, respectively. Bars coloured grey indicate assays in which TAP treatment was not used as a comparison.

## 3.3 Discussion

The work described here confirms that the T170V mutant remains the most suitable candidate for analysing direct entry cleavages *in vitro*, given that the 5' sensor is inactivated in this mutant but basal activity is retained *i.e.* ability to cleave substrates in a 5' monophosphate-independent manner (Figures 3.1 and 3.2). With this mutant, it has been shown that direct entry plays a major role in the maturation of at least some tRNAs, including *argX-hisR-leuT-proM,* which was identified as a direct entry candidate from previous studies (Garrey and Mackie, 2011), as well as *metT-leuW-glnU-glnW-metU-glnV-glnX* and *glyV-glyX-glyY.* As an adequate pool of functional tRNAs is essential to bacterial growth (Berg and Kurland, 1997, Dong et al., 1996), the involvement of direct entry in this pathway means that this mode of cleavage by RNase E is a key aspect of RNA metabolism.

Further analyses of the *met* and *glyV* substrates has revealed that direct entry requires access to single-stranded regions that are adjacent, but not contiguous, to regions where cleavage occurs (Figures 3.6 and 3.9, respectively). This finding fits with the model whereby the simultaneous interaction of two or more single-stranded RNA segments with RNase E can negate the requirement for a 5'-monophosphate group (Kime et al., 2010). The antiparallel arrangement of these two regions flanking the tRNA unit could determine which of the interacting regions is cleaved. Given that the 3'-trailer sequence would always engage one of the RNA-binding channels in the same orientation as 5'-monophosphorylated LU13, it makes sense that this region is cleaved during direct entry. The 5'-leader sequence would engage the other RNA-binding channel in the opposite orientation, and therefore may not be cleaved due to the unsymmetrical nature of the sugar-phosphate backbone. It has been shown that RNase E cleaves RNA due to the conformation of the ribose group that engages the RNA-binding channel (Redko et al., 2003). Simple cooperative interactions of this nature have been reported for other multimeric regulators (Chen and Matthews, 1994, Vossen et al., 1996). Although cooperativity may increase the affinity of the interaction, additional factors may improve the selectivity of the site of cleavage. Despite having low sequence specificity (McDowall et al., 1994, Kaberdin, 2003), RNase E cleaved the *metT* and *glyV* precursors rapidly at only one site. In addition to this, truncations of both substrates showed that there is a requirement for an upstream tRNA unit at the 5' end of the 5'-leader region for cleavage to occur (Figures 3.4 and 3.7). This is possibly indicative of an additional contact whereby the upstream tRNA unit can align the substrate for specific cleavage. This model will be investigated further in Chapter 5. The initiation of tRNA maturation by direct entry may extend to other bacteria. An analysis of 3' trailer sequences of tRNAs has found conserved AU rich regions, preferred substrates for RNase E (McDowall et al., 1994, Kaberdin, 2003), in bacteria with homologues of RNase E (Li et al., 2005).

In addition to elucidating the mechanism of direct entry during the maturation of tRNA precursors, this work has also provided the clearest example to date that a 5'-monophosphorylated end generated by an initial cleavage by RNase E can trigger subsequent cleavages (Figure 5.2). This ability was suggested when the 5'-monophosphate activity of RNase E was first discovered (Mackie, 1998). Cleavage by direct entry at E3 was then followed by cleavage at E5 only in reactions where RNase E still had a functional 5' sensor. Thus, while processing may be initiated at only a few sites by direct entry, subsequent cleavages may occur by the 5' monophosphate-dependent pathway. The location of the 5' sensor in relation to the active site is ideal to engage the 5' monophosphate of the downstream products of cleavage (Callaghan et al., 2005a). Given that these cleavage products have reduced single-stranded regions, the 5' monophosphate may provide the interactions required to increase the affinity for RNase E. The Michaelis-Menten analysis performed in this study has shown that the 5'-monophosphate does not increase the catalytic activity of the enzyme and therefore more likely increases the affinity of the substrate to the enzyme (Figure 3.10). In addition to this, inhibition assays have shown that a 5'-monophosphate group can improve a transcript's ability to compete with LU13 without being cleaved themselves (Figure 3.11). These findings show a large degree of complementarity between the 5' monophosphate-dependent and direct entry models.

# Chapter 4

# Transcriptome-wide prevalence of ‘direct’ entry via RNA seq

## 4.1 Introduction

Although discovered in 1977 as an endonuclease involved in the maturation of rRNA precursors (Gegenheimer et al., 1977, Apirion and Lassar, 1978), wider implications of RNase E in RNA metabolism were not suggested until 12 years later when it was found that *rne*, the gene encoding RNase E, was the same gene as *ams* (Mudd et al., 1990, Babitzke and Kushner, 1991, Melefors and von Gabain, 1991, Taraseviciene et al., 1991), which when mutated resulted in the stabilisation of bulk cellular RNA in *E. coli* (Kuwano et al., 1977, Ono and Kuwano, 1979). Since then, RNase E has been studied extensively as a major player in post-transcriptional regulation with some interesting findings. The degradation of several transcripts in *E. coli* is dependent on an initial cleavage by RNase E enhanced by the presence of a monophosphate at the 5' end of the RNA (Mackie, 1998, Mackie, 2000, Garrey and Mackie, 2011). Crystallographic studies of RNase E have confirmed the presence of a 5'-monophosphate sensor, which contains a horseshoe of polar residues able to make multiple hydrogen bonds with a 5' monophosphate (Callaghan et al., 2005a). More recently, an enzyme named RNA pyrophosphohydrolase (RppH) was discovered in *E. coli* that is responsible for converting the 5' end of nascent transcripts from a triphosphate to a monophosphate, hence providing substrates for the 5' monophosphate-dependent pathway of RNase E (Celesnik et al., 2007).

In contrast, microarrays found that a mutation in *rppH*, the gene encoding RppH, resulted in stabilisation of only 20-25% of transcripts in *E. coli* (Deana et al., 2008). Complementing this finding, it has also been found that cells with a mutation in the 5' sensor of RNase E remain viable (Garrey and Mackie, 2011, Anupama et al., 2011), even though mutations that result in RNase E inactivation are lethal (Apirion and Lassar, 1978). In addition, mutations in the 5' sensor of RNase E (Baker and Mackie, 2003, Garrey and Mackie, 2011) or RppH (Deana et al., 2008) do not significantly alter mRNA stability levels compared to mutations that inactivate RNase E (Ono and Kuwano, 1979, Kuwano et al., 1977). These findings suggest that RNase E is able to cleave RNA in a 5' monophosphate-independent manner. Several substrates have been found to be cleaved *in vitro* and *in vivo* by RNase E independent of the 5' status or functional 5' sensor (Hankins et al., 2007, Kime et al., 2010, Garrey and Mackie, 2011, Kime et al., 2014). However, most of these 5' monophosphate-independent cleavages, termed 'direct' entry sites, have been found mainly in tRNA precursors (Garrey and Mackie, 2011); the highly structured tRNA units may possibly force the flanking single-stranded regions into the correct conformational context to make multiple contacts with the multivalent homotetramer (Kime et al., 2010, Kime et al., 2014). However, given the high degree of flexibility of RNA molecules, as well as the potential to form various structural conformations, it is possible that

direct entry plays a major role in RNA metabolism beyond the maturation of tRNA in *E. coli*. Direct entry also offers simple explanations for the observed interplay between translation and degradation, whereby the passage of ribosomes would limit RNase E access to single-stranded regions (Braun et al., 1998). This would explain how the action of translational-repressing small RNAs (Afonyushkin et al., 2005), sub-optimal ribosome loading (Bardey et al., 2005), and increased RNA polymerisation speed (Iost and Dreyfus, 1995) reduces mRNA stability.

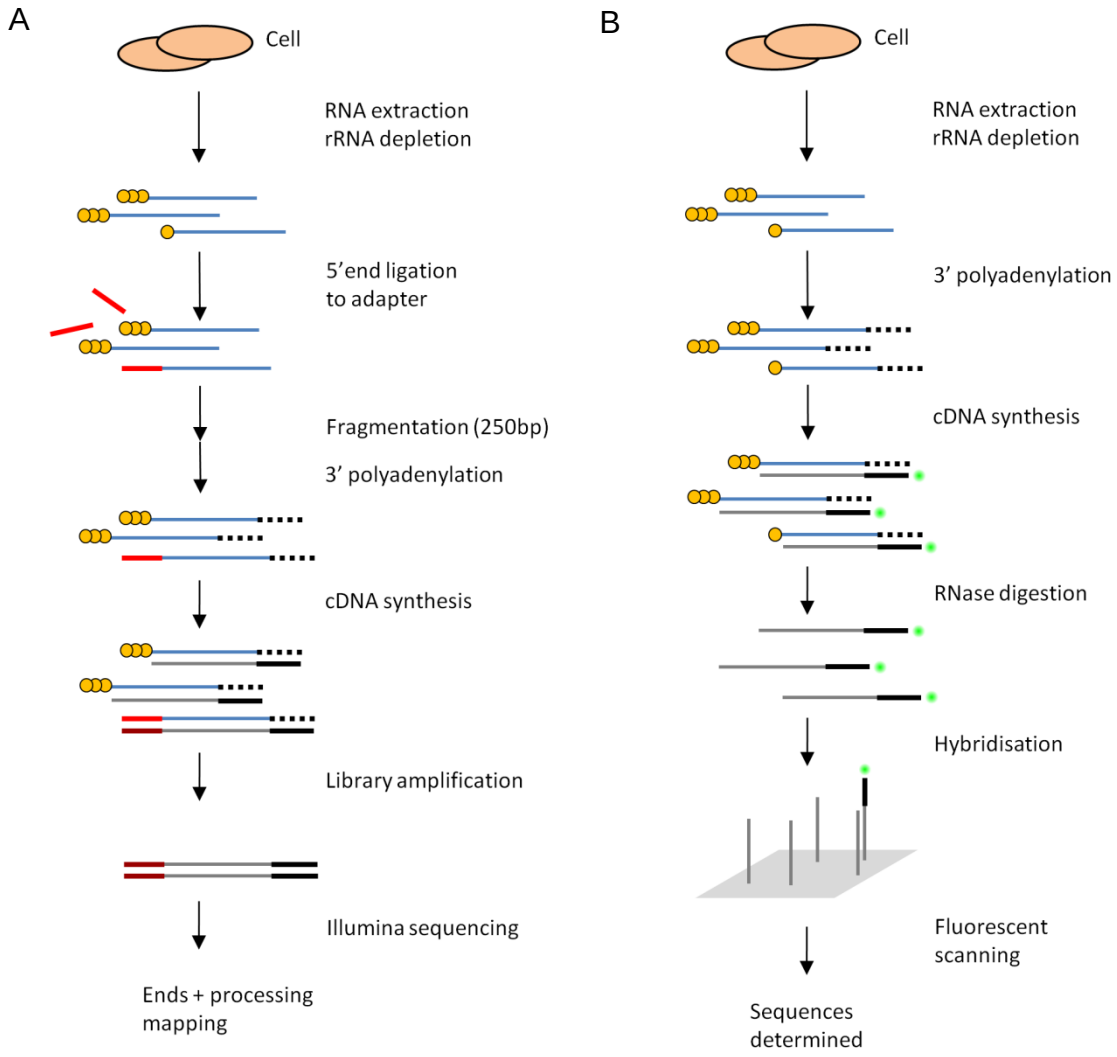


**Figure 4.1 Schematic representations of high-throughput total RNA analyses.** Panels A and B show schematic representations of the differential RNA-seq approach and a microarray-based method, respectively. RNA strands are represented as blue lines, cDNA strands as grey lines, sequencing adaptors as red lines, poly(A) sequences as black dotted lines, green circles as fluorescent labels and 5' phosphates as yellow circles. Diagram adapted from previous work (Lin et al., 2013).

In order to determine the transcriptome-wide prevalence of direct entry and identify additional substrates for biochemical analysis, a high-throughput analysis of RNase E activity on total RNA both *in vivo* and *in vitro* was required. Methods to identify substrates that are stabilised following

inactivation of RNase E *in vivo* have been performed previously using microarray-based approaches but did not provide information on the position of the corresponding cleavages (Lee et al., 2002, Stead et al., 2011). Microarrays involve the construction of fluorescently-labelled cDNA libraries from total RNA that are then hybridised to probe DNA sequences attached to a Chip, as shown in Figure 4.1B. The microarray data output is therefore based primarily on pre-constructed probe libraries; the single-nucleotide resolution that would be beneficial for the identification of sites of endonucleolytic activity is not achieved. The detection of the total cDNA libraries is also limited by the reference sequences used to construct these probes. Furthermore, the variability of hybridisation results in a higher degree of background noise compared to more sensitive technologies. Finally, since products of cleavage will still hybridise, substrates for *in vitro* analyses are not easily identified.

With the advent of high-throughput, low-cost sequencing, RNA seq-based approaches have become increasingly popular for transcriptome-based analyses (Cho et al., 2009, Sharma et al., 2010, Mamanova et al., 2010, Vockenhuber et al., 2011, Raghavan et al., 2012, Lin et al., 2013, Romero A. et al., 2014). This is down to the fact that they provide a genome-wide perspective that allows new factors and patterns of gene regulation to be identified, as well as the establishment of the complete genome sequence of many major model organisms, which ultimately the RNA-seq data is aligned. RNA seq utilises sequencing by synthesis technology, whereby each of the four nucleotides are labelled with a different fluorophore allowing the fragments to be sequenced in real time as they are being produced. In this work, an RNA ligase-dependent method adapted from a previous study to determine transcriptional start sites in *E. coli* was used (Sharma et al., 2010), whereby an adaptor was ligated to the 5' end of the RNA and would provide the site for selective library amplification, as shown in Figure 4.1A. Because ligation only occurs on 5' ends with a monophosphate, which are produced by endonucleolytic cleavage (Misra and Apirion, 1979), specific cleavages by endonucleases could be mapped to the *E. coli* genome by comparison of reads from mutant and wild-type datasets at each nucleotide position *in vivo*, or before and after enzyme incubation datasets *in vitro*.

## 4.2 Results

In this work, total RNA was extracted from cultures of *E. coli* N3431 (*rne*-3071 temperature-sensitive mutant) and N3433 (*rne* wild-type) incubated at 44°C, the non-permissive temperature for the *rne*-3071 mutation (Apirion and Lassar, 1978). RNA was depleted of rRNA and sequenced as described (Section 2.2.2.6) and shown in Figure 4.1A. The comparison of these two sequencing runs forms the *in vivo* dataset. Total RNA was also extracted from *E. coli* culture BW25113, depleted of rRNA,

treated with TAP (5'-triphosphate to -monophosphate group) followed by CIP (5'-monophosphate to -hydroxyl group) and incubated with T170V NTH-RNase E for 0 and 10 min, by Louise Kime. The TAP-CIP treatment ensured that background cleavage products produced *in vivo* before RNA extraction were effectively removed from the *in vitro* RNA-seq data. Both samples were then sequenced as described. The comparison of the 0 and 10 min RNA-seq runs forms the *in vitro* dataset. While the *in vitro* dataset provided the basis for identification of 'direct' entry sites, which can be characterised and studied, the *in vivo* dataset verified the physiological relevance of these sites.

### 4.2.1 Confirming novel sites of cleavage down to single-nucleotide resolution

To confirm the reliability of the *in vivo* dataset, several well-documented sites of RNase E activity were analysed using the UCSC Microbial Genome Browser. As can be seen in Figure 4.2A, end reads associated with sites of cleavage involved in the maturation of the 5' end of 16S rRNA were identified. Tracks for RNase III and G deficient strains, SDF205 (*rnc*-105) and GM11 (*rng::cat*) respectively, compared with their congenic wild-types, SDF204 (*rnc*+) and MC1061 (*rng* wild-type) respectively, are also provided for confirmation of the other processing sites. Absence of RNase III resulted in a decrease of end reads at all 3 sites associated with endonucleolytic cleavage, as well as an accumulation of 5' ends at the site associated with transcription initiation found in a previous study (Romero A. et al., 2014). This confirms that RNase III must make an initial cleavage at position -155 (relative to the start of the functional unit) in order to promote subsequent cleavages by RNase E and G. Inactivation of RNase E results in reduction of end reads at position -66, suggesting only RNase E can cleave at this position. Absence of RNase G results in a slight reduction of ends at position 0, as well as an accumulation of reads at position -66. This suggests that, in the absence of RNase G, the increased steady state levels of the downstream product of RNase E cleavage may drive the subsequent cleavage at position 0 by a "substitute" endonuclease, possibly RNase E. These findings support previous studies (Young and Steitz, 1978, Li et al., 1999a, Li et al., 1999c).

Another established substrate of RNase E is the *rpsT* mRNA, which encodes the ribosomal S20 protein (Mackie, 1992, Mackie et al., 1997, Coburn and Mackie, 1998, Mackie, 2013a). Although the best described site is at position +168 (relative to start codon), it appears that positions +149 and +159 have more 5' ends associated with them in the *rne* wild-type, as seen in Figure 4.2B. However, following inactivation of RNase E, ends associated with all three of these sites are almost completely reduced, suggesting that all three are associated with RNase E. Sites of RNase E cleavage found more recently towards the 5' end of *rpsT* (Mackie, 2013a) are barely detectable in this dataset.

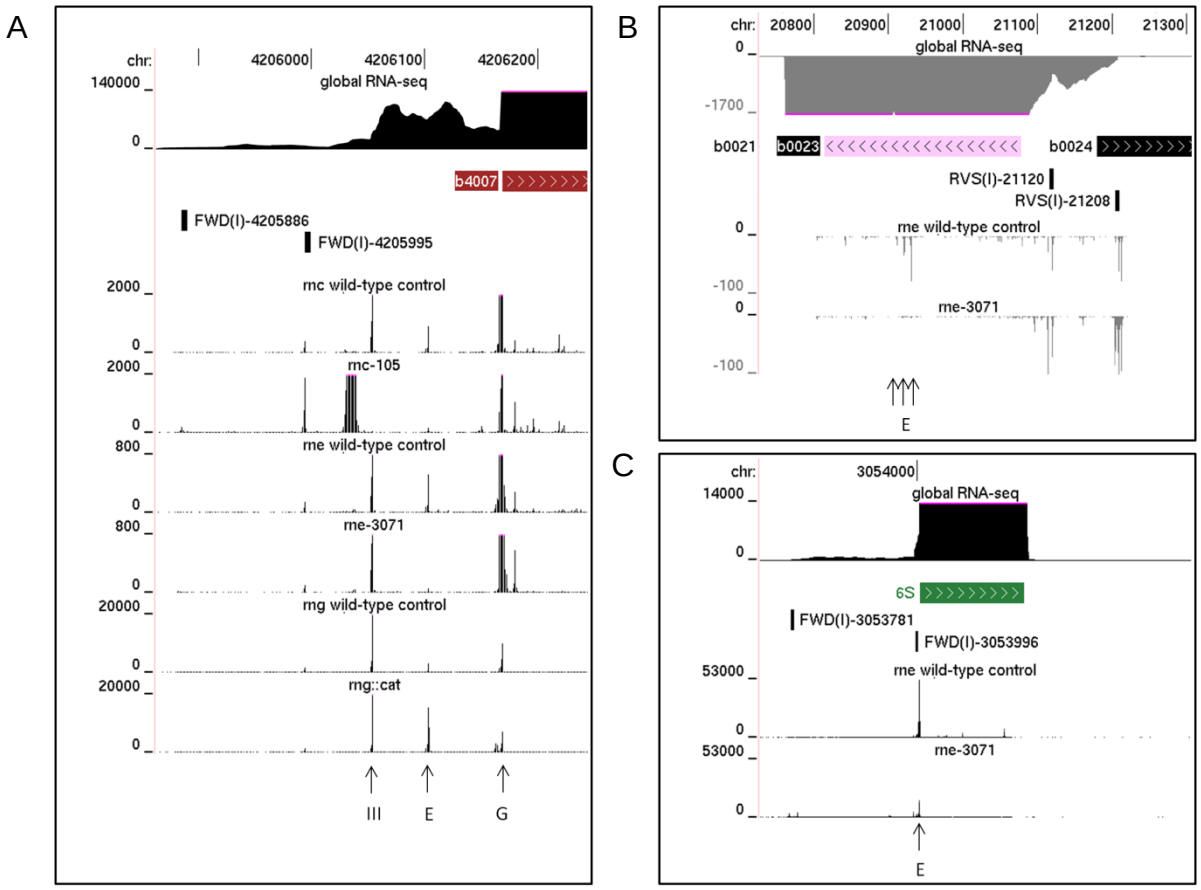


**Figure 4.2 Differential RNA-seq profiles at established endoribonuclease cleavage sites.** Panels A, B and C show sites at the 5' end of the 16S rRNA precursor, within the *rpsT* mRNA coding region, and at the 5' end of the 6S RNA precursor, respectively. The first line on each panel shows the genome position. The top three tracks for each panel show global RNA-seq data (Romero A. et al., 2014), the position of the corresponding gene, and mapped transcription start sites (Romero A. et al., 2014). The remaining tracks below show the reads obtained at each nucleotide position from a dRNA-seq analysis of total RNA extracted from a mutant and its congenic wild-type. For each track, the strain is identified above and the scale of the sequencing reads is shown to the left. Arrows at the bottom of each panel highlight the positions of cleavage by RNase E, III and G. Images were produced by modification of screenshots taken from the UCSC Microbial Genome Browser (Chan et al., 2012). Read values obtained are positive or negative if the corresponding gene is on the forward or reverse strand, respectively.

The final example, shown in Figure 4.2C, is the processing event at the 5' end of 6S RNA (Kim and Lee, 2004). Upon inactivation of RNase E, the mature 5' end reads at position 0 are reduced significantly. However, ends are still present, probably because species produced prior to incubation have not been degraded to completion, given 6S RNA is relatively stable compared to other mRNA substrates (Lee et al., 1978). In addition to the examples shown in Figure 4.2, sites dependent on *rne* have been found, using the RNA-seq data, at the 5' and 3' end of the 9S rRNA precursor (Ghora and Apirion, 1978), within the intergenic region of *pyrG-eno* mRNA (Kime et al., 2008), towards the 3' end of *epd* mRNA (Bardey et al., 2005), at the 3' end of the M1 RNA precursor (Gurevitz et al., 1983),

at the 3' end of the coding sequence for *dnaG* mRNA (Yajnik and Godson, 1993), and at the 3' end of the tmRNA precursor (Lin-Chao et al., 1999).

### 4.2.2 Determining the transcriptome-wide effect of RNase E inactivation

To identify a population of *rne*-dependent sites *in vivo*, as well as provide a visual overview of the dataset, an M-A scatter plot was constructed, whereby M = $\log_2$(reads for wild-type/reads for mutant) and A = [$\log_2$(reads for wild-type) + $\log_2$(reads for mutant)]/2. This was done for each position in the chromosome associated with at least the lowest measureable unit *i.e.* 1 read (Figure 4.3). This graph is similar to a ratio-intensity plot used for microarray analyses, but transforms and rescales the data so that the points become more readily comparable, *i.e.* the separation of a fourfold increase is the same as a fourfold decrease on the y-axis.

The most significant observation of the M-A scatter plot for the RNase E *in vivo* dataset is the lack of a distinctive noise cone; the population of sites in which inactivation of RNase E has no effect should be centred on an M value of 0. In fact, the major population appears to be a cone of points centred on an M value of 1.8, an observation more clear in Figure 4.3B. This finding suggests that the majority of sites of cleavage in the transcriptome of *E. coli* are reduced in an *rne* knockout, supporting previous studies which found that the bulk of transcripts in *E. coli* were stabilised in an RNase E mutant (Kuwano et al., 1977, Ono and Kuwano, 1979).

Due to the lack of two separate populations, establishing strongly *rne*-dependent sites remains difficult and therefore two different boundaries were established. The first boundary, as shown in Figure 4.3A, takes into account the inherent noise found at lower A values while applying less strict criteria on sites with higher A values. This ensures a more realistic population of the *rne*-dependent sites is selected for comparison with sites dependent on other endonucleases *in vivo*. The second boundary, as shown in Figure 4.3B, was established at M value greater than or equal to 5, which corresponds to a 32 fold decrease in peak height in the *rne*-3071 mutant compared to the wild-type at the non-permissive temperature. At this M value, even with reads equal to 1 in the mutant, the reads must be equal to at least 32 in the wild-type, reducing the chances of selecting a site in the noise arms with a positive M value due to random PCR bias between the two datasets. This ensures that only sites with a significant change upon inactivation of *rne* are selected to compare to the sites found from the *in vitro* dataset. Even under this strict requirement, around 7,000 sites of cleavage are classified as being *rne* dependent.

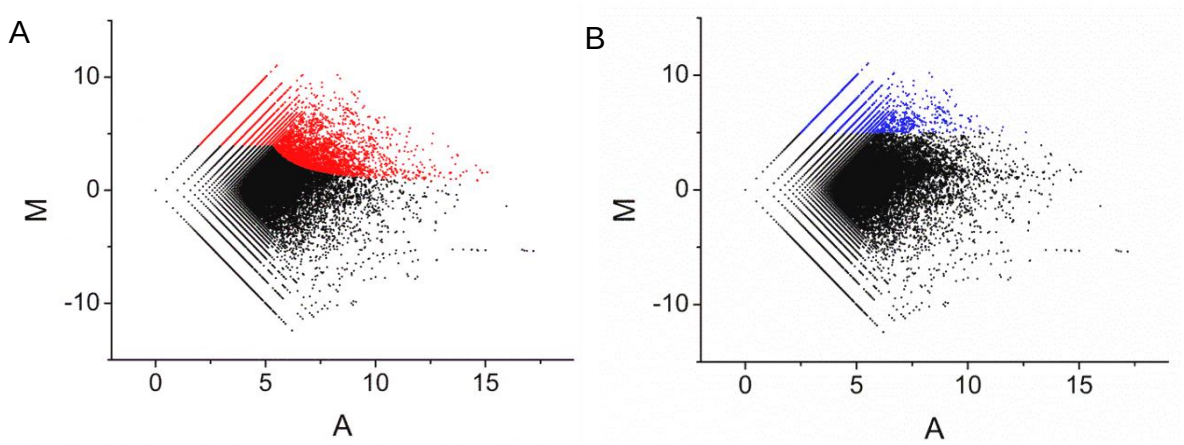


**Figure 4.3 Scatter-plot analysis of the *rne in vivo* dataset.** Panels A and B show an M-A scatter plot that was constructed using the dRNA-seq data obtained from the *rne*-3071 strain and its congenic wild-type partner incubated at the non-permissive temperature of 44°C. The A value was equal to [$\log_2$(reads from wild-type) + $\log_2$(reads from mutant)]/2 and the M value was equal to $\log_2$(reads from wild-type/reads from mutant). The points coloured red in Panel A correspond to sites in the transcriptome with M values ≥ 4 or ≥ (0.9*A/[-2.8+(0.7*A)])-1.1 if the corresponding A values were < or ≥ 5.3, respectively. The points coloured blue in Panel B correspond to sites in the transcriptome with M values ≥ 5.

From the first population, several interesting features have emerged. For example, the cleavage at position -43 from the 3' end of 16S rRNA, which may be responsible for the generation of specialised ribosomes that translate leaderless mRNAs (Vesper et al., 2011), is *rne* dependent (Figure 4.4A).

It is interesting to note that this 43 nt region not only houses the sequence that hybridises with the Shine-Dalgarno element to initiate translation of mRNA (Shine and Dalgarno, 1974), but also associates with the ribosomal protein S1 (Dahlberg and Dahlberg, 1975). Recently it has been found that over expression of ribosome-free S1 leads to stabilisation of several mRNAs, possibly due to the competition with RNase E for AU rich regions (Delvillani et al., 2011). *Salmonella enterica* strains with a temperature-sensitive mutation of *rne* have been found to revert to a wild-type phenotype with subsequent suppressors mutations at other regions of the genome. One of these mutations is located in the *rpsA* gene and results in removal of an RNA-binding region in the ribosomal protein S1. This could suggest that S1 could stabilise mRNAs by blocking access of RNase E (Hammarlof et al., 2015). The production of specialised ribosomes that do not require canonical ribosomal binding sites, as well as the release of ribosomal protein S1 which can compete and block RNase E cleavage, could result in selective stabilisation of mRNAs and represent a complex mode of regulation of RNA decay.

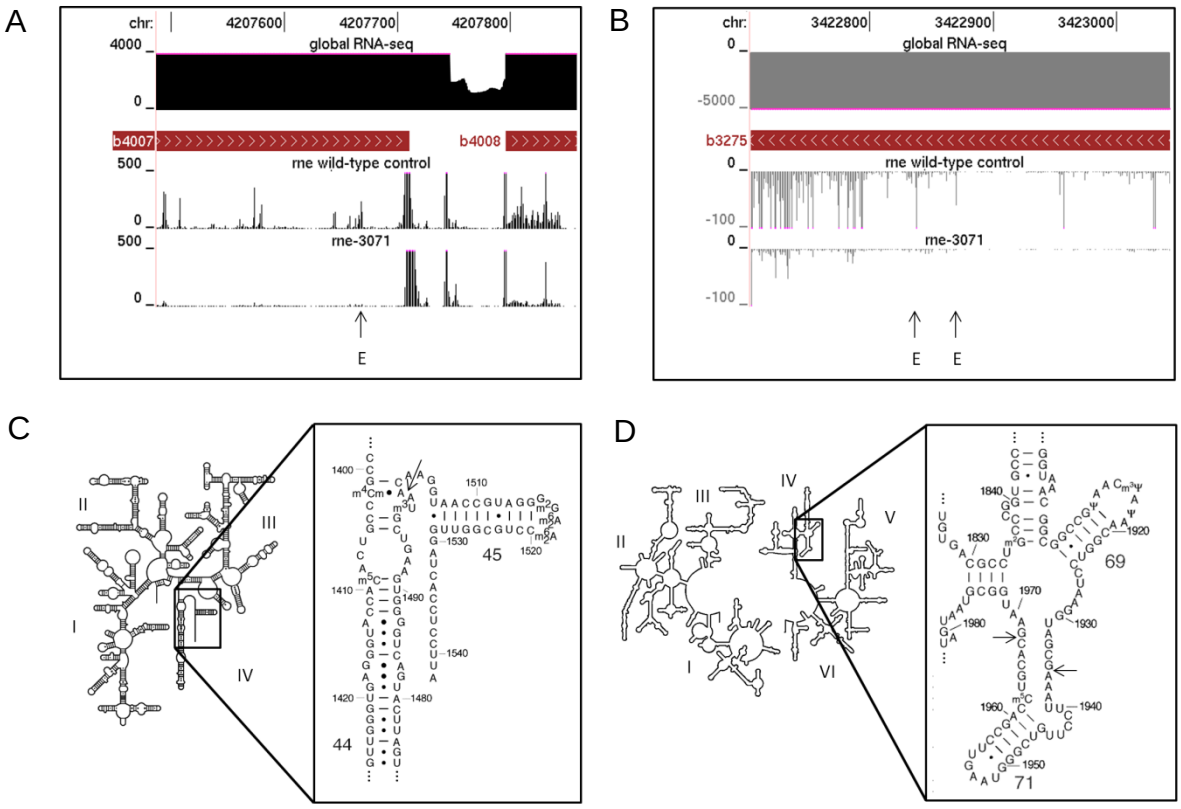


**Figure 4.4 Differential RNA-seq analysis of RNase E cleavage sites within ribosomal RNA.** Panels A and B show dRNA-seq profiles towards the 3' end of 16S rRNA and within the 23S rRNA, respectively. The tracks and labelling are as shown in Figure 4.2. Panel C shows the secondary structure of *E. coli* 16S rRNA. The inset shows the sequence and structure of domain IV with the site of RNase E cleavage marked with an arrow. Panel D shows the secondary structure of *E. coli* 23S rRNA. The inset shows the sequence and structure of helix 69, loop 70, helix 71 and loop 72 where the RNase E cleavage sites are marked with arrows.

The cleavage reported at position -43 of 16S rRNA has been assigned previously to MazF (Vesper et al., 2011), an endoribonuclease in the MazEF toxin-antitoxin system. However, the 5'-hydroxylated downstream products of MazF cleavage would not be detected by the RNA-seq approach used here (Zhang et al., 2005). An additional cleavage by MazF within the helix/loop 70 of 23S rRNA has been reported recently in *Mycobacterium tuberculosis* (Schifano et al., 2013, Schifano et al., 2014). Cleavage at this region also appears to be *rne* dependent in *E. coli*, as shown in Figure 4.4B. Therefore, as suggested initially for MazF family members (Schifano et al., 2013, Schifano et al., 2014), RNase E may also have a role in the regulation of translational activity via a mechanism that does not involve cleavage of mRNA.

These emerging features of RNase E cleavage are not limited to rRNA. Sites reduced upon inactivation of RNase E *in vivo* have been found within regions associated with Clustered Regularly Interspaced Short Palindromic Repeats (CRISPRs), as shown in Figure 4.5.

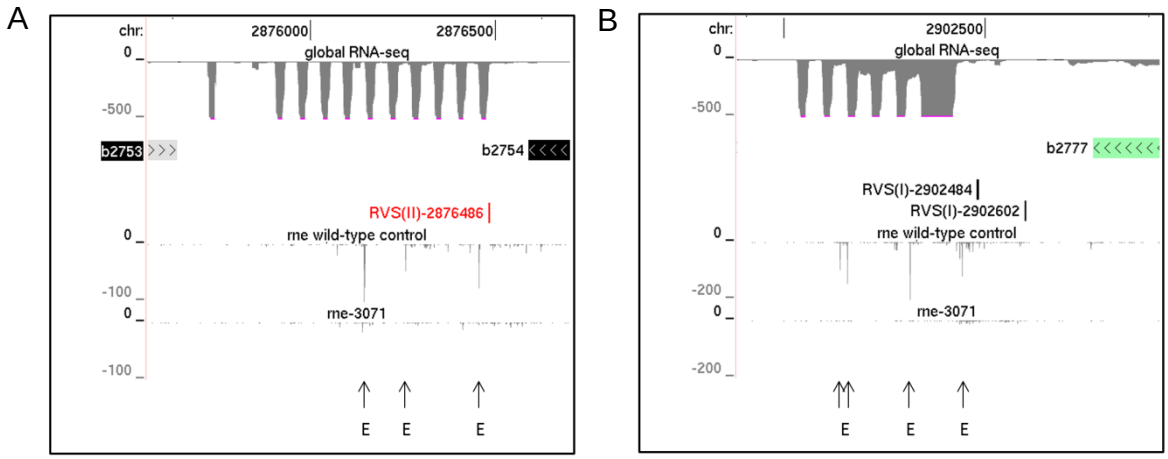


**Figure 4.5 Differential RNA-seq analysis of RNase E cleavages between CRISPRs.** Panels A and B show dRNA-seq profiles of CRISPR Clusters I and II, respectively, as confirmed by the gRNA-seq dataset. The tracks and labelling are as shown in Figure 4.2.

CRISPRs are intergenic repeats spanning 30-40 bp in length that are separated by 30-bp long variable spacers (Nakata et al., 1989). CRISPRs are transcribed as a single unit and processed to yield small mature CRISPR RNAs (crRNAs), which then associate with the Cas complex (Brouns et al., 2008). The function of the Cas-crRNA complex is to protect prokaryotes against potentially harmful mobile genetic elements such as phages, plasmids and transposons (Barrangou et al., 2007, Brouns et al., 2008, Garneau et al., 2010). Hybridisation of the crRNA with a complementary sequence in the target guides cleavage by the Cas proteins resulting in silencing of the infectious agent (Hale et al., 2009). This process is analogous to RNA interference in eukaryotes (Makarova et al., 2006). Previously it has been found that processing of pre-crRNA is coordinated by proteins in the Cas complex (Brouns et al., 2008, Carte et al., 2010, Haurwitz et al., 2010). However, several sites found within the spacer regions of pre-cRNA appear to be *rne* dependent *in vivo* and tend to be found downstream of the 3' end of the mature crRNA unit, as shown in Figure 4.5. In a mechanism reminiscent of tRNA maturation (Li and Deutscher, 2002, Ow and Kushner, 2002), RNase E could be involved in the initial processing of the pre-crRNA at the 3' end, which could then be completed at the 5' end by additional enzymes such as Cse3 (Brouns et al., 2008).

Another interesting feature found in the *rne*-dependent population *in vivo* is the prevalence of cleavages found at sites not associated with high levels of transcription or annotated gene sequences, as shown in Figure 4.6. These sites are found scattered throughout the transcriptome of *E. coli* and perhaps indicate a role for RNase E in removing RNA fragments produced by pervasive transcription, a role attributed to RNase III in *Staphylococcus aureus* (Lioliou et al., 2012).

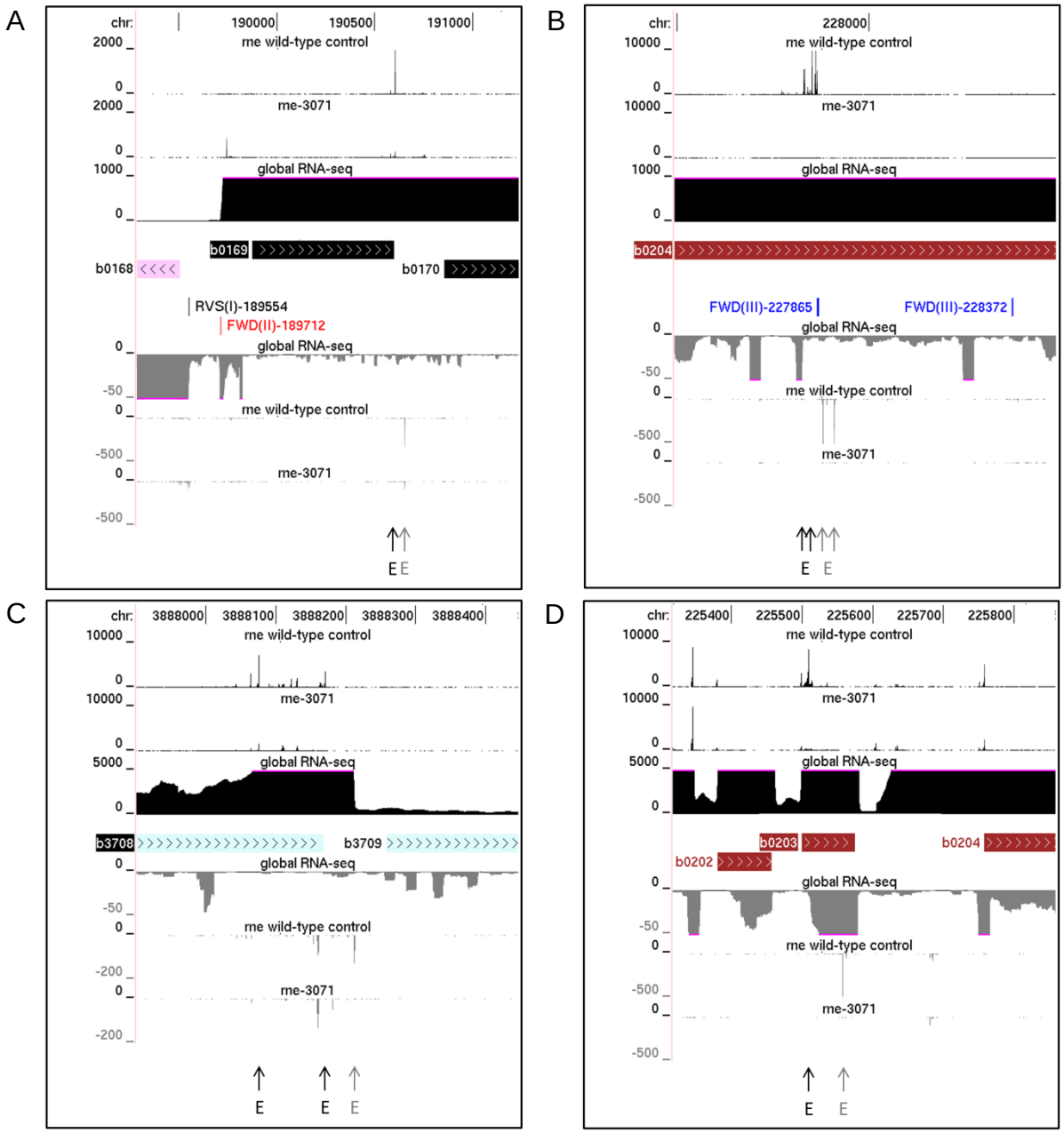


**Figure 4.6 Examples of pervasive transcription and RNase E cleavage.** Panels A, B, C and D show sites of cleavage on both strands between *rpsB* and *tff*, within the *rrlH* functional region, within the *tna* operon, and within the *ileV* functional region, respectively. The first line on each panel shows the genome position. From top to bottom the tracks represent: dRNA-seq reads mapped to the forward strand in the wild-type strain; same as the first track but for the *rne-3071* strain; gRNA-seq data mapped to the forward strand; positions of the corresponding genes; for Panels A and B only mapped transcription starts sites; gRNA-seq data mapped to the reverse strand; same as the first track but for the reverse strand; same as the second track but for the reverse strand. The track descriptions and scales are as described in Figure 4.2. Black and grey vertical arrows at the bottom of each panel highlight the positions of RNase E cleavage in the forward and reverse strand, respectively.

It is also possible that many of these low level transcripts may act as RNA decoys, such that they can bind to and sequester the activity of endonucleases providing another dimension for the regulation of RNA degradation. Multi-layered regulatory mechanisms such as this have been suggested previously (Hansen et al., 2013, Barnhart et al., 2013). It is important to note that the global RNA-seq dataset was obtained using *E. coli* strain BW2113, and therefore, to confirm the results from Figure 4.6, it would be important to perform a global RNA-seq analysis of the N3433 and N3431 strains.

### 4.2.3 Investigating the interplay of additional endonucleases in RNA processing and decay

Although RNase E has been established as the major endonuclease in the initiation of mRNA decay, many RNA processing and degradation events are mediated by other components of the RNA decay machinery. This work presents dRNA-seq analyses of RNase III and G, whereby total RNA was extracted and sequenced from *E. coli* strains SDF205 (*rnc*-105) and GM11 (*rng::cat*), and compared to total RNA sequenced from their congenic wild-type strains SDF204 and MC1061, respectively. Again, the final processed data was uploaded to the UCSC Microbial Genome Browser where screenshots could be produced at notable sites of cleavage, as shown in Figure 4.7.

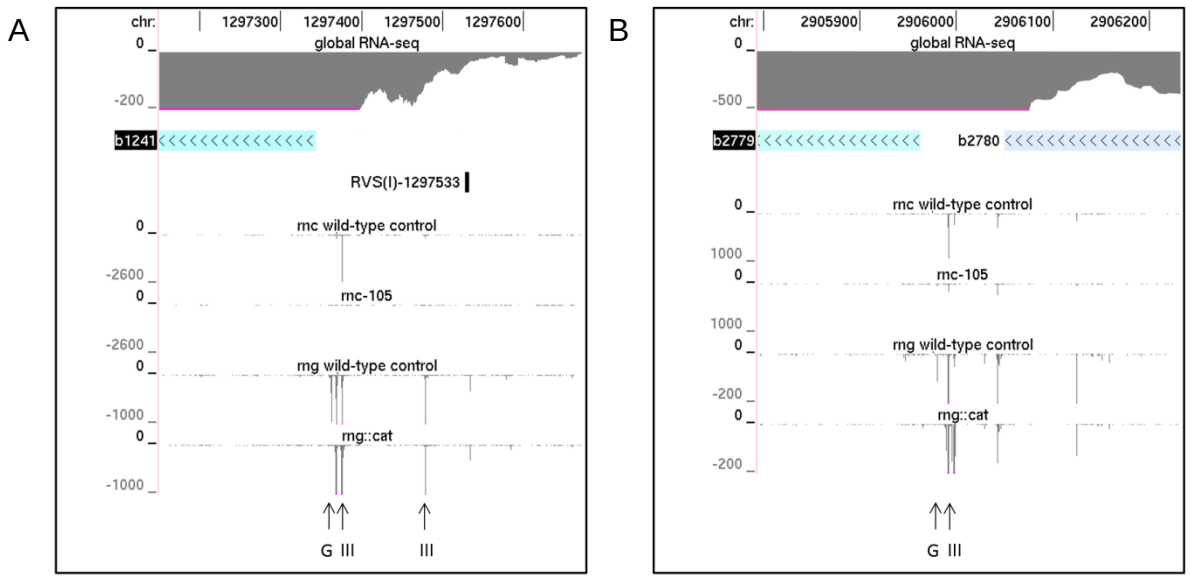


**Figure 4.7 Differential RNA-seq profiles at sites of RNase III and G cleavage.** Panels A and B show sites within the 5' UTR of the *adhE* mRNA and the intergenic region between the *pyrG-eno* mRNA, respectively. The tracks and labelling are as described in Figure 4.2.

As can be seen in Figure 4.7A, the number of 5' ends at position -25 (relative to the start codon) in the *adhE* mRNA is reduced considerably in the absence of functional RNase III (see *rnc* tracks). By cleaving at this site, RNase III reduces the secondary structure of the 5' UTR, exposing the Shine-Dalgarno element to translating ribosomes (Aristarkhov et al., 1996). Previously it has been found

that the *adhE* mRNA is also a substrate for RNase G (Umitsuki et al., 2001, Wachi et al., 2001). As shown in Figure 4.7A, a site at position -19 is reduced in the absence of RNase G, which reflects previous findings (see *rng* tracks) (Ito et al., 2013). The initial cleavage by RNase III may result in a more single-stranded character around the *rng*-dependent site and provide a 5' monophosphate in the downstream product, both of which enhance cleavage by RNase G (Jourdan and McDowall, 2008).

The *adhE* transcript is not the only example whereby sites of RNase III and G activity are found in close proximity. As shown in Figure 4.7B, 5'-ends at position -35 (relative to start codon of the downstream gene) in the *pyrG-eno* mRNA decrease substantially in the absence of functional RNase III. Although this site has not been established previously, one study has found that a mutation in *rnc* has resulted in an accumulation of full length *pyrG-eno* mRNA (Kime et al., 2008). A site at position -17 decreases in the absence of functional RNase G. Mutations in *rng* have been found to result in stabilisation of the *eno* mRNA (Kaga et al., 2002) suggesting the combined action of RNase III and G on the *pyrG-eno* mRNA may serve the same purpose as with the *adhE* mRNA.

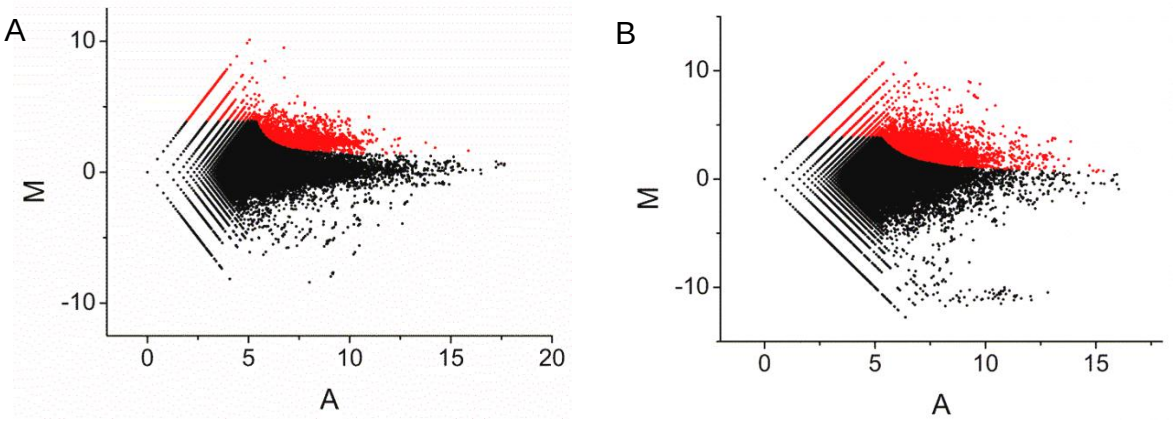


**Figure 4.8 Scatter plot analyses of the *rng* and *rnc in vivo* datasets.** Panels A and B are the same analysis as Figure 4.3 except the values correspond to reads obtained from an *rng::cat* disruption strain and *rnc*-105 strain, respectively, compared to their congenic wild-type partners. The points coloured red for Panel A correspond to those with M values ≥ 4 or ≥ (0.2*A/[-2.4+(0.5*A)])+0.7 if A values were < or ≥ 5.5, respectively. The points coloured red for Panel B correspond to those with M values ≥4 or ≥ (0.9*A/[-2.8+(0.7*A)])-1.1 if A values < or ≥ 5.3, respectively.

As with the *rne in vivo* dataset, an M-A scatter plot for both the *rng* and *rnc in vivo* datasets was constructed as described in Section 3.2.2 (Figure 4.3A). The *rng in vivo* M-A scatter plot showed two characteristic populations, whereby the major cone (cone of "noise") was centred on an M value of 0 and the minor cone (*rng*-dependent population) was centred on an M value of around 2.5, as shown in Figure 4.8A. Because of this clear separation, a boundary was drawn along the edge of the "noise" cone and points with M values ≥ this boundary were highlighted as *rng*-dependent sites. The

difference between the M-A scatter plots of the *rne* and *rng in vivo* datasets reflects the much more restricted role RNase G has in RNA metabolism compared to RNase E (Lee et al., 2002, Ow et al., 2003).

The *rnc in vivo* M-A scatter plot presented a less neatly defined "noise" cone as the *rng in vivo* dataset, as shown in Figure 4.7B. However, a boundary was established by fitting a hyperbole function to the bottom edge of the "noise" cone, where it appears more consistent, and then reflecting the function on the line M = 0. The larger spread of M values in the *rnc in vivo* dataset compared to the *rng in vivo* dataset is consistent with RNase III having a more general role in RNA cleavage compared to RNase G (Stead et al., 2011).

With the establishment of the *in vivo* populations dependent on each of the 3 enzymes, the congruence of the sites was determined by using a Venn diagram as shown in Figure 4.9.

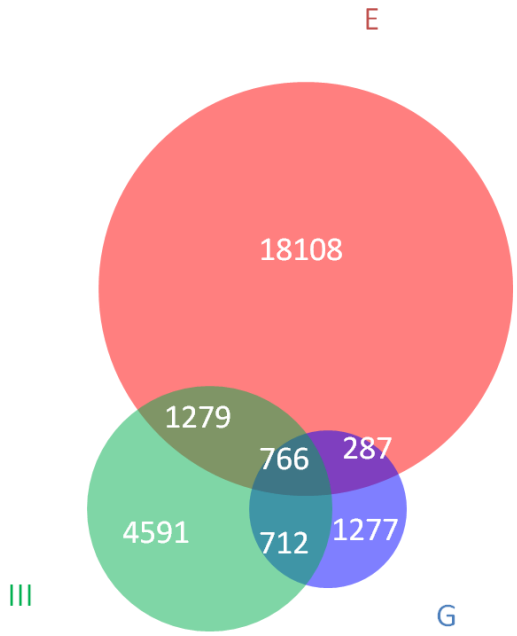


**Figure 4.9 Venn diagram of *rne*, *rng* and *rnc in vivo* datasets.** A venn diagram was constructed whereby the frequency of each site in the three *in vivo* M-A scatter plot populations was determined. Populations from the *rne*, *rng* and *rnc* datasets are labelled as E, G and III, respectively. Image was produced using the BioVenn application (Hulsen et al., 2008).

Although RNase G and the first 470 amino acid residues of RNase E share 50% sequence similarity (McDowall et al., 1993), as well as several structural and functional features (Tock et al., 2000, Briant et al., 2003, Jourdan and McDowall, 2008), it appears that only 9% of the *rng*-dependent sites are also *rne*-dependent. Even more surprisingly, there seems to be 23% overlap of the *rng*-dependent population with the *rnc*-dependent population, despite clear differences in the structural and mechanistic homology between RNase G and III. However, this overlap does not necessarily

represent sites which are cleaved by both enzymes, but may represent cleavages by one enzyme that are enhanced by the initial cleavage elsewhere by the other *e.g.* cleavage by RNase G in the *adhE* 5'UTR is enhanced by upstream cleavage by RNase III (Aristarkhov et al., 1996). This, and the fact that some of the sites in one mutant could be almost completely substituted by the presence of another enzyme, does make the analysis of the *in vivo* dataset complex and would require further experiments *e.g.* RNA-seq analysis of double mutants.

One of the most striking features of the *rng*-dependent population is the arrangement of many of the sites into "clusters", some of which span over 80 nucleotides. Many of these *rng*-dependent clusters overlap with non-coding RNA operons; the clusters tend to be confined within the 5S rRNAs and tRNAs as shown in Figure 4.10.

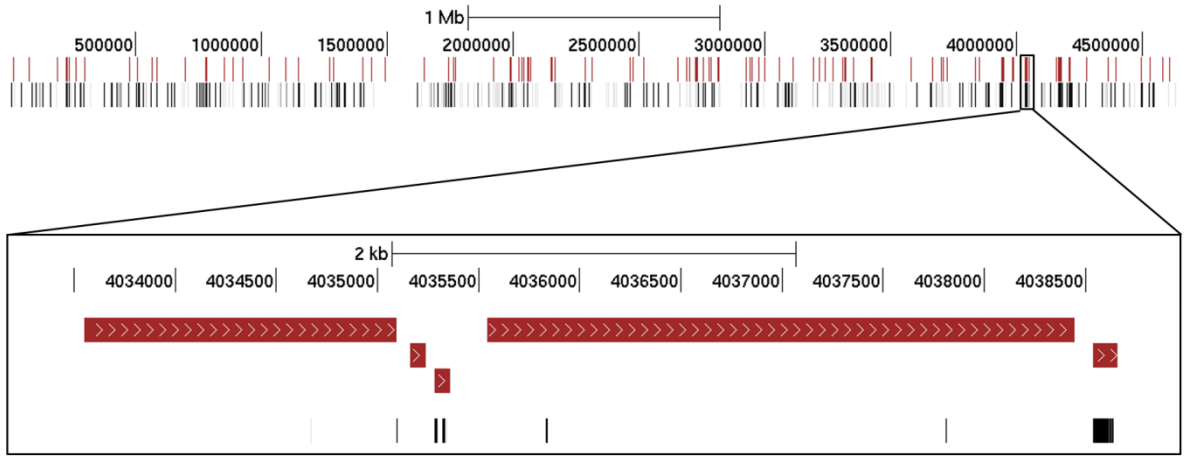


**Figure 4.10 Transcriptome-wide prevalence of *rng*-dependent sites.** In the top panel, the first line represents the genome position. The first track shows the positions of the known non-coding RNA operons in *E. coli*. The second track shows the location of the *rng*-dependent sites, as determined in Figure 4.7. The inset shows clusters of *rng*-dependent sites relative to the *rrnA* operon. Sites on the forward and reverse strands are shown as vertical lines coloured black and grey, respectively.

It is unlikely that these clusters represent an inconsistency in the experimental approach, as analysing the capillary electrophoresis images of the RNA samples prior to fragmentation provided by Vertis Biotechnologies (Figure 4.11) shows a substantial presence of a band that corresponds to tRNAs and 5S rRNA even after mRNA enrichment of the GM11 total RNA.

If these clusters are generated by the direct action of RNase G *in vivo*, this pattern would suggest that RNase G may act as a "pseudo" exonuclease by cleaving small fragments from the 5' end of RNA sequentially. To test this hypothesis, total RNA was extracted from strain MC1061 and enriched for mRNA. The samples were then treated with TAP (5'-triphosphate to -monophosphate group) followed by PNK (5'-hydroxyl to -monophosphate group) to ensure the majority of transcripts were

5’ monophosphorylated. The RNA was then incubated with RNase G for 30 min and sequenced as described previously. An M-A scatter plot was constructed comparing the processed datasets for 0 and 30 min incubation, as shown in Figure 4.12. A population was highlighted which represents the sites that appear in the *rng*-dependent population *in vivo*.

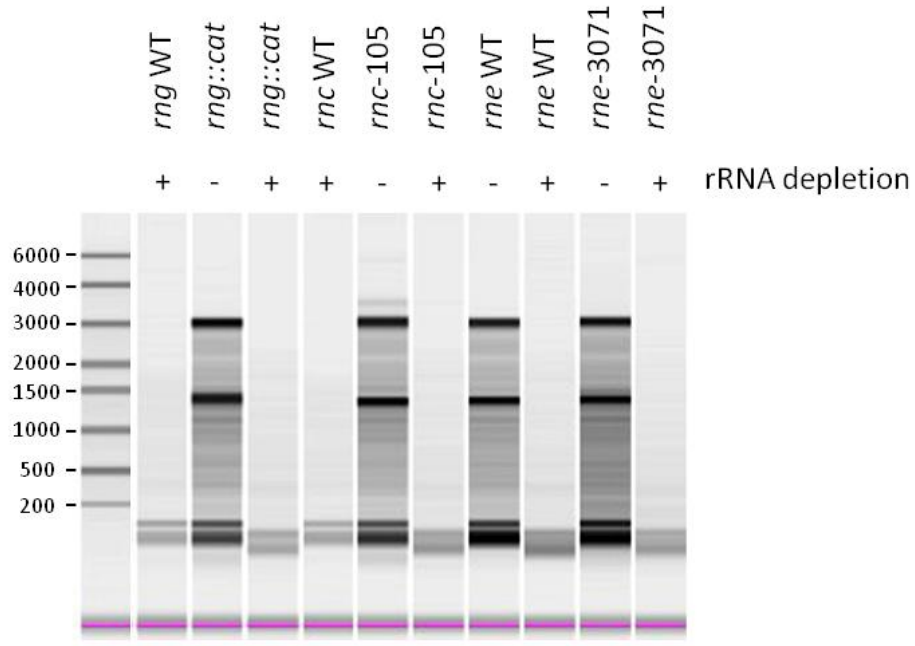


**Figure 4.11 Analysis of the integrity of the total RNA.** Samples were separated on a Shimadzu MultiNA electrophoresis capillary system alongside a RiboRuler$^{TM}$ High Range RNA ladder (ThermoFisher, US). Sample names are labelled above each lane and band sizes (nt) on the left.

These positions have very different M-A values in the RNase G *in vitro* dataset; the boundary of the population appears to be parallel to the “noise” arms on the graph. At an M value of 0, this boundary has an A value of 7.5, which means this population of RNase G sites each have reads ≥181 before incubation with RNase G. Such a spread, whereby most of these points have negative M values, is indicative of trimming activity *in vitro* due to the majority of background products acting as substrates and hence being reduced over time following incubation.

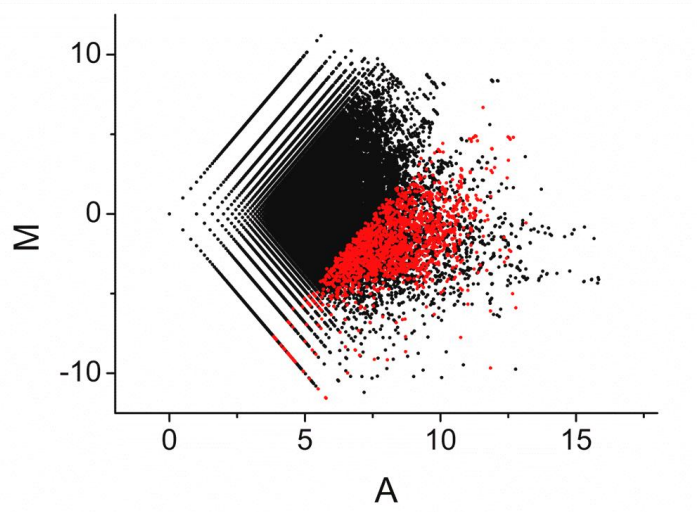


**Figure 4.12 Scatter plot analysis of RNase G *in vitro* dataset.** An M-A scatter plot was constructed using the dRNA-seq data obtained from 5'-monophosphorylated RNA incubated after 0 min and 30 min with RNase G. The A value was equal to [$\log_2$(reads after 30 min) + $\log_2$(reads after 0 min)]/2 and the M value was equal to $\log_2$(reads after 30 min/reads after 0 min). The points coloured red are equivalent to the sites found in the *rng*-dependent population from the *rng in vivo* scatter plot.

Additionally, 25 substrates have been identified where absence of RNase G *in vivo* results in accumulation of 5'-monophosphorylated ends up to <200 nt upstream of ends that are significantly reduced (Table S1), suggesting a wide-spread role for RNase G in the trimming of 5' sequences. However, to truly confirm the mechanistic nature of RNase G on these substrates, further analyses both *in vitro* and *in vivo* will be required.

### 4.2.4 Identifying additional substrates of 'direct' entry

To determine the population of direct entry sites, an M-A scatter plot was constructed for the T170V 10 min *in vitro* dataset in a similar manner to the *rne in vivo* dataset, however M values were equal to $\log_2$(reads after 10 min incubation/reads after 0 min incubation) and A values were equal to [$\log_2$(reads after 10 min incubation) + $\log_2$(reads after 0 min incubation)]/2, as shown in Figure 4.13A.

As with the *rne in vivo* dataset, a suitable boundary was established at an M value ≥ 5, which corresponds to a 32-fold increase in peak height following incubation with T170V for 10 min. However, the position of the noise cone was found to be centred at M value of -1.6, rather than 0. Since the 5' ends of the majority of the RNA in the 0 min sample were hydroxylated, hence reducing the efficiency of ligation of the sequencing adaptor, additional rounds of PCR were required to amplify the correct quantity of cDNA libraries required for sequencing. This was not the case for the 10 min sample, due to the production of RNA fragments with a 5' monophosphate upon incubation

with the hydrolytic T170V NTH-RNase E. Therefore, noise reads would be higher at 0 min than after 10 min incubation, which would result in negative M values and hence the shift downwards of the noise cone. However, this would have affected all ends in this analysis similarly, and so the boundary was shifted down from M = 5 to 3.4 as shown in Figure 4.13B.

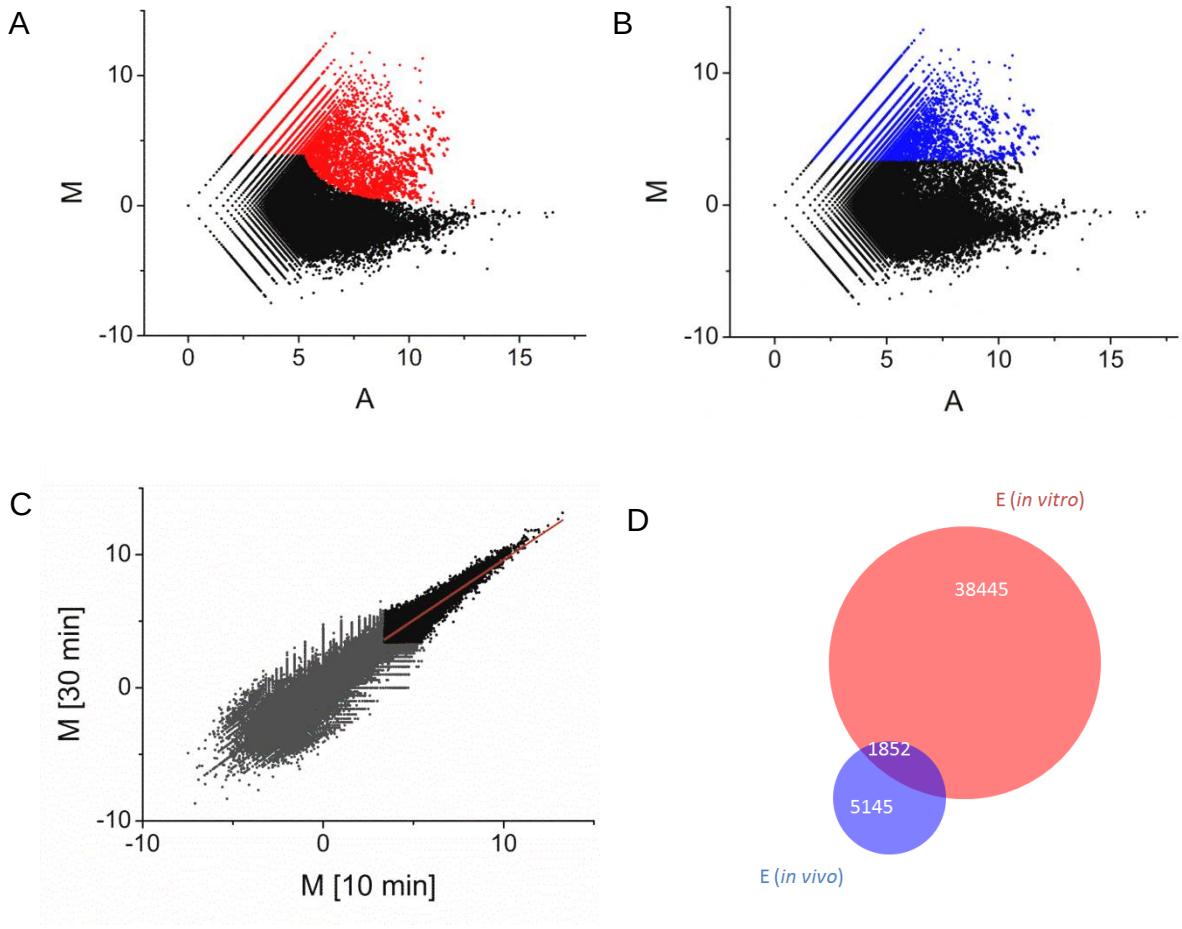


**Figure 4.13 Scatter plot analysis of T170V *in vitro* dataset.** Panels A and B show an M-A scatter plot that was constructed using the dRNA-seq data obtained from 5'-hydroxylated RNA incubated after 0 min and 10 min with NTH-RNase E T170V mutant. The A value was equal to [$\log_2$(reads after 10 min) + $\log_2$(reads after 0 min)]/2 and the M value was equal to $\log_2$(reads after 10 min/reads after 0 min). The points coloured red in Panel A correspond to sites in the transcriptome with M values ≥ 4 or ≥ (0.8*A/[-2.95+(0.7*A)])-1.7 if A values were < or ≥ 5.27, respectively. The points coloured blue in Panel B correspond to sites in the transcriptome with M values ≥ 3.4. The black line represents M = 0 and the grey dotted line is the centre of the cone of noise with M value = -1.6. Panel C shows an M-M scatter plot that was constructed using M values generated from the analysis in Panel A and M values generated from a similar analysis but using data after 30 min incubation with T170V. The points coloured black represent those with M values ≥ 3.4 in both analyses and were used to perform a Spearman's rank correlation coefficient as shown by the red line. The points coloured grey were not used in the statistical analysis. Panel D shows a Venn diagram of the populations from the *rne in vivo* and T170V *in vitro* datasets. The Venn diagram was constructed as described in Figure 4.9.

M values were also calculated for an additional *in vitro* dataset, whereby the sequencing results after 30 min incubation with T170V were compared to the 0 min sample. An M-M scatter plot was

then constructed comparing the M values after 10 min incubation with T170V and the M values after 30 min incubation, as shown in Figure 4.13C. Spearman's rank correlation coefficient was calculated for the significant population *i.e.* the points with M values ≥3.4; the value of a rank coefficient remains unaffected by the obvious positive skewness of both variables. The strong correlation coefficient of 0.82 suggests that much of the cleavage was completed after 10 min incubation, and that the differential RNA-seq approach provides a reproducible measure of the underlying enzymology. This value is significant (p value < $7x10^{-6}$) due to the large size of the population (over 32,000 pairs).

The congruence of the *in vivo* (Figure 4.3B) and *in vitro* (Figure 4.13B) populations was then determined by constructing a Venn diagram, as shown in Figure 4.13D. Around 36% of the *rne*-dependent sites *in vivo* can be recapitulated by NTH-RNase E T170V *in vitro*. Additional factors, such as the presence of a functional 5' sensor and CTH *in vivo*, could explain the 64% of sites found *in vivo* that are not found *in vitro*. The intersecting population is only 5% of the total T170V *in vitro* cleavage population, possibly due to the absence *in vitro* of various competing cellular factors *e.g.* ribosomal coverage of single-stranded regions, reflecting the broad specificity that the NTH-RNase E potentially has.

From this *in vitro* population, candidates were individually selected for analysis *in vitro*, based on several factors such as gene annotation and M values from the *in vivo* dataset. Primers were designed to extend from the known TSS to the transcription terminator where possible. If the known transcriptional unit was too large (>1500 nt), primers were designed to hybridise to regions in the gene not associated with strong secondary structure in the corresponding transcript using the RNAfold web server (Hofacker, 2003). DNA templates were amplified by PCR and transcribed *in vitro* using T7 RNA polymerase as described in Section 2.3.2 and 2.2.3, respectively. Transcripts were incubated with NTH-RNase E T170V and samples taken at several time points were analysed by denaturing PAGE, as shown in Figure 4.14.

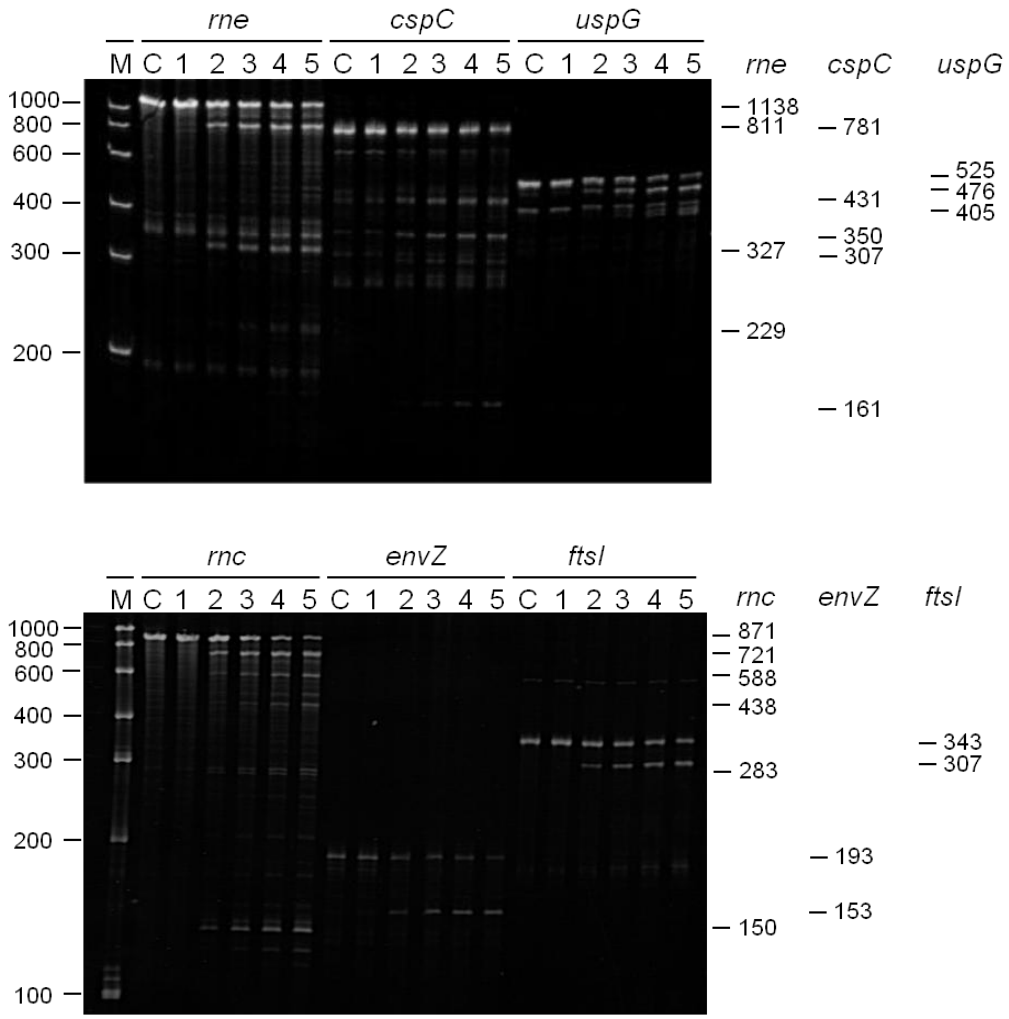


**Figure 4.14 Cleavage of 5'-triphosphorylated RNA by direct entry.** The 5'-triphosphorylated transcripts were generated by *in vitro* transcription as described in Materials and Methods. The gene to which each substrate corresponds is shown at the top of each image. Final substrate and NTH-RNase E T170V concentrations were 180 nM and 20 nM, respectively. Samples were taken after various time points upon incubation, quenched in equal volumes of 2x RNA loading dye, denatured at 95°C, separated on 8% denaturing polyacrylamide gels, and stained with ethidium bromide as described in Chapter 2. Lanes 1-5 contain samples taken at 0, 5, 15, 30 and 60 min after incubation of substrate with enzyme. Lane C contains substrate incubated without enzyme for 60 min. Lane M contains a RiboRuler™ low range RNA ladder with sizes in nt indicated at the left of each image. The sizes in nt of the substrates and cleavage products are shown at the right of each image.

Incubation of 5'-triphosphorylated transcripts with T170V identified cleavages as efficient as those found in the direct entry candidates *cspA* and *argX* (Figure S1) for *rne*, *cspC*, *uspG*, *rnc*, *envZ* and *ftsI* mRNA. Moreover, many of these sites map to sites identified in the RNA-seq analysis both *in vivo* and *in vitro* from Figure 4.13D. However, a minority of these cleavages do not map to sites with highest M values from the *in vitro* dataset, probably because of the fact that the boundaries of the substrates designed *in vitro* were almost certainly different from those that were isolated from *E.*

*coli.* Despite this difference, these results provide evidence that direct entry pervades beyond maturation of tRNA in *E. coli.*

### 4.2.5 Identifying conserved features found at sites of cleavage

Although several studies have determined the cleavage specificity of RNase E using artificial substrates (Lin-Chao et al., 1994, McDowall et al., 1994, Kaberdin, 2003), none of these studies have been performed on a transcriptome-wide scale. For both the *rne in vivo* and T170V *in vitro* populations, the genome sequences flanking 8 nt upstream to 8 nt downstream at each site were extracted and aligned using the Berkley WebLogo application (Figure 4.15).

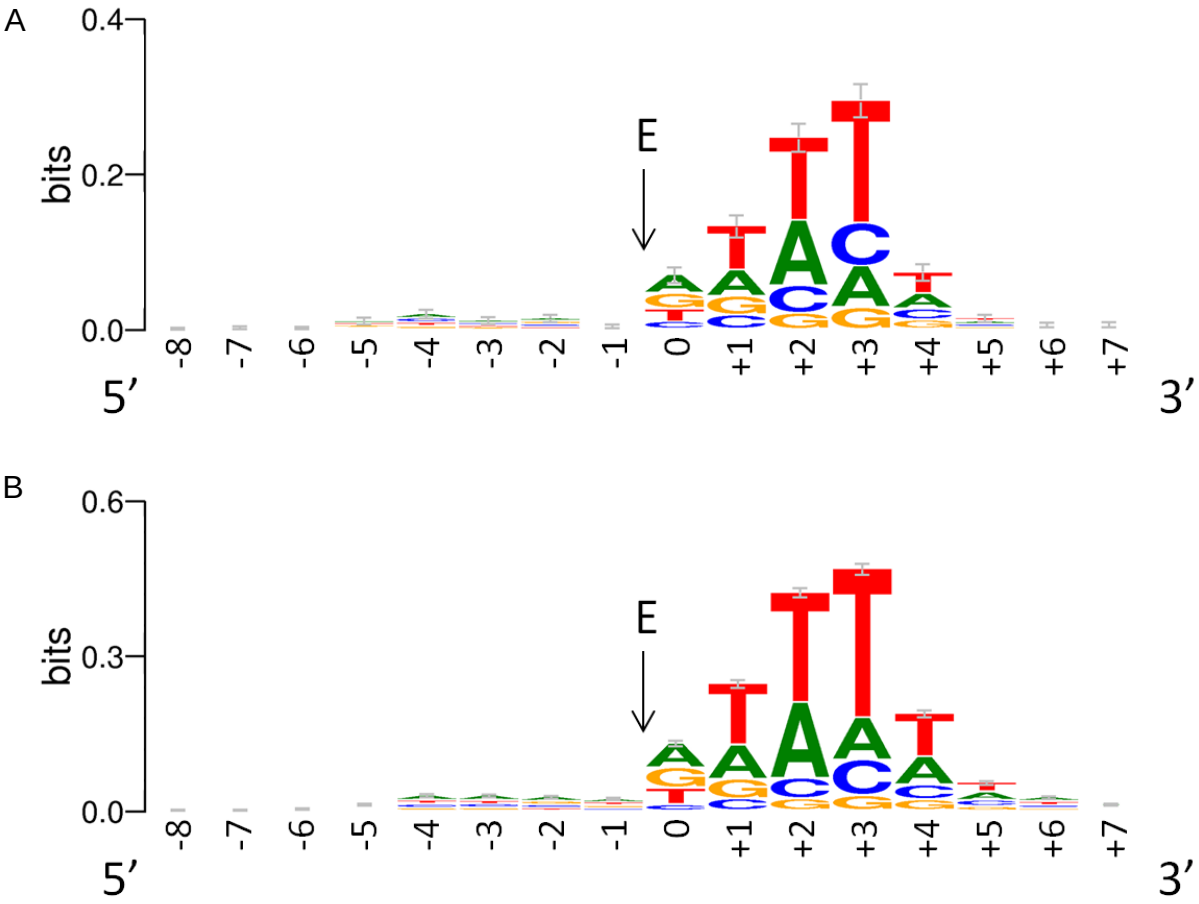


**Figure 4.15 Conserved sequence found at sites of cleavage.** Panels A and B are weblogo representations of the *in vivo* and *in vitro* populations, respectively. The total height of each stack represents the level of sequence conservation at that particular position. The height of each individual nucleotide represents the relative frequency of that nucleotide at each position. Nucleotide positions along the horizontal axis are numbered relative to the nucleotide 3' to the site of cleavage (shown as a vertical arrow). Uridine residues are shown as thymine residues due to the WebLogo software displaying final results as genome sequences. Images were produced using the Berkley WebLogo application (Crooks et al., 2004).

Despite a 36% overlap between the *in vivo* and *in vitro* data sets, the recurring sequence around sites of cleavage appears to be almost identical. The apparent preference for AU rich regions around the sites of cleavage reflects previous studies (McDowall et al., 1994, Kaberdin, 2003), and is probably a consequence of the enzymes requirements for single strandedness. GC rich regions within RNA not only form Watson-Crick base pairs with a higher $T_m$ than AU rich regions, but polyG and C repeats have also been found to form stable motifs such as the G-quadruplex (Pochon and Michelson, 1965) and the i-motif (Gehring et al., 1993), respectively. Complex structures such as these would be less likely to engage the single-stranded RNA binding channel within RNase E. Interestingly, there seems to be more bias for uracil residues compared to adenine. This could be due to the ability of the uracil base to present an exocyclic oxygen to a lysine residue at position 106 on the NTH-RNase E (Callaghan et al., 2005a). This additional contact could increase the affinity of U-rich regions to RNase E during direct entry.

Due to numerous studies that have found evidence for RNase E autoregulation mediated by structural regions within the 5' UTR of its own mRNA (Diwa et al., 2000, Diwa and Belasco, 2002, Schuck et al., 2009), the *rne* substrate from Figure 4.14 was chosen for further analysis of direct entry. Using a similar method as described for the *metT* and *glyV* tRNA precursors in Chapter 3, primers were designed to hybridise to the *rne* gene to produce a truncated RNA ranging from the nucleotide at position +135 to +588 (relative to the first nucleotide of the start codon AUG), as shown in Figure 4.16A. Even though this truncation included the removal of the 5' UTR mentioned above, cleavage at site +447 and at site +545 by T170V occurred at similar rates as found for the full length substrate, as shown in Figure 4.16B. Therefore, the 5' UTR of *rne* mRNA is not required for cleavage at the two major direct entry sites found both *in vitro* and *in vivo*.

A further truncation was performed on this substrate to remove 18 nucleotides at the 3' end, which included the cleavage site at nucleotide position +545, to produce a 409-nt substrate that ranged from the nucleotide at position +135 to +540, as shown in Figure 4.16A. Removal of the +545 site had little to no effect on cleavage at position +447, as shown in Figure 4.16B. Therefore, cleavage of the major site at +447 by RNase E via direct entry does not involve interaction at the minor site at position +545.

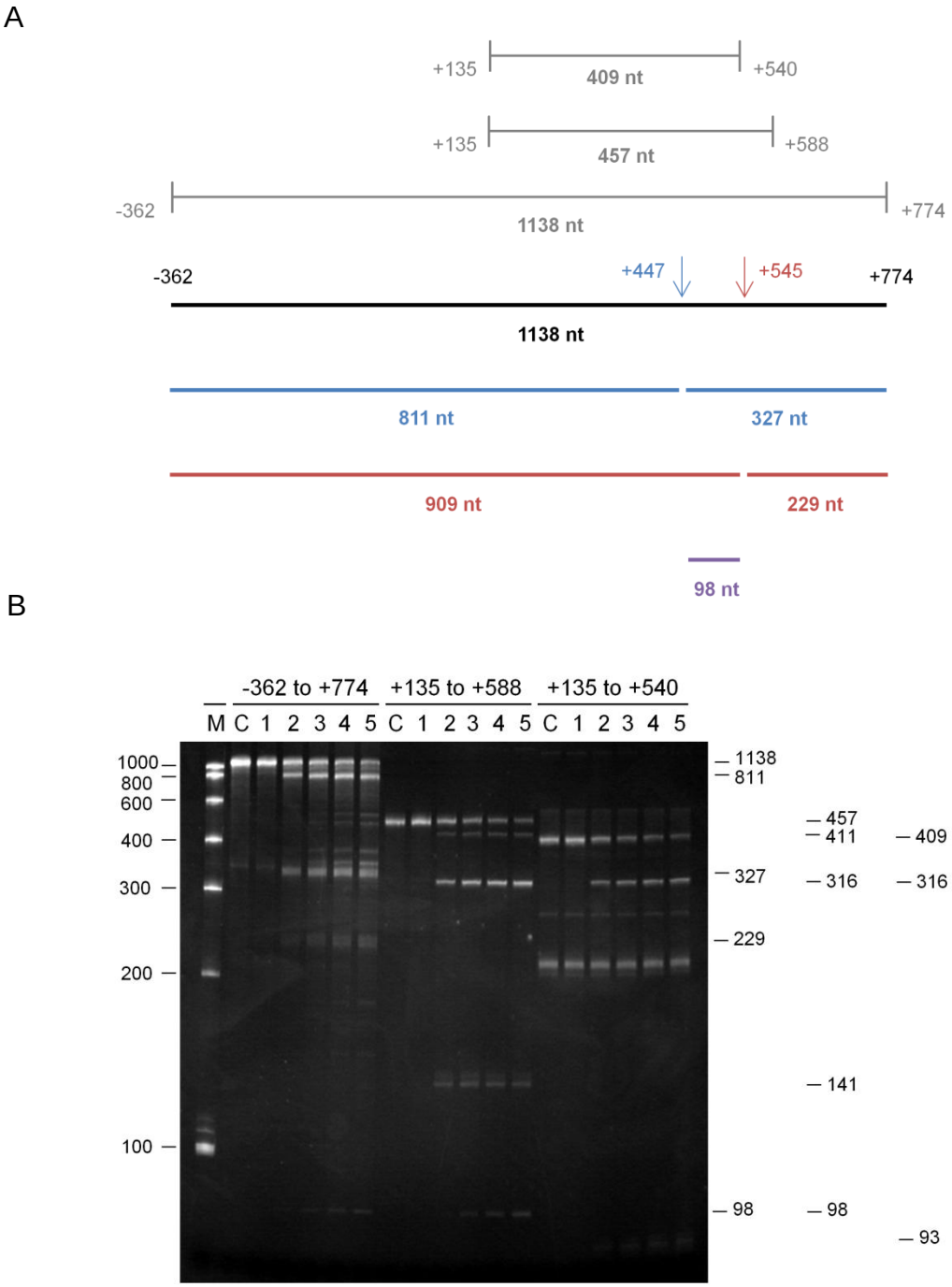


**Figure 4.16 Cleavage of truncated forms of the *rne* substrate.** The 5'-triphosphorylated transcripts were generated by *in vitro* transcription as described in Materials and Methods. Panel A shows a schematic representation of the *rne* substrate used in this analysis (black line). The blue lines represent the products of T170V cleavage at nucleotide position +447. The red lines represent the products of T170V cleavage at nucleotide position +545. The purple line represents the additional product after T170V cleavage at both sites. The size of the substrate and products are shown below each line. In addition, the boundaries of the truncated substrates are shown above in grey, with the start and end nucleotide of each truncation located at either end. Panel B shows the cleavage assay results of each substrate. The identity of each truncation is shown at the top of the image. Further details are as described in Figure 4.14.

To locate the secondary interaction where RNase E may make contact during direct entry, complementary DNA oligonucleotides were hybridised to the 409-nt fragment. The positions of these DNA oligonucleotides were confirmed by RNase H digests (data not shown). The hybridised samples were then incubated with T170V and analysed for cleavage as before, as shown in Figure 4.17. By blocking the first 20 nt (shown as b9 on Figure 4.17), the rate of cleavage at position +447 by T170V was reduced significantly. Blocking a 20 nt segment only 17 nt downstream of b9 (shown as b10) had no effect on cleavage at this site. As a control, a 22 nt segment encompassing the cleavage site at position +447 was also blocked (shown as b11), which, as expected, prevented access of T170V and hence abolished cleavage. Therefore, efficient cleavage at position +447 by direct entry appears to be dependent on the accessibility of RNase E to a region between +135 and +155.

A further truncation of this 409-nt substrate was performed, whereby 57 nt were removed from the 5' end to produce a 352-nt fragment ranging from the nucleotide at position +197 to +540, as shown in Figure 4.18A. This truncation included removal of the two regions to which DNA oligonucleotides b9 and b10 hybridised.

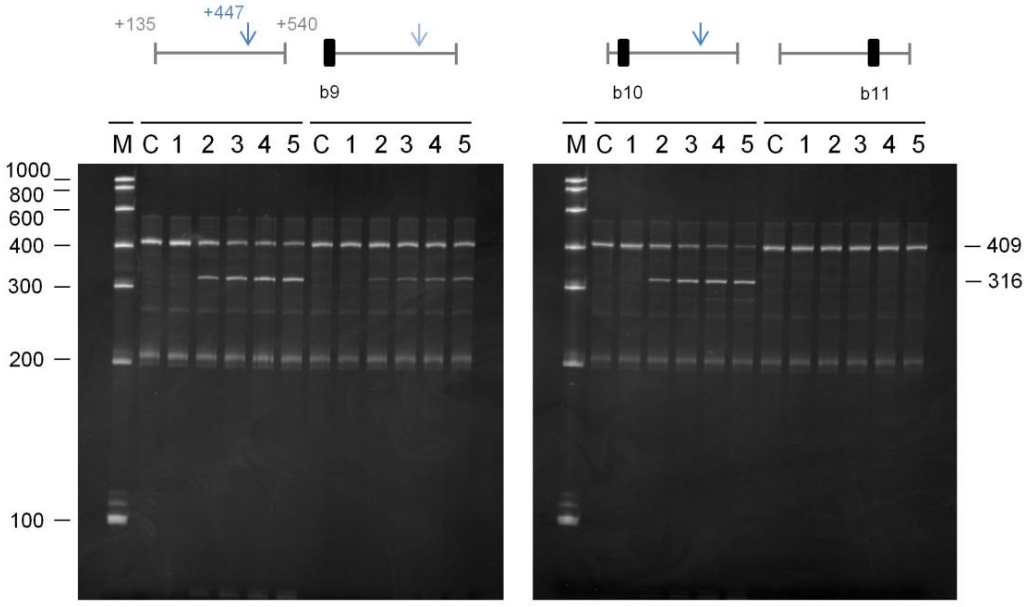


**Figure 4.17 Cleavage of truncated *rne* mRNA hybridised with various blocking oligonucleotides.** Truncated *rne* transcript ranging from nucleotide position +135 to +540 was incubated with 3-fold Molar excess of DNA oligonucleotides complimentary to the regions highlighted in black above the gel image. The positions of hybridisation were confirmed by RNase H digests. The sequences of the DNA oligonucleotides are shown in Table 2.1 in Section 2.2.3.7. The hybridised samples were incubated with T170V and cleavages were analysed as described in Figure 4.14. Lighter arrows indicate cleavage that was reduced, but not abolished.

As shown in Figure 4.18B (second panel), the rate of cleavage at position +447 in this 352-nt substrate is similar to the rate seen in the 409-nt substrate when hybridised with the DNA oligonucleotide b9. The residual cleavage at the +447 site suggests an alternative interaction that could occur in the 352-nt substrate to allow direct entry. This region must be between +192 and +277, as removal of this segment effectively blocked cleavage at +447, as shown in Figure 4.18B (third panel). Interestingly, cleavage at +447 could be restored by addition of the 48 nt back to the 3' end encompassing the +545 nt cleavage site to produce a 315-nt fragment as shown in Figure 4.18B (fourth panel). Therefore, it appears that cleavage at position +447 via direct entry can be supported by a secondary interaction at either the 5' or 3' side with RNase E.

A

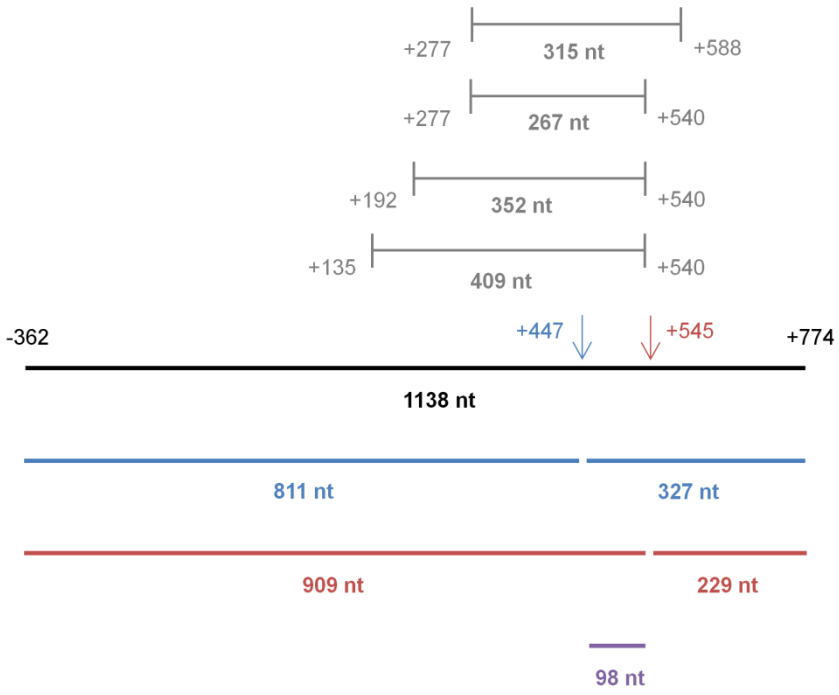


B

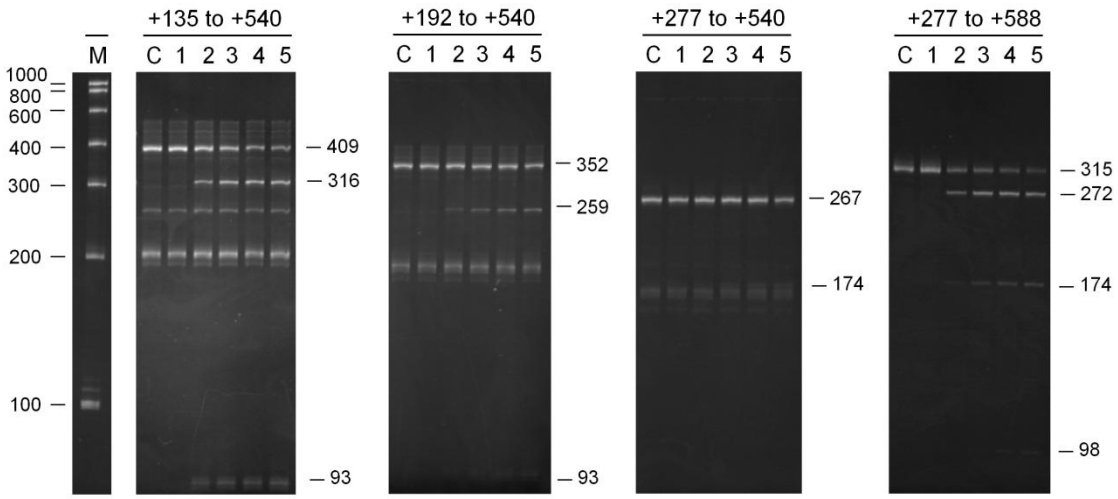

**Figure 4.18 Cleavage of further truncations of the *rne* substrate.** Both Panels A and B are labelled as described in Figure 4.16.

Hybridisation of the DNA oligonucleotide b11 to block the region encompassing the +447 cleavage site had little effect on the cleavage rate at the +545 site, as shown in Figure 4.19. In addition, hybridisation of a DNA oligonucleotide to block a 20 nt region encompassing the +545 site (shown as b12 on Figure 4.19) had no effect on the cleavage rate at the +447 site. This result confirms that cleavage by direct entry at one of these sites is independent of the other.

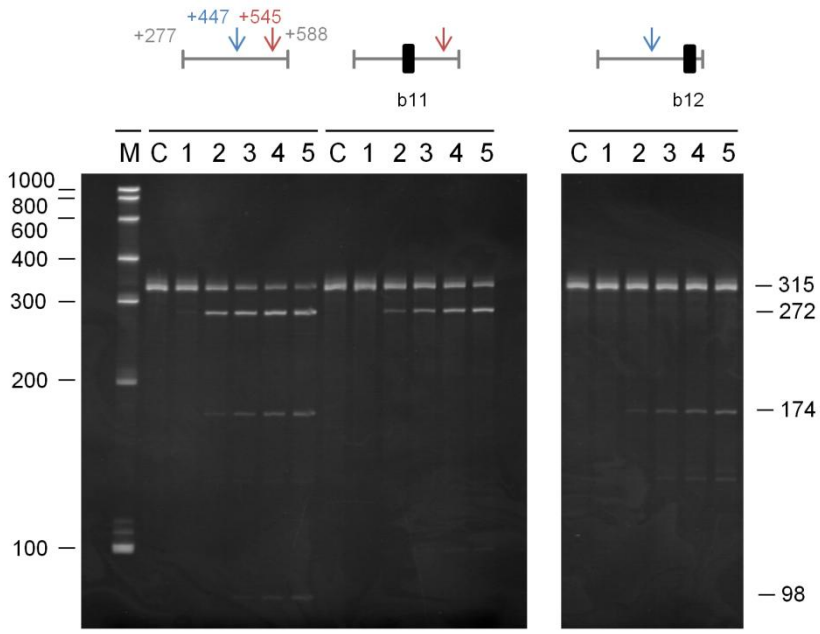


**Figure 4.19 Cleavage of further truncations of *rne* mRNA hybridised with blocking oligonucleotides.** Truncated *rne* transcript ranging from nucleotide position +277 to +588 was incubated with 3-fold molar excess of DNA oligonucleotides complementary to regions highlighted in black above the gel image. Labelling is as described in Figure 4.17.

It appears that RNase E possesses flexibility with regard to the locations of unpaired regions in mRNA substrates that it can bind to initiate direct entry cleavage. This finding is expected, given the relative flexibility and length of mRNA compared to tRNA precursors as well as the simple requirements for direct entry. It is likely that these regions are brought closer together for simultaneous interaction with NTH-RNase E by structural elements within the RNA.

## 4.3 Discussion

The work described here shows that cleavages by RNase E can be found throughout the transcriptome of *E. coli*. This reinforces the evidence found previously that RNase E is the major endonuclease involved in initiating mRNA decay in *E. coli* (Babitzke and Kushner, 1991, Stead et al.,

2011). However, sites dependent on *rne* are not limited to mRNA decay or tRNA maturation, and have been implicated in the quality control of ribosomes, processing of CRISPR RNAs, and in regions not associated with high levels of transcription. Because of this potential involvement in various cellular processes, the role of RNase E in post-transcriptional gene regulation may extend much further than initiating mRNA decay by endonucleolytic cleavage.

Additionally it has been found that the hallmark property of RNase E to interact with a 5' monophosphate is not required for a large proportion of RNase E cleavages. Therefore, it appears that direct entry has a major role beyond tRNA maturation and is potentially the major pathway by which mRNA decay is initiated. In addition, these cleavages also seem to occur in the absence of the C-terminal half, which provides the scaffold for the RNA degradosome, and therefore represents a growing list of substrates that can be reconstituted *in vitro* using just the NTH of RNase E (For reviews see (Carpousis et al., 2009, Mackie, 2013b). Such substrates will be of value in further biochemical characterisation of direct entry, as well as controls for the analysis of the contribution of the CTH to RNase E cleavage. Although mutations in the CTH alone do not affect cell viability (Leroy et al., 2002), the CTH is indispensable in cells with a mutation in either RppH (Anupama et al., 2011) or the 5' sensor (Garrey et al., 2009, Garrey and Mackie, 2011). This suggests that the CTH has some role in direct entry, possibly by providing additional interactions with RNA via the arginine-rich domains (Taraseviciene et al., 1995, Kaberdin et al., 2000) or by localising the components of the RNA degradosome, which may actively degrade products of cleavage that would otherwise remain tightly bound to RNase E (for further discussion, see later chapters).

As found with the *metT* and *glyV* tRNA precursors (see Chapter 3), evidence has been provided that direct entry cleavage within the *rne* transcript requires access to unpaired regions in addition to those that are cleaved. The simultaneous binding of two or perhaps more regions within the transcript to RNase E may increase the overall affinity (Kime et al., 2010, Kime et al., 2014). In addition, new evidence has found that RNase E possesses flexibility in relation to the binding of unpaired regions. Cleavage at the +447 site in a 409-nt substrate, which is abolished by removal of regions found upstream of the site, can be restored by subsequent addition of the region found downstream of the site. Complementing this finding, work performed alongside this study by Louise Kime has found that direct entry cleavages in the *rnc* and *uspF* mRNAs are actually shifted when blocked by DNA oligonucleotides (Clarke et al., 2014). Therefore, not only can RNase E cleave at the same site while being able to change the position which it makes an additional contact, but it can also keep hold of the additional contact while changing the site of cleavage. This flexibility in the position of binding and/or cleavage suggests that RNase E can bypass the inhibitory effects of high

ribosomal traffic and transient secondary structure, which are more common in mRNAs compared to tRNA precursors. However, it is still unclear what role the 5' UTR of the *rne* transcript plays in auto regulation, given that it is not required for rapid cleavage by direct entry *in vitro*. This topic will be analysed further in the next chapter.

This work has also found a more limited role for cleavages by RNase G, and RNase III to some extent, in the decay of the RNA pool. In accordance with previous findings, the congruence between sites of cleavage by RNase G and RNase E is actually low despite their structural similarities (Lee et al., 2002, Ow et al., 2003). More surprising, some of the results from this work have implied that the mechanistic nature of RNase G may be very different to what has previously been suspected. The clustering of sites at the 5' end of 5S rRNAs and tRNAs suggests RNase G may act by trimming fragments from the 5' end sequentially, acting in a "pseudo" 5'-exonucleolytic manner. RNase J from *Bacillus subtilis* and other bacterial species (Even et al., 2005, Bugrysheva and Scott, 2010) displays both an endonucleolytic and a 5' to 3' exonucleolytic function (Mathy et al., 2007). Interestingly, the endonucleolytic function, which is homologous to RNase E activity in *E. coli* (Even et al., 2005), tends to occur on transcripts with a 5'-triphosphate group (de la Sierra-Gallay et al., 2008). Only substrates with a 5' monophosphate, which is also a requirement for RNase G (Tock et al., 2000, Jourdan and McDowall, 2008), can be degraded in an exonucleolytic manner by RNase J (de la Sierra-Gallay et al., 2008). Although this is only speculative, perhaps the requirement for a 5' monophosphate by RNase G limits its activity to 5' trimming, whereas the ability of RNase E to cleave substrates regardless of the 5'-phosphorylation status allows it to make endonucleolytic cleavages at sites central to transcripts.

# Chapter 5

# Investigating the binding capabilities of RNase E

## 5.1 Introduction

As stated in the previous chapters, RNase E has a major role in controlling the cellular levels of all classes of RNA by mediating their processing and/or turnover (Carpousis et al., 2009, Mackie, 2013b). Two temperature-sensitive mutations have shown that RNase E is essential for cell viability and RNA metabolism (Apirion and Lassar, 1978, Ono and Kuwano, 1979). These mutations, which result in substitutions of glycine to serine and leucine to phenylalanine at positions 66 and 68 respectively (McDowall et al., 1993), are found within the core of an S1-like RNA-binding domain (Schubert et al., 2004). Comparison of the structures of the RNase E apoprotein and when bound to oligonucleotide substrates has revealed that the S1 domain can close down onto the DNase I-like domain (Koslover et al., 2008) to form an elongated RNA-binding channel that can accommodate single-stranded RNA (Callaghan et al., 2005a). Within this channel, two aspartate residues at positions 303 and 346 on the DNase I-like domain coordinate a magnesium ion that mediates hydrolytic attack of the adjacent phosphodiester backbone, which is aligned by the interaction of the base at the 3' side of the susceptible bond with the hydrophobic pouch located on the S1-like domain. This hydrophobic pouch consists of two phenylalanine residues at positions 57 and 67, between which the base is stacked, and the side chain of a lysine residue at position 112 (Diwa et al., 2002, Callaghan et al., 2005a). Interestingly, the Gly66 and Leu68 residues are found buried directly beneath the hydrophobic pocket (Diwa et al., 2002), suggesting that the temperature-sensitive phenotypes observed with mutations in either of these two residues could be a result of disruption on the hydrophobic binding pocket directly above.

The NTH-RNase E self-associates to form a principle dimer, with the S1-like domain of one protomer forming the RNA-binding channel with the DNase I-like domain of the other protomer. Therefore, the principle dimer is the minimal structural unit required for NTH-RNase E to display endonucleolytic activity (Caruthers et al., 2006). Two dimers can then self-associate to form a homotetramer, which has maximum activity (Callaghan et al., 2003, Caruthers et al., 2006, Callaghan et al., 2005b). Thus, the catalytic domain has the capacity to interact with up to four single-stranded regions within four RNA-binding channels (Callaghan et al., 2003). Evidence has been provided that suggests that the simultaneous binding of two or more single-stranded regions could provide a simple mechanism by which RNase E can associate with transcripts (Kime et al., 2010, Kime et al., 2014, Clarke et al., 2014). However, in other cases interaction of a transcript with RNase E involves the recognition of a 5'-monophosphorylated end (Mackie, 1998, Mackie, 2000, Garrey et al., 2009). Indeed, a 5'-monophosphate sensor, consisting of hydrophilic interactions provided by arginine and

threonine residues at positions 169 and 170 respectively, at the beginning of the RNA-binding channel has been located on RNase E (Callaghan et al., 2005a).

Interactions between RNA and NTH-RNase E are not limited to the RNA-binding channel. One of the most well characterised substrates of RNase E is the *rne* transcript, which is stabilised and expressed *in vivo* following inactivation of RNase E (Jain and Belasco, 1995). Further analysis of this substrate found that two conserved stem-loop structures, named hairpin (hp) 2 and 3, on the 5' UTR were responsible for increasing susceptibility of the transcript to RNase E-mediated degradation, as shown in Figure 5.1 (Diwa et al., 2000). In particular, it was found that a uridine residue in a "bulge" region of hp2 made direct contact with an asparagine residue found at position 323, a site in the DNase I-like domain situated away from the RNA-binding channel (Diwa and Belasco, 2002, Schuck et al., 2009).

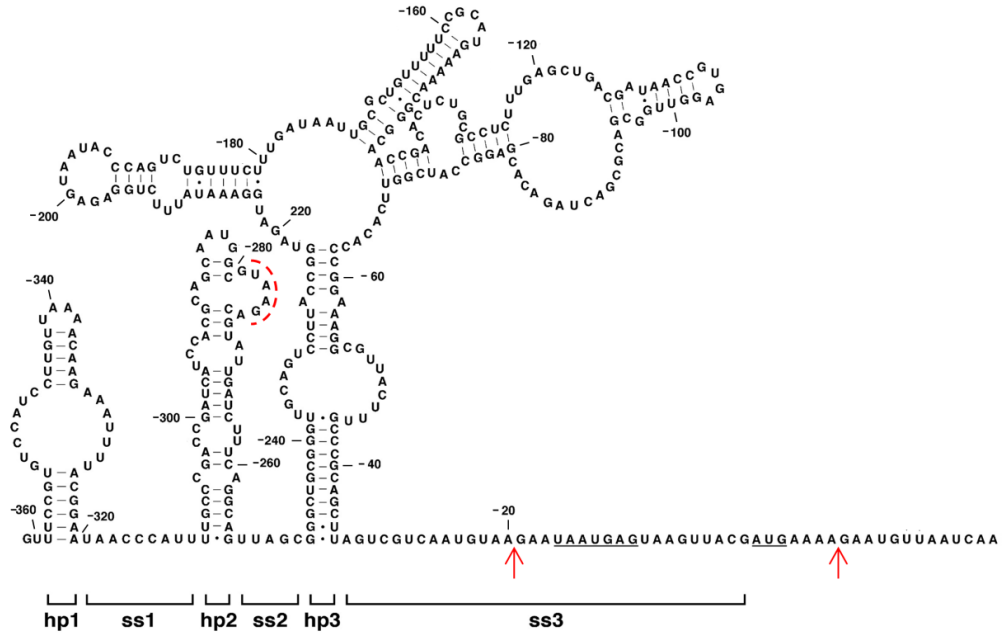


**Figure 5.1 The 5' UTR of the *rne* mRNA.** The secondary structure of the *rne* 5' UTR as determined previously (Diwa et al., 2000). The brackets highlight the boundaries of each structural domain where hp and ss are shorthand for hairpin and single strand, respectively. The numbering indicates the relative distance from the first nucleotide in the start codon, which, alongside the Shine-Dalgarno element, is underlined. The positions of two minor cleavage sites observed in the dRNA-seq data from Chapter 4 are shown as red arrows. The "bulge" region of hp2 that has been identified as a direct binding site of NTH-RNase E is shown as a dashed line (Diwa and Belasco, 2002).

Two other residues, tyrosine and glutamine at positions 25 and 36 within the RNase H-like domain, have been suggested to provide an alternative binding site for RNA within NTH-RNase E (Go et al., 2011, Kim et al., 2014). Interestingly, mutation of the glutamine to an arginine residue at position 36 actually resulted in a 3-fold increase in activity of NTH-RNase E. A combination of UV-crosslinking

and mass spectrometry showed that RNA could bind to a site on the RNase H-like domain by simultaneous interaction with the Gln36 and Tyr25 residues, and that mutation of Gln36 actually allowed RNA to relocate to the S1 like-domain (Kim et al., 2014). In addition, the Q36R mutation resulted in an increase in both the $K_M$ and $k_{cat}$ values, suggesting that, in the wild-type NTH-RNase E, this residue may play a role in uncompetitive autoregulation (Go et al., 2011). Mutation of the tyrosine to an alanine residue at position 25 resulted in a 1.3-fold decrease in activity of NTH-RNase E. Further mass spectrometry analysis found that the Y25A mutation caused the RNA to bind to an allosteric site found between residues at positions 427 and 433 on the small domains of NTH-RNase E, suggesting that other regions within RNase E may have a role in allosteric regulation (Kim et al., 2014). In addition to this, two mutations within the RNase H-like domain of RNase G, a paralogue of NTH-RNase E that is not required for cell viability, have led to complementation in RNase E-deficient cells (Chung et al., 2010). Although the structure of RNase G with and without these mutations has not been fully confirmed, it is clear that the RNase H-like domain of both proteins plays an important role in RNA degradation.

## 5.2 Results

In this chapter, the RNA-binding abilities of RNase E will be assessed in order to further elaborate the mechanism of direct entry. A competition-based assay was chosen so that the relative binding affinities could be determined under the same conditions, and so that each of the transcripts did not have to be individually labelled. Moreover, by also incorporating direct binding assays it was possible to determine if RNase E could interact with substrates beyond contacts made with the labelled reporter substrate used in the competition assay.

### 5.2.1 RNase E can bind to oligonucleotide quadruplexes

The first step toward developing a competition-based binding assay was to identify a suitable reporter substrate, which should have one of the lowest $K_d$ values of any of the substrates. Using an inhibition-based assay as described in Chapter 3, which involved titration of transcripts into RNase E cleavage assays of 5'-monophosphorylated LU13 and determining the concentration at which the cleavage rate was reduced by 50%, $IC_{50}$ values for several transcripts were found to be between 100-300 nM. Therefore, it was decided that a suitable reporter for competition-binding assays would have to have a $K_d$ value of 100 nM or less for NTH-RNase E. Initially, the model substrate 5'-monophosphorylated LU13 (Kime et al., 2010) was suggested, given that it is cleaved at one of the highest rates compared to other substrates and previous studies have shown that it engages the RNA-binding channel of RNase E (Callaghan et al., 2005a). However, Michaelis-Menten analyses from

Chapter 3 and previous studies (Redko et al., 2003, Kime et al., 2010) has shown that the $K_M$ of RNase E for 5'-monophosphorylated LU13 is around 3-6 µM. This suggests that a high concentration of NTH-RNase E would be required to saturate the 5'-monophosphorylated LU13 for competition assays, and therefore would result in an overestimation of the $IC_{50}$ values. A more suitable reporter was identified using information from a previous study, where it was found that 5'-hydroxylated BR13 that was pre-cooled, promoting formation of an intermolecular quadruplex via the string of three guanine residues at the 5' end, had a $K_M$ of around 190 nM (Kime et al., 2010). The reporter substrate used here, termed as BR15, was designed to have a string of five guanine residues at the 5' end to greatly enhance the stability of the G-quadruplex (Mergny et al., 2005). In addition, the remaining sequence of 10 nt was 2' *O*-methylated to prevent cleavage but retain binding of the substrate (Feng et al., 2002, Redko et al., 2003) and contained a 3'-fluorescein group for detection. BR15 was kept in conditions of 100 mM KCl to promote quadruplex formation (Mergny et al., 2005).

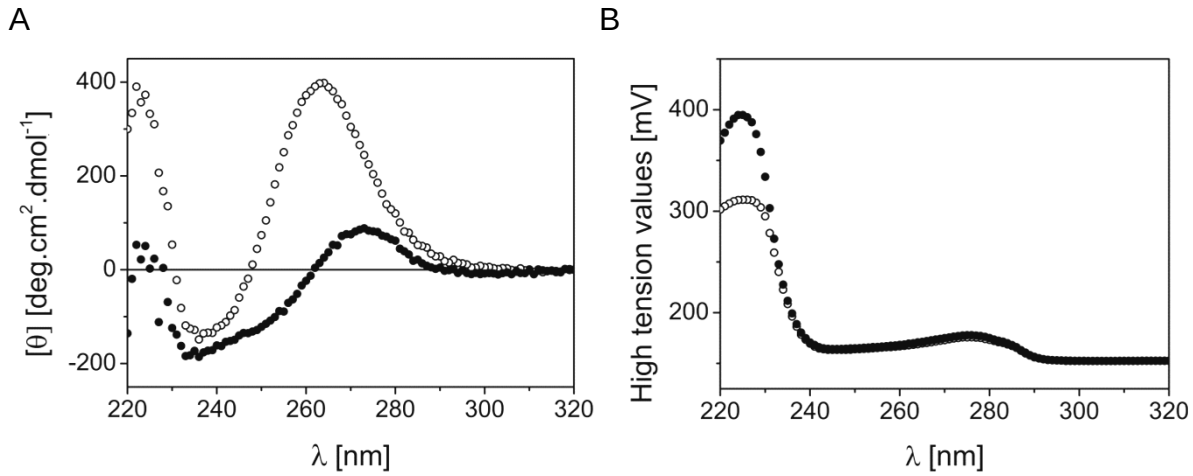


**Figure 5.2 Circular Dichroism spectrum of an oligonucleotide quadruplex.** The 5'-hydroxylated LU13 and BR15 substrates were synthesised by MWG operons (Eurofins, Germany). Substrates were diluted to 7.5 µM in 25 mM *bis*-Tris Propane (pH 8.3), 100 mM KCl, 15 mM $MgCl_2$, 0.1% (v/v) Triton X-100, and 1 mM DTT. The CD spectra were obtained at 37°C. Panel A shows the molar ellipticity ([θ]) recorded at 5 nm wavelength (λ) intervals between 220 and 320 nm. Panel B shows the high tension values at the same wavelengths. The closed and open circles represent the data obtained for LU13 and BR15, respectively.

The next step was to confirm that BR15 adopted a G-quadruplex conformation at 37°C. Previous work used circular dichroism to achieve this goal (Kime et al., 2010). BR15 gives the characteristic peak at 260 nm that is indicative of parallel G-quadruplex stacking, as shown in Figure 5.2A. Confirming this, antiparallel G-quadruplex stacking gives a peak at 285 nm, which is not observed in this spectrum (Balagurumoorthy et al., 1992, Lu et al., 1992). As a control, 5'-hydroxylated LU13, which has the same sequence as BR15 except that the central guanine in the 5'GGG sequence is

replaced with an adenine residue, gave a spectrum characteristic of RNA that does not form stable intermolecular complexes. High tension values remained under 500 mV for both substrates throughout the wavelength range used here, confirming a high signal-to-noise ratio as shown in Figure 5.2B.

After confirming that the reporter formed a stable quadruplex under reaction conditions, the next step was to establish the conditions for binding to NTH-RNase E. Optimised assay conditions for RNase E cleavage have been used extensively as described throughout this work. Therefore, these conditions were used for binding assays, with several ionic substitutions of the reaction buffer.

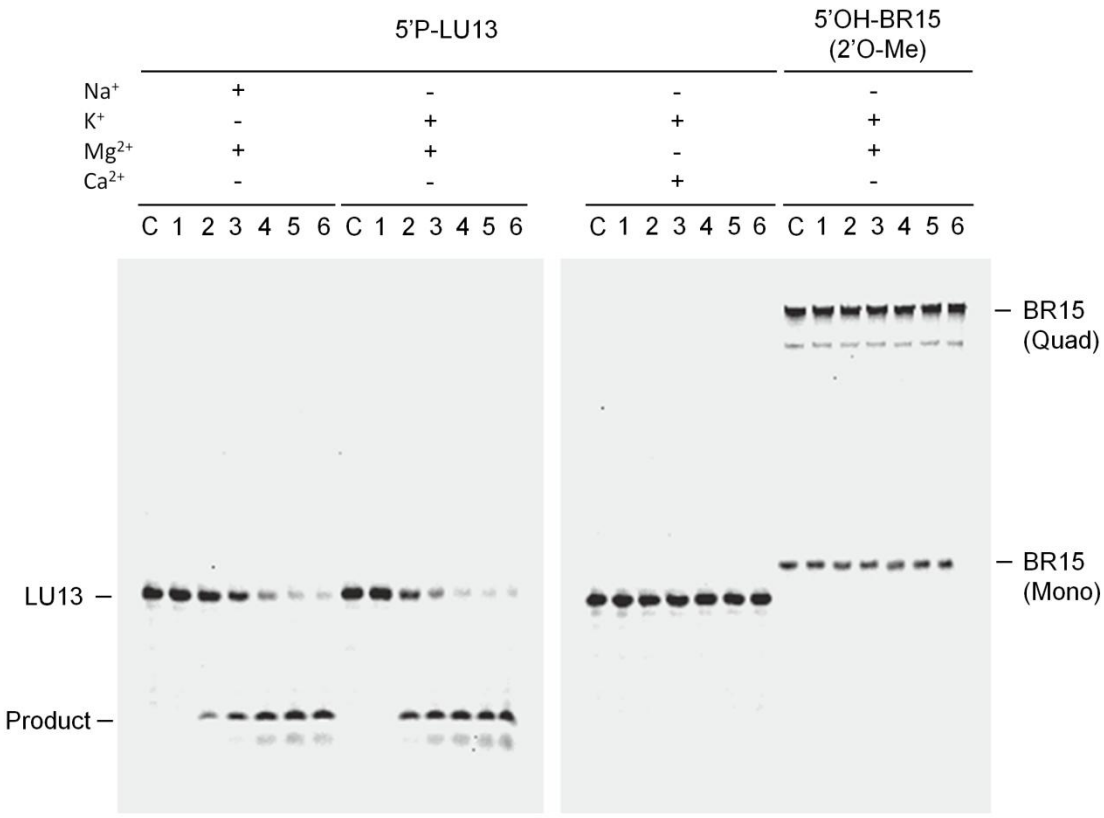


**Figure 5.3 Activity of NTH-RNase E under different substrate and buffer conditions.** Substrates were synthesised by Eurofins MWG operons as described previously and contain a fluorescein label at the 3' end. The identity of each substrate and composition of the reaction buffers are shown at the top of each image. Final substrate and NTH-RNase E concentrations were 250 nM and 5 nM, respectively. Samples were taken after various time points upon incubation, quenched in equal volumes of 2x RNA loading dye, denatured at 95°C, separated on 8% denaturing polyacrylamide gels, and scanned for fluorescence as described in Chapter 2. Lanes 1-6 contain samples taken at 0, 2, 5, 15, 60 and 120 min after incubation of substrate with enzyme. Lane C contains substrate incubated without enzyme for 120 min. The identities of the substrates and cleavage products are shown at the sides of the image.

Potassium was substituted for sodium to maintain the stability of BR15. As shown in Figure 5.3, cleavage of 5'-monophosphorylated LU13 is not reduced in the presence of potassium chloride

compared to sodium chloride at the same concentration (compare first assay with second assay). Next, calcium was substituted for magnesium to prevent cleavage of competing transcripts used in the competition assays. Cleavage of 5'-monophosphorylated LU13 was abolished in the presence of calcium chloride compared to magnesium chloride at the same concentration (compared third assay to second assay). Furthermore, cleavage of BR15 is not observed even when magnesium is present, confirming that the 2' *O*-methyl modifications do prevent cleavage (compare forth assay with second assay). Interestingly, even after quenching the reactions in formamide loading dye, heating to 95°C for 3 min and separating in polyacrylamide gels containing 7 M urea, the majority of the BR15 still appears to be in the quadruplex form.

Having obtained suitable conditions for the competition assays, the next step was to perform a binding assay of the reporter, whereby fixed concentrations of BR15 (5' hydroxylated) were titrated with increasing concentrations of NTH-RNase E. BR15 was used at the lowest concentration that allowed detection (7.5 nM), as $K_d$ values cannot be determined accurately below the concentration of labelled substrate. In this way, $K_d$, the concentration of free enzyme required to cause 50% of the reporter to be bound, could be estimated from the total enzyme concentration. Two distinct complexes were detected, as shown in Figure 5.4A. The first complex, which has been labelled 1:1 (BR15:NTH-RNase E), appears to have a $K_d$ of around 8 nM, whereas the second binding state, which has been labelled 1:2, appears to have a $K_d$ of around 150 nM, estimated from the double sigmoidal binding curve shown in Figure 5.4B. The first binding event is most likely the engagement of two of the single-stranded regions of quadruplexed BR15 with one of the two principal dimers of RNase E. The second binding event could be the binding of the two remaining single-stranded regions of quadruplexed BR15 with another molecule of RNase E. The affinity of this second interaction is presumed to be lower because of spatial constraints imposed by the first.

The same assay was performed under conditions with magnesium (data not shown). The migration of the bands showed a very similar pattern to the first assay, indicating that substitution of magnesium with calcium did not affect binding. However, the separation between the unbound and 1:1 binding bands on the gel image was not as clear with magnesium. It is not known why this would be the case. However, it did not detract from the competition assays as these used calcium unless otherwise stated.

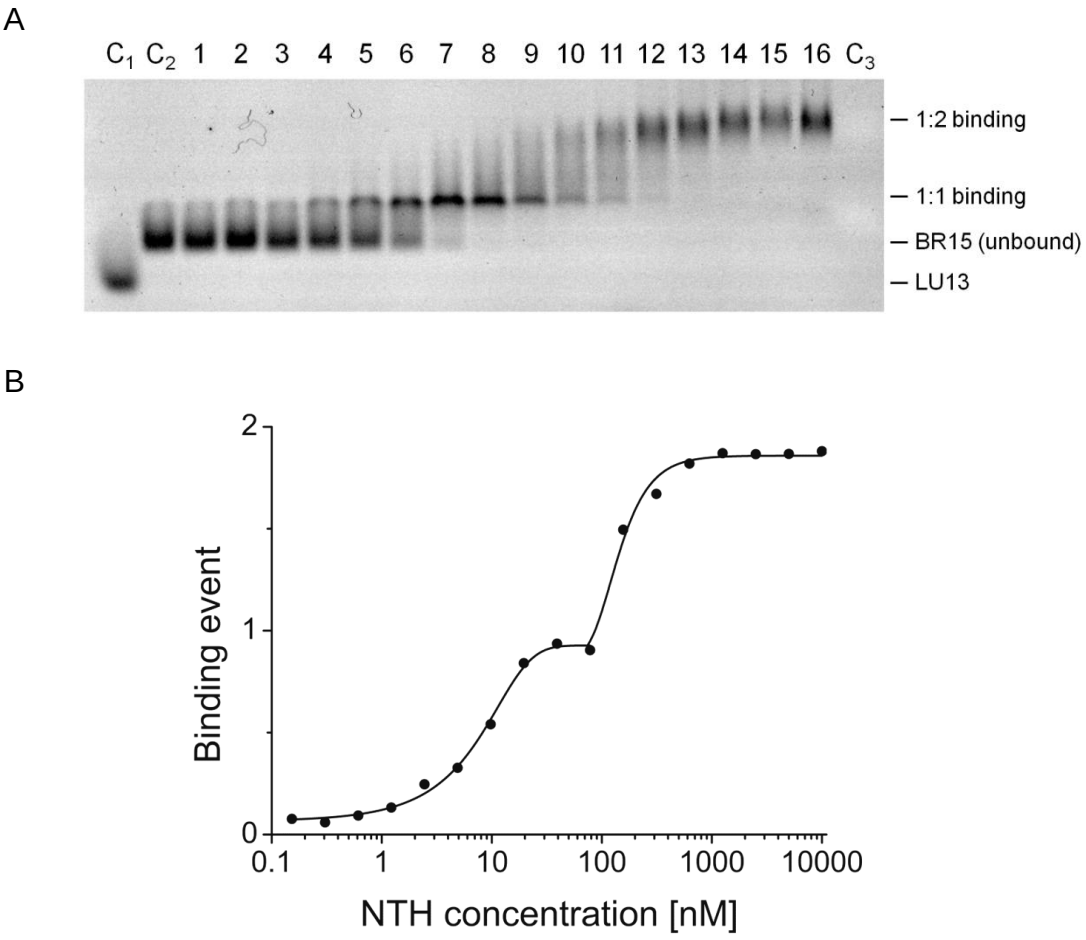


**Figure 5.4 Binding of BR15 to NTH-RNase E.** Panel A shows an electrophoretic mobility shift assay (EMSA) of the quadruplex BR15 incubated with increasing concentrations of NTH-RNase E. Reactions were incubated at 37°C for 20 min, separated on 1% (w/v) agarose gels and scanned for fluorescence as described in Chapter 2. Lanes 1-16 contain 7.5 nM BR15 (quadruplex) incubated with 0.3, 0.6, 1.2, 2.4, 4.9, 9.8, 19.5, 39, 78.1, 156.3, 312.5, 625 nM, 1.25, 2.5, 5, and 10 µM wild-type NTH-RNase E. Lanes $C_1$, $C_2$ and $C_3$ contain 30 nM LU13, 7.5 nM BR15 and 10 µM wild-type NTH-RNase E, respectively. The binding states of each band are shown at the right of the image. Panel B shows a binding curve of BR15 to NTH-RNase E. The proportion of BR15 in each binding state was calculated from the band intensities by 2D densitometry.

From the BR15 binding assays, a concentration of 20 nM NTH-RNase E was used in the subsequent competition assays as this was the lowest concentration at which almost all of the BR15 was bound by NTH-RNase E. The next step was to confirm that the binding of BR15 was dependent on contacts with RNase E that were also required for the binding of monomeric single-stranded oligonucleotides. The first competitor substrate to be analysed was 5'-monophosphorylated LU13, given that it is cleaved rapidly by RNase E and that previous crystallographic studies confirmed it is engaged within the RNA-binding channel of the closed conformation of RNase E (Callaghan et al., 2005a). As shown in Figure 5.5, the $IC_{50}$, *i.e.* the concentration of 5'-monophosphorylated LU13 required to displace 50% of the labelled BR15 reporter from catalytic domain of RNase E was 154 nM. As BR15 does not

have a 5′-monophosphate group, and LU13 does not form a G quadruplex, this result confirms that substrates competing with BR15 are competing for contacts used in the binding of single-stranded regions of RNA.

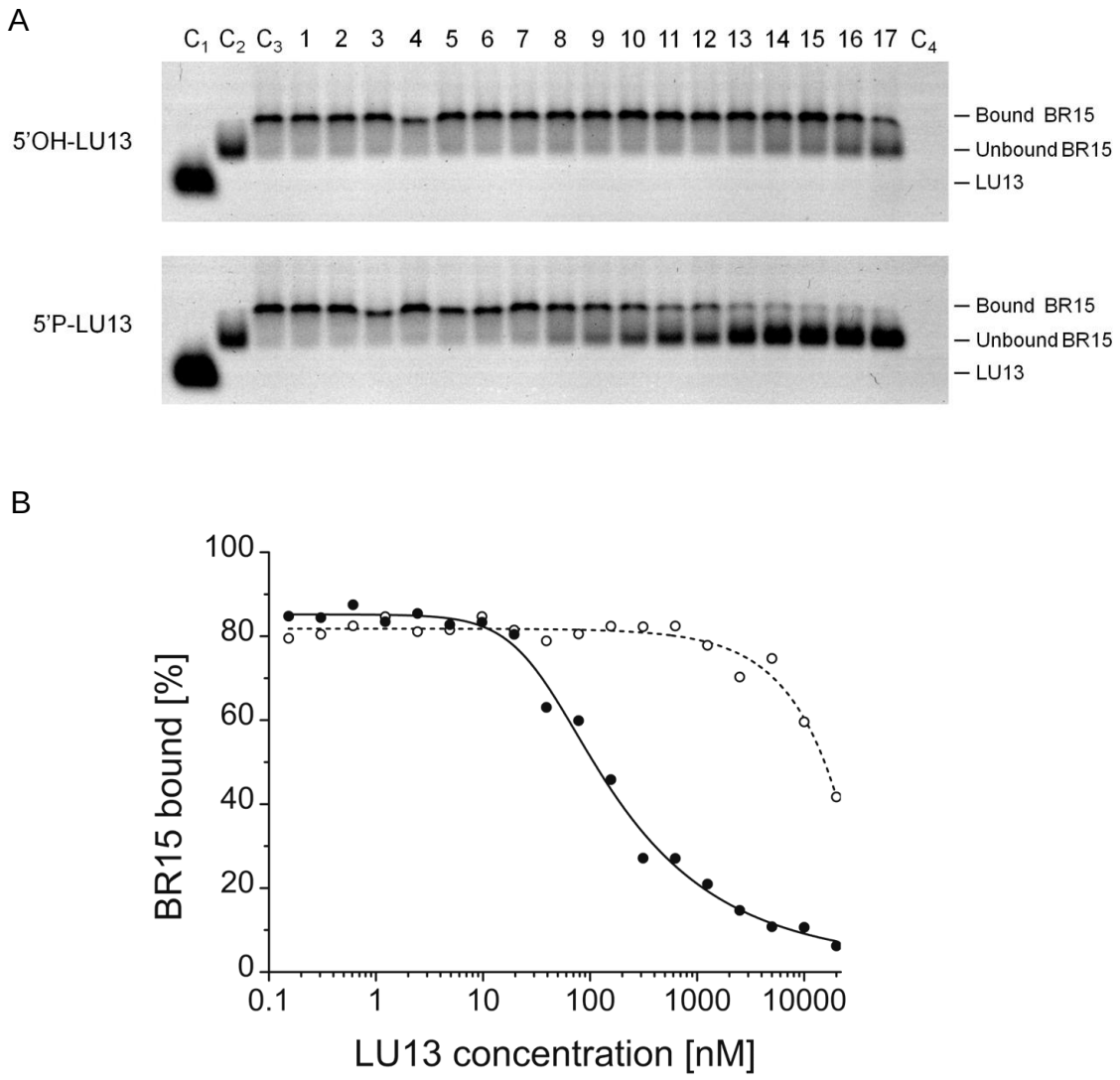


**Figure 5.5 Competition between LU13 and BR15 for binding to NTH-RNase E.** Panel A shows an electrophoretic mobility shift assay (EMSA) of the BR15-NTH complex incubated with increasing concentrations of unlabelled LU13. Reactions were performed and analysed as described in Figure 5.3A. Lanes 1-17 contain 7.5 nM BR15 (quadruplex) and 20 nM NTH-RNase E incubated with 0.3, 0.6, 1.2, 2.4, 4.9, 9.8, 19.5, 39, 78.1, 156.3, 312.5, 625 nM, 1.25, 2.5, 5, 10, and 20 µM LU13. Lanes $C_1$, $C_2$, $C_3$ and $C_4$ contain 30 nM LU13 with a 3′-fluorescein label, 7.5 nM BR15, 7.5 nM BR15 incubated with 20 nM wild-type NTH-RNase E, and 20 nM NTH-RNase E incubated with 20 µM unlabelled LU13. The binding states of each band are shown at the right of each image. The top and bottom image used 5′-hydroxylated and 5′-monophosphorylated LU13 as the competitor, respectively. Panel B shows a competition binding curve of this data. The proportion of BR15 bound to NTH-RNase E compared to the unbound state was calculated from the band intensities by 2D densitometry. The closed and open circles represent the data obtained from the 5′-monophosphorylated and 5′-hydroxylated LU13, respectively.

The 5'-hydroxylated LU13, a substrate that has been shown using the Michaelis-Menten analysis performed in Chapter 3 to occupy the active site of RNase E only at very high concentrations, had a much greater $IC_{50}$ of ≥ 20 µM. The higher level of competition with 5'-monophosphorylated LU13 indicates that while it competes with BR15 for contacts made with single-stranded regions, its ability to compete is enhanced by the additional contact with the 5'-monophosphorylated end.

The first control lane in the competition assays (labelled $C_1$) contains only the LU13 substrate to illustrate the migration distance of the non-quadruplex form. The second control ($C_2$) contains only BR15 to show the migration distance of unbound BR15. The third control ($C_3$) contains BR15 with NTH-RNase E to show the migration distance of fully bound BR15. The fourth control ($C_4$) contains just NTH-RNase E to show that this molecule does not exhibit a fluorescent signal.

### 5.2.2 Implications for RNase E in non-nucleolytic control of translation

The major direct entry cleavages found in the *rne* transcript were actually located far into the coding region of the mRNA and were still evident even after removal of the 5' UTR (For details see Chapter 4). Previous studies have shown that the 5' UTR of *rne* is required for RNase E autoregulation, which destabilises the transcript and reduces translation (Diwa et al., 2000). This suggests that destabilisation of *rne* via interaction with the 5' UTR and cleavage by direct entry within the coding region are two separate events during RNase E autoregulation. Given that the direct entry sites of *rne* are likely blocked by high ribosomal traffic *in vivo*, it is likely that interaction of RNase E with the 5' UTR is the primary event. Binding of RNase E to the 5' UTR could block ribosomal association, therefore exposing the downstream direct entry sites to subsequent RNase E cleavage. Cleavage within these sites would ensure the inactivation of the mRNA is irreversible. Therefore, cleavage assays were performed to determine if the 5' UTR (labelled as -361 to +134; numbering is the nt position with respect to the first nt in the start codon AUG) is a substrate for direct entry cleavage, by comparing the cleavage rate to those of full length *rne* substrate (labelled as -361 to +774) and the coding-region fragment (labelled as +135 to +558), as shown in Figure 5.6.

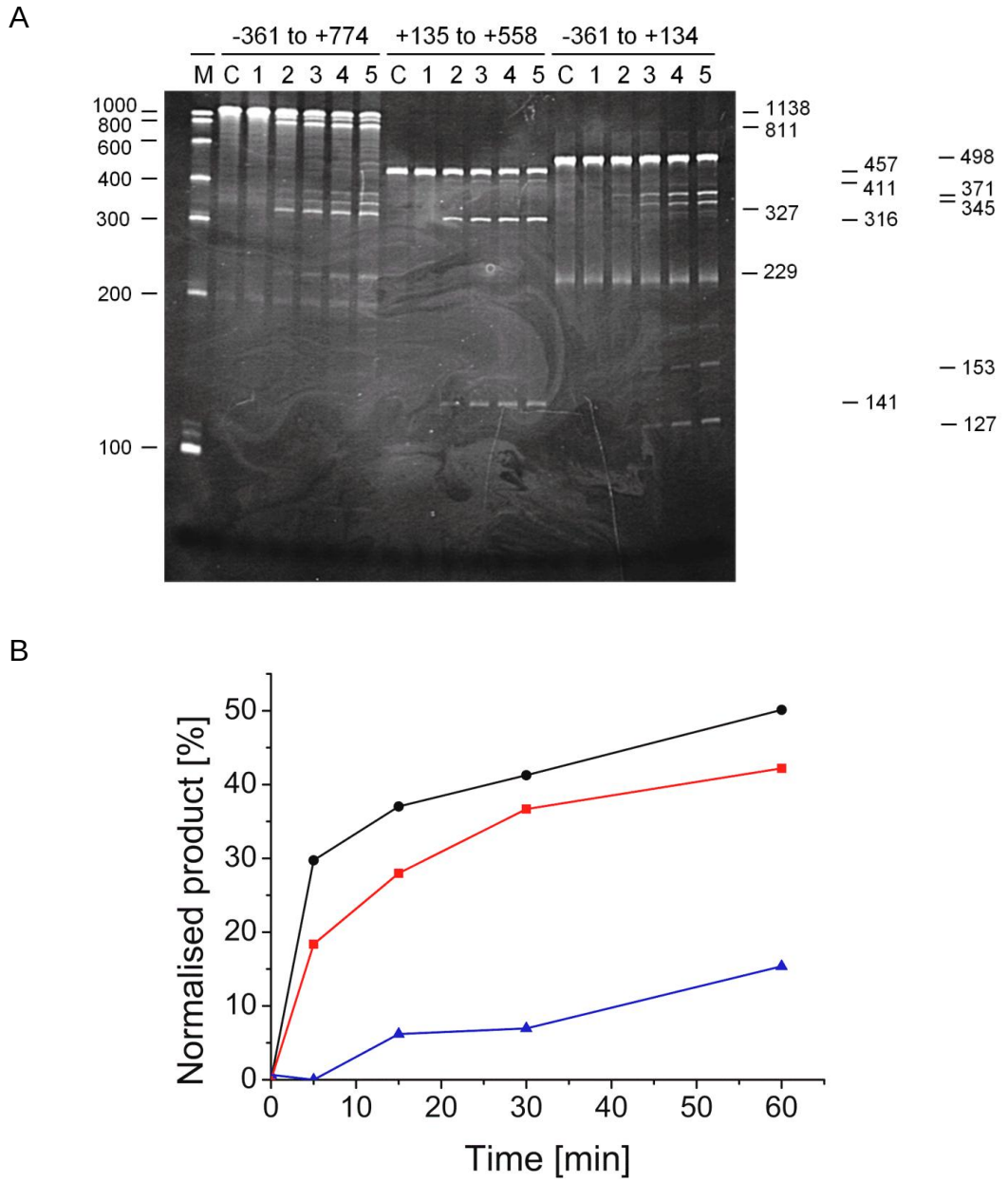


**Figure 5.6 Cleavage of *rne* fragments by NTH-RNase E T170V.** Panel A shows discontinuous cleavage assays of the *rne* fragments by T170V. The 5'-triphosphorylated transcripts were generated by *in vitro* transcription as described in Materials and Methods. The boundaries of each fragment are shown at the top of the image. Final substrate and NTH-RNase E T170V concentrations were 180 nM and 20 nM, respectively. Samples were taken after various time points upon incubation, quenched in equal volumes of 2x RNA loading dye, denatured at 95°C, separated on 8% denaturing polyacrylamide gels, and stained with ethidium bromide as described in Chapter 2. Lanes 1-5 contain samples taken at 0, 5, 15, 30 and 60 min after incubation of substrate with enzyme. Lane C contains substrate incubated without enzyme for 60 min. Lane M contains a RiboRuler™ low range RNA ladder with sizes in nt indicated at the left of each image. The sizes in nt of the substrates and cleavage products are shown at the right of each image. Panel B shows a graph of the proportion of product generated by T170V cleavage compared to substrate over time. The black, blue and red curves represent the data obtained from the *rne* fragments -361 to +774, -361 to +134 and +135 to +558, respectively.

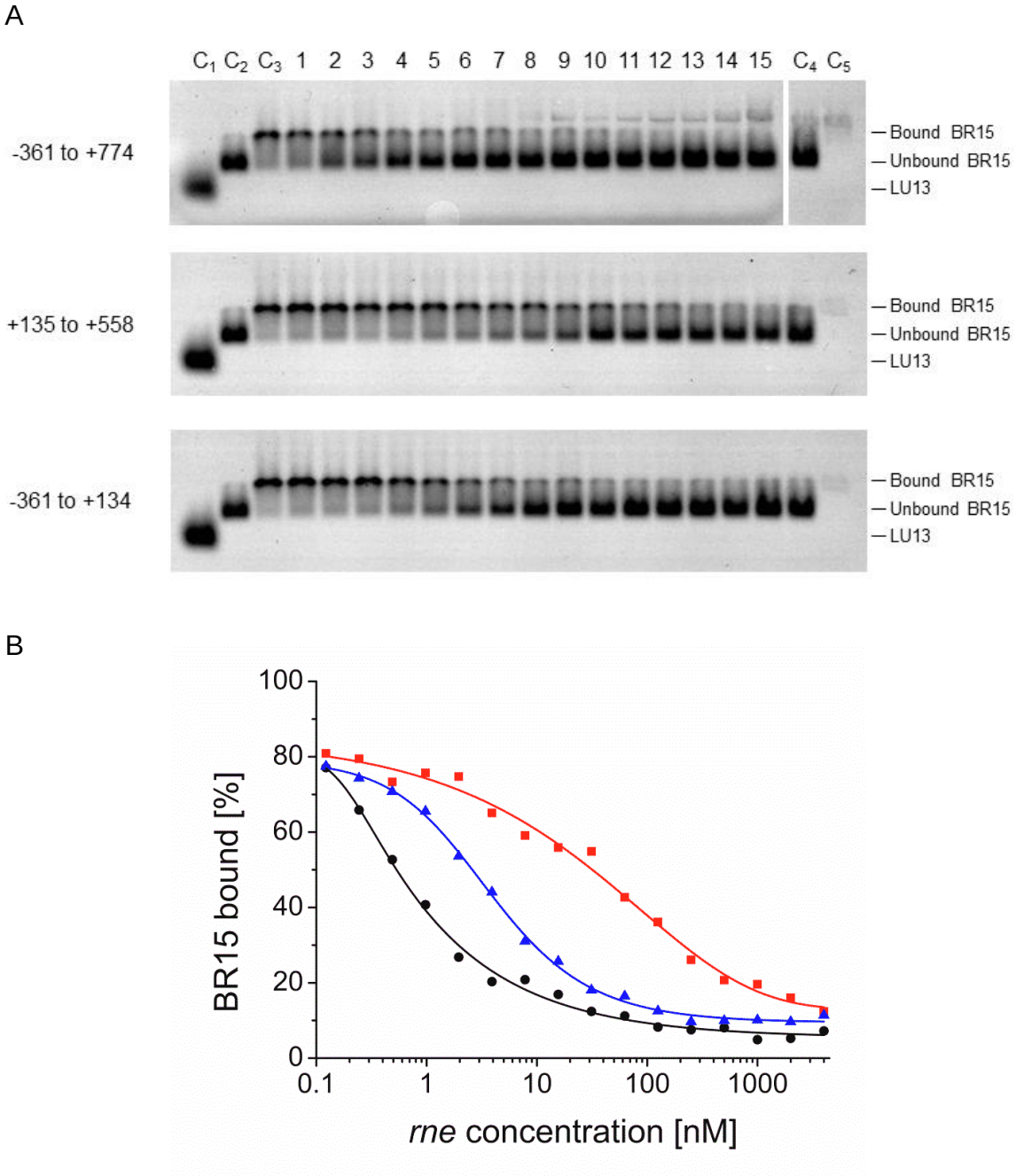


**Figure 5.7 Competition assays of the *rne* transcript.** Panel A shows an electrophoretic mobility shift assay (EMSA) of the BR15-NTH complex incubated with increasing concentrations of *rne* RNA fragments. Reactions were performed and analysed as described in Figure 5.5A. Lanes 1-15 contain 7.5 nM BR15 (quadruplex) and 20 nM NTH-RNase E incubated with 0.3, 0.6, 1.2, 2.4, 4.9, 9.8, 19.5, 39, 78.1, 156.3, 312.5, 625 nM, 1.25, 2.5, and 5 µM of RNA fragments. Lanes $C_1$, $C_2$, $C_3$, $C_4$ and $C_5$ contain 30 nM LU13 with a 3'-fluorescein label, 7.5 nM BR15, 7.5 nM BR15 incubated with 20 nM wild-type NTH-RNase E, 7.5 nM BR15 incubated with 5 µM RNA fragments, and 20 nM NTH-RNase E incubated with 5 µM RNA fragments, respectively. The binding states of each band are shown at the right of each image. RNA fragment boundaries are shown at the left of each image. Panel B shows competition binding curves of this data, obtained as described in Figure 5.4B. The colouring is the same as for Figure 5.5B.

As also seen in Chapter 4, cleavage at the two major direct entry sites in the full length *rne* occurs at similar rates as with the coding-region fragment, confirming that the 5' UTR is not able to exert control over the cleavage rate at the internal site. In addition, the 5' UTR itself is cleaved at a much slower rate at two minor sites and therefore would not be considered a good substrate for direct entry cleavage. Therefore, there is a clear missing link between the *in vitro* data presented here and the *in vivo* data presented previously. This is most likely due to the absence of "protective" ribosomes *in vitro* (Deana and Belasco, 2005). Therefore, it appears that interaction of RNase E with the 5' UTR, in the absence of endonucleolytic cleavage, must cause this reduction in ribosomal traffic and hence destabilisation of *rne*.

Previous work has shown that the ability of the 5' UTR to enhance autoregulation of *rne* lies in its ability to interact with RNase E, and there is no evidence of major cleavages occurring as a result of this binding (Diwa and Belasco, 2002, Schuck et al., 2009). Therefore, competition assays were performed using the three *rne* fragments, as shown in Figure 5.7. As expected, even though the 5'-UTR fragment (-361 to +134) was cleaved at a significantly slower rate compared to the coding-region fragment (+135 to +558), it actually competes with BR15 in binding to RNase E at an even lower concentration, with an $IC_{50}$ of 3.7 nM, than the coding-region fragment does, with an $IC_{50}$ of 36 nM. Therefore, it appears that the 5' UTR can bind the catalytic domain of RNase E with relatively high affinity, via contacts that interact with single-stranded regions, without necessarily being cleaved efficiently.

It should be noted that the full-length *rne* (-361 to +774) has a very low $IC_{50}$ of around 0.75 nM. Under conditions of 1:1 binding, $IC_{50}$ values are limited to [S]/2. However, competing substrates that can provide multiple-binding sites to the protein, which is evident with the full length *rne* due to the fact that both the 5' UTR and the coding region have been shown to interact independently with RNase E, can have lower $IC_{50}$ values.

To further identify the regions that RNase E interacts with, dissections of the 5' UTR were performed and analysed using competition assays, as shown in Figure 5.8. The boundaries of each dissection coincided with the boundaries of several structural elements present in the *rne* 5' UTR, as determined from previous studies by others and shown in Figure 5.1 (Diwa et al., 2000). Removal of hairpin 1 (hp1) and single-stranded region 1 (ss1) have no effect on the ability of the remaining 5' UTR fragment to compete with BR15 (compare the right assay of the first panel and left assay of the second panel with the left assay of the first panel, respectively).

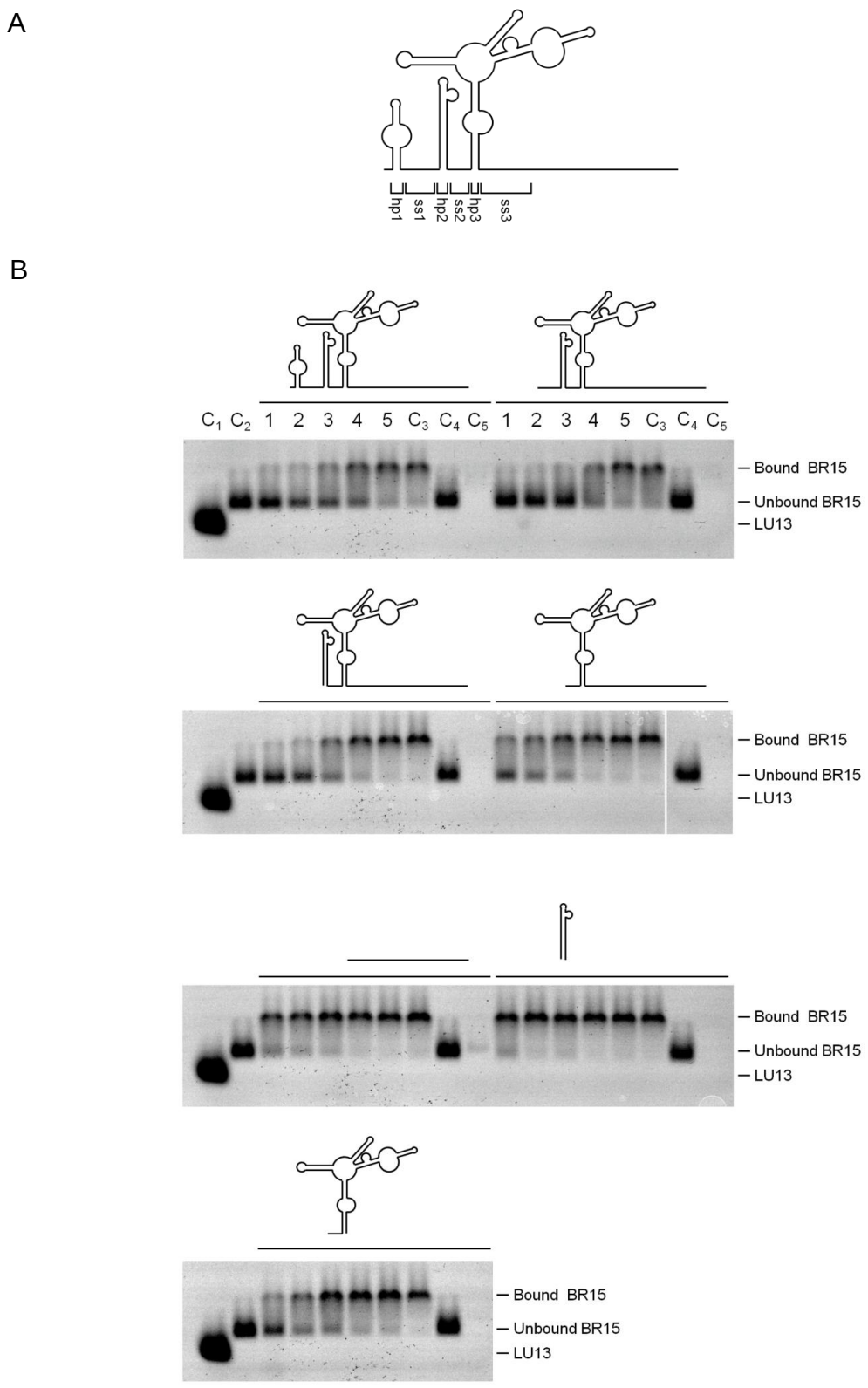


**Figure 5.8 Competition assays of the *rne* 5'UTR.** Panel A shows a schematic of the *rne* 5' UTR as detailed in Figure 5.1. Panel B shows competition assays of the 5' UTR. Labelling and reactions conditions are as described in Figure 5.7A, except lanes 1-5 contain NTH-RNase E concentrations of 156.3, 39, 9.8, 2.4, and 0.6 nM, respectively. A schematic is provided above each assay to highlight the structure of the resulting fragments.

Removal of hp2 has a more apparent effect, with a moderate reduction in the ability of the remaining 5' UTR to compete (compare right assay of the second panel with the left assay of the second panel). Previous work has found that removal of hp2 causes an increase in stability and expression of *rne* (Diwa et al., 2000). In fact, a direct interaction between the "bulge" regions of hp2 and an asparagine residue at position 323 on NTH-RNase E has been found (Diwa and Belasco, 2002, Schuck et al., 2009).The most significant effect comes with the subsequent removal of ss2 and hp3 from the 5' UTR (compare left assay of the third panel with the right assay of the second panel). Given that ss2 has been ruled out as an important region involved in *rne* autoregulation in previous studies (Diwa et al., 2000), it is most likely that hp3 is required for the competition with BR15. Similar results were previously observed *in vivo* by others. Autoregulation, although diminished, was still evident following removal of hp2, suggesting that other regions of the 5' UTR were involved. Removal of hp3 showed similar effects to removal of hp2, suggesting that hp3 could be one of these other regions (Diwa et al., 2000). However, because it was less evolutionary conserved compared to hp2, further analyses of this region were not performed (Diwa and Belasco, 2002).

The hp2 structural element on its own does not compete with BR15 (see right assay of the third panel), which is in accordance with previous results that suggest hp2 interacts with a region of RNase E that is not associated with the active site (Schuck et al., 2009) and therefore on its own would not block BR15 binding. Surprisingly, the fragment encompassing ss2 and hp3 on its own appears to show as strong competition as ss2 and hp3 with the remaining downstream region of the 5' UTR (compare assay in fourth panel with right assay in second panel). This would suggest that the majority of binding between the 5' UTR and the catalytic domain of RNase E is via contacts with single-stranded regions of hp3, a region that is not cleaved and is highly structured.

### 5.2.3 Role of RNA structural elements in RNase E interactions

In Chapter 3 it was confirmed that a tRNA unit presented two flanking single-stranded regions so that each could interact with RNase E via contacts made with single-stranded regions of RNA, promoting direct entry cleavage within the downstream region. However, it was found that a "supporting" tRNA unit was also required at the 5' end of the upstream flanking region for efficient cleavage (Figures 3.4 and 3.7). Interestingly, hp3, a region of RNA that has been shown in this chapter to bind to RNase E strongly without being cleaved, bears at least a superficial resemblance to tRNA in as much as it contains three hairpins that form a clover leaf-like secondary structure. Therefore, it was decided to investigate the interactions between these "supporting" tRNA units and RNase E.

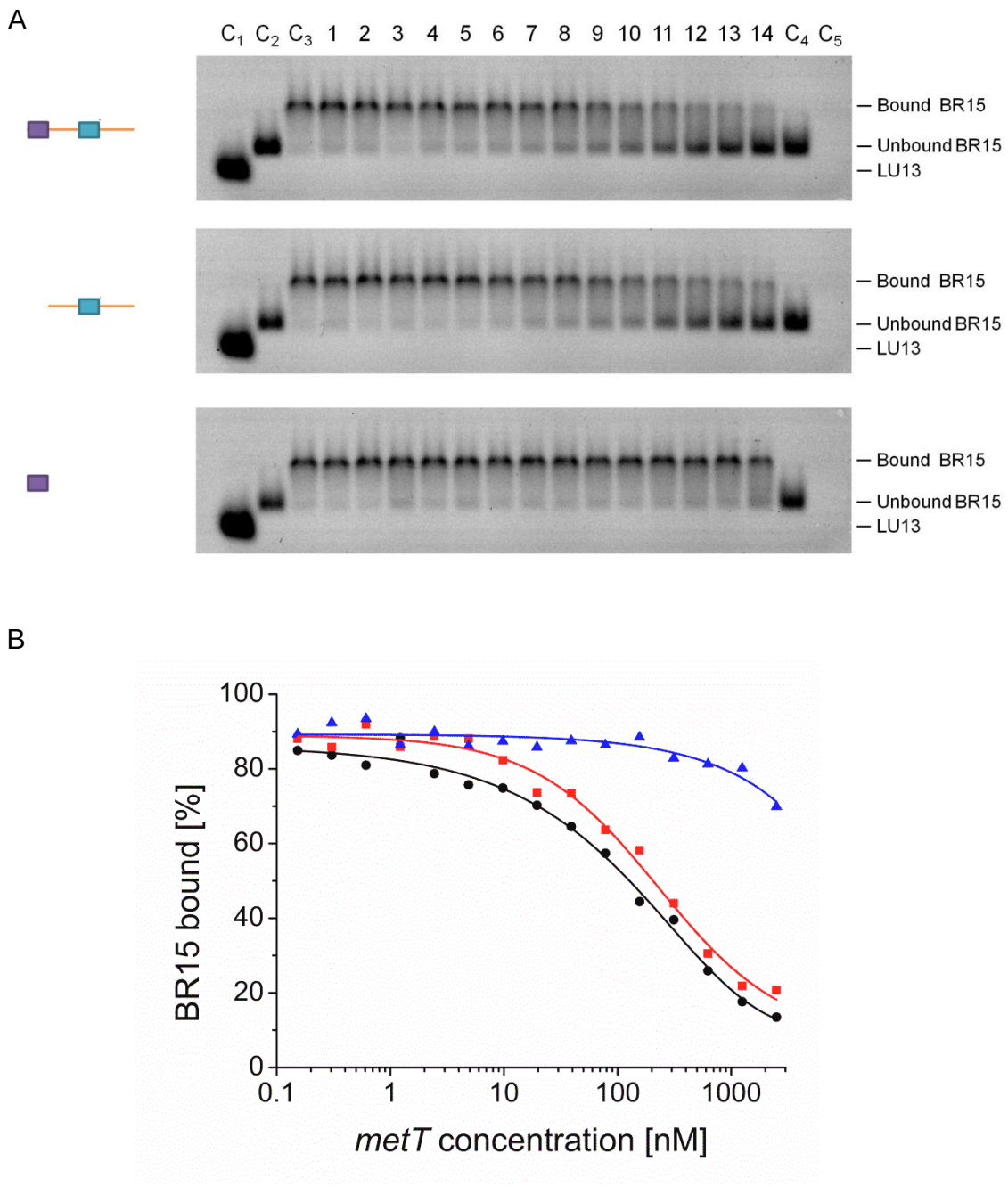


**Figure 5.9 Competition assays of the *metT* tRNA precursor.** Panel A shows an electrophoretic mobility shift assay (EMSA) of the BR15-NTH complex incubated with increasing concentrations of *metT* RNA fragments. Reactions were performed and analysed as described in Figure 5.5A. Labelling is as Figure 5.7A. The first, second and third panels show competition images of the 217-, 142- and 78-nt fragments, respectively. A schematic is provided for all three fragments at the left of the images and colour coding of the tRNA units is as described in Figure 3.4A. Panel B shows competition binding curves of these data, obtained as described in Figure 5.5B. The black, blue and red curves represent the data obtained from the 217-, 142- and 78-nt fragments, respectively.

Competition assays were first performed with three dissections around the *glnW-metU* units, as shown in Figure 5.9. The first substrate was a 217-nt fragment that contains the *glnW-metU* units as well as the 3' flanking region of *metU* that contains the site of direct entry cleavage (shown in the

top panel). The second substrate is a 142-nt fragment that contains a truncation so that the *glnW* tRNA, the unit required to promote or support cleavage, is removed (shown in the second panel). The third substrate is a 78-nt fragment that just consists of the *glnW* tRNA unit (shown in third panel). Despite the abolishment in cleavage upon removal of the *glnW* tRNA (see Chapter 3), competition of the 142-nt fragment with BR15 is just as strong as the 217-nt fragment, with $IC_{50}$ values of 229 nM and 147 nM, respectively (compare second panel with first panel). The 78-nt fragment on its own shows very little competition with BR15 in binding to RNase E and therefore it is unlikely that *glnW* itself interacts with the catalytic domain of RNase E, at least via contacts made with single-stranded regions channel (see third panel). Competition requires the two single-stranded regions flanking *metU* consistent with the simplest iteration of our model for direct entry.

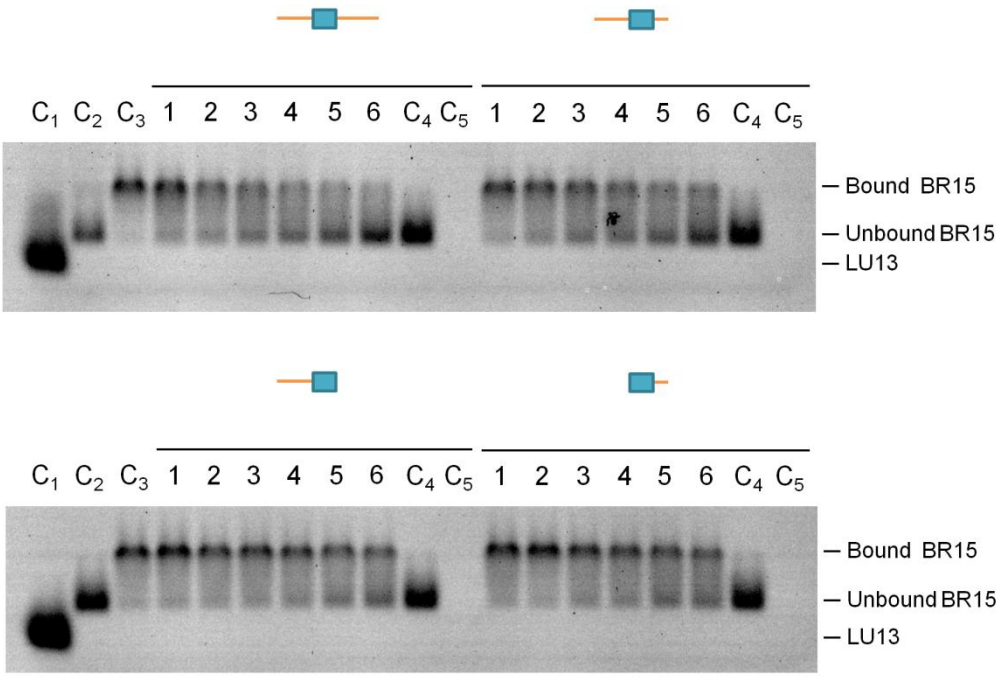


**Figure 5.10 Competition assays of further dissections of the *metT* tRNA precursor.** Labelling and reactions conditions are as described in Figure 5.9A, except lanes 1-6 contain NTH-RNase E concentrations of 39, 78.1, 156.3, 312.5, 625 nM and 1.25 µM, respectively. The left and right assay of the top panel show competition EMSAs of the 142- and 105-nt fragments, respectively. The left and right assay of the bottom panel show competitions EMSAs of the 95- and 90-nt fragments, respectively.

To confirm that the two single-stranded regions flanking *metU* are required for binding to the catalytic domain of RNase E, competition assays were performed with further dissections of the 142-nt fragment, as shown in Figure 5.10. Removal of the last 38 nt from the 3' end (region labelled as b3 from Figure 3.6) had minimal effect on the ability of the remaining 105-nt fragment to compete with

BR15 (compare right assay on the top panel with left assay on the top panel). This is as expected, as blocking of b3 with DNA oligonucleotides had no effect on direct entry cleavage (Figure 3.6).

Removal of the remaining 10 nt on the 3' flanking region of *metU* that encompassed the cleavage site (region labelled as b2 in Figure 3.6) had a much more significant effect on the ability of the resulting 95-nt fragment to compete with BR15 (compare left assay on second panel to right assay on first panel). Again, this is expected given that blocking of b2 abolished cleavage by direct entry. Removal of the first 15 nt from the 5' end (region labelled as b1 in Figure 3.6), while retaining the 10 nt downstream of *metU* encompassing the cleavage site, also showed a significant reduction in the ability of the remaining 90-nt fragment to compete with BR15 (compare right assay of second panel to right assay on first panel). This result confirms that the simultaneous interaction of both the 5' leader and 3' trailer sequences of *metU* with contacts also required for interaction of single-stranded RNAs with RNase E increases the affinity of the substrate for the enzyme, hence promoting direct entry cleavage.

Given that *glnW* is dispensable for binding of the 142-nt fragment to the catalytic domain of RNase E, but is required for cleavage downstream of *metU*, ligand binding assays were performed to establish if *glnW* can interact with another region on NTH-RNase E (Figure 5.11). Fixed concentrations of the 217-nt fragment that is cleaved, the 142-nt fragment that is not cleaved, but able to compete with BR15 for binding to RNase E, and the 78-nt fragment that is not cleaved nor able to compete with BR15 for binding to RNase E were each titrated with increasing concentrations of NTH-RNase E and binding was analysed by migration through agarose gels. The version of NTH-RNase E used in ligand binding assays had a mutation that resulted in substitution of aspartate at position 346 in the DNase I-like domain to asparagine. The D346N mutation reduces the ability of the enzyme to chelate magnesium at the active site, hence abolishing cleavage that would be observed at high enzyme concentrations in these assays (Callaghan et al., 2005a). Work performed alongside this study by Jonah Ciccone confirmed that the D346N mutant, while unable to cleave RNA rapidly, still retains a similar affinity for BR15 compared to the wild-type.

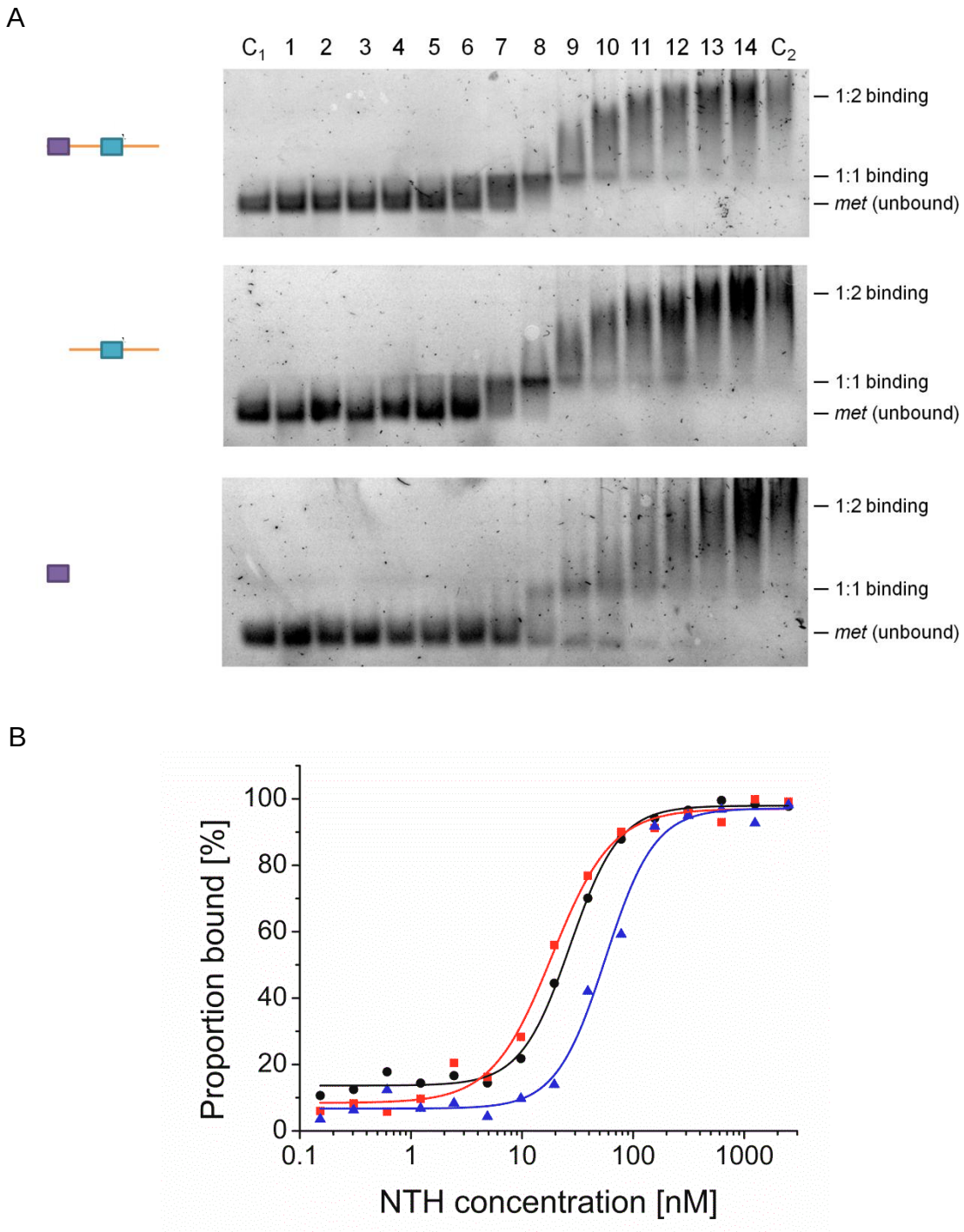


**Figure 5.11 Direct binding of RNase E to the *metT* tRNA precursor.** Panel A shows EMSAs of *metT* RNA fragments incubated with increasing concentrations of NTH-RNase E D346N. The reactions were set up and analysed as previously described in Figure 5.4, except the gels were stained with SYBR® Gold Nucleic acid stain to visualise the RNA. Lanes 1-14 contain 20 nM RNA fragments incubated with 0.3, 0.6, 1.2, 2.4, 4.9, 9.8, 19.5, 39, 78.1, 156.3, 312.5, 625 nM, 1.25, and 2.5 µM NTH-RNase E D346N, respectively. Lanes $C_1$ and $C_2$ contain 20 nM RNA fragments and 2.5 µM NTH-RNase E D346N, respectively. The first, second and third panels show EMSAs of the 217-, 142- and 78-nt fragments, respectively. A schematic is provided for all three fragments at the left of the images and colour coding of the tRNA units is as described in Figure 3.4A. Panel B shows binding curves of these data,

obtained as described in Figure 5.4B. The black, blue and red curves represent the data obtained from the 217-, 142- and 78-nt fragments, respectively.

As expected from the results of Figure 5.9, the 142-nt fragment bound to RNase E with a similar affinity as the 217-nt fragment, with $K_d$ values of 18.6 and 27.1 nM, respectively. Interestingly, the $K_d$ value for the 78-nt fragment was not much higher at 56.3 nM, suggesting that *glnW* interacts with RNase E as well, but not using contacts that interact with single-stranded regions. Therefore, *glnW* appears to interact with an allosteric site on NTH-RNase E, increasing the rate of cleavage by direct entry without contributing to an increase in affinity between the remaining 142-nt fragment and the catalytic domain of RNase E. Because it has been shown that the *glyX* tRNA is required for direct entry cleavage on the 3' trailer of *glyY* (Figure 3.7), and that *hisR* is required for direct entry cleavage on the 3' trailer of *argX* (Kime et al., 2014), it is possible that many tRNA units have the potential to interact with an allosteric site on RNase E in a similar manner.

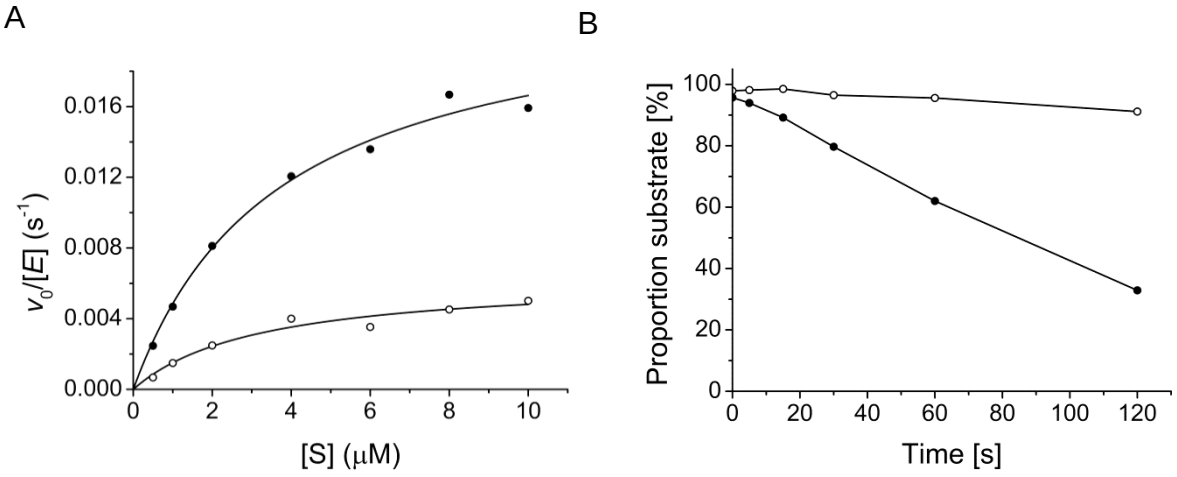


**Figure 5.12 Kinetic analyses of *metT* RNA dissections.** Panel A shows a Michaelis-Menten graph for the cleavage of the 217- (black circles) and 142-nt (open circles) RNA fragments, respectively. The concentration of NTH-RNase E T170V (monomer) in each reaction was 40 nM. Rates normalised against enzyme concentration ($v_0/[E]$) were calculated, plotted against substrate concentration ([*S*]), and were fitted to the Michaelis-Menten equation. Panel B shows a graph of the proportion of substrate over time following incubation with T170V under single-turnover conditions. The concentration of substrate and NTH-RNase E T170V (monomer) in each reaction was 5 nM and 200 nM, respectively. Reactions were performed as in Chapter 3, except that the final gels were stained with SYBR® Gold Nucleic acid stain to visualise the low RNA concentrations. The colouring is the same as for Panel A.

Further kinetic analyses were then performed to determine how the interaction of *glnW* with an allosteric site on RNase E increases the cleavage rate at the site downstream of *metU.* A Michaelis-Menten analysis was first performed whereby the cleavage rates of both the 217- and 142-nt RNA fragments by NTH-RNase E T170V were measured at increasing substrate concentrations, as shown in Figure 5.12A. Values of 3.7 μM and 3.2 μM were obtained for the $K_M$ of the 217- and 142-nt

fragments, respectively, which is consistent with the observation that both substrates have a similar affinity for the active site. Values of 2.28 x $10^{-2}$ $s^{-1}$ and 6.35 x $10^{-3}$ $s^{-1}$ were obtained for the $k_{cat}$ of the 217- and 142-nt fragments, respectively, suggesting that the removal of the *glnW* tRNA diminished the turnover of the 142-nt fragment by 3.6-fold. This suggests that the interaction between the *glnW* tRNA and the allosteric site of RNase E enhances the catalytic step of the reaction.

However, it is important to note that the Michaelis-Menten equation fails to address the distinction between the actual step of catalysis and the subsequent step of product release, both of which impact the value of $k_{cat}$. Under multiple-turnover conditions, products of cleavage that are generated rapidly by the enzyme but are not subsequently released effectively deplete enzyme from the reaction and therefore reduce the apparent rate of reaction. Under single-turnover conditions, whereby there is an excess of enzyme over substrate, the concentration of enzyme remains constant throughout the reaction and therefore the true rate of reactions that are limited by product release will be much higher than under multiple-turnover conditions (Jones et al., 2008). Therefore, cleavage assays were performed whereby the 217- and 142-nt fragments were incubated with NTH-RNase E T170V under single-turnover conditions, as shown in Figure 5.12B. Values of 1.43 x $10^{-4}$ $s^{-1}$ and 1.16 x $10^{-5}$ $s^{-1}$ were obtained for normalised cleavage rates of the 217- and 142-nt fragments, respectively. The 10-fold reduction of cleavage under single-turnover conditions when *glnW* is removed from the substrate suggests that the upstream tRNA unit is not responsible for assisting product release, and therefore must be allosterically activating the enzyme.

### 5.2.4 Possible amino acid interactions that govern the conformation of NTH-RNase E

Interestingly, recent work has found an allosteric RNA-binding site present on the small domains of RNase E, whereby a lysine residue at position 433 was found to interact with RNA, presumably by an ionic interaction with the negative phosphodiester backbone (Kim et al., 2014). It is possible that the supporting tRNA unit could engage this site on the small domains of the principal dimer, given that its position in the hypothetical complex would be at the exit of one of the RNA-binding channels of RNase E. How the engagement of the supporting tRNA unit with the allosteric site on the small domain enhances the activity of RNase E is unknown. However, it is interesting to note that one of the major differences in the quaternary structure of the RNase E tetramer of the “open” form compared to the “closed” form is the presence of a kink of around 40° within the dimer-dimer interface, as shown in Figure 5.13A (Koslover et al., 2008). This kink is a result of a 20° rotation in the positions of the small domains relative to the large domains, as shown in Figure 5.13B. As a hypothetical model, interaction of the supporting tRNA unit to the allosteric site on the small domain could cause a shift in the small domains so that the kink is reduced, which could then force

the enzyme to adopt the “closed” conformation, possibly resulting in cleavage in the 3’ trailer of *metU*.

The allosteric model suggested above implies that several inter-domain interactions are required to mediate a “cascade of conformational changes” within the whole of NTH-RNase E, forcing it to adopt a closed conformation. This cascade is likely activated by interaction of the supporting tRNA unit with the allosteric site found on the small domain, as described above. One of the domain-domain interaction(s) that may be important in this cascade is between the small and large domains. It is likely that this interaction involves residue(s) on the RNase H-like domain, given that the relative position of the small domains is beneath the RNase H-like domain in both confirmations (Koslover et al., 2008). The anionic glutamate at position 12 of the RNase H-like domain and cationic lysine at position 455 on the small domain appear to come in to close contact when the NTH-RNase E is in the “closed” conformation. When the 40° kink is reduced in the homotetramer, the small domains rotate so that Lys455 comes into closer contact with the RNase H-like domain. It is possible that this could stabilise the salt bridge between the two domains, forcing the RNase H-like domain to stay in this position (See Figure 5.13B).

Another set of interactions that may be important in this model is between the RNase H-like domain and the 5’-sensing domain, as shown in Figure 5.17C. One particular interaction between these two domains may occur between the anionic glutamate at position 210 and the cationic arginine at position 219. Supporting the E210-R219 salt bridge appears to be another interaction between a histidine residue at position 190 and another histidine at position 208. Although both residues are both cationic, the orientation of the two residues perpendicular to each other suggests the interaction could occur via the hydrogen-π interface (Hughes and Waters, 2006, Liao et al., 2013). Through both of these interactions, the shift in the position of the RNase H-like domain could force a shift in the position of the 5’-sensing domain, causing the S1-like domain to then clamp down onto the DNase I-like domain.

Given that the structure of the RNase E-RNA complex has only been elucidated using single-stranded oligonucleotide substrates (Callaghan et al., 2005a, Koslover et al., 2008), and that the structure of RNase E in the open conformation has only ever been determined in its unbound state (Koslover et al., 2008), previous findings cannot confirm the molecular simulation proposed in Figure 5.13.

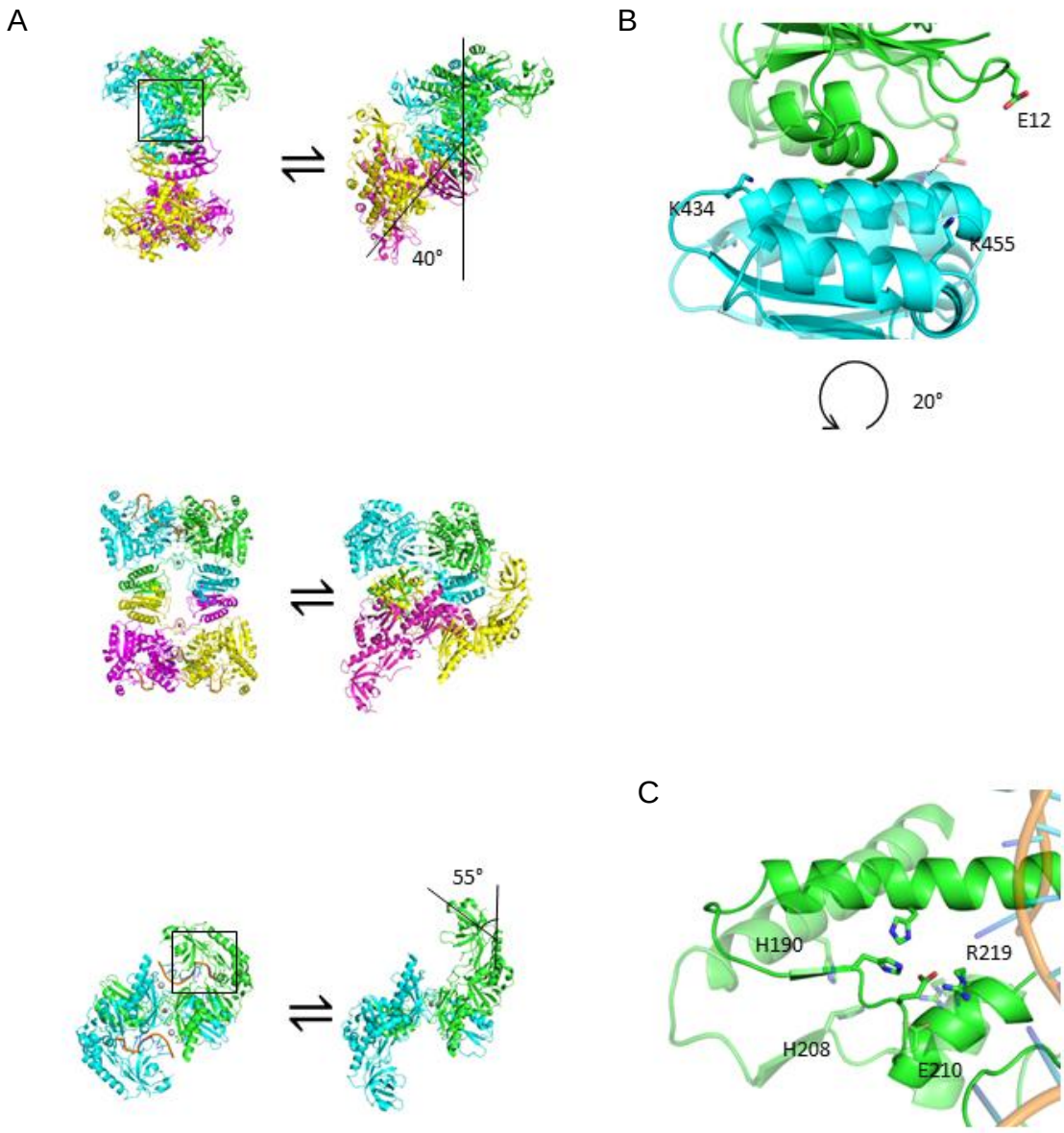


**Figure 5.13 Structure of RNase E highlighting specific residues involved in conformational changes.** The RNase E tetramer in the closed and open conformations was downloaded from the RCSB Protein Data Bank (PDB ID's 2C0B and 2VMK, respectively). Panel A shows the full homotetrameric structure of both conformations viewed at different angles. Panel B shows a higher resolution image of the region highlighted in the first image of Panel A. The open conformation is shown as solid, whereas the closed conformation, which has been aligned onto the open structure, is shown as semi-transparent. Panel C shows a higher resolution image of the region highlighted in the third image of Panel A. Colouring is as before, and the RNA is shown in orange. Amino acid residues are highlighted.

## 5.3 Discussion

Work in the previous chapter indicated that cleavage of RNA by a direct entry mechanism that appears to require interaction with multiple-single-stranded regions had a major role in the processing and degradation of RNA in *E. coli* and presumably the other organisms that contain homologues of RNase E. In this chapter, two observations are made that may have an equal impact on the way in which the regulation of gene expression by RNase E is viewed. The first is that, although direct entry cleavage within the 5' UTR of *rne* is inefficient compared to that in the coding region, the affinity for the catalytic domain of RNase E is actually much stronger. This suggests that the catalytic domain is not restricted to the binding of single-stranded RNAs as previously proposed, and that interaction with regions of RNase E also involved in binding to single-stranded RNA does not necessarily commit the RNA to cleavage. One possible way that RNase E binding could result in regulation of translation, particularly in the *rne* 5' UTR, is to bind to and block the association of the 30S ribosomal subunit to the Shine-Dalgarno sequence, preventing the initiation of canonical translation. This would explain why RNase E has such a strong ability to reduce its own expression by interacting with the 5' UTR of *rne* (Diwa et al., 2000). Studies have shown that high ribosomal occupancy of the 5' UTR of *ompA* protects it from RNase E-mediated degradation, suggesting that there is competition for binding between the 30S subunit and RNase E (Emory et al., 1992).

Work performed alongside this study by Paul Cowling has shown that many other transcripts that are not cleaved by RNase E *in vitro* can still interact with the enzyme at sites required for binding of single-stranded RNA, suggesting that this feature may not be specific to the *rne* mRNA. However, the binding of several of these transcripts is not limited towards the 5' UTR. Perhaps another role RNase E plays in the regulation of translation is to bind to regions of mRNA and sequester the transcript from the pool of translational machinery and locate it to the inner membrane, where it can be subsequently degraded by the localised RNA decay machinery. This would explain the observed compartmentalisation of bacterial cells (Taghbalout et al., 2014, Bakshi et al., 2012), which is beginning to be appreciated as a major factor in post-transcriptional gene regulation (Mackie, 2013b, Bandyra et al., 2013, Taghbalout et al., 2014, Strahl et al., 2015).

Highly structured RNAs could interact with regions of RNase E that are also involved in the binding of single-stranded RNA possibly due to the NTH adopting two conformations. It has been suggested before that, although RNase E has only been shown to adopt the closed conformation when bound to single-stranded RNA (Callaghan et al., 2005a, Koslover et al., 2008), given the relative mobility of the S1-like domain, more complex structures could accommodate catalytic domain in the "open" conformation (Gorna et al., 2012). This could also explain why many regions of RNA seem to be able

to bind to RNase E without being cleaved. Perhaps the NTH of RNase E adopts the "open" conformation to accommodate various regions of RNA, allowing it to locate most transcripts to the degradosome, and that cleavage is a secondary event for some RNAs, whereby the enzyme subsequently adopts the "closed" confirmation. This sequential occurrence of the binding and then cleavage events ensures that only when the last of the already translating ribosomes completed their course of translation could the NTH of RNase E then cleave the major direct entry sites within the coding region. In this way, non-nucleolytic inactivation by RNase E ensures that there is a temporal gap between completion of translation and RNase E-initiated degradation of the transcript, reducing the chances of producing stalled ribosomes and prematurely terminated polypeptides. Although both of these can be removed by the action of tmRNA (Moore and Sauer, 2007), their production is inconsistent with an organism that is renowned for maximising growth potential and not being wasteful.

The second observation, which is not unrelated to the first, is that the catalytic domain of RNase E can clearly interact with some RNAs using contacts not required for the binding of single-stranded regions. These other contacts are sufficient on their own, but can also be made in addition to contacts with single-stranded regions of RNA. In fact, the latter point is illustrated by the fact that interaction of RNA at the allosteric site of RNase E appears to enhance the catalytic step at the direct entry cleavage site within the 3' trailer of *metU.* Although this mechanism appears to be limited to tRNA processing, due to the unique secondary structure of tRNAs, work performed alongside this study by Louise Kime has found that these supporting tRNAs can be substituted with simple stem loops, such as the one found in the *rpsO-pnp* mRNA. This suggests that the requirement of a supporting stem-loop structure for direct entry cleavage may not be limited to tRNA precursors and may be a general feature involved in the initiation of mRNA decay. Indeed, cleavage by RNase E has been shown to be dependent on the presence of stem loop structures in several mRNA substrates (Ehretsmann et al., 1992, Cormack and Mackie, 1992, Mackie and Genereaux, 1993). One possible reason for this selectivity could be to ensure that RNase E makes rapid direct entry cleavages upstream of stem loop structures to allow 3'-exonucleases to bypass these stabilising elements.

The work described in this chapter also confirms that oligonucleotide quadruplexes can bind to RNase E with high affinity, probably due to their ability to present multiple single-stranded regions to the RNA-binding channels in a cooperative manner. In addition, further proof is shown that a monophosphate group at the 5' end increases the affinity of single-stranded oligonucleotides for RNase E, complementing the Michaelis-Menten analysis from Chapter 3 and previous studies (Kime et al., 2010, Kime et al., 2014). Therefore, it appears that the 5'-monophosphate group does not

enhance the catalytic activity of RNase E, and is more likely a requirement for shorter RNA substrates that do not contain the requirements for binding via direct entry. Complementing the binding analysis of the 5' monophosphate-dependent substrates, work in this chapter has confirmed that the requirement of single-stranded regions within both the 5' leader and 3' trailer of tRNA precursors to permit direct entry lies in the fact that these two regions enhance the affinity of the substrate for the catalytic domain of RNase E in a cooperative manner (Kime et al., 2010). The proposed model for mRNA degradation is that long nascent transcripts are substrates for direct entry by RNase E, and the shorter cleavage products are subsequently cleaved via the 5' monophosphate-dependent pathway. Finally, the binding assays developed in this chapter are also the first examples of EMSAs performed with RNase E that have given quantitative results and therefore will make very important tools for further analysis of RNase E as well as re-analysis and/or confirmation of previous studies.

# Chapter 6

# Discussion and future work

## 6.1 Summary of work

The work provided in this thesis has confirmed that the T170V mutant of NTH-RNase E remains a suitable candidate for investigating 5' end-independent cleavages, and therefore was used to analyse the requirements for 'direct' entry cleavage within tRNA precursors. It was confirmed that, during direct entry, RNase E requires simultaneous access to two single-stranded regions separated by a tRNA unit. This structural element probably presents the 5' leader and 3' trailer sequences in the correct conformational context so that they can engage both RNA-binding channels in the RNase E principle dimer simultaneously.

Interestingly, another requirement for direct entry was also found. A supporting tRNA unit was required at the 5' end of the leader sequence for efficient cleavage. This upstream tRNA unit does not contribute to the affinity of the substrate for the catalytic domain of RNase E, but can interact with another region within the NTH. Further kinetic analysis revealed that the presence of this upstream tRNA unit enhances the catalytic activity of RNase E, possibly by binding to an allosteric site and causing a shift in the conformation of the NTH. Further molecular modelling has suggested that changes in the positions of the small domain may be responsible for determining the conformation of RNase E.

This work has also shown that, contrary to previous studies (Jiang and Belasco, 2004), a 5'-monophosphate group does not enhance the catalytic activity of RNase E, and that this group may actually be required to enhance the affinity of the interaction in substrates that do not possess the basic requirement for direct entry *i.e.* two adjacent single-stranded regions in the correct conformational context. This finding explains how RNase E can bypass the 5' monophosphate-dependent pathway both *in vitro* (Hankins et al., 2007, Kime et al., 2010) and *in vivo* (Garrey and Mackie, 2011, Deana et al., 2008, Anupama et al., 2011).

Using an RNA-seq approach, it was shown that the majority of cleavage sites in *E. coli* were attributable to RNase E *in vivo*, in accordance with its role as the initiator of mRNA decay (Kuwano et al., 1977). In addition, 36% of these sites could be recapitulated by just the NTH of RNase E with a T170V mutation *in vitro*. Therefore, direct entry does play a major role in RNase E-mediated degradation as speculated previously (Kime et al., 2014). Further analysis of some of these substrates has found that RNase E can switch between single-stranded regions to cleave at a particular site, or even switch the cleavage site while retaining hold of a particular single-stranded region. This finding illustrates the flexibility that the direct entry mechanism has for the sites of binding and cleavage. The flexibility in binding is mirrored in the fact that RNase E also appears to be

able to interact with regions of RNA without necessarily cleaving them. This could suggest the function of RNase E may be to bind to RNA and prevent further ribosome association and/or to localise the RNA to the inner membrane, where the majority of RNA decay machinery is compartmentalised. Therefore, the role of RNase E during post-transcriptional gene regulation may also extend beyond its ability to make endonucleolytic cleavages.

## 6.2 Future work

### 6.2.1 Further characterisation of the supporting tRNA unit required for direct entry

One of the first issues in analysing the tRNA precursors is that assumptions are made about the structures of the RNA fragments. Before further analysis could be performed, it would be beneficial to determine the structures of many of these truncations. This could be performed using 2'-hydroxyl acylation analysed by primer extension (SHAPE). SHAPE has been used successfully to determine the structure of the direct entry substrate *cspA* (Kime et al., 2010), and would likely give more definite results for tRNA precursors due to the higher theoretical stability of the tRNA units.

Following SHAPE analyses, further dissections of the supporting tRNA units could be performed to confirm the findings in Section 5.3, whereby the supporting structural unit required for direct entry could just be a simple stem-loop structure. Substrates would be generated that have the T- and/or D-loop arms of the supporting *glnW* tRNA removed, whereas others would have *glnW* entirely replaced with the stem loop found in *rpsO*. These substrates would then be subjected to both cleavage and binding assays to investigate the biochemical requirements for the supporting structural elements during direct entry. Following this, the importance of these supporting stem loops *in vivo* could be established, by cloning DNA fragments that encode these tRNA precursors with and without the supporting tRNA unit, as well as with the *rpsO* stem loop replacement, into plasmids that would be transformed into *E. coli* cells. Following rifampicin treatment, which inhibits transcription, RNA would be isolated from samples of culture taken after various time points and the half-life of the substrates would be analysed by Northern blotting.

It would then be interesting to establish the region within the NTH whereby these substrates interact. One such method could be the use of fast photochemical oxidation of proteins (FPOP) combined with mass spectrometry (Maleknia and Downard, 2014). During FPOP, the NTH of RNase E and the NTH-RNA complex would be exposed to oxidative free radicals, which would cause damage to the protein side chains except in regions protected by interacting RNA. The two protein species would then be analysed by denaturing mass spectrometry, allowing the regions where the RNA was interacting to be mapped to RNase E. This could confirm that two single-stranded regions of RNA

interact with the two RNA-binding channels of the principle dimer of RNase E simultaneously during direct entry. In addition, FPOP would also provide a location within the NTH-RNase E for the interaction of the supporting tRNA/stem loop. However, it is important to note that conformational changes in the NTH-RNase E could cause changes in solvent accessibility as well. Therefore, a detailed protein footprinting analysis would also benefit from using techniques such as hydrogen-deuterium exchange mass spectrometry, which can map specific regions of interaction between binding partners by following the movement of deuterium groups within macromolecules (Tsutsui and Wintrode, 2007).

After confirming the molecular recognition of these stem loops, it would be interesting to determine the prevalence of these structural elements within the pool of direct entry substrates. An RNA structurome of *E. coli* could be obtained, using a combination of SHAPE and RNA-seq (Kwok et al., 2015), which could then be compared to the T170V *in vitro* RNA-seq dataset from Chapter 2. Substrates that contain structural regions adjacent to direct entry cleavages would be identified and synthesised. These mRNA substrates could then be dissected and analysed as performed for the tRNA subsrates in this work to test whether supporting structural elements are required for the majority of direct entry cleavages within the mRNA pool. Establishing the importance of these stem loops in initiating RNase E cleavage by direct entry could contribute to advancements in *E. coli* protein expression systems. Expression of a particular protein could be enhanced by removing these "destabilising" features from the corresponding mRNA. In addition, these findings could have applications in synthetic biology, whereby multiple genes could be coordinated at different levels by adding these features to the corresponding transcripts.

### 6.2.2 Interplay of RNase E and 30S subunit binding to mRNA

Several studies have shown that RNase E interacts with its own mRNA by making contact with hp2 on the 5' UTR of *rne*, which results in destabilisation of the transcript and repression of translation. However, this work has found that RNase E binds primarily to another site within hp3. In order to determine the exact regions of hp3 that interact with RNase E, mutagenesis of the sequence within the "bulge" regions of the substrate could be performed and the effects on binding analysed by EMSAs.

Interestingly, interaction of RNase E with hp3 does not result in significant destabilisation of the 5' UTR and is not required for direct entry cleavage within the coding region of *rne in vitro*. However, *in vivo* it has been shown that the 5' UTR of *rne* actually results in destabilisation of the transcript, and hence reduced expression of RNase E. One hypothesis in this work has suggested that binding of

RNase E to the 5' UTR actually blocks the association of the 30S subunit to the *rne* transcript. This reduces ribosomal traffic on the transcript, exposing the major direct entry sites within the coding region of *rne* for subsequent cleavage. To confirm this model, it would first be necessary to show that the sites of RNase E binding and 30S binding overlap, possibly by using an RNA-footprinting analysis such as SHAPE. Following this, the effect of RNase E on translation could be examined using an *in vitro* transcription-translation assay (T-T assays). Plasmids would be designed to contain a gene encoding the green fluorescent protein fused with various truncations of the *rne* 5' UTR. The T-T assays could then be incubated with wild-type and D346N mutants of NTH-RNase E, to confirm that binding of RNase E to hp3 inhibits translation. As a negative control, mutants of RNase E that are suspected to reduce binding to RNA, such as F57A (Garrey et al., 2009), could be used to show that they do not inhibit translation. EMSAs would first have to be performed using the F57A mutant to show that this mutation gave the predicted phenotype.

Another hypothesis as to why RNase E binds to the 5' UTR of *rne* without cleaving it is to localise the mRNA to the inner membrane. In this way, RNase E would sequester the 5' UTR away from the translational machinery instead of directly blocking it. This could ensure that already translated ribosomes were allowed to complete their round of translation and dissociate from the transcript, but new ribosomes would not associate, allowing RNase E to make subsequent cleavages within the coding region without the risk of producing stalled ribosomes. One possible way to prove this hypothesis is using an *in vivo* approach (Diwa et al., 2000). Plasmids containing a *lacZ* gene fused with various truncations of the *rne* 5' UTR would be introduced into *E. coli* strains that contain either a truncation in the CTH of RNase E that retains or removes the membrane-binding segment A. As a positive control, similar analyses would have to be performed using congenic *E. coli* strains with full length wild-type RNase E.

If either of these two hypotheses is found to be possible, it would then be important to establish how prevalent the ability of RNase E to bind but not cleave is in the *E. coli* transcriptome. One such method termed individual-nucleotide resolution cross-linking and immuno-precipitation (iCLIP) could be used (Huppertz et al., 2014). The iCLIP strategy would combine UV crosslinking of RNA to RNase E, followed by immunoprecipitation of the RNase E-RNA complex, and protease digestion of RNase E to yield RNA cross-linked to very short peptide fragments. RNA seq would yield truncated cDNA fragments due to the inability of reverse transcriptase to remaining associated at regions of RNA that are cross-linked to amino acids. This multi-step technique would allow single nucleotide-resolution, transcriptome-wide maps of RNase E interactions to be obtained, which could be compared to the *rne in vivo* RNA-seq dataset from Chapter 4 to establish regions within the *E. coli*

transcriptome that are associated with RNase E binding in the absence of cleavage *in vivo*. This information could contribute significantly to the understanding of leaderless mRNAs and specialised ribosomes, translational regulation by sRNAs, cellular compartmentalisation, and the relevance of the *trans*-translation pathway. Establishing the ability of RNase E to bind to RNAs without cleaving them could also have implications in gene expression, by developing decoy mRNAs that could bind to the active site of RNase E and sequester its activity from mRNAs encoding desired proteins.

### 6.2.3 Conformational changes in RNase E

Work in Chapter 5 has suggested that RNase E is catalytically activated by the interaction of supporting tRNA units to an allosteric site on the NTH-RNase E. Allosteric activation is most likely due to a conformational change that results in the NTH-RNase E adopting the "closed" conformation. Therefore, this model suggests that in the absence of supporting tRNA units, the direct entry substrate can still bind to the principal dimer but cannot cause the enzyme to adopt the "closed" conformation and therefore cleave at the site of direct entry cleavage. One possible technique that could be used to confirm this model is small angle X-ray scattering (SAXS). SAXS has been used before to successfully monitor conformational changes within NTH-RNase E and has the advantages that structural information can be obtained in non-crystalline conditions (Callaghan et al., 2003, Koslover et al., 2008). However, due to the random orientation of dissolved molecules, there is a loss of structural information compared to techniques such as X-ray crystallography.

Another method that could be used to visualise the conformational changes of RNase E upon binding to different RNA substrates is cryogenic electron microscopy (cryo-EM). Like SAXS, cryo-EM allows the samples to be incubated under native conditions. However, following this step, samples are then subjected rapidly to cryogenic temperatures and analysed via transmission electron microscopy. Given that these molecules are effectively "fixed", cryo-EM data has an advantage over SAXS data that less structural information is lost. However, because the molecules are "fixed", to gain high resolution maps many molecules in various orientations need to be imaged and then aligned.

After identifying a useful technique for analysing the conformation of NTH-RNase E, the residues of the protein that are involved in this conformational change could be identified, either by random mutagenesis or by structural modelling (Figure 5.13). These residues could include those which are involved in interacting with supporting RNA structural elements at the allosteric site; interactions within the heterologous interface between the large and small domains of the principal dimer; and interactions that allow the 5'-sensing domain and S1-like domain to clamp down onto the DNase I-

like domain. Further analyses of these residues could confirm the hypotheses suggested in this work and reveal further information for the RNA recognition mechanism of RNase E.

# Chapter 7

# References

AFONYUSHKIN, T., VECEREK, B., MOLL, I., BLASI, U. & KABERDIN, V. R. 2005. Both RNase E and RNase III control the stability of *sodB* mRNA upon translational inhibition by the small regulatory RNA RyhB. *Nucleic Acids Research,* 33**,** 1678-1689.

AIBA, H. 2007. Mechanism of RNA silencing by Hfq-binding small RNAs. *Current Opinion in Microbiology,* 10**,** 134-139.

AIZENMAN, E., ENGELBERG-KULKA, H. & GLASER, G. 1996. An *Escherichia coli* chromosomal "addiction module" regulated by guanosine [corrected] 3',5'-bispyrophosphate: a model for programmed bacterial cell death. *Proceedings of the National Academy of Sciences of the United States of America,* 93**,** 6059-6063.

ALTMAN, S., BAER, M., GOLD, H., GUERRIER-TAKADA, C., KIRSEBOM, L., LAWRENCE, N., LUMELSKY, N. & VIOQUE, A. 1987. Cleavage of RNA by RNase P. *Molecular Biology of RNA: New Perspectives***,** 3-15.

AMITAI, S., KOLODKIN-GAL, I., HANANYA-MELTABASHI, M., SACHER, A. & ENGELBERG-KULKA, H. 2009. *Escherichia coli* MazF leads to the simultaneous selective synthesis of both "death proteins'' and "survival proteins''. *PLoS Genetics,* 5.

ANDRADE, J. M., HAJNSDORF, E., REGNIER, P. & ARRAIANO, C. M. 2009a. The poly(A)-dependent degradation pathway of *rpsO* mRNA is primarily mediated by RNase R. *RNA-a Publication of the RNA Society,* 15**,** 316-326.

ANDRADE, J. M., POBRE, V., SILVA, I. J., DOMINGUES, S. & ARRAIANO, C. M. 2009b. The role of 3'-5' exoribonucleases in RNA degradation. *In:* CONDON, C. (ed.) *Molecular Biology of RNA Processing and Decay in Prokaryotes.* Academic Press.

ANUPAMA, K., LEELA, J. K. & GOWRISHANKAR, J. 2011. Two pathways for RNase E action in *Escherichia coli in vivo* and bypass of its essentiality in mutants defective for Rho-dependent transcription termination. *Molecular Microbiology,* 82**,** 1330-1348.

APIRION, D. & LASSAR, A. B. 1978. Conditional lethal mutant of *Escherichia coli* which affects processing of ribosomal RNA. *Journal of Biological Chemistry,* 253**,** 1738-1742.

APIRION, D., NEIL, J. & WATSON, N. 1976a. Consequences of losing ribonuclease III on the *Escherichia coli* cell. *Molecular General Genetics,* 144**,** 185-190.

APIRION, D., NEIL, J. & WATSON, N. 1976b. Revertants from RNase III negative strains of *Escherichia coli. Molecular General Genetics,* 149**,** 201-210.

ARISTARKHOV, A., MIKULSKIS, A., BELASCO, J. G. & LIN, E. C. C. 1996. Translation of the *adhE* transcript to produce ethanol dehydrogenase requires RNase III cleavage in *Escherichia coli*. *Journal of Bacteriology,* 178**,** 4327-4332.

ARNOLD, T. E., YU, J. & BELASCO, J. G. 1998. mRNA stabilization by the ompA 5 ' untranslated region: Two protective elements hinder distinct pathways for mRNA degradation. *RNA-a Publication of the RNA Society,* 4**,** 319-330.

AWANO, N., RAJAGOPAL, V., ARBING, M., PATEL, S., HUNT, J., INOUYE, M. & PHADTARE, S. 2010. *Escherichia coli* RNase R has dual activities, helicase and RNase. *Journal of Bacteriology,* 192**,** 1344-1352.

BABA, T., ARA, T., HASEGAWA, M., TAKAI, Y., OKUMURA, Y., BABA, M., DATSENKO, K. A., TOMITA, M., WANNER, B. L. & MORI, H. 2006. Construction of *Escherichia coli* K-12 in-frame, single-gene knockout mutants: the Keio collection. *Molecular Systems Biology,* 2**,** 2006 0008.

BABITZKE, P., GRANGER, L., OLSZEWSKI, J. & KUSHNER, S. R. 1993. Analysis of messenger RNA decay and ribosomal RNA processing in *Escherichia coli* multiple mutants carrying a deletion in RNase III. *Journal of Bacteriology,* 175**,** 229-239.

BABITZKE, P. & KUSHNER, S. R. 1991. The *ams* (altered messenger RNA stability) protein and ribonuclease E are encoded by the same structural gene of *Escherichia coli*. *Proceedings of the National Academy of Sciences of the United States of America,* 88**,** 1-5.

BAKER, K. E. & MACKIE, G. A. 2003. Ectopic RNase E sites promote bypass of 5'-end-dependent mRNA decay in *Escherichia coli*. *Molecular Microbiology,* 47**,** 75-88.

BAKSHI, S., SIRYAPORN, A., GOULIAN, M. & WEISSHAAR, J. C. 2012. Superresolution imaging of ribosomes and RNA polymerase in live *Escherichia coli* cells. *Molecular Microbiology,* 85**,** 21-38.

BALAGURUMOORTHY, P., BRAHMACHARI, S. K., MOHANTY, D., BANSAL, M. & SASISEKHARAN, V. 1992. Hairpin and parallel quartet structures for telomeric sequences. *Nucleic Acids Research,* 20**,** 4061-4067.

BANDYRA, K. J., BOUVIER, M., CARPOUSIS, A. J. & LUISI, B. F. 2013. The social fabric of the RNA degradosome. *Biochimica et Biophysica Acta,* 1829**,** 514-522.

BANDYRA, K. J., SAID, N., PFEIFFER, V., GORNA, M. W., VOGEL, J. & LUISI, B. F. 2012. The seed region of a small RNA drives the controlled destruction of the target mRNA by the endoribonuclease RNase E. *Molecular Cell,* 47**,** 943-953.

BARBAS, A., MATOS, R. G., AMBLAR, M., LOPEZ-VINAS, E., GOMEZ-PUERTAS, P. & ARRAIANO, C. M. 2008. New insights into the mechanism of RNA degradation by ribonuclease II - Identification of the residue responsible for setting the RNase II end product. *Journal of Biological Chemistry,* 283**,** 13070-13076.

BARBOSA, E. & MOSS, B. 1978. mRNA(nucleoside-2'-)-methyltransferase from vaccinia virus. Characteristics and substrate specificity. *Journal of Biological Chemistry,* 253**,** 7698-7702.

BARDEY, V., VALLET, C., ROBAS, N., CHARPENTIER, B., THOUVENOT, B., MOUGIN, A., HAJNSDORF, E., REGNIER, P., SPRINGER, M. & BRANLANT, C. 2005. Characterization of the molecular mechanisms involved in the differential production of erythrose-4-phosphate dehydrogenase, 3-phosphoglycerate kinase and class II fructose-1,6-bisphosphate aldolase in *Escherichia coli*. *Molecular Microbiology,* 57**,** 1265-1287.

BARNHART, M. D., MOON, S. L., EMCH, A. W., WILUSZ, C. J. & WILUSZ, J. 2013. Changes in cellular mRNA stability, splicing, and polyadenylation through HuR protein sequestration by a cytoplasmic RNA virus. *Cell Reports,* 5**,** 909-917.

BARRANGOU, R., FREMAUX, C., DEVEAU, H., RICHARDS, M., BOYAVAL, P., MOINEAU, S., ROMERO, D. A. & HORVATH, P. 2007. CRISPR provides acquired resistance against viruses in prokaryotes. *Science,* 315**,** 1709-1712.

BELASCO, J. G., NILSSON, G., VONGABAIN, A. & COHEN, S. N. 1986. The stability of *Escherichia coli* gene transcripts is dependent on determinants localized to specific messenger RNA segments. *Cell,* 46**,** 245-251.

BERG, O. G. & KURLAND, C. G. 1997. Growth rate-optimised tRNA abundance and codon usage. *Journal of Molecular Biology,* 270**,** 544-550.

BERNSTEIN, J. A., KHODURSKY, A. B., LIN, P. H., LIN-CHAO, S. & COHEN, S. N. 2002. Global analysis of mRNA decay and abundance in *Escherichia coli* at single-gene resolution using two-color fluorescent DNA microarrays. *Proceedings of the National Academy of Sciences of the United States of America,* 99**,** 9697-9702.

BERNSTEIN, J. A., LIN, P. H., COHEN, S. N. & LIN-CHAO, S. 2004. Global analysis of *Escherichia coli* RNA degradosome function using DNA microarrays. *Proceedings of the National Academy of Sciences of the United States of America,* 101**,** 2758-2763.

BLUM, E., CARPOUSIS, A. J. & HIGGINS, C. F. 1999. Polyadenylation promotes degradation of 3 '-structured RNA by the *Escherichia coli* mRNA degradosome *in vitro*. *Journal of Biological Chemistry,* 274**,** 4009-4016.

BOUVET, P. & BELASCO, J. G. 1992. Control of RNase E-mediated RNA degradation by 5'-terminal base-pairing in *Escherichia coli*. *Nature,* 360**,** 488-491.

BRAM, R. J., YOUNG, R. A. & STEITZ, J. A. 1980. The ribonuclease III site flanking 23S sequences in the 30S ribosomal precursor RNA of *E. coli*. *Cell,* 19**,** 393-401.

BRANDT, F., ETCHELLS, S. A., ORTIZ, J. O., ELCOCK, A. H., HARTL, F. U. & BAUMEISTER, W. 2009. The native 3D organization of bacterial polysomes. *Cell,* 136**,** 261-271.

BRANTL, S. 2007. Regulatory mechanisms employed by cis-encoded antisense RNAs. *Current Opinions in Microbiology,* 10**,** 102-109.

BRAUN, F., HAJNSDORF, E. & REGNIER, P. 1996. Polynucleotide phosphorylase is required for the rapid degradation of the RNase E-processed *rpsO* mRNA of *Escherichia coli* devoid of its 3' hairpin. *Molecular Microbiology,* 19**,** 997-1005.

BRAUN, F., LE DEROUT, J. & REGNIER, P. 1998. Ribosomes inhibit an RNase E cleavage which induces the decay of the *rpsO* mRNA of *Escherichia coli*. *EMBO Journal,* 17**,** 4790-4797.

BRIANT, D. J., HANKINS, J. S., COOK, M. A. & MACKIE, G. A. 2003. The quaternary structure of RNase G from *Escherichia coli*. *Molecular Microbiology,* 50**,** 1381-1390.

BRICKER, A. L. & BELASCO, J. G. 1999. Importance of a 5 ' stem-loop for longevity of *papA* mRNA in *Escherichia coli*. *Journal of Bacteriology,* 181**,** 3587-3590.

BRITTON, R. A. 2009. Role of GTPases in bacterial ribosome assembly. *Annual Reviews of Microbiology,* 63**,** 155-176.

BRITTON, R. A., WEN, T. Y., SCHAEFER, L., PELLEGRINI, O., UICKER, W. C., MATHY, N., TOBIN, C., DAOU, R., SZYK, J. & CONDON, C. 2007. Maturation of the 5 ' end of *Bacillus subtilis* 16S rRNA by the essential ribonuclease YkqC/RNase J1. *Molecular Microbiology,* 63**,** 127-138.

BROUNS, S. J., JORE, M. M., LUNDGREN, M., WESTRA, E. R., SLIJKHUIS, R. J., SNIJDERS, A. P., DICKMAN, M. J., MAKAROVA, K. S., KOONIN, E. V. & VAN DER OOST, J. 2008. Small CRISPR RNAs guide antiviral defense in prokaryotes. *Science,* 321**,** 960-964.

BUGRYSHEVA, J. V. & SCOTT, J. R. 2010. The ribonucleases J1 and J2 are essential for growth and have independent roles in mRNA decay in *Streptococcus pyogenes*. *Molecular Microbiology,* 75**,** 731-743.

BURGE, S., PARKINSON, G. N., HAZEL, P., TODD, A. K. & NEIDLE, S. 2006. Quadruplex DNA: sequence, topology and structure. *Nucleic Acids Research,* 34**,** 5402-5415.

BURGERS, P. M. & ECKSTEIN, F. 1979. Stereochemistry of internucleotide bond formation by polynucleotide phosphorylase from *Micrococcus luteus*. *Biochemistry,* 18**,** 450-454.

BYCROFT, M., HUBBARD, T. J., PROCTOR, M., FREUND, S. M. & MURZIN, A. G. 1997. The solution structure of the S1 RNA binding domain: a member of an ancient nucleic acid-binding fold. *Cell,* 88**,** 235-242.

CAHOVA, H., WINZ, M. L., HOFER, K., NUBEL, G. & JASCHKE, A. 2015. NAD captureSeq indicates NAD as a bacterial cap for a subset of regulatory RNAs. *Nature,* 519**,** 374-377.

CALLAGHAN, A. J., AURIKKO, J. P., IIAG, L. L., GROSSMANN, J. G., CHANDRAN, V., KUHNEL, K., POLJAK, L., CARPOUSIS, A. J., ROBINSON, C. V., SYMMONS, M. F. & LUISI, B. F. 2004. Studies of the RNA degradosome-organizing domain of the *Escherichia coli* ribonuclease RNase E. *Journal of Molecular Biology,* 340**,** 965-979.

CALLAGHAN, A. J., GROSSMANN, J. G., REDKO, Y. U., ILAG, L. L., MONCRIEFFE, M. C., SYMMONS, M. F., ROBINSON, C. V., MCDOWALL, K. J. & LUISI, B. F. 2003. Quaternary structure and catalytic activity of the *Escherichia coli* ribonuclease E amino-terminal catalytic domain. *Biochemistry,* 42**,** 13848-13855.

CALLAGHAN, A. J., MARCAIDA, M. J., STEAD, J. A., MCDOWALL, K. J., SCOTT, W. G. & LUISI, B. F. 2005a. Structure of *Escherichia coli* RNase E catalytic domain and implications for RNA turnover. *Nature,* 437**,** 1187-1191.

CALLAGHAN, A. J., REDKO, Y., MURPHY, L. M., GROSSMANN, J. G., YATES, D., GARMAN, E., ILAG, L. L., ROBINSON, C. V., SYMMONS, M. F., MCDOWALL, K. J. & LUISI, B. F. 2005b. "Zn-Link": A metal-sharing interface that organizes the quaternary structure and catalytic site of the endoribonuclease, RNase E. *Biochemistry,* 44**,** 4667-4675.

CALLAHAN, C., NERI-CORTES, D. & DEUTSCHER, M. P. 2000. Purification and characterization of the tRNA-processing enzyme RNase BN. *Journal of Biological Chemistry,* 275**,** 1030-1034.

CANNISTRARO, V. J. & KENNELL, D. 1989. Purification and characterization of ribonuclease M and mRNA degradation in *Escherichia coli*. *European Journal of Biochemistry,* 181**,** 363-370.

CAO, G. J. & SARKAR, N. 1992. Poly(A) RNA in *Escherichia coli*: nucleotide sequence at the junction of the *lpp* transcript and the polyadenylate moiety. *Proceedings of the National Academy of Sciences of the United States of America,* 89**,** 7546-7550.

CARABETTA, V. J., SILHAVY, T. J. & CRISTEA, I. M. 2010. The response regulator SprE (RssB) is required for maintaining poly(A) polymerase I-degradosome association during stationary phase. *Journal of Bacteriology,* 192**,** 3713-3721.

CARPOUSIS, A. J., LUISI, B. F. & MCDOWALL, K. J. 2009. Endonucleolytic initiation of mRNA decay in *Escherichia coli*. *In:* CONDON, C. (ed.) *Molecular Biology of RNA Processing and Decay in Prokaryotes.* Academic Press.

CARPOUSIS, A. J., VAN HOUWE, G. & KRISCH, H. M. 1994. Copurification of *Escherichia coli* RNase E and PNPase: Evidence for a specific association between two enzymes important in RNA processing and degradation. *Journal of Cellular Biochemistry***,** 146-146.

CARTE, J., PFISTER, N. T., COMPTON, M. M., TERNS, R. M. & TERNS, M. P. 2010. Binding and cleavage of CRISPR RNA by Cas6. *RNA-a Publication of the RNA Society ,* 16**,** 2181-2188.

CARUTHERS, J. M., FENG, Y. N., MCKAY, D. B. & COHEN, S. N. 2006. Retention of core catalytic functions by a conserved minimal ribonuclease E peptide that lacks the domain required for tetramer formation. *Journal of Biological Chemistry,* 281**,** 27046-27051.

CARUTHERS, J. M. & MCKAY, D. B. 2002. Helicase structure and mechanism. *Current Opinions in Structural Biology,* 12**,** 123-133.

CARZANIGA, T., BRIANI, F., ZANGROSSI, S., MERLINO, G., MARCHI, P. & DEHO, G. 2009. Autogenous Regulation of *Escherichia coli* Polynucleotide Phosphorylase Expression Revisited. *Journal of Bacteriology,* 191**,** 1738-1748.

CASADABAN, M. J. & COHEN, S. N. 1980. Analysis of gene control signals by DNA fusion and cloning in *Escherichia coli*. *Journal of Molecular Biology,* 138**,** 179-207.

CASTANO, J. G., TOBIAN, J. A. & ZASLOFF, M. 1985. Purification and characterization of an endonuclease from *Xenopus laevis* ovaries which accurately processes the 3' terminus of human pre-tRNA-Met(i) (3' pre-tRNase). *Journal of Biological Chemistry,* 260**,** 9002-9008.

CELESNIK, H., DEANA, A. & BELASCO, J. G. 2007. Initiation of RNA decay in *Escherichia coli* by 5'-pyrophosphate removal. *Molecular Cell,* 27**,** 79-90.

CHAMPOUX, J. J. & SCHULTZ, S. J. 2009. Ribonuclease H: properties, substrate specificity and roles in retroviral reverse transcription. *FEBS Journal,* 276**,** 1506-1516.

CHAN, P. P., HOLMES, A. D., SMITH, A. M., TRAN, D. & LOWE, T. M. 2012. The UCSC Archaeal Genome Browser: 2012 update. *Nucleic Acids Research,* 40**,** D646-52.

CHANDRAN, V., CALLAGHAN, A., LONG, J., ZAID, O., AURIKKA, J., ILAG, L., ROBINSON, C., CARPOUSIS, A. J., SYMMONS, M. & LUISI, B. F. 2004. Protein-protein interactions in the RNA degradosome. *Protein Science,* 13**,** 144-144.

CHANDRAN, V. & LUISI, B. F. 2006. Recognition of enolase in the *Escherichia coli* RNA degradosome. *Journal of Molecular Biology,* 358**,** 8-15.

CHANDRAN, V., POLJAK, L., VANZO, N. F., LEROY, A., MIGUEL, R. N., FERNANDEZ-RECIO, J., PARKINSON, J., BURNS, C., CARPOUSIS, A. J. & LUISI, B. F. 2007. Recognition and cooperation between the ATP-dependent RNA helicase RhIB and ribonuclease RNase e. *Journal of Molecular Biology,* 367**,** 113-132.

CHEN, C. Y. A., BEATTY, J. T., COHEN, S. N. & BELASCO, J. G. 1988. An intercistronic stem-loop structure functions as a messenger RNA decay terminator necessary but insufficient for *puf* messenger RNA stability. *Cell,* 52**,** 609-619.

CHEN, J. & MATTHEWS, K. S. 1994. Subunit dissociation affects DNA binding in a dimeric lac repressor produced by C-terminal deletion. *Biochemistry,* 33**,** 8728-8735.

CHEN, L. H., EMORY, S. A., BRICKER, A. L., BOUVET, P. & BELASCO, J. G. 1991. Structure and function of a bacterial messenger RNA stabilizer: Analysis of the 5' untranslated region of *ompA* messenger RNA. *Journal of Bacteriology,* 173**,** 4578-4586.

CHEN, Y. G., KOWTONIUK, W. E., AGARWAL, I., SHEN, Y. & LIU, D. R. 2009. LC/MS analysis of cellular RNA reveals NAD-linked RNA. *Nature Chemical Biology,* 5**,** 879-881.

CHENG, Z. F. & DEUTSCHER, M. P. 2002. Purification and characterization of the Escherichia coli exoribonuclease RNase R. Comparison with RNase II. *Journal of Biological Chemistry,* 277**,** 21624-21629.

CHENG, Z. F. & DEUTSCHER, M. P. 2003. Quality control of ribosomal RNA mediated by polynucleotide phosphorylase and RNase R. *Proceedings of the National Academy of Sciences of the United States of America,* 100**,** 6388-6393.

CHENG, Z. F., ZUO, Y., LI, Z., RUDD, K. E. & DEUTSCHER, M. P. 1998. The *vacB* gene required for virulence in *Shigella flexneri* and *Escherichia coli* encodes the exoribonuclease RNase R. *Journal of Biological Chemistry,* 273**,** 14077-14080.

CHO, B. K., ZENGLER, K., QIU, Y., PARK, Y. S., KNIGHT, E. M., BARRETT, C. L., GAO, Y. & PALSSON, B. O. 2009. The transcription unit architecture of the *Escherichia coli* genome. *Nature Biotechnology,* 27**,** 1043-1049.

CHO, E. J., TAKAGI, T., MOORE, C. R. & BURATOWSKI, S. 1997. mRNA capping enzyme is recruited to the transcription complex by phosphorylation of the RNA polymerase II carboxy-terminal domain. *Genes & Development,* 11**,** 3319-3326.

CHRISTENSEN, S. K., PEDERSEN, K., HANSEN, F. G. & GERDES, K. 2003. Toxin-antitoxin loci as stress-response-elements: ChpAK/MazF and ChpBK cleave translated RNAs and are counteracted by tmRNA. *Journal of Molecular Biology,* 332**,** 809-819.

CHUNG, D. H., MIN, Z., WANG, B. C. & KUSHNER, S. R. 2010. Single amino acid changes in the predicted RNase H domain of *Escherichia coli* RNase G lead to complementation of RNase E deletion mutants. *RNA-a Publication of the RNA Society,* 16**,** 1371-1385.

CLARKE, J. E., KIME, L., ROMERO A., D. & MCDOWALL, K. J. 2014. Direct entry by RNase E is a major pathway for the degradation and processing of RNA in *Escherichia coli*. *Nucleic Acids Research,* 42, 11733-11751.

COBURN, G. A. & MACKIE, G. A. 1996a. Differential sensitivities of portions of the mRNA for ribosomal protein S20 to 3'-exonucleases dependent on oligoadenylation and RNA secondary structure. *Journal of Biological Chemistry,* 271**,** 15776-15781.

COBURN, G. A. & MACKIE, G. A. 1996b. Overexpression, purification, and properties of *Escherichia coli* ribonuclease II. *Journal of Biological Chemistry,* 271**,** 1048-1053.

COBURN, G. A. & MACKIE, G. A. 1998. Reconstitution of the degradation of the mRNA for ribosomal protein S20 with purified enzymes. *Journal of Molecular Biology,* 279**,** 1061-1074.

COBURN, G. A. & MACKIE, G. A. 1999. Degradation of mRNA in *Escherichia coli*: an old problem with some new twists. *Progressions in Nucleic Acid Research and Molecular Biology,* 62**,** 55-108.

COBURN, G. A., MIAO, X., BRIANT, D. J. & MACKIE, G. A. 1999. Reconstitution of a minimal RNA degradosome demonstrates functional coordination between a 3 ' exonuclease and a DEAD-box RNA helicase. *Genes & Development,* 13**,** 2594-2603.

COLLER, J. M., GRAY, N. K. & WICKENS, M. P. 1998. mRNA stabilization by poly(A) binding protein is independent of poly(A) and requires translation. *Genes & Development,* 12**,** 3226-3235.

COMMICHAU, F. M., ROTHE, F. M., HERZBERG, C., WAGNER, E., HELLWIG, D., LEHNIK-HABRINK, M., HAMMER, E., VOLKER, U. & STULKE, J. 2009. Novel activities of glycolytic enzymes in *Bacillus subtilis*: interactions with essential proteins involved in mRNA processing. *Molecular & Cellular Proteomics,* 8**,** 1350-1360.

CONDON, C. & PUTZER, H. 2002. The phylogenetic distribution of bacterial ribonucleases. *Nucleic Acids Research,* 30**,** 5339-5346.

CORDIN, O., BANROQUES, J., TANNER, N. K. & LINDER, P. 2006. The DEAD-box protein family of RNA helicases. *Gene,* 367**,** 17-37.

CORMACK, R. S. & MACKIE, G. A. 1992. Structural requirements for the processing of *Escherichia coli* 5S ribosomal RNA by RNase E *in vitro*. *Journal of Molecular Biology,* 228**,** 1078-1090.

COWLING, V. H. 2010. Regulation of mRNA cap methylation. *Biochemical Journal,* 425**,** 295-302.

CROOKS, G. E., HON, G., CHANDONIA, J. M. & BRENNER, S. E. 2004. WebLogo: A sequence logo generator. *Genome Research,* 14**,** 1188-1190.

DAHLBERG, A. E. & DAHLBERG, J. E. 1975. Binding of ribosomal protein S1 of *Escherichia coli* to the 3' end of 16S rRNA. *Proceedings of the National Academy of Sciences of the United States of America,* 72**,** 2940-2944.

DANCHIN, A. 2009. A Phylogenetic View of Bacterial Ribonucleases. *In:* CONDON, C. (ed.) *Molecular Biology of RNA Processing and Decay in Prokaryotes.* Academic Press.

DAOU-CHABO, R. & CONDON, C. 2009. RNase J1 endonuclease activity as a probe of RNA secondary structure. *RNA-a Publication of the RNA Society,* 15**,** 1417-1425.

DAVIES, B. W., KOHRER, C., JACOB, A. I., SIMMONS, L. A., ZHU, J., ALEMAN, L. M., RAJBHANDARY, U. L. & WALKER, G. C. 2010. Role of Escherichia coli YbeY, a highly conserved protein, in rRNA processing. *Molecular Microbiology,* 78**,** 506-518.

DE LA SIERRA-GALLAY, I. L., PELLEGRINI, O. & CONDON, C. 2005. Structural basis for substrate binding, cleavage and allostery in the tRNA maturase RNase Z. *Nature,* 433**,** 657-661.

DE LA SIERRA-GALLAY, I. L., ZIG, L., JAMALLI, A. & PUTZER, H. 2008. Structural insights into the dual activity of RNase J. *Nature Structural & Molecular Biology,* 15**,** 206-212.

DEANA, A. & BELASCO, J. G. 2005. Lost in translation: The influence of ribosomes on bacterial mRNA decay. *Genes & Development,* 19**,** 2526-2533.

DEANA, A., CELESNIK, H. & BELASCO, J. G. 2008. The bacterial enzyme RppH triggers messenger RNA degradation by 5'-pyrophosphate removal. *Nature,* 451**,** 355-358.

DELVILLANI, F., PAPIANI, G., DEHO, G. & BRIANI, F. 2011. S1 ribosomal protein and the interplay between translation and mRNA decay. *Nucleic Acids Researcg,* 39**,** 7702-7715.

DEUTSCHER, M. P. 2003. Degradation of stable RNA in bacteria. *Journal of Biological Chemistry,* 278**,** 45041-45044.

DEUTSCHER, M. P. 2006. Degradation of RNA in bacteria: Comparison of mRNA and stable RNA. *Nucleic Acids Research,* 34**,** 659-666.

DEUTSCHER, M. P. 2009. Maturation and degradation of ribosomal RNA in bacteria. *In:* CONDON, C. (ed.) *Molecular Biology of RNA Processing and Decay in Prokaryotes.* Academic press.

DEUTSCHER, M. P., LIN, J. J. & EVANS, J. A. 1977. Transfer RNA metabolism in *Escherichia coli* cells deficient in tRNA nucleotidyltransferase. *Journal of Molecular Biology,* 117**,** 1081-1094.

DEUTSCHER, M. P., MARLOR, C. W. & ZANIEWSKI, R. 1984. Ribonuclease T: new exoribonuclease possibly involved in end-turnover of tRNA. *Proc Natl Acad Sci U S A,* 81**,** 4290-3.

DEUTSCHER, M. P. & REUVEN, N. B. 1991. Enzymatic basis for hydrolytic versus phosphorolytic mRNA degradation in *Escherichia coli* and *Bacillus subtilis*. *Proceedings of the National Academy of Sciences of the United States of America,* 88**,** 3277-3280.

DIWA, A., BRICKER, A. L., JAIN, C. & BELASCO, J. G. 2000. An evolutionarily conserved RNA stem-loop functions as a sensor that directs feedback regulation of RNase E gene expression. *Genes & Development,* 14**,** 1249-1260.

DIWA, A. A. & BELASCO, J. G. 2002. Critical features of a conserved RNA stem-loop important for feedback regulation of RNase E synthesis. *Journal of Biological Chemistry,* 277**,** 20415-20422.

DIWA, A. A., JIANG, X. Q., SCHAPIRA, M. & BELASCO, J. G. 2002. Two distinct regions on the surface of an RNA-binding domain are crucial for RNase E function. *Molecular Microbiology,* 46**,** 959-969.

DONG, H., NILSSON, L. & KURLAND, C. G. 1996. Co-variation of tRNA abundance and codon usage in *Escherichia coli* at different growth rates. *Journal of Molecular Biology,* 260**,** 649-663.

DONOVAN, W. P. & KUSHNER, S. R. 1986. Polynucleotide phosphorylase and Ribonuclease II are required for cell viability and messenger RNA turnover in *Escherichia coli* K12. *Proceedings of the National Academy of Sciences of the United States of America,* 83**,** 120-124.

DUNCKLEY, T. & PARKER, R. 1999. The DCP2 protein is required for mRNA decapping in *Saccharomyces cerevisiae* and contains a functional MutT motif. *EMBO Journal,* 18**,** 5411-5422.

DUNCKLEY, T., TUCKER, M. & PARKER, R. 2001. Two related proteins, Edc1p and Edc2p, stimulate mRNA decapping in *Saccharomyces cerevisiae*. *Genetics,* 157**,** 27-37.

DUNN, J. J. & STUDIER, F. W. 1973. T7 early RNAs and *Escherichia coli* ribosomal RNAs are cut from large precursor RNAs *in vivo* by ribonuclease 3. *Proceedings of the National Academy of Sciences of the United States of America,* 70**,** 3296-3300.

DURAN-FIGUEROA, N. V., PINA-ESCOBEDO, A., SCHROEDER, I., SIMONS, R. W. & GARCIA-MENA, J. 2006. Polynucleotide phosphorylase interacts with ribonuclease E through a betabetaalphabetabetaalpha domain. *Biochimie,* 88**,** 725-735.

DURAND, S., GILET, L., BESSIERES, P., NICOLAS, P. & CONDON, C. 2012. Three essential ribonucleases-RNase Y, J1, and III-control the abundance of a majority of *Bacillus subtilis* mRNAs. *PLoS Genet,* 8**,** e1002520.

DURRENBERGER, M., BJORNSTI, M. A., UETZ, T., HOBOT, J. A. & KELLENBERGER, E. 1988. Intracellular location of the histonelike protein HU in *Escherichia coli*. *Journal of Bacteriology,* 170**,** 4757-4768.

DUTTA, T. & DEUTSCHER, M. P. 2009. Catalytic properties of RNase BN/RNase Z from *Escherichia coli*: RNase BN is both an exo- and endoribonuclease. *Journal of Biological Chemistry,* 284**,** 15425-15431.

DUTTA, T. & DEUTSCHER, M. P. 2010. Mode of action of RNase BN/RNase Z on tRNA precursors: RNase BN does not remove the CCA sequence from tRNA. *Journal of Biological Chemistry,* 285**,** 22874-22881.

DUTTA, T., MALHOTRA, A. & DEUTSCHER, M. P. 2012. Exoribonuclease and endoribonuclease activities of RNase BN/RNase Z both function *in vivo*. *Journal of Biological Chemistry,* 287**,** 35747-35755.

EHRETSMANN, C. P., CARPOUSIS, A. J. & KRISCH, H. M. 1992. Specificity of *Escherichia coli* endoribonuclease RNase E: *in vivo* and *in vitro* analysis of mutants in a bacteriophage T4 messenger RNA processing site. *Genes & Development,* 6**,** 149-159.

EMORY, S. A. & BELASCO, J. G. 1990. The *ompA* 5' untranslated RNA segment functions in *Escherichia coli* as a growth-rate-regulated messenger RNA stabilizer whose activity is related to translationa efficiency. *Journal of Bacteriology,* 172**,** 4472-4481.

EMORY, S. A., BOUVET, P. & BELASCO, J. G. 1992. A 5'-terminal stem-loop structure can stabilize messenger RNA in *Escherichia coli*. *Genes & Development,* 6**,** 135-148.

EVEN, S., PELLEGRINI, O., ZIG, L., LABAS, V., VINH, J., BRECHEMMIER-BAEY, D. & PUTZER, H. 2005. Ribonucleases J1 and J2: two novel endoribonucleases in *B. subtilis* with functional homology to *E. coli* RNase E. *Nucleic Acids Research,* 33**,** 2141-2152.

EZRATY, B., DAHLGREN, B. & DEUTSCHER, M. P. 2005. The RNase Z homologue encoded by Escherichia coli elaC gene is RNase BN. *Journal of Biological Chemistry,* 280**,** 16542-16545.

FABREGA, C., SHEN, V., SHUMAN, S. & LIMA, C. D. 2003. Structure of an mRNA capping enzyme bound to the phosphorylated carboxy-terminal domain of RNA polymerase II. *Molecular Cell,* 11**,** 1549-1561.

FARNHAM, P. J. & PLATT, T. 1981. Rho-independent termination: dyad symmetry in DNA causes RNA polymerase to pause during transcription in vitro. *Nucleic Acids Research,* 9**,** 563-577.

FENG, Y. & COHEN, S. N. 2000. Unpaired terminal nucleotides and 5' monophosphorylation govern 3' polyadenylation by *Escherichia coli* poly(A) polymerase I. *Proceedings of the National Academy of Sciences of the United States of America,* 97**,** 6415-6420.

FENG, Y. A., VICKERS, T. A. & COHEN, S. N. 2002. The catalytic domain of RNase E shows inherent 3' to 5' directionality in cleavage site selection. *Proceedings of the National Academy of Sciences of the United States of America,* 99**,** 14746-14751.

FORCONI, M. & HERSCHLAG, D. 2009. Metal ion-based RNA cleavage as a structural probe. *Methods in Enzymology,* 468**,** 91-106.

FORD, L. P., BAGGA, P. S. & WILUSZ, J. 1997. The poly(A) tail inhibits the assembly of a 3'-to-5' exonuclease in an *in vitro* RNA stability system. *Molecular &Cellular Biology,* 17**,** 398-406.

FRAZAO, C., MCVEY, C. E., AMBLAR, M., BARBAS, A., VONRHEIN, C., ARRAIANO, C. M. & CARRONDO, M. A. 2006. Unravelling the dynamics of RNA degradation by ribonuclease II and its RNA-bound complex. *Nature,* 443**,** 110-114.

FRENDEWEY, D., DINGERMANN, T., COOLEY, L. & SOLL, D. 1985. Processing of precursor tRNAs in Drosophila. Processing of the 3' end involves an endonucleolytic cleavage and occurs after 5' end maturation. *Journal of Biological Chemistry,* 260**,** 449-454.

GARNEAU, J. E., DUPUIS, M. E., VILLION, M., ROMERO, D. A., BARRANGOU, R., BOYAVAL, P., FREMAUX, C., HORVATH, P., MAGADAN, A. H. & MOINEAU, S. 2010. The CRISPR/Cas bacterial immune system cleaves bacteriophage and plasmid DNA. *Nature,* 468**,** 67-71.

GARREY, S. M., BLECH, M., RIFFELL, J. L., HANKINS, J. S., STICKNEY, L. M., DIVER, M., HSU, Y. H. R., KUNANITHY, V. & MACKIE, G. A. 2009. Substrate binding and active site residues in RNases E and G: role of the 5' sensor. *Journal of Biological Chemistry,* 284**,** 31843-31850.

GARREY, S. M. & MACKIE, G. A. 2011. Roles of the 5'-phosphate sensor domain in RNase E. *Molecular Microbiology,* 80**,** 1613-1624.

GEGENHEIMER, P., WATSON, N. & APIRION, D. 1977. Multiple pathways for primary processing of ribosomal RNA in *Escherichia coli*. *Journal of Biological Chemistry,* 252**,** 3064-3073.

GEHRING, K., LEROY, J. L. & GUERON, M. 1993. A tetrameric DNA structure with protonated cytosine.cytosine base pairs. *Nature,* 363**,** 561-565.

GEISSMANN, T. A. & TOUATI, D. 2004. Hfq, a new chaperoning role: binding to messenger RNA determines access for small RNA regulator. *EMBO Journal,* 23**,** 396-405.

GHORA, B. K. & APIRION, D. 1978. Structural analysis and *in vitro* processing to p5 ribosomal RNA of a 9S RNA molecule isolated from an *rne* mutant of *Escherichia coli*. *Cell,* 15**,** 1055-1066.

GHOSH, S. & DEUTSCHER, M. P. 1999. Oligoribonuclease is an essential component of the mRNA decay pathway. *Proceedings of the National Academy of Sciences of the United States of America,* 96**,** 4372-4377.

GO, H., MOORE, C. J., LEE, M., SHIN, E., JEON, C. O., CHA, C. J., HAN, S. H., KIM, S. J., LEE, S. W., LEE, Y., HA, N. C., KIM, Y. H., COHEN, S. N. & LEE, K. 2011. Upregulation of RNase E activity by mutation of a site that uncompetitively interferes with RNA binding. *RNA Biology,* 8**,** 1022-1034.

GOLDSTEIN, J., POLLITT, N. S. & INOUYE, M. 1990. Major cold shock protein of *Escherichia coli*. *Proceedings of the National Academy of Sciences of the United States of America,* 87**,** 283-287.

GORNA, M. W., CARPOUSIS, A. J. & LUISI, B. F. 2012. From conformational chaos to robust regulation: the structure and function of the multi-enzyme RNA degradosome. *Quarterly Reviews of Biophysics,* 45**,** 105-145.

GUARNEROS, G. & PORTIER, C. 1991. Different specificities of ribonuclease II and polynucleotide phosphorylase in 3'mRNA decay. *Biochimie,* 73**,** 543-549.

GUPTA, R. S., KASAI, T. & SCHLESSINGER, D. 1977. Purification and some novel properties of *Escherichia coli* RNase II. *Journal of Biological Chemistry,* 252**,** 8945-8949.

GUREVITZ, M., JAIN, S. K. & APIRION, D. 1983. Identification of a precursor molecular for the RNA moiety of the processing enzyme RNase P. *Proceedings of the National Academy of Sciences of the United States of America,* 80**,** 4450-4454.

HAJNSDORF, E., BRAUN, F., HAUGEL-NIELSEN, J. & REGNIER, P. 1995. Polyadenylylation destabilizes the *rpsO* mRNA of *Escherichia coli*. *Proceedings of the National Academy of Sciences of the United States of America,* 92**,** 3973-3977.

HAJNSDORF, E., CARPOUSIS, A. J. & REGNIER, P. 1994a. Nucleolytic inactivation and degradation of the RNase-III processed *pnp* message encoding polynucleotide phosphorylase of *Escherichia coli*. *Journal of Molecular Biology,* 239**,** 439-454.

HAJNSDORF, E. & REGNIER, P. 2009. Poly(A)-assisted RNA decay and modulators of RNA stability *In:* CONDON, C. (ed.) *Molecular Biology of Rna Processing and Decay in Prokaryotes.* San Diego: Academic Press, Elsevier Inc.

HAJNSDORF, E., STEIER, O., COSCOY, L., TEYSSET, L. & REGNIER, P. 1994b. Roles of RNase E, RNase II and PNPase in the degradation of the *rpsO* transcripts of *Escherichia coli*: Stabilizing function of RNase II and evidence for efficient degradation in an *ams-pnp-rnb* mutant. *EMBO Journal,* 13**,** 3368-3377.

HALE, C. R., ZHAO, P., OLSON, S., DUFF, M. O., GRAVELEY, B. R., WELLS, L., TERNS, R. M. & TERNS, M. P. 2009. RNA-guided RNA cleavage by a CRISPR RNA-Cas protein complex. *Cell,* 139**,** 945-956.

HAMMARLOF, D. L., BERGMAN, J. M., GARMENDIA, E. & HUGHES, D. 2015. Turnover of mRNAs is one of the essential functions of RNase E. *Molecular Microbiology,* 98**,** 34-45.

HAN, T. K., ZHU, Z. & DAO, M. L. 2004. Identification, molecular cloning, and sequence analysis of a deoxyribose aldolase in *Streptococcus mutans* GS-5. *Current Microbiology,* 48**,** 230-236.

HANKINS, J. S., ZAPPAVIGNA, C., PRUD'HOMME-GENEREUX, A. & MACKIE, G. A. 2007. Role of RNA structure and susceptibility to RNase E in regulation of a cold shock mRNA, *cspA* mRNA. *Journal of Bacteriology,* 189**,** 4353-4358.

HANSEN, T. B., JENSEN, T. I., CLAUSEN, B. H., BRAMSEN, J. B., FINSEN, B., DAMGAARD, C. K. & KJEMS, J. 2013. Natural RNA circles function as efficient microRNA sponges. *Nature,* 495**,** 384-8.

HARTMANN, R. K., GOSSRINGER, M., SPATH, B., FISCHER, S. & MARCHFELDER, A. 2009. The Making of tRNAs and More - RNase P and tRNase Z. *In:* CONDON, C. (ed.) *Molecular Biology of RNA Processing and Decay in Prokaryotes.* Academic Press.

HAURWITZ, R. E., JINEK, M., WIEDENHEFT, B., ZHOU, K. & DOUDNA, J. A. 2010. Sequence- and structure-specific RNA processing by a CRISPR endonuclease. *Science,* 329**,** 1355-1358.

HAYES, C. S. & SAUER, R. T. 2003. Cleavage of the A site mRNA codon during ribosome pausing provides a mechanism for translational quality control. *Molecular Cell,* 12**,** 903-911.

HAZAN, R. & ENGELBERG-KULKA, H. 2004. *Escherichia coli* mazEF-mediated cell death as a defense mechanism that inhibits the spread of phage P1. *Molecular Genetics Genomics,* 272**,** 227-234.

HENGGE-ARONIS, R. 2002. Signal transduction and regulatory mechanisms involved in control of the sigma(S) (RpoS) subunit of RNA polymerase. *Microbiology and Molecular Biology Reviews,* 66**,** 373-395.

HOFACKER, I. L. 2003. Vienna RNA secondary structure server. *Nucleic Acids Research,* 31**,** 3429-3431.

HUA, Q., YANG, C., OSHIMA, T., MORI, H. & SHIMIZU, K. 2004. Analysis of gene expression in Escherichia coli in response to changes of growth-limiting nutrient in chemostat cultures. *Applied Environmental Microbiology,* 70**,** 2354-2366.

HUANG, H. J., LIAO, J. & COHEN, S. N. 1998. Poly(A)- and poly(U)-specific RNA 3' tail shortening by *E coli* ribonuclease E. *Nature,* 391**,** 99-102.

HUGHES, R. M. & WATERS, M. L. 2006. Effects of lysine acetylation in a beta-hairpin peptide: comparison of an amide-pi and a cation-pi interaction. *Journal of the American Chemical Society,* 128**,** 13586-13591.

HULSEN, T., DE VLIEG, J. & ALKEMA, W. 2008. BioVenn - a web application for the comparison and visualization of biological lists using area-proportional Venn diagrams. *BMC Genomics,* 9**,** 488.

HUPPERTZ, I., ATTIG, J., D'AMBROGIO, A., EASTON, L. E., SIBLEY, C. R., SUGIMOTO, Y., TAJNIK, M., KONIG, J. & ULE, J. 2014. iCLIP: protein-RNA interactions at nucleotide resolution. *Methods,* 65**,** 274-287.

IOST, I. & DREYFUS, M. 1995. The stability of *Escherichia coli lacZ* messenger RNA depends upon the simultaneity of its synthesis and translation. *EMBO Journal,* 14**,** 3252-3261.

ITO, K., HAMASAKI, K., KAYAMORI, A., NGUYEN, P. A., AMAGAI, K. & WACHI, M. 2013. A secondary structure in the 5' untranslated region of *adhE* mRNA required for RNase G-dependent regulation. *Bioscience Biotechnology, and Biochemistry,* 77**,** 2473-2479.

IZAURRALDE, E., LEWIS, J., GAMBERI, C., JARMOLOWSKI, A., MCGUIGAN, C. & MATTAJ, I. W. 1995. A cap-binding protein complex mediating U snRNA export. *Nature,* 376**,** 709-712.

JAIN, C. & BELASCO, J. G. 1995. RNase E autoregulates its synthesis by controlling the degradation rate of its own messenger RNA in *Escherichia coli*: Unusual sensitivity of the *rne* transcript to RNase E activity. *Genes & Development,* 9**,** 84-96.

JARRIGE, A. C., MATHY, N. & PORTIER, C. 2001. PNPase autocontrols its expression by degrading a double-stranded structure in the *pnp* mRNA leader. *EMBO Journal,* 20**,** 6845-6855.

JEROME, L. J., VAN BIESEN, T. & FROST, L. S. 1999. Degradation of FinP antisense RNA from F-like plasmids: the RNA-binding protein, FinO, protects FinP from ribonuclease E. *Journal of Molecular Biology,* 285**,** 1457-1473.

JIANG, X. Q. & BELASCO, J. G. 2004. Catalytic activation of multimeric RNase E and RNase G by 5'-monophosphorylated RNA. *Proceedings of the National Academy of Sciences of the United States of America,* 101**,** 9211-9216.

JONES, B. N., QUANG-DANG, D. U., OKU, Y. & GROSS, J. D. 2008. A kinetic assay to monitor RNA decapping under single- turnover conditions. *Methods in Enzymology,* 448**,** 23-40.

JOURDAN, S. S., KIME, L. & MCDOWALL, K. J. 2010. The sequence of sites recognised by a member of the RNase E/G family can control the maximal rate of cleavage, while a 5'-monophosphorylated end appears to function cooperatively in mediating RNA binding. *Biochemical and Biophysical Research Communications,* 391**,** 879-883.

JOURDAN, S. S. & MCDOWALL, K. J. 2008. Sensing of 5' monophosphate by *Escherichia coli* RNase G can significantly enhance association with RNA and stimulate the decay of functional mRNA transcripts *in vivo*. *Molecular Microbiology,* 67**,** 102-115.

KABERDIN, V. R. 2003. Probing the substrate specificity of *Escherichia coli* RNase E using a novel oligonucleotide-based assay. *Nucleic Acids Research,* 31**,** 4710-4716.

KABERDIN, V. R., WALSH, A. P., JAKOBSEN, T., MCDOWALL, K. J. & VON GABAIN, A. 2000. Enhanced cleavage of RNA mediated by an interaction between substrates and the arginine-rich domain of *E. coli* ribonuclease E. *Journal of Molecular Biology,* 301**,** 257-264.

KAGA, N., UMITSUKI, G., NAGAI, K. & WACHI, M. 2002. RNase G-dependent degradation of the *eno* mRNA encoding a glycolysis enzyme enolase in *Escherichia coli*. *Bioscience Biotechnology, and Biochemistry,* 66**,** 2216-2220.

KEILER, K. C. 2008. Biology of trans-Translation. *Annual Review of Microbiology,* 62**,** 133-151.

KELLY, K. O. & DEUTSCHER, M. P. 1992. The presence of only one of five exoribonucleases is sufficient to support the growth of *Escherichia coli*. *Journal of Bacteriology,* 174**,** 6682-6684.

KELLY, K. O., REUVEN, N. B., LI, Z. & DEUTSCHER, M. P. 1992. RNase PH is essential for tRNA processing and viability in RNase-deficient Escherichia coli cells. *Journal of Biological Chemistry,* 267**,** 16015-16018.

KESELER, I. M., MACKIE, A., PERALTA-GIL, M., SANTOS-ZAVALETA, A., GAMA-CASTRO, S., BONAVIDES-MARTINEZ, C., FULCHER, C., HUERTA, A. M., KOTHARI, A., KRUMMENACKER, M., LATENDRESSE, M., MUNIZ-RASCADO, L., ONG, Q., PALEY, S., SCHRODER, I., SHEARER, A. G., SUBHRAVETI, P., TRAVERS, M., WEERASINGHE, D., WEISS, V., COLLADO-VIDES, J., GUNSALUS, R. P., PAULSEN, I. & KARP, P. D. 2013. EcoCyc: fusing model organism databases with systems biology. *Nucleic Acids Research,* 41**,** D605-D612.

KHEMICI, V. & CARPOUSIS, A. J. 2004. The RNA degradosome and poly(A) polymerase of *Escherichia coli* are required *in vivo* for the degradation of small mRNA decay intermediates containing REP-stabilizers. *Molecular Microbiology,* 51**,** 777-790.

KHEMICI, V., POLJAK, L., LUISI, B. F. & CARPOUSIS, A. J. 2008. The RNase E of *Escherichia coli* is a membrane-binding protein. *Molecular Microbiology,* 70**,** 799-813.

KHEMICI, V., POLJAK, L., TOESCA, I. & CARPOUSIS, A. J. 2005. Evidence *in vivo* that the DEAD-box RNA helicase RhlB facilitates the degradation of ribosome-free mRNA by RNase E. *Proceedings of the National Academy of Sciences of the United States of America,* 102**,** 6913-6918.

KHEMICI, V., TOESCA, I., POLJAK, L., VANZO, N. F. & CARPOUSIS, A. J. 2004. The RNase E of *Escherichia coli* has at least two binding sites for DEAD-box RNA helicases: functional replacement of RhlB by RhlE. *Molecular Microbiology,* 54**,** 1422-1430.

KIDO, M., YAMANAKA, K., MITANI, T., NIKI, H., OGURA, T. & HIRAGA, S. 1996. RNase E polypeptides lacking a carboxyl-terminal half suppress a *mukB* mutation in *Escherichia coli*. *Journal of Bacteriology,* 178**,** 3917-3925.

KIM, D., SONG, S., LEE, M., GO, H., SHIN, E., YEOM, J. H., HA, N. C., LEE, K. & KIM, Y. H. 2014. Modulation of RNase E activity by alternative RNA binding sites. *PLoS One,* 9**,** e90610.

KIM, K. S. & LEE, Y. 2004. Regulation of 6S RNA biogenesis by switching utilization of both sigma factors and endoribonucleases. *Nucleic Acids Research,* 32**,** 6057-6068.

KIM, S., SIM, S. & LEE, Y. 1999. *In vitro* analysis of processing at the 3' end of precursors of M1 RNA, the catalytic subunit of *Escherichia coli* RNase P: multiple pathways and steps for the processing. *Nucleic Acids Research,* 27**,** 895-902.

KIME, L., CLARKE, J. E., ROMERO, A. D., GRASBY, J. A. & MCDOWALL, K. J. 2014. Adjacent single-stranded regions mediate processing of tRNA precursors by RNase E direct entry. *Nucleic Acids Research,* 42**,** 4577-4589.

KIME, L., JOURDAN, S. S. & MCDOWALL, K. J. 2008. Identifying and characterizing substrates of the RNase E/G family of enzymes. *In:* MAQUAT, L. E. & ARRAIANO, C. M. (eds.) *Methods in Enzymology: RNA Turnover in Bacteria, Archaea and Organelles.* Academic Press.

KIME, L., JOURDAN, S. S., STEAD, J. A., HIDALGO-SASTRE, A. & MCDOWALL, K. J. 2010. Rapid cleavage of RNA by RNase E in the absence of 5'-monophosphate stimulation. *Molecular Microbiology,* 76**,** 590-604.

KIME, L., VINCENT, H. A., GENDOO, D. M., JOURDAN, S. S., FISHWICK, C. W., CALLAGHAN, A. J. & MCDOWALL, K. J. 2015. The first small-molecule inhibitors of members of the ribonuclease E family. *Scientific Reports,* 5**,** 8028.

KING, T. C., SIRDESHMUKH, R. & SCHLESSINGER, D. 1984. RNase III cleavage is obligate for maturation but not for function of *Escherichia coli* pre-23S rRNA. *Proceedings of the National Academy of Sciences of the United States of America,* 81**,** 185-188.

KIRBY, A. J. Y., M. 1970. The reactivity of phosphate esters. Diester hydrolysis. *Journal of the Chemical. Society B***,** 510-513.

KIVITY-VOGEL, T. & ELSON, D. 1967. On the metabolic inactivation of messenger RNA in *Escherichia coli*: ribonuclease I and polynucleotide phosphorylase. *Biochimica et Biophysica Acta,* 138**,** 66-75.

KOLODKIN-GAL, I. & ENGELBERG-KULKA, H. 2006. Induction of *Escherichia coli* chromosomal mazEF by stressful conditions causes an irreversible loss of viability. *Journal of Bacteriology,* 188**,** 3420-3423.

KOLODKIN-GAL, I., HAZAN, R., GAATHON, A., CARMELI, S. & ENGELBERG-KULKA, H. 2007. A linear pentapeptide is a quorum-sensing factor required for mazEF-mediated cell death in *Escherichia coli*. *Science,* 318**,** 652-655.

KOSLOVER, D. J., CALLAGHAN, A. J., MARCAIDA, M. J., GARMAN, E. F., MARTICK, M., SCOTT, W. G. & LUISI, B. F. 2008. The crystal structure of the *Escherichia coli* RNase E apoprotein and a mechanism for RNA degradation. *Structure,* 16**,** 1238-1244.

KUWANO, M., ONO, M., ENDO, H., HORI, K., NAKAMURA, K., HIROTA, Y. & OHNISHI, Y. 1977. Gene affecting longevity of messenger RNA: Mutant of *Escherichia coli* with altered messenger RNA stability. *Molecular & General Genetics,* 154**,** 279-285.

KWOK, C. K., TANG, Y., ASSMANN, S. M. & BEVILACQUA, P. C. 2015. The RNA structurome: transcriptome-wide structure probing with next-generation sequencing. *Trends in Biochemical Science,* 40**,** 221-232.

LAALAMI, S., BESSIERES, P., ROCCA, A., ZIG, L., NICOLAS, P. & PUTZER, H. 2013. *Bacillus subtilis* RNase Y activity *in vivo* analysed by tiling microarrays. *PLoS One,* 8**,** e54062.

LACAVA, J., HOUSELEY, J., SAVEANU, C., PETFALSKI, E., THOMPSON, E., JACQUIER, A. & TOLLERVEY, D. 2005. RNA degradation by the exosome is promoted by a nuclear polyadenylation complex. *Cell,* 121**,** 713-724.

LAMPHEAR, B. J., KIRCHWEGER, R., SKERN, T. & RHOADS, R. E. 1995. Mapping of functional domains in eukaryotic protein synthesis initiation factor 4G (eIF4G) with picornaviral proteases. Implications for cap-dependent and cap-independent translational initiation. *Journal of Biological Chemistry,* 270**,** 21975-21983.

LASSERRE, J. P., BEYNE, E., PYNDIAH, S., LAPAILLERIE, D., CLAVEROL, S. & BONNEU, M. 2006. A complexomic study of *Escherichia coli* using two-dimensional blue native/SDS polyacrylamide gel electrophoresis. *Electrophoresis,* 27**,** 3306-3321.

LEASE, R. A. & BELFORT, M. 2000. A trans-acting RNA as a control switch in *Escherichia coli*: DsrA modulates function by forming alternative structures. *Proceedings of the National Academy of Sciences of the United States of America,* 97**,** 9919-9924.

LEASE, R. A., CUSICK, M. E. & BELFORT, M. 1998. Riboregulation in *Escherichia coli*: DsrA RNA acts by RNA:RNA interactions at multiple loci. *Proceedings of the National Academy of Sciences of the United States of America,* 95**,** 12456-12461.

LEASE, R. A. & WOODSON, S. A. 2004. Cycling of the Sm-like protein Hfq on the DsrA small regulatory RNA. *Journal of Molecular Biology,* 344**,** 1211-1223.

LEE, K., BERNSTEIN, J. A. & COHEN, S. N. 2002. RNase G complementation of *rne* null mutation identifies functional interrelationships with RNase E in *Escherichia coli*. *Molecular Microbiology,* 43**,** 1445-1456.

LEE, S. Y., BAILEY, S. C. & APIRION, D. 1978. Small stable RNAs from *Escherichia coli*: evidence for existence of new molecules and for a new ribonucleoprotein particle containing 6S RNA. *Journal of Bacteriology,* 133**,** 1015-1023.

LEHNIK-HABRINK, M., NEWMAN, J., ROTHE, F. M., SOLOVYOVA, A. S., RODRIGUES, C., HERZBERG, C., COMMICHAU, F. M., LEWIS, R. J. & STULKE, J. 2011. RNase Y in *Bacillus subtilis*: a Natively disordered protein that is the functional equivalent of RNase E from *Escherichia coli*. *Journal of Bacteriology,* 193**,** 5431-5441.

LEHNIK-HABRINK, M., PFORTNER, H., REMPETERS, L., PIETACK, N., HERZBERG, C. & STULKE, J. 2010. The RNA degradosome in *Bacillus subtilis*: identification of CshA as the major RNA helicase in the multiprotein complex. *Molecular Microbiology,* 77**,** 958-971.

LEROY, A., VANZO, N. F., SOUSA, S., DREYFUS, M. & CARPOUSIS, A. J. 2002. Function in *Escherichia coli* of the non-catalytic part of RNase E: role in the degradation of ribosome-free mRNA. *Molecular Microbiology,* 45**,** 1231-1243.

LI, Y., COLE, K. & ALTMAN, S. 2003. The effect of a single, temperature-sensitive mutation on global gene expression in Escherichia coli. *RNA-a Publication of the RNA Society,* 9**,** 518-532.

LI, Z. & DEUTSCHER, M. P. 1996. Maturation pathways for *E. coli* tRNA precursors: a random multienzyme process *in vivo*. *Cell,* 86**,** 503-512.

LI, Z., GONG, X., JOSHI, V. H. & LI, M. 2005. Co-evolution of tRNA 3'- trailer sequences with 3'-processing enzymes in bacteria. *RNA-a Publication of the RNA Society,* 11**,** 567-577.

LI, Z., PANDIT, S. & DEUTSCHER, M. P. 1999a. The CafA protein (RNase G) together with RNase E is required for the maturation of 16S rRNA in *Escherichia coli*. *FASEB Journal,* 13**,** A1410-A1410.

LI, Z., PANDIT, S. & DEUTSCHER, M. P. 1999b. Maturation of 23S ribosomal RNA requires the exoribonuclease RNase T. *RNA-a Publication of the RNA Society,* 5**,** 139-146.

LI, Z. W. & DEUTSCHER, M. P. 1995. The transfer RNA processing enzyme RNase T is essential for maturation of 5S RNA. *Proceedings of the National Academy of Sciences of the United States of America,* 92**,** 6883-6886.

LI, Z. W. & DEUTSCHER, M. P. 2002. RNase E plays an essential role in the maturation of *Escherichia coli* tRNA precursors. *RNA-a Publication of the RNA Society,* 8**,** 97-109.

LI, Z. W., PANDIT, S. & DEUTSCHER, M. P. 1998a. 3 ' exoribonucleolytic trimming is a common feature of the maturation of small, stable RNAs in *Escherichia coli*. *Proceedings of the National Academy of Sciences of the United States of America,* 95**,** 2856-2861.

LI, Z. W., PANDIT, S. & DEUTSCHER, M. P. 1998b. Polyadenylation of stable RNA precursors *in vivo*. *Proceedings of the National Academy of Sciences of the United States of America,* 95**,** 12158-12162.

LI, Z. W., PANDIT, S. & DEUTSCHER, M. P. 1999c. RNase G (CafA protein) and RNase E are both required for the 5 ' maturation of 16S ribosomal RNA. *EMBO Journal,* 18**,** 2878-2885.

LI, Z. W., REIMERS, S., PANDIT, S. & DEUTSCHER, M. P. 2002. RNA quality control: Degradation of defective transfer RNA. *EMBO Journal,* 21**,** 1132-1138.

LIAO, S. M., DU, Q. S., MENG, J. Z., PANG, Z. W. & HUANG, R. B. 2013. The multiple roles of histidine in protein interactions. *Chemistry Central Journal,* 7**,** 44.

LIN-CHAO, S. & COHEN, S. N. 1991. The rate of processing and degradation of antisense RNAI regulates the replication of ColE1-type plasmids *in vivo*. *Cell,* 65**,** 1233-1242.

LIN-CHAO, S., WEI, C. L. & LIN, Y. T. 1999. RNase E is required for the maturation of *ssrA* RNA and normal *ssrA* RNA peptide-tagging activity. *Proceedings of the National Academy of Sciences of the United States of America,* 96**,** 12406-12411.

LIN-CHAO, S., WONG, T. T., MCDOWALL, K. J. & COHEN, S. N. 1994. Effects of nucleotide sequence on the specificity of *rne*-dependent and RNase E-mediated cleavages of RNAI encoded by the pBR322 plasmid. *Journal of Biological Chemistry,* 269**,** 10797-10803.

LIN, Y. F., A, D. R., GUAN, S., MAMANOVA, L. & MCDOWALL, K. J. 2013. A combination of improved differential and global RNA-seq reveals pervasive transcription initiation and events in all stages of the life-cycle of functional RNAs in *Propionibacterium acnes*, a major contributor to wide-spread human disease. *BMC Genomics,* 14**,** 620.

LIOLIOU, E., SHARMA, C. M., CALDELARI, I., HELFER, A. C., FECHTER, P., VANDENESCH, F., VOGEL, J. & ROMBY, P. 2012. Global regulatory functions of the *Staphylococcus aureus* endoribonuclease III in gene expression. *PLoS Genetics,* 8**,** e1002782.

LIOU, G. G., CHANG, H. Y., LIN, C. S. & LIN-CHAO, S. 2002. DEAD box RhlB RNA helicase physically associates with exoribonuclease PNPase to degrade double-stranded RNA independent of the degradosome-assembling region of RNase E. *Journal of Biological Chemistry,* 277**,** 41157-41162.

LIOU, G. G., JANE, W. N., COHEN, S. N., LIN, N. S. & LIN-CHAO, S. 2001. RNA degradosomes exist *in vivo* in *Escherichia coli* as multicomponent complexes associated with the cytoplasmic membrane via the N-terminal region of ribonuclease E. *Proceedings of the National Academy of Sciences of the United States of America,* 98**,** 63-68.

LOPEZ, P. J., MARCHAND, I., JOYCE, S. A. & DREYFUS, M. 1999. The C-terminal half of RNase E, which organizes the *Escherichia coli* degradosome, participates in mRNA degradation but not rRNA processing *in vivo*. *Molecular Microbiology,* 33**,** 188-199.

LU, F. & TAGHBALOUT, A. 2013. Membrane association via an amino-terminal amphipathic helix is required for the cellular organization and function of RNase II. *Journal of Biological Chemistry,* 288**,** 7241-7251.

LU, M., GUO, Q. & KALLENBACH, N. R. 1992. Structure and stability of sodium and potassium complexes of $dT_4G_4$ and $dT_4G_4T$. *Biochemistry,* 31**,** 2455-2459.

LUCIANO, D. J., HUI, M. P., DEANA, A., FOLEY, P. L., BELASCO, K. J. & BELASCO, J. G. 2012. Differential control of the rate of 5' end-dependent mRNA degradation in *Escherichia coli*. *Journal of Bacteriology,* 194**,** 6233-6239.

MACKIE, G. A. 1991. Specific endonucleolytic cleavage of the messenger RNA for ribosomal protein S20 of *Escherichia coli* requires the product of the *ams* gene *in vivo* and *in vitro*. *Journal of Bacteriology,* 173**,** 2488-2497.

MACKIE, G. A. 1992. Secondary structure of the messenger RNA for ribosomal protein S20: Implications for cleavage by ribonuclease E. *Journal of Biological Chemistry,* 267**,** 1054-1061.

MACKIE, G. A. 1998. Ribonuclease E is a 5'-end-dependent endonuclease. *Nature,* 395**,** 720-723.

MACKIE, G. A. 2000. Stabilization of circular *rpsT* mRNA demonstrates the 5'-end dependence of RNase E action *in vivo*. *Journal of Biological Chemistry,* 275**,** 25069-25072.

MACKIE, G. A. 2013a. Determinants in the *rpsT* mRNAs recognized by the 5'-sensor domain of RNase E. *Molecular Microbiology,* 89**,** 388-402.

MACKIE, G. A. 2013b. RNase E: at the interface of bacterial RNA processing and decay. *Nature Reviews Microbiology,* 11**,** 45-57.

MACKIE, G. A. & GENEREAUX, J. L. 1993. The role of RNA structure in determining RNase E-dependent cleavage sites in the messenger RNA for ribosomal protein S20 *in vitro*. *Journal of Molecular Biology,* 234**,** 998-1012.

MACKIE, G. A., GENEREAUX, J. L. & MASTERMAN, S. K. 1997. Modulation of the activity of RNase E *in vitro* by RNA sequences and secondary structures 5' to cleavage sites. *Journal of Biological Chemistry,* 272**,** 609-616.

MAJDALANI, N., CUNNING, C., SLEDJESKI, D., ELLIOTT, T. & GOTTESMAN, S. 1998. DsrA RNA regulates translation of RpoS message by an anti-antisense mechanism, independent of its action as an antisilencer of transcription. *Proceedings of the National Academy of Sciences of the United States of America,* 95**,** 12462-12467.

MAKAROVA, K. S., GRISHIN, N. V., SHABALINA, S. A., WOLF, Y. I. & KOONIN, E. V. 2006. A putative RNA-interference-based immune system in prokaryotes: computational analysis of the predicted enzymatic machinery, functional analogies with eukaryotic RNAi, and hypothetical mechanisms of action. *Biology Direct,* 1**,** 7.

MAKEYEV, A. V., EASTMOND, D. L. & LIEBHABER, S. A. 2002. Targeting a KH-domain protein with RNA decoys. *RNA-a Publication of the RNA Society,* 8**,** 1160-1173.

MALEKNIA, S. D. & DOWNARD, K. M. 2014. Advances in radical probe mass spectrometry for protein footprinting in chemical biology applications. *Chemical Society Reviews,* 43**,** 3244-3258.

MAMANOVA, L., ANDREWS, R. M., JAMES, K. D., SHERIDAN, E. M., ELLIS, P. D., LANGFORD, C. F., OST, T. W. B., COLLINS, J. E. & TURNER, D. J. 2010. FRT-seq: amplification-free, strand-specific transcriptome sequencing. *Nature Methods,* 7**,** 130-U63.

MANASHEROB, R., MILLER, C., KIM, K. S. & COHEN, S. N. 2012. Ribonuclease E modulation of the bacterial SOS response. *PLoS One,* 7**,** e38426.

MARCAIDA, M. J., DEPRISTO, M. A., CHANDRAN, V., CARPOUSIS, A. J. & LUISI, B. F. 2006. The RNA degradosome: Life in the fast lane of adaptive molecular evolution. *Trends in Biochemical Sciences,* 31**,** 359-365.

MARCK, C. & GROSJEAN, H. 2002. tRNomics: analysis of tRNA genes from 50 genomes of Eukarya, Archaea, and Bacteria reveals anticodon-sparing strategies and domain-specific features. *RNA-a Publication of the RNA Society,* 8**,** 1189-1232.

MARCOTRIGIANO, J., GINGRAS, A. C., SONENBERG, N. & BURLEY, S. K. 1997a. Cocrystal structure of the messenger RNA 5' cap-binding protein (eIF4E) bound to 7-methyl-GDP. *Cell,* 89**,** 951-961.

MARCOTRIGIANO, J., GINGRAS, A. C., SONENBERG, N. & BURLEY, S. K. 1997b. X-ray studies of the messenger RNA 5' cap-binding protein (eIF4E) bound to 7-methyl-GDP. *Nucleic Acids Symposium Series***,** 8-11.

MARIANOVSKY, I., AIZENMAN, E., ENGELBERG-KULKA, H. & GLASER, G. 2001. The regulation of the *Escherichia coli* mazEF promoter involves an unusual alternating palindrome. *Journal of Biology Chemistry,* 276**,** 5975-5984.

MARTIN, S. A., PAOLETTI, E. & MOSS, B. 1975. Purification of mRNA guanylyltransferase and mRNA (guanine-7-) methyltransferase from vaccinia virions. *Journal of Biological Chemistry,* 250**,** 9322-9329.

MARUJO, P. E., HAJNSDORF, E., LE DEROUT, J., ANDRADE, R., ARRAIANO, C. M. & REGNIER, P. 2000. RNase II removes the oligo(A) tails that destabilize the *rpsO* mRNA of *Escherichia coli*. *RNA-a Publication of the RNA Society,* 6**,** 1185-1193.

MARZI, S. & ROMBY, P. 2012. RNA mimicry, a decoy for regulatory proteins. *Molecular Microbiology,* 83**,** 1-6.

MASSE, E., ESCORCIA, F. E. & GOTTESMAN, S. 2003. Coupled degradation of a small regulatory RNA and its mRNA targets in *Escherichia coli*. *Genes & Development,* 17**,** 2374-2383.

MASSE, E. & GOTTESMAN, S. 2002. A small RNA regulates the expression of genes involved in iron metabolism in *Escherichia coli*. *Proceedings of the National Academy of Sciences of the United States of America,* 99**,** 4620-4625.

MATHY, N., BENARD, L., PELLEGRINI, O., DAOU, R., WEN, T. Y. & CONDON, C. 2007. 5'-to-3' exoribonuclease activity in bacteria: Role of RNase J1 in rRNA maturation and 5 ' stability of mRNA. *Cell,* 129**,** 681-692.

MATHY, N., HEBERT, A., MERVELET, P., BENARD, L., DORLEANS, A., LI DE LA SIERRA-GALLAY, I., NOIROT, P., PUTZER, H. & CONDON, C. 2010. *Bacillus subtilis* ribonucleases J1 and J2 form a complex with altered enzyme behaviour. *Molecular Microbiology,* 75**,** 489-498.

MATOS, R. G., BARBAS, A. & ARRAIANO, C. M. 2009. RNase R mutants elucidate the catalysis of structured RNA: RNA-binding domains select the RNAs targeted for degradation. *Biochemical Journal,* 423**,** 291-301.

MATOS, R. G., BARBAS, A., GOMEZ-PUERTAS, P. & ARRAIANO, C. M. 2011. Swapping the domains of exoribonucleases RNase II and RNase R: conferring upon RNase II the ability to degrade ds RNA. *Proteins,* 79**,** 1853-1867.

MCDOWALL, K. J. & COHEN, S. N. 1996. The N-terminal domain of the *rne* gene product has RNase E activity and is non-overlapping with the arginine-rich RNA-binding site. *Journal of Molecular Biology,* 255**,** 349-355.

MCDOWALL, K. J., HERNANDEZ, R. G., LIN-CHAO, S. & COHEN, S. N. 1993. The *ams-1* and *rne-3071* temperature-sensitive mutations in the *ams* gene are in close proximity to each other and cause substitutions within a domain that resembles a product of the *Escherichia coli mre* locus. *Journal of Bacteriology,* 175**,** 4245-4249.

MCDOWALL, K. J., KABERDIN, V. R., WU, S. W., COHEN, S. N. & LIN-CHAO, S. 1995. Site-specific RNase E cleavage of oligonucleotides and inhibition by stem-loops. *Nature,* 374**,** 287-290.

MCDOWALL, K. J., LIN-CHAO, S. & COHEN, S. N. 1994. A+U content rather than a particular nucleotide order determines the specificity of RNase E cleavage. *Journal of Biological Chemistry,* 269**,** 10790-10796.

MCLAREN, R. S., NEWBURY, S. F., DANCE, G. S. C., CAUSTON, H. C. & HIGGINS, C. F. 1991. Messenger RNA degradation by processive 3'-5' exoribonucleases *in vitro* and the implications for prokaryotic messenger RNA decay *in vivo*. *Journal of Molecular Biology,* 221**,** 81-95.

MCSWIGGEN, J. A. & CECH, T. R. 1989. Stereochemistry of RNA cleavage by the Tetrahymena ribozyme and evidence that the chemical step is not rate-limiting. *Science,* 244**,** 679-683.

MELEFORS, O. & VON GABAIN, A. 1991. Genetic studies of cleavage initiated messenger RNA decay and processing of ribosomal 9S RNA show that the *Escherichia coli ams* and *rne* loci are the same. *Molecular Microbiology,* 5**,** 857-864.

MERGNY, J. L., DE CIAN, A., GHELAB, A., SACCA, B. & LACROIX, L. 2005. Kinetics of tetramolecular quadruplexes. *Nucleic Acids Research,* 33**,** 81-94.

MICZAK, A., KABERDIN, V. R., WEI, C. L. & LIN-CHAO, S. 1996. Proteins associated with RNase E in a multicomponent ribonucleolytic complex. *Proceedings of the National Academy of Sciences of the United States of America,* 93**,** 3865-3869.

MICZAK, A., SRIVASTAVA, R. A. K. & APIRION, D. 1991. Location of the RNA processing enzymes RNase III, RNase E and RNase P in the *Escherichia coli* cell. *Molecular Microbiology,* 5**,** 1801-1810.

MILLER, O. L., JR., HAMKALO, B. A. & THOMAS, C. A., JR. 1970. Visualization of bacterial genes in action. *Science,* 169**,** 392-395.

MILNER-WHITE, E. J., PIETRAS, Z. & LUISI, B. F. 2010. An ancient anion-binding structural module in RNA and DNA helicases. *Proteins,* 78**,** 1900-1908.

MISRA, T. K. & APIRION, D. 1979. RNase E, an RNA processing enzyme from *Escherichia coli*. *Journal of Biological Chemistry,* 254**,** 1154-1159.

MITCHELL, P., PETFALSKI, E., SHEVCHENKO, A., MANN, M. & TOLLERVEY, D. 1997. The exosome: a conserved eukaryotic RNA processing complex containing multiple 3'-->5' exoribonucleases. *Cell,* 91**,** 457-466.

MOHANTY, B. K. & KUSHNER, S. R. 1999. Analysis of the function of *Escherichia coli* poly(A) polymerase I in RNA metabolism. *Molecular Microbiology,* 34**,** 1094-1108.

MOHANTY, B. K. & KUSHNER, S. R. 2000. Polynucleotide phosphorylase functions both as a 3 '-> 5 ' exonuclease and a poly(A) polymerase in *Escherichia coli*. *Proceedings of the National Academy of Sciences of the United States of America,* 97**,** 11966-11971.

MOHANTY, B. K. & KUSHNER, S. R. 2002. Polyadenylation of *Escherichia coli* transcripts plays an integral role in regulating intracellular levels of polynucleotide phosphorylase and RNase E. *Molecular Microbiology,* 45**,** 1315-1324.

MOHANTY, B. K. & KUSHNER, S. R. 2003. Genomic analysis in *Escherichia coli* demonstrates differential roles for polynucleotide phosphorylase and RNase II in mRNA abundance and decay. *Molecular Microbiology,* 50**,** 645-658.

MOHANTY, B. K. & KUSHNER, S. R. 2006. The majority of *Escherichia coli* mRNAs undergo post-transcriptional modification in exponentially growing cells. *Nucleic Acids Research,* 34**,** 5695-5704.

MOLL, I., AFONYUSHKIN, T., VYTVYTSKA, O., KABERDIN, V. R. & BLASI, U. 2003. Coincident Hfq binding and RNase E cleavage sites on mRNA and small regulatory RNAs. *RNA-a Publication of the RNA Society,* 9**,** 1308-1314.

MOORE, S. D. & SAUER, R. T. 2007. The tmRNA system for translational surveillance and ribosome rescue. *Annual Review of Biochemistry,* 76**,** 101-124.

MORITA, T., KAWAMOTO, H., MIZOTA, T., INADA, T. & AIBA, H. 2004. Enolase in the RNA degradosome plays a crucial role in the rapid decay of glucose transporter mRNA in the response to phosphosugar stress in *Escherichia coli*. *Molecular Microbiology,* 54**,** 1063-1075.

MORITA, T., MAKI, K. & AIBA, H. 2005. RNase E-based ribonucleoprotein complexes: mechanical basis of mRNA destabilization mediated by bacterial noncoding RNAs. *Genes & Development,* 19**,** 2176-2186.

MORITA, T., MOCHIZUKI, Y. & AIBA, H. 2006. Translational repression is sufficient for gene silencing by bacterial small noncoding RNAs in the absence of mRNA destruction. *Proceedings of the National Academy of Sciences of the United States of America,* 103**,** 4858-4863.

MOTT, J. E., GALLOWAY, J. L. & PLATT, T. 1985. Maturation of *Escherichia coli* tryptophan operon mRNA: evidence for 3'-exonucleolytic processing after rho-dependent termination. *EMBO Journal,* 4**,** 1887-1891.

MUDD, E. A., KRISCH, H. M. & HIGGINS, C. F. 1990. RNase E, an endoribonuclease, has a general role in the chemical decay of *Escherichia coli* messenger RNA: Evidence that *rne* and *ams* are the same genetic locus. *Molecular Microbiology,* 4**,** 2127-2135.

MUHLRAD, D., DECKER, C. J. & PARKER, R. 1994. Deadenylation of the unstable mRNA encoded by the yeast MFA2 gene leads to decapping followed by 5'-->3' digestion of the transcript. *Genes &Development,* 8**,** 855-866.

MURASHKO, O. N., KABERDIN, V. R. & LIN-CHAO, S. 2012. Membrane binding of *Escherichia coli* RNase E catalytic domain stabilizes protein structure and increases RNA substrate affinity. *Proceedings of the National Academy of Sciences of the United States of America,* 109**,** 7019-7024.

NAKATA, A., AMEMURA, M. & MAKINO, K. 1989. Unusual nucleotide arrangement with repeated sequences in the *Escherichia coli* K-12 chromosome. *Journal of Bacteriology,* 171**,** 3553-3556.

NEU, H. C. & HEPPEL, L. A. 1964. Some observations on the "latent" ribonuclease of *Escherichia coli*. *Proceedings of the National Academy of Sciences of the United States of America,* 51**,** 1267-1274.

NEWBURY, S. F., SMITH, N. H., ROBINSON, E. C., HILES, I. D. & HIGGINS, C. F. 1987. Stabilization of translationally active messenger RNA by prokaryotic REP sequences. *Cell,* 48**,** 297-310.

NICHOLSON, A. W. 1999. Function, mechanism and regulation of bacterial ribonucleases. *FEMS Microbiology Reviews,* 23**,** 371-390.

NURMOHAMED, S., MCKAY, A. R., ROBINSON, C. V. & LUISI, B. F. 2010. Molecular recognition between *Escherichia coli* enolase and ribonuclease E. *Acta Crystallographica Section D-Biological Crystallography,* 66**,** 1036-1040.

NURMOHAMED, S., VAIDIALINGAM, B., CALLAGHAN, A. J. & LUISI, B. F. 2009. Crystal Structure of *Escherichia coli* Polynucleotide Phosphorylase Core Bound to RNase E, RNA and Manganese: Implications for Catalytic Mechanism and RNA Degradosome Assembly. *Journal of Molecular Biology,* 389**,** 17-33.

NURMOHAMED, S., VINCENT, H. A., TITMAN, C. M., CHANDRAN, V., PEARS, M. R., DU, D., GRIFFIN, J. L., CALLAGHAN, A. J. & LUISI, B. F. 2011. Polynucleotide phosphorylase activity may be modulated by metabolites in *Escherichia coli*. *Journal of Biological Chemistry,* 286**,** 14315-14323.

O'HARA, E. B., CHEKANOVA, J. A., INGLE, C. A., KUSHNER, Z. R., PETERS, E. & KUSHNER, S. R. 1995. Polyadenylylation helps regulate messenge RNA decay in *Escherichia coli*. *Proceedings of the National Academy of Sciences of the United States of America,* 92**,** 1807-1811.

OKADA, Y., WACHI, M., HIRATA, A., SUZUKI, K., NAGAI, K. & MATSUHASHI, M. 1994. Cytoplasmic axial filaments in *Escherichia coli* cells: possible function in the mechanism of chromosome segregation and cell division. *Journal of Bacteriology,* 176**,** 917-922.

ONO, M. & KUWANO, M. 1979. Conditional lethal mutation in an *Escherichia coli* strain with a longer chemical lifetime of messenger RNA. *Journal of Molecular Biology,* 129**,** 343-357.

OST, K. A. & DEUTSCHER, M. P. 1990. RNase PH catalyzes a synthetic reaction, the addition of nucleotides to the 3' end of RNA. *Biochimie,* 72**,** 813-818.

OW, M. C. & KUSHNER, S. R. 2002. Initiation of tRNA maturation by RNase E is essential for cell viability in *E. coli*. *Genes & Development,* 16**,** 1102-1115.

OW, M. C., LIU, Q. & KUSHNER, S. R. 2000. Analysis of mRNA decay and rRNA processing in *Escherichia coli* in the absence of RNase E-based degradosome assembly. *Molecular Microbiology,* 38**,** 854-866.

OW, M. C., PERWEZ, T. & KUSHNER, S. R. 2003. RNase G of *Escherichia coli* exhibits only limited functional overlap with its essential homologue, RNase E. *Molecular Microbiology,* 49**,** 607-622.

PARKINSON, G. N. 2006. Fundamentals of quadruplex structures. *In:* S, N. & S, B. (eds.) *Quadruplex Nucleic Acids.* Cambridge: Royal Society of Chemistry.

PATEL, A. M. & DUNN, S. D. 1992. RNase E-dependent cleavages in the 5' and 3' regions of the *Escherichia coli unc* messenger RNA. *Journal of Bacteriology,* 174**,** 3541-3548.

PATEL, A. M. & DUNN, S. D. 1995. Degradation of *Escherichia coli uncB* messenger RNA by multiple endonucleolytic cleavages. *Journal of Bacteriology,* 177**,** 3917-3922.

PELLEGRINI, O., NEZZAR, J., MARCHFELDER, A., PUTZER, H. & CONDON, C. 2003. Endonucleolytic processing of CCA-less tRNA precursors by RNase Z in *Bacillus subtilis*. *EMBO Journal,* 22**,** 4534-4543.

PERWEZ, T., HAMI, D., MAPLES, V. F., MIN, Z., WANG, B. C. & KUSHNER, S. R. 2008. Intragenic suppressors of temperature-sensitive *rne* mutations lead to the dissociation of RNase E activity on mRNA and tRNA substrates in *Escherichia coli*. *Nucleic Acids Research,* 36**,** 5306-5318.

PFLEGER, B. F., PITERA, D. J., D SMOLKE, C. & KEASLING, J. D. 2006. Combinatorial engineering of intergenic regions in operons tunes expression of multiple genes. *Nature Biotechnology,* 24**,** 1027-1032.

PICHON, C., DU MERLE, L., LEQUEUTRE, I. & LE BOUGUENEC, C. 2013. The AfaR small RNA controls expression of the AfaD-VIII invasin in pathogenic *Escherichia coli* strains. *Nucleic Acids Research,* 41**,** 5469-5482.

POCHON, F. & MICHELSON, A. M. 1965. Polynucleotides. VI. Interaction between polyguanylic acid and polycytidylic acid. *Proceedings of the National Academy of Sciences of the United States of America,* 53**,** 1425-1430.

POLACH, K. J. & UHLENBECK, O. C. 2002. Cooperative binding of ATP and RNA substrates to the DEAD/H protein DbpA. *Biochemistry,* 41**,** 3693-3702.

PORTIER, C., DONDON, L., GRUNBERG-MANAGO, M. & REGNIER, P. 1987. The first step in the functional inactivation of the *Escherichia coli* polynucleotide phosphorylase messenger is a ribonuclease III processing at the 5' end. *EMBO Journal,* 6**,** 2165-2170.

PREISS, T. & HENTZE, M. W. 1998. Dual function of the messenger RNA cap structure in poly(A)-tail-promoted translation in yeast. *Nature,* 392**,** 516-520.

PRUD'HOMME-GENEREUX, A., BERAN, R. K., IOST, I., RAMEY, C. S., MACKIE, G. A. & SIMONS, R. W. 2004. Physical and functional interactions among RNase E, polynucleotide phosphorylase and the cold-shock protein, CsdA: evidence for a 'cold shock degradosome'. *Molecular Microbiology,* 54**,** 1409-1421.

PY, B., CAUSTON, H., MUDD, E. A. & HIGGINS, C. F. 1994. A protein complex mediating messenger RNA degradation in *Escherichia coli*. *Molecular Microbiology,* 14**,** 717-729.

PY, B., HIGGINS, C. F., KRISCH, H. M. & CARPOUSIS, A. J. 1996. A DEAD-box RNA helicase in the *Escherichia coli* RNA degradosome. *Nature,* 381**,** 169-172.

RAGHAVAN, R., SLOAN, D. B. & OCHMAN, H. 2012. Antisense transcription is pervasive but rarely conserved in enteric bacteria. *MBio,* 3.

RAUHUT, R. & KLUG, G. 1999. mRNA degradation in bacteria. *FEMS Microbiol Rev,* 23**,** 353-70.

REDKO, Y., DE LA SIERRA-GALLAY, I. L. & CONDON, C. 2007. When all's zed and done: the structure and function of RNase Z in prokaryotes. *Nature Reviews Microbiology,* 5**,** 278-286.

REDKO, Y., TOCK, M. R., ADAMS, C. J., KABERDIN, V. R., GRASBY, J. A. & MCDOWALL, K. J. 2003. Determination of the catalytic parameters of the N-terminal half of *Escherichia coli* ribonuclease E and the identification of critical functional groups in RNA substrates. *Journal of Biological Chemistry,* 278**,** 44001-44008.

REGNIER, P. & GRUNBERG-MANAGO, M. 1990. RNase III cleavages in non-coding leaders of *Escherichia coli* transcripts control mRNA stability and genetic expression. *Biochimie,* 72**,** 825-834.

REGNIER, P. & HAJNSDORF, E. 1991. Decay of messenger RNA encoding ribosomal protein S15 of *Escherichia coli* is initiated by an RNase E-dependent endonucleolytic cleavage that removes the 3' stabilizing stem and loop structure. *Journal of Molecular Biology,* 217**,** 283-292.

REGNIER, P. & PORTIER, C. 1986. Initiation, attenuation and RNase III processing of transcripts from the *Escherichia coli* operon encoding ribosomal protein S15 and polynucleotide phosphorylase. *Journal of Molecular Biology,* 187**,** 23-32.

RESCH, A., AFONYUSHKIN, T., LOMBO, T. B., MCDOWALL, K. J., BLASI, U. & KABERDIN, V. R. 2008. Translational activation by the noncoding RNA DsrA involves alternative RNase III processing in the *rpoS* 5'-leader. *RNA-a Publication of the RNA Society,* 14**,** 454-459.

RICHARDS, J., LIU, Q., PELLEGRINI, O., CELESNIK, H., YAO, S., BECHHOFER, D. H., CONDON, C. & BELASCO, J. G. 2011. An RNA pyrophosphohydrolase triggers 5'-exonucleolytic degradation of mRNA in *Bacillus subtilis*. *Molecular Cell,* 43**,** 940-949.

RICHARDS, J., LUCIANO, D. J. & BELASCO, J. G. 2012. Influence of translation on RppH-dependent mRNA degradation in *Escherichia coli*. *Molecular Microbiology,* 86**,** 1063-1072.

ROBERT-LE MEUR, M. & PORTIER, C. 1994. Polynucleotide phosphorylase of *Escherichia coli* induces the degradation of its RNase III-processed messenger by preventing its translation. *Nucleic Acids Research,* 22**,** 397-403.

ROBERTSON, H. D., WEBSTER, R. E. & ZINDER, N. D. 1967. A nuclease specific for double-stranded RNA. *Virology,* 32**,** 718-719.

ROBERTSON, H. D., WEBSTER, R. E. & ZINDER, N. D. 1968. Purification and properties of ribonuclease III from *Escherichia coli*. *Journal of Biological Chemistry,* 243**,** 82-91.

ROBINOW, C. & KELLENBERGER, E. 1994. The bacterial nucleoid revisited. *Microbiology Reviews,* 58**,** 211-232.

ROMERO A., D., HASAN, A., LIN, Y.-F., KIME, L., KABERDIN, V. R., RUIZ-LARRABEITI, O., SMITH, C. P., LAING, E. E., VAN WEZEL, G. P., UREM, M., MAMANOVA, L. & MCDOWALL, K. J. 2014. A comparison and analysis of key aspects of gene regulation in *Streptomyces coelicolor* and *Escherichia coli* using equivalent nucleotide-resolution transcription maps produced by global and differential RNA-sequencing. (in press).

ROZEN, S. & SKALETSKY, H. 2000. Primer3 on the WWW for general users and for biologist programmers. *Methods in Molecular Biology,* 132**,** 365-386.

SAKAI, T., NAKAMURA, N., UMITSUKI, G., NAGAI, K. & WACHI, M. 2007. Increased production of pyruvic acid by *Escherichia coli* RNase G mutants in combination with *cra* mutations. *Applied Microbiology and Biotechnology,* 76**,** 183-192.

SAMBROOK, J. & RUSSELL, D. W. 2001. *Molecular cloning: A laboratory manual,* New York, Cold Spring Harbor Laboratories.

SCHIFANO, J. M., EDIFOR, R., SHARP, J. D., OUYANG, M., KONKIMALLA, A., HUSSON, R. N. & WOYCHIK, N. A. 2013. Mycobacterial toxin MazF-mt6 inhibits translation through cleavage of 23S rRNA at the ribosomal A site. *Proceedings of the National Academy of Sciences of the United States of America,* 110**,** 8501-8506.

SCHIFANO, J. M., VVEDENSKAYA, I. O., KNOBLAUCH, J. G., OUYANG, M., NICKELS, B. E. & WOYCHIK, N. A. 2014. An RNA-seq method for defining endoribonuclease cleavage specificity identifies dual rRNA substrates for toxin MazF-mt3. *Nature Communications,* 5**,** 3538.

SCHMIDT, F. J. 1975. A novel function of Escherichia coli transfer RNA nucleotidyltransferase. Biosynthesis of the C-C-A sequence in a phage T4 transfer RNA precursor. *Journal of Biological Chemistry,* 250**,** 8399-8403.

SCHUBERT, M., EDGE, R. E., LARIO, P., COOK, M. A., STRYNADKA, N. C. J., MACKIE, G. A. & MCINTOSH, L. P. 2004. Structural characterization of the RNase E S1 domain and identification of its oligonucleotide-binding and dimerization interfaces. *Journal of Molecular Biology,* 341**,** 37-54.

SCHUCK, A., DIWA, A. & BELASCO, J. G. 2009. RNase E autoregulates its synthesis in *Escherichia coli* by binding directly to a stem-loop in the *rne* 5' untranslated region. *Molecular Microbiology,* 72**,** 470-478.

SELINGER, D. W., SAXENA, R. M., CHEUNG, K. J., CHURCH, G. M. & ROSENOW, C. 2003. Global RNA half-life analysis in *Escherichia coli* reveals positional patterns of transcript degradation. *Genome Research,* 13**,** 216-223.

SHAHBABIAN, K., JAMALLI, A., ZIG, L. & PUTZER, H. 2009. RNase Y, a novel endoribonuclease, initiates riboswitch turnover in *Bacillus subtilis*. *EMBO Journal,* 28**,** 3523-33.

SHARMA, C. M., HOFFMANN, S., DARFEUILLE, F., REIGNIER, J., FINDEISS, S., SITTKA, A., CHABAS, S., REICHE, K., HACKERMULLER, J., REINHARDT, R., STADLER, P. F. & VOGEL, J. 2010. The primary transcriptome of the major human pathogen *Helicobacter pylori*. *Nature,* 464**,** 250-255.

SHATKIN, A. J. 1976. Capping of eucaryotic mRNAs. *Cell,* 9**,** 645-653.

SHI, Z., YANG, W. Z., LIN-CHAO, S., CHAK, K. F. & YUAN, H. S. 2008. Crystal structure of *Escherichia coli* PNPase: central channel residues are involved in processive RNA degradation. *RNA-a Publication of the RNA Society,* 14**,** 2361-2371.

SHINE, J. & DALGARNO, L. 1974. 3'-terminal sequence of *Escherichia coli* 16S rRNA: possible role in initiation and termination of protein synthesis. *Proceedings of the Australian Biochemical Society,* 7**,** 72-72.

SHIRAISHI, H. & SHIMURA, Y. 1995. Genetic analysis of the structure and function of RNase P from *E. coli*. *Molecular Biology Reports,* 22**,** 111-114.

SMOLKE, C. D. & KEASLING, J. D. 2002. Effect of gene location, mRNA secondary structures, and RNase sites on expression of two genes in an engineered operon. *Biotechnology and Bioengineering,* 80**,** 762-776.

SODERBOM, F., SVARD, S. G. & KIRSEBOM, L. A. 2005. RNase E cleavage in the 5' leader of a tRNA precursor. *Journal of Molecular Biology,* 352**,** 22-27.

SPAHR, P. F. & HOLLINGWORTH, B. R. 1961. Purification and Mechanism of Action of Ribonuclease from *Escherichia coli* Ribosomes *Journal of Biological Chemistry,* 236**,** 823-831.

SPRINZL, M. & CRAMER, F. 1979. The -C-C-A end of tRNA and its role in protein biosynthesis. *Progressions in Nucleic Acid Research and Molecular Biology,* 22**,** 1-69.

STEAD, M. B., MARSHBURN, S., MOHANTY, B. K., MITRA, J., CASTILLO, L. P., RAY, D., VAN BAKEL, H., HUGHES, T. R. & KUSHNER, S. R. 2011. Analysis of *Escherichia coli* RNase E and RNase III activity *in vivo* using tiling microarrays. *Nucleic Acids Research,* 39**,** 3188-3203.

STRAHL, H., TURLAN, C., KHALID, S., BOND, P. J., KEBALO, J. M., PEYRON, P., POLJAK, L., BOUVIER, M., HAMOEN, L., LUISI, B. F. & CARPOUSIS, A. J. 2015. Membrane recognition and dynamics of the RNA degradosome. *PLoS Genetics,* 11**,** e1004961.

SUBBARAYAN, P. R. & DEUTSCHER, M. P. 2001. *Escherichia coli* RNase M is a multiply altered form of RNase I. *RNA-a Publication of the RNA Society,* 7**,** 1702-1707.

SULTHANA, S. & DEUTSCHER, M. P. 2013. Multiple exoribonucleases catalyze maturation of the 3' terminus of 16S ribosomal RNA (rRNA). *Journal of Biological Chemistry,* 288**,** 12574-12579.

SUNOHARA, T., JOJIMA, K., YAMAMOTO, Y., INADA, T. & AIBA, H. 2004. Nascent-peptide-mediated ribosome stalling at a stop codon induces mRNA cleavage resulting in nonstop mRNA that is recognized by tmRNA. *RNA-a Publication of the RNA Society,* 10**,** 378-386.

SVITKIN, Y. V., PAUSE, A., HAGHIGHAT, A., PYRONNET, S., WITHERELL, G., BELSHAM, G. J. & SONENBERG, N. 2001. The requirement for eukaryotic initiation factor 4A (eIF4A) in translation is in direct proportion to the degree of mRNA 5' secondary structure. *RNA-a Publication of the RNA Society,* 7**,** 382-394.

SYMMONS, M. F., JONES, G. H. & LUISI, B. F. 2000. A duplicated fold is the structural basis for polynucleotide phosphorylase catalytic activity, processivity, and regulation. *Structure,* 8**,** 1215-1226.

SYMMONS, M. F., WILLIAMS, M. G., LUISI, B. F., JONES, G. H. & CARPOUSIS, A. J. 2002. Running rings around RNA: a superfamily of phosphate-dependent RNases. *Trends in Biochemical Sciences,* 27**,** 11-18.

TAGHBALOUT, A. & ROTHFIELD, L. 2007. RNaseE and the other constituents of the RNA degradosome are components of the bacterial cytoskeleton. *Proceedings of the National Academy of Sciences of the United States of America,* 104**,** 1667-1672.

TAGHBALOUT, A. & ROTHFIELD, L. 2008. RNaseE and RNA helicase B play central roles in the cytoskeletal organization of the RNA degradosome. *Journal of Biological Chemistry,* 283**,** 13850-13855.

TAGHBALOUT, A., YANG, Q. & ARLUISON, V. 2014. The *Escherichia coli* RNA processing and degradation machinery is compartmentalized within an organized cellular network. *Biochemical Journal,* 458**,** 11-22.

TAKATA, R., MUKAI, T. & HORI, K. 1987. RNA processing by RNase III is involved in the synthesis of *Escherichia coli* polynucleotide phosphorylase. *Molecular General Genetics,* 209**,** 28-32.

TALKAD, V., ACHORD, D. & KENNELL, D. 1978. Altered mRNA metabolism in ribonuclease III-deficient strains of *Escherichia coli*. *Journal of Bacteriology,* 135**,** 528-541.

TARASEVICIENE, L., BJORK, G. R. & UHLIN, B. E. 1995. Evidence for an RNA binding region in the *Escherichia coli* processing endoribonuclease RNase E. *Journal of Biological Chemistry,* 270**,** 26391-26398.

TARASEVICIENE, L., MICZAK, A. & APIRION, D. 1991. The gene specifying RNase E (*rne*) and a gene affecting messenger RNA stability (*ams*) are the same gene. *Molecular Microbiology,* 5**,** 851-855.

TARUN, S. Z., JR. & SACHS, A. B. 1996. Association of the yeast poly(A) tail binding protein with translation initiation factor eIF-4G. *EMBO Journal,* 15**,** 7168-7177.

THOMPSON, K. J., ZONG, J. & MACKIE, G. A. 2015. Altering the divalent metal ion preference of RNase E. *Journal of Bacteriology,* 197**,** 477-482.

TOCK, M. R., WALSH, A. P., CARROLL, G. & MCDOWALL, K. J. 2000. The CafA protein required for the 5'-maturation of 16S rRNA is a 5'-end-dependent ribonuclease that has context-dependent broad sequence specificity. *Journal of Biological Chemistry,* 275**,** 8726-8732.

TOURRIERE, H., CHEBLI, K. & TAZI, J. 2002. mRNA degradation machines in eukaryotic cells. *Biochimie,* 84**,** 821-837.

TSUTSUI, Y. & WINTRODE, P. L. 2007. Hydrogen/deuterium exchange-mass spectrometry: a powerful tool for probing protein structure, dynamics and interactions. *Current Medicinal Chemistry,* 14**,** 2344-2358.

TUTAS, D. J. & PAOLETTI, E. 1977. Purification and characterization of core-associated polynucleotide 5'-triphosphatase from Vaccinia virus. *Journal of Biological Chemistry,* 252**,** 3092-3098.

UDEKWU, K. I., DARFEUILLE, F., VOGEL, J., REIMEGARD, J., HOLMQVIST, E. & WAGNER, E. G. 2005. Hfq-dependent regulation of OmpA synthesis is mediated by an antisense RNA. *Genes & Development,* 19**,** 2355-2366.

UMITSUKI, G., WACHI, M., TAKADA, A., HIKICHI, T. & NAGAI, K. 2001. Involvement of RNase G in *in vivo* mRNA metabolism in *Escherichia coli*. *Genes To Cells,* 6**,** 403-410.

VANACOVA, S., WOLF, J., MARTIN, G., BLANK, D., DETTWILER, S., FRIEDLEIN, A., LANGEN, H., KEITH, G. & KELLER, W. 2005. A new yeast poly(A) polymerase complex involved in RNA quality control. *PLoS Biology,* 3**,** e189.

VANDERPOOL, C. K. 2007. Physiological consequences of small RNA-mediated regulation of glucose-phosphate stress. *Current Opinion in Microbiology,* 10**,** 146-151.

VANZO, N. F., LI, Y. S., PY, B., BLUM, E., HIGGINS, C. F., RAYNAL, L. C., KRISCH, H. M. & CARPOUSIS, A. J. 1998. Ribonuclease E organizes the protein interactions in the *Escherichia col*i RNA degradosome. *Genes & Development,* 12**,** 2770-2781.

VECEREK, B., MOLL, I., AFONYUSHKIN, T., KABERDIN, V. & BLASI, U. 2003. Interaction of the RNA chaperone Hfq with mRNAs: direct and indirect roles of Hfq in iron metabolism of *Escherichia coli*. *Molecular Microbiology,* 50**,** 897-909.

VENKATESAN, S., GERSHOWITZ, A. & MOSS, B. 1980. Modification of the 5' end of mRNA. Association of RNA triphosphatase with the RNA guanylyltransferase-RNA (guanine-7-)methyltransferase complex from vaccinia virus. *Journal of Biological Chemistry,* 255**,** 903-908.

VESPER, O., AMITAI, S., BELITSKY, M., BYRGAZOV, K., KABERDINA, A. C., ENGELBERG-KULKA, H. & MOLL, I. 2011. Selective translation of leaderless mRNAs by specialized ribosomes generated by MazF in *Escherichia coli*. *Cell,* 147**,** 147-157.

VIEGAS, S. C. & ARRAIANO, C. M. 2008. Regulating the regulators. *RNA Biology,* 5**,** 230-243.

VIEGAS, S. C., MIL-HOMENS, D., FIALHO, A. M. & ARRAIANO, C. M. 2013. The virulence of *Salmonella enterica Serovar Typhimurium* in the insect model *Galleria mellonella* is impaired by mutations in RNase E and RNase III. *Applied and Environmental Microbiology,* 79**,** 6124-6133.

VINCENT, H. A. & DEUTSCHER, M. P. 2006. Substrate recognition and catalysis by the exoribonuclease RNase R. *Journal of Biological Chemistry,* 281**,** 29769-29775.

VISA, N., IZAURRALDE, E., FERREIRA, J., DANEHOLT, B. & MATTAJ, I. W. 1996. A nuclear cap-binding complex binds Balbiani ring pre-mRNA cotranscriptionally and accompanies the ribonucleoprotein particle during nuclear export. *Journal of Cellular Biology,* 133**,** 5-14.

VOCKENHUBER, M. P., SHARMA, C. M., STATT, M. G., SCHMIDT, D., XU, Z. J., DIETRICH, S., LIESEGANG, H., MATHEWS, D. H. & SUESS, B. 2011. Deep sequencing-based identification of small non-coding RNAs in *Streptomyces coelicolor*. *RNA Biology,* 8**,** 468-477.

VOSSEN, K. M., STICKLE, D. F. & FRIED, M. G. 1996. The mechanism of CAP-lac repressor binding cooperativity at the *E. coli* lactose promoter. *Journal of Molecular Biology,* 255**,** 44-54.

WACHI, M., KAGA, N., UMITSUKI, G., CLARK, D. P. & NAGAI, K. 2001. A novel RNase G mutant that is defective in degradation of *adhE* mRNA but proficient in the processing of 16S rRNA precursor. *Biochemical and Biophysical Research Communications,* 289**,** 1301-1306.

WACHI, M., UMITSUKI, G. & NAGAI, K. 1997. Functional relationship between *Escherichia coli* RNase E and the CafA protein. *Molecular General Genetics,* 253**,** 515-519.

WACHI, M., UMITSUKI, G., SHIMIZU, M., TAKADA, A. & NAGAI, K. 1999. *Escherichia coli cafA* gene encodes a novel RNase, designated as RNase G, involved in processing of the 5' end of 16S rRNA. *Biochemical and Biophysical Research Communications,* 259**,** 483-488.

WALSH, A. P., TOCK, M. R., MALLEN, M. H., KABERDIN, V. R., VON GABAIN, A. & MCDOWALL, K. J. 2001. Cleavage of poly(A) tails on the 3'-end of RNA by ribonuclease E of *Escherichia coli*. *Nucleic Acids Research,* 29**,** 1864-1871.

WILLIAMSON, J. R. 2003. After the ribosome structures: how are the subunits assembled? *RNA-a Publication of the RNA Society,* 9**,** 165-167.

WORRALL, J. A., HOWE, F. S., MCKAY, A. R., ROBINSON, C. V. & LUISI, B. F. 2008. Allosteric activation of the ATPase activity of the *Escherichia coli* RhlB RNA helicase. *Journal of Biological Chemistry,* 283**,** 5567-5576.

XIONG, Y. & STEITZ, T. A. 2004. Mechanism of transfer RNA maturation by CCA-adding enzyme without using an oligonucleotide template. *Nature,* 430**,** 640-645.

XU, F. F., LINCHAO, S. & COHEN, S. N. 1993. The *Escherichia coli pcnB* gene promotes adenylylation of antisense RNAI of ColE1-type plasmids *in vivo* and degradation of RNAI decay intermediates. *Proceedings of the National Academy of Sciences of the United States of America,* 90**,** 6756-6760.

YAJNIK, V. & GODSON, G. N. 1993. Selective decay of *Escherichia coli dnaG* messenger RNA is initiated by RNase E. *Journal of Biological Chemistry,* 268**,** 13253-13260.

YANG, J., JAIN, C. & SCHESSER, K. 2008. RNase E regulates the *Yersinia* type 3 secretion system. *Journal of Bacteriology,* 190**,** 3774-3778.

YAO, S. Y. & BECHHOFER, D. H. 2010. Initiation of Decay of *Bacillus subtilis rpsO* mRNA by Endoribonuclease RNase Y. *Journal of Bacteriology,* 192**,** 3279-3286.

YEHUDAI-RESHEFF, S. & SCHUSTER, G. 2000. Characterization of the *E.coli* poly(A) polymerase: nucleotide specificity, RNA-binding affinities and RNA structure dependence. *Nucleic Acids Research,* 28**,** 1139-1144.

YOUNG, R. A. & STEITZ, J. A. 1978. Complementary sequences 1700 nucleotides apart form a ribonuclease III cleavage site in *Escherichia coli* ribosomal precursor RNA. *Proceedings of the National Academy of Sciences of the United States of America,* 75**,** 3593-3597.

ZHANG, X., ZHU, L. & DEUTSCHER, M. P. 1998. Oligoribonuclease is encoded by a highly conserved gene in the 3'-5' exonuclease superfamily. *Journal of Bacteriology,* 180**,** 2779-2781.

ZHANG, Y., ZHANG, J., HARA, H., KATO, I. & INOUYE, M. 2005. Insights into the mRNA cleavage mechanism by MazF, an mRNA interferase. *Journal of Biological Chemistry,* 280**,** 3143-3150.

ZHANG, Y., ZHANG, J., HOEFLICH, K. P., IKURA, M., QING, G. & INOUYE, M. 2003. MazF cleaves cellular mRNAs specifically at ACA to block protein synthesis in *Escherichia coli*. *Molecular Cell,* 12**,** 913-923.

ZHU, L. & DEUTSCHER, M. P. 1987. tRNA nucleotidyltransferase is not essential for *Escherichia coli* viability. *EMBO Journal,* 6**,** 2473-2477.

ZILHAO, R., CAIRRAO, F., REGNIER, P. & ARRAIANO, C. M. 1996. PNPase modulates RNase II expression in *Escherichia coli*: implications for mRNA decay and cell metabolism. *Molecular Microbiology,* 20**,** 1033-1042.

ZUO, Y. & DEUTSCHER, M. P. 2001. Exoribonuclease superfamilies: structural analysis and phylogenetic distribution. *Nucleic Acids Research* 29**,** 1017-1026.

ZUO, Y. & DEUTSCHER, M. P. 2002a. Mechanism of action of RNase T. I. Identification of residues required for catalysis, substrate binding, and dimerization. *Journal of Biological Chemistry,* 277**,** 50155-50159.

ZUO, Y. & DEUTSCHER, M. P. 2002b. Mechanism of action of RNase T. II. A structural and functional model of the enzyme. *Journal of Biological Chemistry,* 277**,** 50160-50164.

ZUO, Y., ZHENG, H., WANG, Y., CHRUSZCZ, M., CYMBOROWSKI, M., SKARINA, T., SAVCHENKO, A., MALHOTRA, A. & MINOR, W. 2007. Crystal structure of RNase T, an exoribonuclease involved in tRNA maturation and end turnover. *Structure,* 15**,** 417-428.

ZUO, Y. H., VINCENT, H. A., ZHANG, J. W., WANG, Y., DEUTSCHER, M. P. & MALHOTRA, A. 2006. Structural basis for processivity and single-strand specificity of RNase II. *Molecular Cell,* 24**,** 149-156.

# Chapter 8

# Appendix

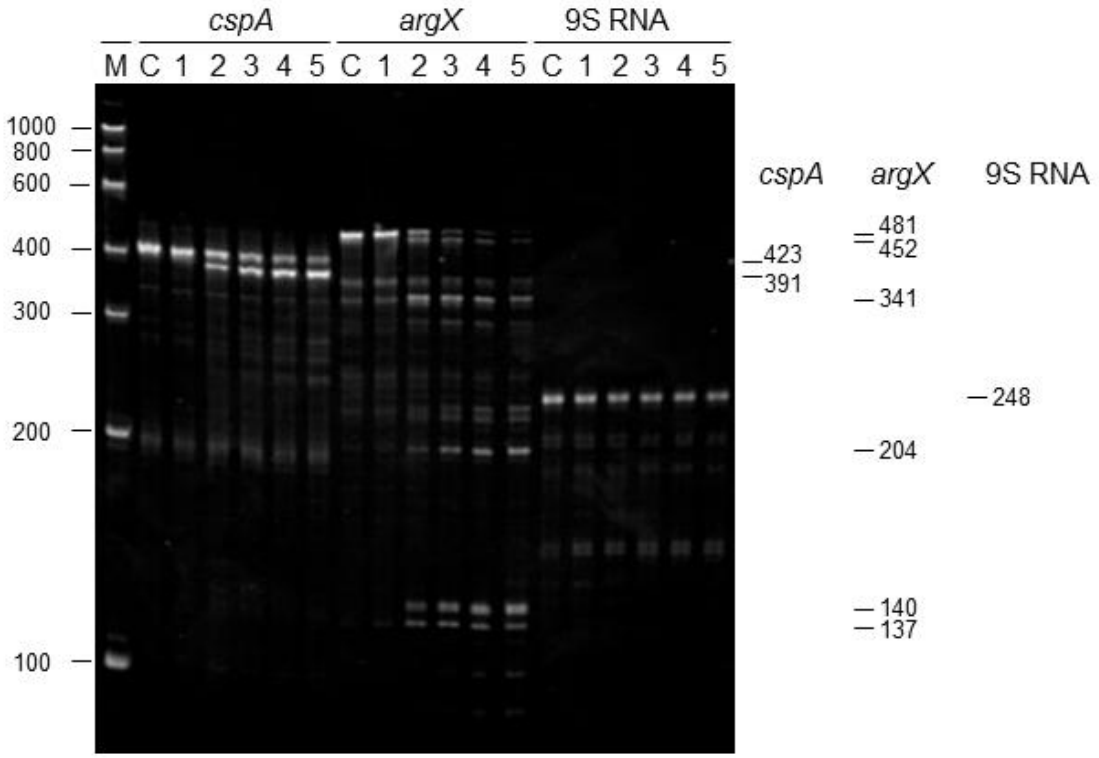


**Figure S1 Cleavage of 5'-triphosphorylated direct entry controls.** The 5'-triphosphorylated transcripts were generated by *in vitro* transcription as described in Materials and Methods. The gene to which each substrate corresponds is shown at the top of each image. Final substrate and NTH-RNase E T170V concentrations were 180 nM and 20 nM, respectively. Samples were taken after various time points upon incubation, quenched in equal volumes of 2x RNA loading dye, denatured at 95°C, separated on 8% denaturing polyacrylamide gels, and stained with ethidium bromide as described in Chapter 2. Lanes 1-5 contain samples taken at 0, 5, 15, 30 and 60 min after incubation of substrate with enzyme. Lane C contains substrate incubated without enzyme for 60 min. Lane M contains a RiboRuler™ low range RNA ladder with sizes in nt indicated at the left of each image. The sizes in nt of the substrates and cleavage products are shown at the right of each image.